



The University of
Nottingham

UNITED KINGDOM • CHINA • MALAYSIA

Continuous flow photooxidation of *p*-substituted phenols using singlet oxygen in supercritical CO₂ applied to telescoped syntheses

Bruna Lacerda da Silva Abreu, BSc

Thesis submitted to The University of Nottingham for the degree of
Doctor of Philosophy

Supervisors: Prof. Mike George and Prof. Martyn Poliakoff

June / 2021

Acknowledgements

Firstly, I would like to thank my supervisors Prof. Mike George and Prof. Martyn Poliakoff for providing me the opportunity to join their research group and to fulfil my dream of doing a PhD in a renowned university in the UK.

I am grateful to the University of Nottingham for awarding me with the Vice-Chancellor's Scholarship for Research Excellence, which is funding my course, and the EPSRC Photo-Electro programme grant for financial support.

I express my warm thanks to all the members of our research group, which are around 35 people. In particular, Dr. Lingqiao Wu and Dr. Hamza Boufroua who worked closely with me throughout my PhD, giving me guidance with the high-pressure system and organic reactions. I would also like to thank Dr. Rowena Howie for her support in flow chemistry; Drs. Jonathan Moore, Darren Lee, Marcos Hernando, Rodolfo Teixeira and Amy Flinn, as well as Kateryna Zhyvitska, Jonathan Hunter and Toby Waldron for sharing their organic chemistry knowledge with me and revising my thesis chapters.

I also thank all the technicians from the University of Nottingham's workshop; Dr. Steve Argent for XRD measurements; Shaz Aslam for NMR support; Sue and Melissa Richardson for always being so lovely with me. I would also like to thank Dr. Sam Tang and Dr. Charlotte Clark for their incredible support to help me develop teaching skills.

A special thanks to a few of my close friends and lab mates Amy Flinn, Kateryna Zhyvitska, Agata Rogalska, and Jonathan Hunter, for being incredibly amazing people whom I share great moments during and after work; and my best friends from Brazil Lucas Martoni and Amanda Ramos for always being there for me for years and years.

Finally, I am extremely grateful to my beloved parents Elaine and Marcelo, grandparents Laisse and Manoel, and aunt Ivone, for all the love, emotional support and encouragement since I was a child for me to pursue my dreams. Special thanks for my dogs Meg, Kika, and Talinha for have given me unconditionally love. My dearest fiancée Joe Millard who relentlessly helped me throughout the whole process, revising my applications for the PhD and my reports, loving me in every possible way. Joe's family for being supportive and caring specially during COVID-19 pandemic lockdown, inviting us to stay at their house during part of my writing.

Abstract

Interest in photochemical processes both in academia and industry is increasing, but uptake is still limited due to low efficiency and/or scalability of current processes. Photochemical synthesis of highly reactive hydroperoxides so-called '*p*-peroxyquinols' is of particular interest for synthetic organic chemistry and pharmaceutical manufacturing, given their involvement in the synthesis of antimalarial drugs and complex natural products. Batch synthesis of *p*-peroxyquinols in large scale can be challenging, given its instability in flammable solvents and long reaction times of up to 48 h. Continuous flow photooxidation of *p*-substituted phenols using singlet oxygen and supercritical CO₂ could be a suitable alternative. In this Thesis, this methodology is explored in telescoped syntheses of compounds with potential pharmaceutical interest.

Chapter 1 gives an introduction to flow chemistry including an overview of parameters and concepts used in the field. It highlights the advantages, challenges, and applications of flow chemistry both in academia and industry. A brief description of continuous flow photochemistry is also given, including recent advances using singlet oxygen in supercritical CO₂. Chapter 2 describes the high-pressure batch and flow reactors used in this work, as well as the Standard Operating Procedures (SOP) for each system.

Chapters 3 and 4 explore the continuous flow dearomatisation of *p*-substituted phenols using singlet oxygen in supercritical CO₂ (Chapter 3) and its applications in the telescoped synthesis of 1,2,4-trioxanes, a scaffold present in antimalarial drugs such as Artemisinin (Chapter 4). The dearomatisation of *p*-substituted phenols was carried out using a photosensitiser and Light Emitting Diodes (LEDs) to generate singlet oxygen. 1,2,4-trioxanes were then synthesised via an acid catalysed acetalization/oxa-Michael addition cascade with aldehydes. The substrate scope was expanded to a variety of *p*-peroxyquinols and 1,2,4-trioxanes, investigating functional group robustness, degree of substitution, and type of substituent.

Chapter 5 reports the telescoped synthesis of 2-substituted-1,4-benzoquinones, an important class of compounds with a variety of medicinal properties. The *p*-peroxyquinols formed through dearomatisation of *p*-substituted phenols, following the methodology developed in Chapter 3, were converted into 2-substituted-1,4-benzoquinones via acid-catalysed 1,2-alkyl shift of *p*-peroxyquinols. Optimisation of reaction conditions was initially carried out in batch, and the best conditions were then transferred to the continuous flow

system. Several packed bed reactor designs were investigated in order to optimise the reaction yields.

Chapters 6 and 7 present studies for the telescoped synthesis of 1,2,4-dioxazinanes and 1,3-oxazolidines, respectively. For both target compounds, an amination/aza-Michael addition step using either a *N*-sulfinyl imine or *N*-sulfonyl imine was involved in the process. In Chapter 6, the synthesis of 1,2,4-dioxazinanes was investigated as this scaffold has been shown to have antimalarial activity, but synthetic methodologies to produce these compounds are scarce in the literature. The reaction conditions for both the asymmetric and racemic synthesis of 1,2,4-dioxazinanes were attempted in batch using a *p*-peroxyquinol and *N*-sulfonyl/sulfinyl imines previously synthesised. In Chapter 7, a synthetic route was designed for the asymmetric synthesis of 1,3-oxazolidines in four steps starting from the dearomatisation of *p*-substituted phenols. The reduction of *p*-peroxyquinols was examined in batch, and subsequent experiments were carried out to make 1,3-oxazolidines from *p*-quinols and *N*-sulfinyl imines.

In Chapter 8, a summary of the work developed in this Thesis is outlined, highlighting the main findings and challenges in exploring the continuous flow photooxidation of *p*-substituted phenols in telescoped syntheses. The discussion is guided by the Thesis aims defined in the introduction chapter. Ideas for potential future work are also presented.

Declaration

I declare that the work presented in this Thesis is a record of my own work for the period of October 2018 to June 2021. This Thesis has not been accepted in partial or complete fulfilment of any other degree or personal qualification. Where any work has been carried out in collaboration, the relevant researcher or researchers have been acknowledged both below specifically and within each chapter.

Chapters 3 and 4 were written up for publication in *Organic Process Research & Development*, in collaboration with Wu, L.; Blake, A. J.; Taylor, L. J.; Argent, S. P.; Poliakoff, M.; Boufroura, H.; George, M. W. (*in press*, DOI: <https://doi.org/10.1021/acs.oprd.1c00111>)

Chapter 5 results have been written up for publication in a special issue of *Molecules*, entitled “singlet oxygen-photooxygenation of organic compounds”, in collaboration with Boufroura, H.; Moore, J. C.; Poliakoff, M.; George, M. W.

A handwritten signature in black ink that reads "Bruna Abreu". The signature is written in a cursive, flowing style with a long horizontal line extending from the end of the name.

Bruna Lacerda da Silva Abreu, 25th June 2021

Abbreviation List

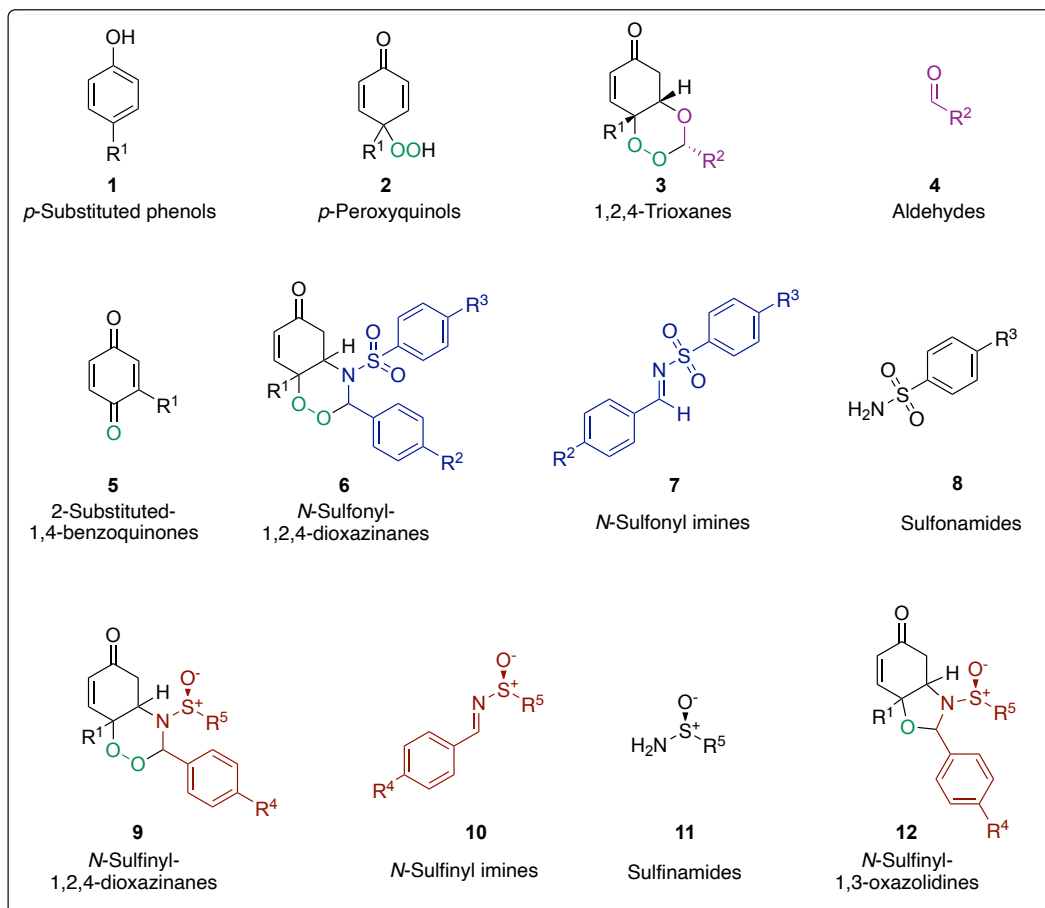
ρ_c	Critical Density
τ	Lifetime of Singlet Oxygen
k_Δ	Rate of Decay of Singlet Oxygen
$^1\text{O}_2$	Singlet Oxygen
$^3\text{O}_2$	Triplet Oxygen
API	Active Pharmaceutical Ingredient
Amb	Amberlyst-15
ACT	Artemisinin-based Combination Therapy
BPR	Back-Pressure Regulator
Boc ₂ O	Di- <i>tert</i> -Butyl Dicarboxylate
CSA	Camphorsulfonic Acid
dr	Diastereomeric Ratio
DABCO	4-Diazabicyclo[2.2.2]octane
DDQ	2,3-Dichloro-5,6-dicyanobenzoquinone
DCE	Dichloroethane
DCM	Dichloromethane
DMAP	Dimethylaminopyridine
DMC	Dimethyl Carbonate
DMF	Dimethylformamide
DMS	Dimethyl Sulfide
DMSO	Dimethyl Sulfoxide
EDG	Electron-Donating Group
EWG	Electron-Withdrawing Group
ESI-MS	Electrospray Ionisation Mass Spectrometry
ee	Enantiomeric Excess
Et	Ethyl
EPDM	Ethylene Propylene Diene Monomer
EC	External Conversion
FEP	Fluorinated Ethylene Propylene
F8	Highly fluorinated modified TFPFPP
HFE	3-Ethoxyperfluoro(2-methylhexane)
HFIP	Hexafluoro-2-propanol
HOMO	Highest-Occupied Molecular Orbital

HPLC	High performance liquid chromatography
IC	Internal Conversion
ISC	Intersystem Crossing
LED	Light Emitting Diodes
LOC	Limiting Oxygen Concentration
LUMO	Lowest-Unoccupied Molecular Orbital
Me	Methyl
Ms	Mesyl
NMR	Nuclear Magnetic Resonance
OAc	Acetate
O.D.	Outer Diameter
Oxone	Potassium Peroxymonosulfate
P_c	Critical Pressure
PVC	Polyvinyl Chloride
PPQ	<i>p</i> -Peroxyquinol
PTSA	<i>p</i> -Toluenesulfonic Acid
RDS	Rate-determining step
S_1	First Excited Singlet State
Sens	Photosensitiser
S_0	Singlet Ground State
STY	Space-time yield
SOP	Standard Operating Procedures
S_c	Supercritical
SCF	Supercritical Fluid
T_c	Critical Temperature
T_1	Lowest Excited Triplet State
TRIP	(<i>R</i>)-3,3'-Bis(2,4,6-triisopropylphenyl)-1,1'-binaphthyl-2,2'-diyl hydrogenphosphate
TBHP	<i>tert</i> -Butyl Hydroperoxide
TBSCI	<i>tert</i> -Butyldimethylsilylchloride
TBAF	Tetrabutylammonium Fluoride
TDCPP	5,10,15,20-Tetrakis(2,6-dichlorophenyl)porphyrin
THF	Tetrahydrofuran
TPFPP	5,10,15,20-Tetrakis(pentafluorophenyl) porphyrin
TPP	5,10,15,20-Tetraphenylporphyrin
TR	Thermo reactor

TLC	Thin Layer Chromatography
TATP	Triacetone Triperoxide
TEA	Triethylamine
Tf	Triflate
TFA	Trifluoroacetic Acid
TMSOTf	Trimethylsilyl Trifluoromethanesulfonate
UV-Vis	Ultraviolet-Visible
XRD	X-ray Diffraction

Compound numbering guide

All compounds synthesised in this Thesis were numbered according to their class, as shown in Scheme 1. By-products and intermediates were numbered in relation to the compound that originated them.



Scheme 1. Summary of classes of compounds synthesised in this Thesis and their respective numbering guide.

Table of Contents

ACKNOWLEDGEMENTS	2
ABSTRACT	3
DECLARATION	5
ABBREVIATION LIST.....	6
COMPOUND NUMBERING GUIDE	9
1. INTRODUCTION	12
1.1. FLOW CHEMISTRY: THE TRANSITION FROM FLASKS TO TUBES.....	12
1.2. CONTINUOUS FLOW PHOTOCHEMISTRY AND APPLICATIONS IN TELESCOPED SYNTHESSES	18
1.3. THESIS AIMS.....	33
2. METHODS AND MATERIALS	34
2.1. HIGH-PRESSURE CONTINUOUS FLOW SYSTEM FOR PHOTOOXIDATION AND TELESCOPED SYNTHESIS	34
2.2. HIGH-PRESSURE VIEW CELL	55
2.3. GENERAL REMARKS AND ANALYTICAL METHODS	59
3. CONTINUOUS FLOW DEAROMATISATION OF <i>P</i>-SUBSTITUTED PHENOLS USING SINGLET OXYGEN IN SUPERCRITICAL CO₂.....	61
3.1. INTRODUCTION	61
3.2. AIMS AND GENERAL STRATEGY	66
3.3. RESULTS AND DISCUSSION	68
3.4. CONCLUSIONS.....	78
3.5. EXPERIMENTAL PROCEDURES	80
4. CONTINUOUS FLOW TELESCOPED SYNTHESIS OF 1,2,4-TRIOXANES.....	94
4.1. INTRODUCTION	94
4.2. AIMS AND GENERAL STRATEGY	101
4.3. RESULTS AND DISCUSSION	103
4.4. CONCLUSIONS.....	122
4.5. EXPERIMENTAL PROCEDURES	126
5. CONTINUOUS FLOW TELESCOPED SYNTHESIS OF 2-SUBSTITUTED 1,4-BENZOQUINONES	
160	
5.1. INTRODUCTION	160
5.2. AIMS AND GENERAL STRATEGY	168
5.3. RESULTS AND DISCUSSION	169
5.4. CONCLUSIONS.....	192

5.5.	EXPERIMENTAL PROCEDURES.....	198
5.6.	APPENDIX	223
6.	CONTINUOUS FLOW TELESCOPED SYNTHESIS OF 1,2,4-DIOXAZINANES.....	230
6.1.	INTRODUCTION	230
6.2.	AIMS AND GENERAL STRATEGY.....	233
6.3.	RESULTS AND DISCUSSION	235
6.4.	CONCLUSIONS.....	246
6.5.	EXPERIMENTAL PROCEDURES.....	248
6.6.	APPENDIX	256
7.	CONTINUOUS FLOW TELESCOPED SYNTHESIS OF 1,3-OXAZOLIDINES	261
7.1.	INTRODUCTION	261
7.2.	AIMS AND GENERAL STRATEGY.....	267
7.3.	RESULTS AND DISCUSSION	268
7.4.	CONCLUSIONS.....	273
7.5.	EXPERIMENTAL PROCEDURES.....	274
8.	FINAL CONCLUSIONS AND FUTURE WORK	277
8.1.	FINAL WORDS	287
9.	REFERENCES	288

1. Introduction

1.1. Flow chemistry: the transition from flasks to tubes

The majority of chemicals and pharmaceuticals are still produced using batch processes,¹ with large vessels or continuous stirred tank reactors. The advantages of batch processes include the robustness, simplicity, and relative low cost of equipment required.² However, there are challenges that still need to be overcome including inefficient heat and mass transfer, reproducibility, safety hazards, and light penetration for photochemical reactions.³

Over the past ten years, there has been an increased use of flow rather than batch chemistry, which has been driven by both academia and the pharmaceutical industry^{2, 4-10}, in helping to address the challenges previously mentioned for batch reactions. Indeed, a Web of Science search showed that the number of publications returned from the search term “flow chemistry” has increased since 2010 (Figure 1).

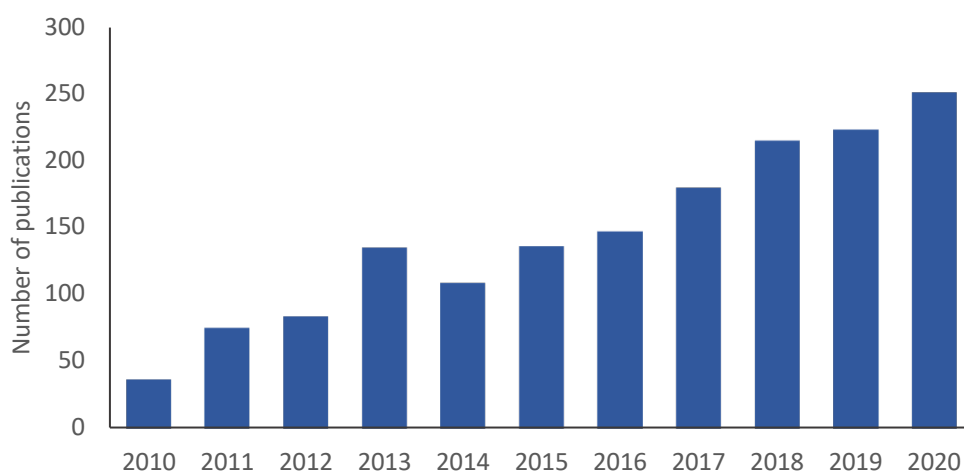


Figure 1. Number of publications between 2010 and 2020 returned from the search term “flow chemistry” (Web of Science).

What is flow chemistry? Flow chemistry consists of pumping reagents through channels or tubing to perform reactions in a continuous stream rather than in a traditional flask.³ Continuous flow systems can be designed from a variety of commercially available flow reactors (Figure 2) or customised depending on the reaction needs.



Figure 2. Examples of commercially available flow reactors: Vapourtec R-series,¹¹ Tube-in-tube membrane reactor,¹² and Ammonite electrolysis flow cell.¹³

1.1.1. Advantages and applications of flow chemistry

There are numerous possible advantages for a continuous flow approach over a batch process, such as increased heat and mass transfer; reduced reaction time; increased safety; easy screening, optimisation and automation; in-line analysis and purification; and scaling-up.⁶ These advantages will be discussed in the following paragraphs.

Efficient heat and mass transfer are achieved due to the reduced diameters of the flow tubing, which increases the surface-to-volume ratio.^{14, 15} As these parameters are better controlled in flow, reactions often have an enhanced selectivity and yield. For example, the batch synthesis of monoprotected diamines is usually problematic in batch, forming a mixture of protected products. In 2015, Bradley and Jong reported continuous flow monoprotection of diamines with high selectivity and yields up to 91%.¹⁶

Reaction time is often shortened in flow because of the efficient mixing inside the tubing. For example, Noël and co-workers have shown that trifluoromethylation of styrenes could be achieved with a reduced reaction time from 24 h in batch to 2 h in flow, both at a scale of 1.5 mmol, 5 mL using a flow photomicroreactor.¹⁷

Exposure to hazardous and/or explosive chemicals is of great concern in batch reactions, especially at large scale. Therefore, researchers have been developing continuous flow strategies for the safe generation of these compounds.¹⁸ For instance, Lehmann developed a simple and safe continuous flow formation of highly reactive and unstable diazomethane from non-hazardous *N*-methylurea at a multi-gram scale of 4.9 g/h.¹⁹

Reaction screening, optimisation and automation are also facilitated using a flow approach. A review written by Wu and co-workers showed that automation combined with flow chemistry enabled a facile design of experiments, which can often be time-consuming

and laborious in batch. Through screening a variety of parameters such as catalysts, solvents, and substrates, reaction conditions could be rapidly and automatically optimised.²⁰

Flow reactions can also be analysed and purified in-line. For instance, Ley and co-workers have reported a controlled flow synthesis of piperazine-2-carboxamide using in-line infrared spectroscopy.²¹ This technique enabled real-time analysis, thus reducing the overall time required for reaction optimisation. Regarding the use of in-line purification, a recent review on the use of scavenger columns, distillation, nanofiltration, and extraction methods in-line highlighted the potential of these techniques in medicinal chemistry.²² Moreover, Jamison and co-workers published one of the first studies using a liquid-liquid extraction membrane (called Zaiput) in the flow synthesis of an anticholinergic drug, Atropine.²³

In contrast to batch processes, in which the size of the reactor defines the scale of the reaction, flow systems are easier to scale-up. This is because by adding multiple reactors in series or running the reaction for longer periods of time, reactions can be scaled-up from milligram to kilogram-scale.²⁴

1.1.2. Main parameters and concepts in flow chemistry

The main parameters and concepts to be considered in developing a flow process are the stoichiometry, residence time, steady state, space-time yield (STY), and productivity, which are typically different from a batch setup.³

The stoichiometry of flow reactions (Equation 1)³ is calculated considering the molar flow rate of each reagent, \dot{n} , which is the product between its volumetric flow rate, \dot{q} , and molar concentration, M . This applies particularly where each reagent involved is pumped into the flow reactor from separate feedstocks. In batch conditions, stoichiometry is determined by the molar concentration of reagents in the reaction medium.

$$\dot{n} = \dot{q}M \quad (1)$$

Residence time, RT, is the time that the reagents spend in the reactor zone and can be estimated by the ratio of the reactor volume, V , to the overall flow rate, q , (Equation 2).³ This is the equivalent to the reaction time in batch, which is the time a given mixture is held under fixed conditions. Estimating the residence time can be challenging because other factors need to be considered such as the dead volume in packed bed reactors, and the solubility of gas in liquid-gas transformations.³

$$RT = \frac{V}{q} \quad (2)$$

In flow chemistry, there is a concentration gradient throughout the reactor zone, in which the concentration of the substrate decreases along the tubing.³ A steady state is reached when the concentration of substrate and product at a given position in the reactor zone remains constant. Conversion and yield are often calculated under steady state conditions and in-line analysis is a powerful tool to continuously monitor the time taken to reach steady-state.

Pressure-driven delivery of solutions in flow systems typically operate under a laminar flow regime with a characteristic parabolic velocity profile.²⁵ This velocity profile is a consequence of the fluid moving in layers, varying its speed from zero at the tubing walls, in which the fluid encounters the highest resistance to movement, reaching its maximum velocity in the centre of the tube. This is different from batch processes, where the concentration of starting material decreases with time and is assumed to be homogeneous in the flask.

Other parameters commonly reported in flow chemistry experiments are STY and productivity. STY is defined as the product quantity, n , per volume of reactor, V , and time, t (Equation 3). Productivity is the ratio between product quantity and time (Equation 4).³

$$STY = \frac{n}{Vt} \quad (3)$$

$$Productivity = \frac{n}{t} \quad (4)$$

1.1.3. Telescoped syntheses

The syntheses of fine chemicals and complex molecular frameworks both at bench and industrial scale are traditionally carried out in a stepwise manner in batch.²⁶⁻²⁸ Nonetheless, the energy and time demand, risk of exposure to hazardous intermediates, and the environmental impact in downstream processing (*e.g.* work-up and purification) have prompted researchers to find alternative technologies to perform multi-step processes.

Continuous flow telescoped synthesis is a multi-step process in which reagents are added one at a time without isolation of intermediates. The most common difficulties in developing a telescoped process in flow are identifying solvents compatible with all

reactions, and by-product formation which can interfere in subsequent steps of the process. These challenges have been addressed in recent years and flow chemistry has emerged as an enabling tool for the efficient synthesis of complex molecules, natural products and Active Pharmaceutical Ingredients (APIs). It also enables a safe generation and use of hazardous intermediates in multi-step synthesis.²⁹⁻³³

A recent example of continuous flow telescoped synthesis of an API was reported by Thompson and co-workers in 2019. They developed a methodology for the synthesis of an anticancer agent lomustine,³⁴ used for the treatment of brain tumour and lymphoma (Figure 3). The flow system designed was built using Fluorinated Ethylene Propylene (FEP) tubing and Zaiput liquid-liquid flow extractor. The synthesis consists of a carbamylation followed by a nitrosation, with a total residence time of 9 min, representing more than thirteenfold reduction in reaction time compared to previous batch processes. The reaction conditions were rapidly optimised using a Desorption Electrospray Ionisation Mass Spectrometry (DESI-MS) method and Chemtrix microreactor with autosampler. Pure lomustine was obtained by further extraction and washing, avoiding wasteful chromatography methods.

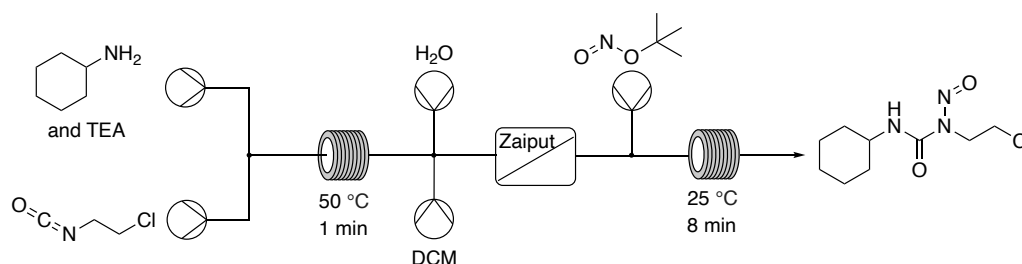


Figure 3. Continuous flow telescoped synthesis of lomustine by Thompson and co-workers using FEP tubing reactors and Zaiput liquid-liquid extractor. Reprinted (adapted) with permission from ref 34. Copyright 2019 American Chemical Society.³⁴

A second example from 2019 was the convergent flow synthesis of antibacterial drug linezolid in seven continuous steps, with an isolated yield of 73%.³⁵ The total reaction time was substantially reduced from the reported batch process (> 60 h) to less than 5 h in flow to produce 3.8g of Linezolid. At the time, it was the highest number of reaction steps ever carried out in continuous flow without intermediate purification or solvent exchange (Figure 4).

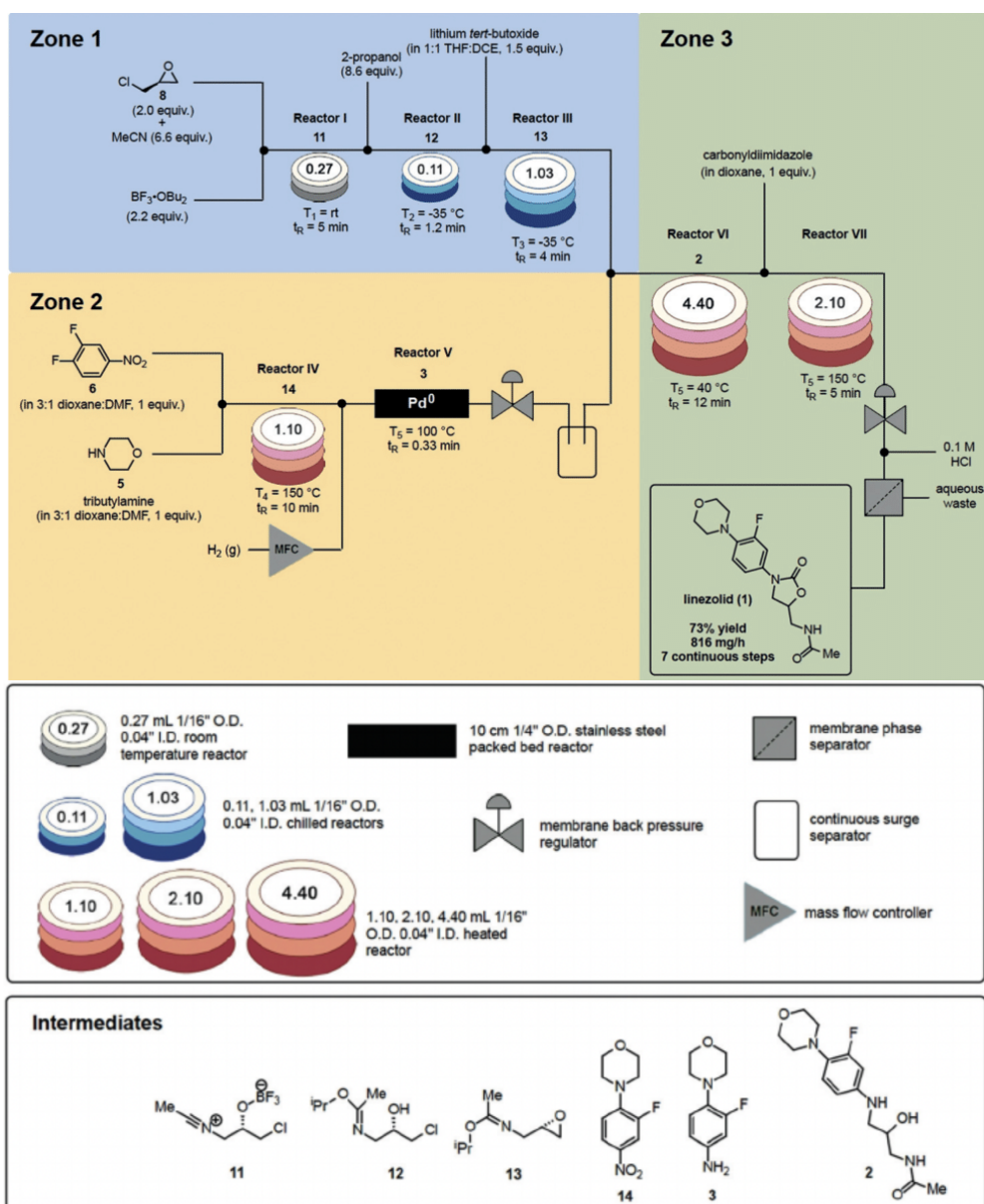


Figure 4. Continuous flow telescoped synthesis of linezolid by Jamison and co-workers separated in three main zones: zone 1, generation of epoxide **13** from **8**; zone 2, generation of aniline **3** from **5** and **6**; and zone three; coupling of **3** and **13** from zones 1 and 2, followed by formation of oxazolidinone ring to form linezolid.³⁵

1.1.4. Challenges and future perspectives in flow chemistry

Despite the many advantages that flow chemistry offers compared to batch processes, there are still challenges to be overcome for a wider implementation at industrial scale. These include handling of solids, cost of investment, background knowledge, and cultural barriers, which will be depicted below.

The use and generation of solids can cause serious blockages.³⁶ Ley and co-workers addressed the issue of solid generation in the oxidation of nitroalkanes using potassium

permanganate.³⁷ The fouling caused by the formation of insoluble aggregates of manganese dioxide was circumvented by submerging the T-piece mixer in an ultrasound bath. Other ways to avoid blockages are to use diluted streams of reactants, large diameter tubing, or multiphasic systems.^{38,39}

Another issue is the cost to implement flow systems. Owing to the high price of commercially available flow reactors, researchers have been encouraged to build their own flow setups to meet the reactions needs,⁴⁰⁻⁴² which can reduce the overall cost of the process.⁴³

An insufficient number of chemists with flow chemistry knowledge is one of the reasons why this technique is still not widely implemented in industries.⁴⁴ Therefore, it is essential that continuous flow chemistry is acknowledged at every level of chemical education. Moreover, chemists have been performing synthesis in batch for many years. Changing their attitude towards new technologies such as flow chemistry is necessary to drive significant advances in industrial processes.⁶

The possibility to extend the processing window and easily access unusual reaction conditions such as extremely high temperatures, use of unstable intermediates, and photochemistry are promising areas for further development and industrial implementation. An interesting new development was highlighted by Jamison and Jensen who recently published an integrated robotic platform for the synthesis of drug substances in continuous flow.⁴⁵ In combination with Artificial Intelligence planning and automation, their research shows the potential of a future with fully autonomous synthesis of chemicals, in which chemists spend less time on laborious tasks and more time creating new ideas.

1.2. Continuous flow photochemistry and applications in telescoped syntheses

1.2.1. *The origins, advantages, and hurdles of photochemistry*

Photochemistry is a branch of chemistry that studies chemical transformations induced by light. Some photochemical reactions occur naturally in the presence of sunlight: from the synthesis of vitamin D in our skins to one of the most important processes for our survival – the production of oxygen by photosynthesis.

The first ever described synthetic photochemical reaction was published in 1834 by Trommsdorff.⁴⁶ He observed that when the sesquiterpene lactone santonin was exposed to

sunlight, it turned yellow and its crystals were fragmented. However, it was only in 1912 in “*The photochemistry of the future*” by Ciamician that photochemistry finally emerged as a promising area of research.⁴⁷ He highlighted the importance of photochemistry as a potential clean alternative to conventional synthesis and foresaw a future in which light would be widely implemented in industry.

“On the arid lands there will spring up industrial colonies without smoke and without smokestacks; forests of glass tubes will extend over the plains and glass buildings will rise everywhere; inside of these will take place the photochemical processes that hitherto have been the guarded secret of the plants, but that will have been mastered by human industry which will know how to make them bear even more abundant fruit than nature, for nature is not in a hurry and mankind is.”

Giacomo Ciamician (1912)

The advantages of photochemical transformations are numerous. Light not only provides the energy necessary for the reactions, but also generates excited-state molecules which can undergo chemical transformations that are difficult to achieve in their ground states.⁴⁸ In addition, photons are regarded as traceless reagents and photochemistry is therefore considered an attractive strategy for the development of sustainable methodologies.⁴⁹

However, photochemistry remains an underdeveloped research area and its industrial applications are limited to a few well-established processes. This includes the synthesis of Nylon 6 precursor caprolactam (Toray),⁵⁰ rose oxide (Symrise),⁵¹ and antimalarial drug Artemisinin (Sanofi).⁵²

One of the reasons for the low industrial and academic uptake of photochemistry is that traditional batch processes are often limited in scale due to poor light penetration.⁵³ According to the Beer-Lambert law, in which I_0 is the incident intensity and ϵ is the molar absorption coefficient, the intensity of light transmitted, I , decreases exponentially with the path length, l , and concentration, c , as shown in Equation 5. Another common issue is the short lifetime of excited-state molecules for reactions that require more time in order to achieve completion.⁴⁸

$$I = I_0 10^{-\epsilon cl} \quad (5)$$

The advantages of continuous flow approaches to photochemical transformations have driven an increasing interest in the area and numerous reviews have been published in recent years.⁵⁴⁻⁵⁷ This is in part due to the small tubing used in flow reactors, which increases light penetration. In addition, light exposure is easily controlled by adjusting the flow rate, avoiding the formation of side-products by over irradiation, another common issue in batch photochemistry.⁵⁵

Flow chemistry has also facilitated the safe and efficient utilisation of singlet oxygen in photooxidations. This particular reaction and its main features such as singlet oxygen and CO₂ as an alternative solvent will be discussed in the next sections.

1.2.2. Singlet oxygen (¹O₂)

"I don't understand it Dr. von Tappeiner. The paramecia were all wiggling just fine a minute ago, but now these over by the window seem to be dead."

Oscar Raab (1898)

In the 1890s Oscar Raab, a medical researcher working on the toxicity of a natural dye acridine derivative on a single-celled organism, observed that the experiments carried out with oxygen in the presence of light showed much higher lethality than those in the dark.⁵⁸ However, the electronic structure of the Reactive Oxygen Species (ROS) involved in the photooxygenation of the microorganism was yet unknown.

In the 1920s, Mullikan described the electronic structure of molecular oxygen, arguing that it would originate a triplet ground state (³Σ_g) as well as two excited singlet states (¹Δ_g and ¹Σ_g).^{59, 60} Three years later, Kautsky attempted to characterise the ROS involved in the photooxidation of leucomalachite green, which was assumed to have a ¹Σ_g electronic configuration.⁶¹ However, Gaffron showed that the energy transfer between a hematoporphyrin dye (146 kJ/mol) and the suggested ¹Σ_g oxygen species (157 kJ/mol) would be incompatible.⁶² Kautsky then reformulated his hypothesis and assigned the reactive singlet oxygen state as ¹Δ_g.⁶³

Although the first studies on the electronic structure of singlet oxygen were reported in the 1930s, it was only thirty years later when the scientific community widely recognised the existence of singlet oxygen, owing to the discovery of its chemiluminescence in NaOCl-H₂O₂ solutions.⁶⁴ Further investigations on singlet oxygen structure and reactivity were published in a seminal work by Foote,⁶⁵ some of which will be further explored in the next sections.

Structure and reactivity of $^1\text{O}_2$

Singlet oxygen is the first electronically excited state of molecular oxygen. The ground state molecular orbitals of oxygen help to explain the low reactivity of O_2 ($^3\Sigma_g$) towards most diamagnetic organic molecules by a spin restriction. This is because the π^* orbitals in the triplet ground state of the paramagnetic molecular oxygen possess aligned spins and hence would have to accept a pair of electrons with the same orientation to fill the orbitals.⁶⁶ For this reason, the reactivity of ground state oxygen is mainly limited to single-electron transfers from, for example, transition metals and organic radicals.⁶⁷ To enhance the oxidising power of molecular oxygen by removing the spin restriction, energy transfer enables the formation of two excited states ($^1\Delta_g$ and $^1\Sigma_g$) in which the electrons have opposite spins and therefore, can oxidise a wide range of molecules. The lifetime of singlet oxygen (τ) for the second excited state $^1\Sigma_g$ is very short in gas-phase ($\tau = 12$ s) and reactions involving this species have never been reported.^{68, 69} $^1\Sigma_g$ rapidly decays through a spin-allowed transition to its analogous $^1\Delta_g$ often called “singlet oxygen”, whose lifetime is much longer in gas-phase ($\tau = 45$ min) due to a forbidden transition to the triplet ground state⁷⁰ (Figure 5).

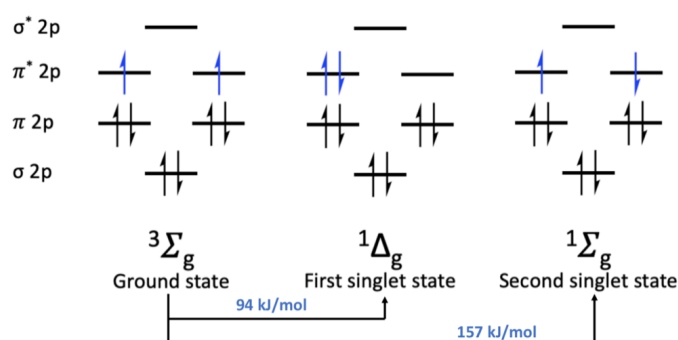


Figure 5. Molecular orbitals for ground state ($^3\Sigma_g$) and excited states ($^1\Delta_g$ and $^1\Sigma_g$) of oxygen. The energy levels of the singlet states are relative to the triplet ground state.

Although the lifetime of singlet oxygen is high in gas-phase ($\tau = 45$ min), it drastically decreases to microseconds in solution.⁷¹ This is due to a collisional energy transfer to the vibrational modes of the solvent. The lifetime of singlet oxygen is also affected by other parameters such as isotope effects, photosensitiser concentration, and light source power, which will be discussed below.⁷²

The isotope effect down-shifts the solvent vibrational frequencies, resulting in poor overlap with the vibronic transitions of $^1\text{O}_2$ and, consequently, less $^1\text{O}_2$ quenching (Figure 6 - left).⁷³ For example, solvents containing C-H bonds have vibrational frequencies (3050 cm^{-1}) that are closer to $^1\text{O}_2$ vibronic transition $0 \rightarrow 3$ (3286 cm^{-1}) when compared to their

deuterated form C-D (2240 cm⁻¹). This off-resonance factor of deuterated solvents results in a longer lifetime of singlet oxygen, when compared to the correspondent non-deuterated solvents (Figure 6 - right).

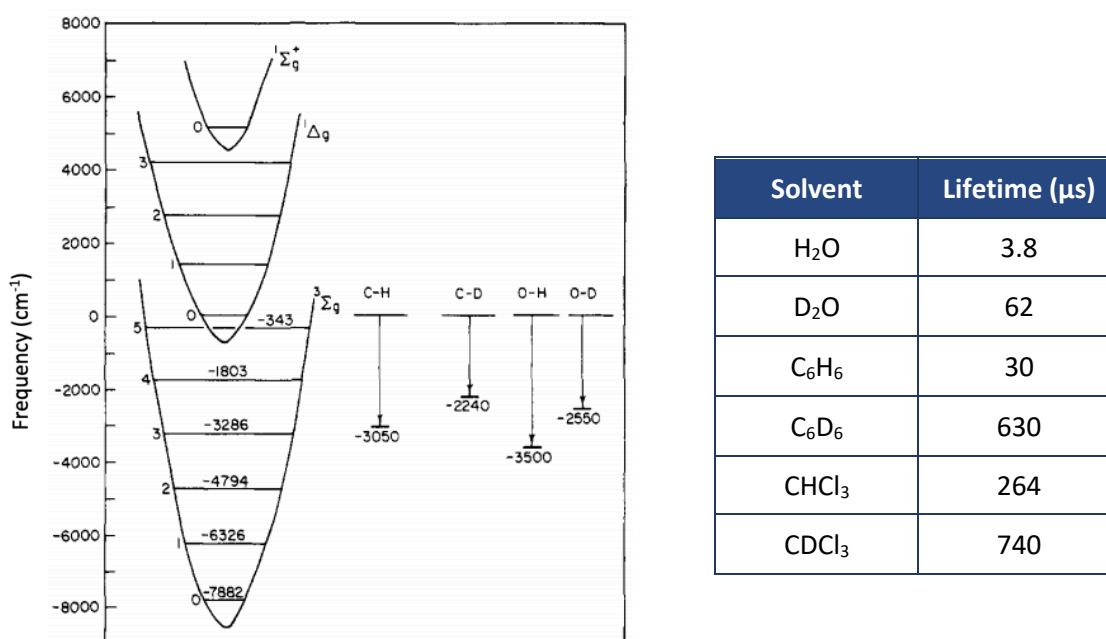
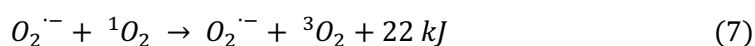
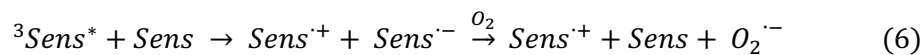
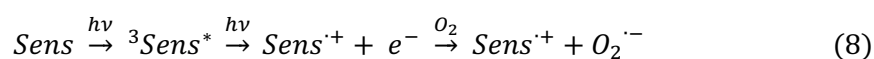


Figure 6. Left: oxygen vibronic transitions compared to the frequencies of solvent vibrational modes. C-H and C-D bonds are derived from aromatic solvents and O-H and O-D bonds from water or alcohols;⁷³ Right: singlet oxygen lifetime comparison between non-deuterated and deuterated solvents.⁷¹

Increased concentrations of photosensitiser (Sens) can also cause the deactivation of ¹O₂, through the formation of a radical ion pair between the excited triplet-state (³Sens*) and ground state (Sens) of the photosensitiser (Equation 6). The following electron-transfer from the radical anion (Sens^{•-}) to molecular oxygen forms a superoxide radical anion (O₂^{•-}). This highly reactive species subsequently quenches ¹O₂ to ground state molecular oxygen (³O₂) (Equation 7).⁷²



High-power light sources facilitate electron ejection from photosensitisers with low ionisation potential, such as commonly used porphyrins (Equation 8).⁷⁴ The formation of superoxide further deactivates singlet oxygen, as previously shown in Equation 7.



Thermal and photochemical pathways to generate 1O_2

The thermal reaction of hydrogen peroxide with sodium hypochlorite,⁷⁵ arene endoperoxides,⁷⁶ or potassium peroxymonosulfate (Oxone),⁷⁷ forms singlet oxygen through a chemical reaction. However, the use of strong oxidants is not desirable as they can react directly with the substrate, have a poor functional group tolerance, and have low atom economy.⁷⁸ On the other hand, singlet oxygen can be generated photochemically by using molecular oxygen, a light source, and a photosensitiser. Visible light photosensitisers are coloured conjugated compounds capable of initiating a chemical reaction by absorbing light and transferring energy it to a reactant, in this case, molecular oxygen. In solution, oxygen is colourless and absorbs only small amounts of light and thus, a photosensitiser is needed for the excitation of oxygen to its singlet state. The most common photosensitisers used for photooxidation are methylene blue,⁷⁹ rose bengal,⁸⁰ and 5,10,15,20-tetraphenylporphyrin (TPP)⁸¹ (Figure 7). For the energy transfer occur, the photosensitiser triplet state needs to be higher in energy than the oxygen singlet state (94 kJ/mol).

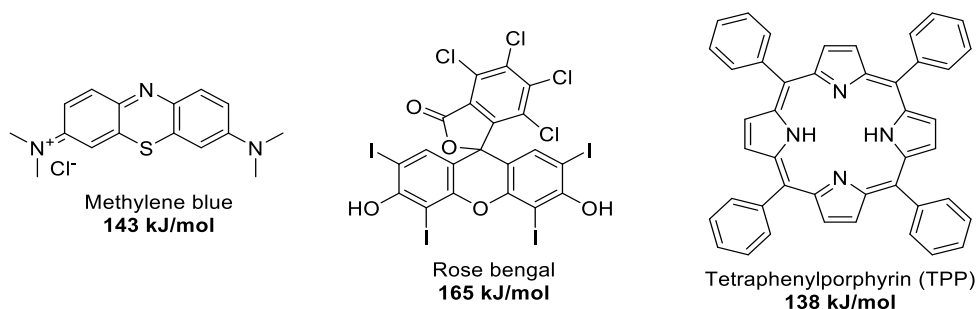


Figure 7. Common photosensitisers for photooxidations and their respective triplet state energies.^{82, 83}

In some instances sunlight can be an economical light source, employed for example in the synthesis of rose oxide,⁸⁴ oxidation of naphthalene,⁸⁵ and other photochemical reactions.⁸⁶ However, these processes rely on solar irradiance, the intensity of which varies with the location, weather, and time of day, directly affecting the reproducibility of experiments.⁴⁹ Due to the difficulty of controlling solar radiation, xenon arc, metal-halide, and mercury artificial lamps are commonly used in this type of reaction.⁸⁷ In recent years, LEDs have received significant attention due to their advantages over traditional lamps, such as low cost, narrow light emission spectra, high efficiency, and long radiative lifetime. A number of photooxidations using LED sources have been reported in the literature.⁸⁸

Photooxidations can occur in two different pathways: Type I and Type II as shown in Figure 8.⁸⁹ Initially, the photosensitiser is excited to a higher energetic state by absorption of

a photon. At this stage, this species can react with either the substrate or solvent (Type I), or with molecular oxygen (Type II).

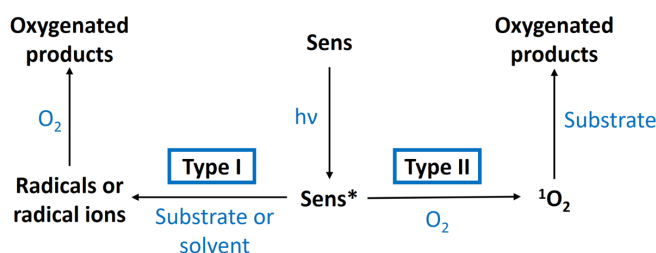


Figure 8. Types I and II pathways of photosensitisation.

In Type I photooxidations, radicals or radical ions are formed through either electron or hydrogen transfer between the photosensitiser and the substrate or solvent, yielding oxygenated products after reacting with ground state oxygen. This process is favoured by high concentrations of substrate as the excited photosensitiser reacts firstly with the substrate. Photosensitiser loss is one of the problems that can occur since the photosensitiser radical anion generated in this process can be oxidised by molecular oxygen and therefore, cannot be regenerated.⁹⁰ Over long irradiation times, traces of oxygen radicals may cause photobleaching: a photochemical alteration of the photosensitiser that makes it permanently unreactive.⁹¹

In Type II (Figure 9), the photosensitiser in the ground state (S_0) absorbs a photon, exciting an electron to the first excited state (S_1). After a radiationless intersystem crossing (ISC) to the excited triplet state (T_1), an external conversion (EC) transfers energy to the ground state of molecular oxygen forming singlet oxygen and regenerating the ground state photosensitiser. The decay of the excited state can also occur through side processes, such as internal conversion (IC), fluorescence, and phosphorescence. The major advantage of Type II photooxidation is that the photosensitiser is regenerated and thus can be reused. This process is favoured by low concentration of photosensitiser and oxygen, low reactivity of T_1 , and high intersystem crossing yield of the photosensitiser.⁹²

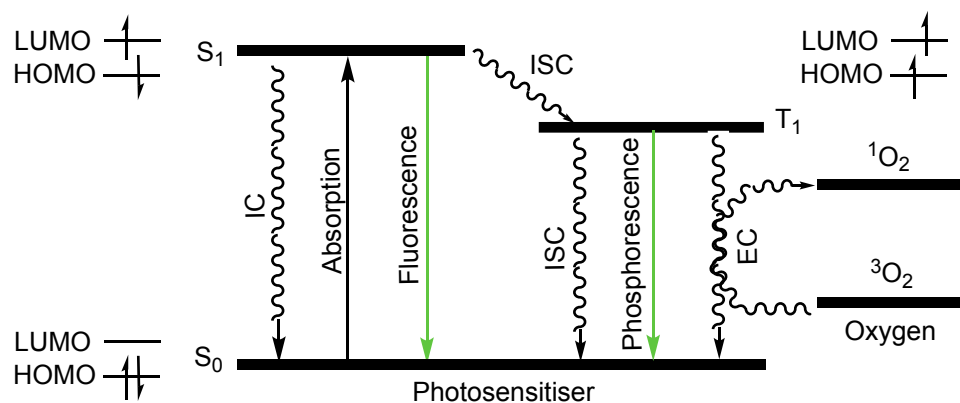


Figure 9. Jablonski diagram for the Type II photosensitised generation of singlet oxygen.

To perform photooxidations in a sustainable manner, the photochemical pathway to generate singlet oxygen was chosen for this Thesis. This is because molecular oxygen is considered a “green reagent”, as it is harmless to the environment, and replaces toxic and corrosive oxidants. Molecular oxygen is also inexpensive, readily available, and reactions involving O_2 have high atom efficiency, as the two atoms of oxygen are incorporated in the final molecule.⁹³ On the other hand, there are some challenges with photochemical oxidations. In particular, the low solubility of oxygen in most organic solvents and water, low mass transfer, and risk of explosion when using oxygen in flammable solvents.⁹⁴ These challenges have been addressed by performing photooxidations using singlet oxygen in an alternative medium such as CO_2 .

1.2.3. Supercritical CO_2 ($scCO_2$) as an alternative solvent

Most solvents used in the chemical and pharmaceutical industries are volatile organic compounds (VOCs).⁹⁵ Chlorofluorocarbons, for example, are VOCs which are known to have a negative impact on the environment through depletion of the ozone layer.⁹⁶ The discovery of these harms led to an increase in industrial and scientific interest in using alternative solvents such as ionic liquids and supercritical fluids (SCFs).⁹⁷ For the purpose of this Thesis, SCFs were chosen as the reaction medium given their low impact on the environment, research group’s expertise, and desirable properties, which will be further discussed.

A supercritical fluid state is reached when the pressure (P_c), temperature (T_c) and density (ρ_c) of a fluid is raised beyond its critical point, in which the liquid-gas phase boundary no longer exists.⁹⁸ Supercritical systems are found in nature in geothermal systems of volcanoes,⁹⁹ and the interior and atmosphere of gas giants such as Jupiter and Saturn.¹⁰⁰

Supercritical fluids have properties similar to both liquids and gases, such as low viscosity, and high diffusivity and density. These properties can be easily tuned by adjusting the pressure and temperature in small increments. SCFs are fully miscible with gases, which increases the mass transfer and reaction kinetics compared to biphasic gas-liquid systems. The density of a supercritical fluid is directly related to the solvent strength, and it often increases with pressure and decreases with temperature.¹⁰¹

The most commonly used supercritical fluids found in the literature are water and carbon dioxide.^{102, 103} This is due to their low toxicity, high abundance, and versatility to partake in a variety of chemical reactions. However, processes that employ supercritical water encounter some challenges,¹⁰⁴ such as inconvenient high temperature and pressure needed to maintain the critical conditions ($T_c = 374\text{ °C}$ and $P_c = 221\text{ bar}$), requiring high investments in terms of equipment, and the formation of corrosive chemicals and salt precipitation. For these and other reasons that will be further explored in the next section, CO_2 was chosen as the reaction medium for this Thesis.

Applications of scCO_2

Carbon dioxide is an abundant, nontoxic and inexpensive gas. It is often obtained as a by-product from other processes in industry such as production of ammonia¹⁰⁵ and reused in supercritical conditions (73.8 bar and 31.1 °C).¹⁰⁶ The phase diagram for CO_2 is shown in Figure 10.

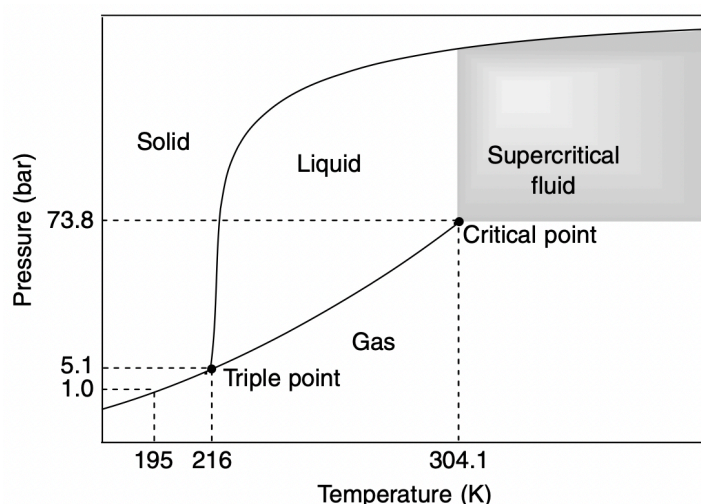


Figure 10. Phase diagram of carbon dioxide showing its critical point (73.8 bar and $304.1\text{ K} = 31.1\text{ °C}$).¹⁰⁷

In the 1970s, Zosel patented one of the first and most important applications of scCO₂, substituting dichloromethane as an extraction medium for the decaffeination of coffee on an industrial scale.¹⁰⁸ Since then, supercritical CO₂ has been employed in a variety of processes such as extraction of natural products,¹⁰¹ eluent for chromatography,¹⁰⁹ synthesis of polymers,¹¹⁰ and textile processing.¹¹¹ More recently, it has been used as a coolant for nuclear engineering,¹¹² and as a solvent or additive for the synthesis of drug nanoparticles.¹¹³

Singlet oxygen in supercritical CO₂

Supercritical CO₂ is a highly desirable solvent for oxidations using singlet oxygen. It is fully oxidised and thus non-flammable; easily removed by reducing the system pressure; and is fully miscible with oxygen, facilitating mass transfer and increasing reaction kinetics.¹¹⁴

The lifetime of ¹O₂ in supercritical CO₂ (5.1 ms at 150 bar and 41 °C) was first reported by Worrall.¹¹⁵ In this study, the overall rate of decay of singlet oxygen (k_{Δ}) was analysed in terms of pressure and temperature (Figure 11 - left). It was shown that k_{Δ} increases with oxygen concentration and scCO₂ fluid density. Moreover, the rate constant of decay of singlet oxygen by ground state oxygen was determined as $1.9 \times 10^4 \text{ dm}^3 \cdot \text{mol}^{-1} \cdot \text{s}^{-1}$ at 150 bar and 41 °C, a value comparable to other organic solvents. Regarding the scCO₂ fluid density, low density, which is favoured in high temperature and low pressure (Figure 11 - right), results in lower k_{Δ} and longer ¹O₂ lifetime.

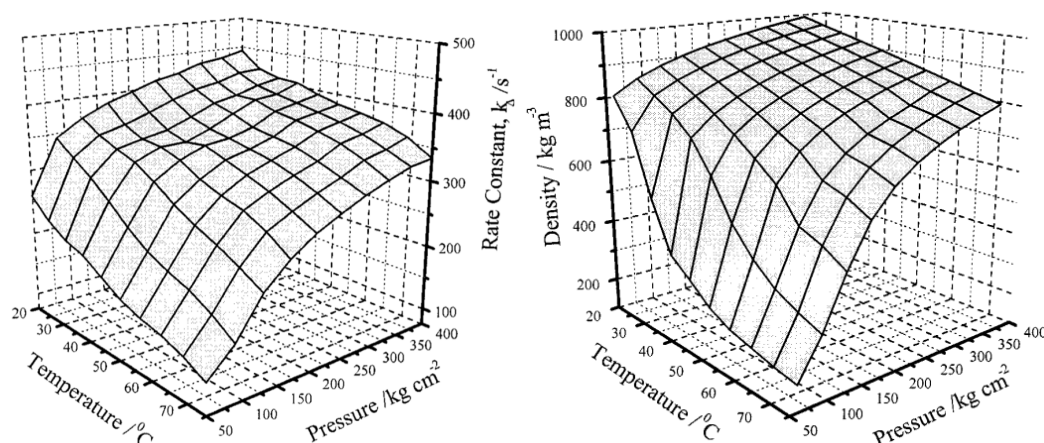


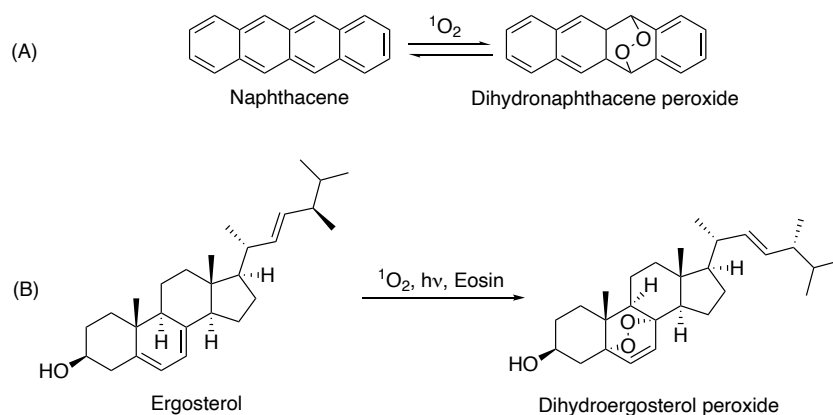
Figure 11. Left: rate constant of the decay of singlet oxygen (k_{Δ}) dependence on temperature and pressure in scCO₂; Right: density of scCO₂ as a function of temperature and pressure.¹¹⁵

Despite the high solubility of O₂ in scCO₂, the solubility of organic molecules in this solvent can be difficult as carbon dioxide is a linear molecule with a small dipole, only capable

of solvating small and weakly polar solutes.¹¹⁶ Fortunately this physicochemical issue can be addressed by the addition of a polar co-solvent¹¹⁷ or surfactants.¹¹⁶

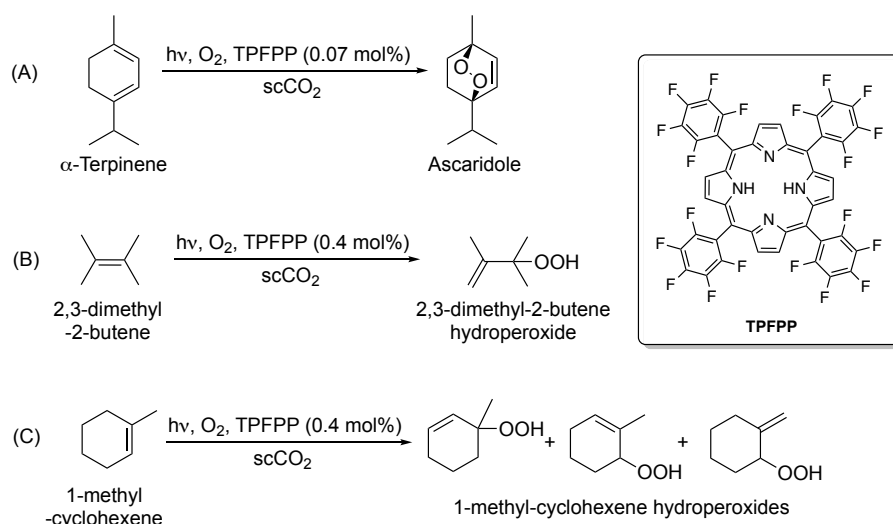
1.2.4. Continuous flow photooxidations using $^1\text{O}_2$ in scCO_2

One of the earliest studies of photooxidations involving singlet oxygen occurred in 1867, when Fritzsche performed a 1,4-cycloaddition of $^1\text{O}_2$ to naphthacene (Scheme 2 - A).¹¹⁸ The first compound isolated from this type of reaction was dihydroergosterol peroxide, a transannular peroxide formed from the eosin-sensitised oxidation of ergosterol^{119, 120} (Scheme 2 - B). Since then, numerous compounds have been synthesised using singlet oxygen, with recent reviews of the literature demonstrating its use in the synthesis of natural products and drugs.^{78, 121}



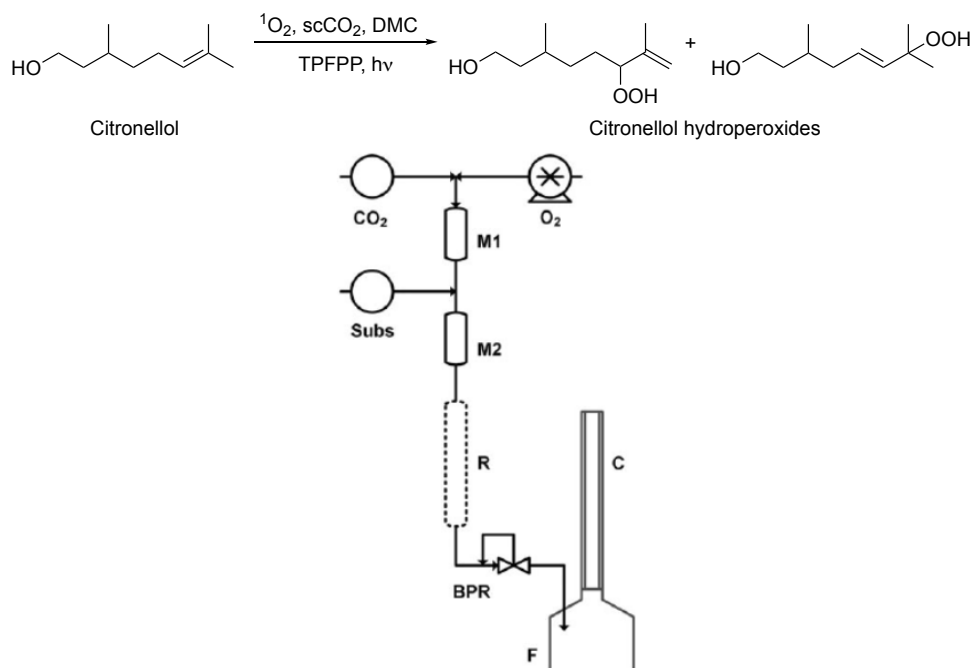
Scheme 2. Photooxidation of naphthacene (A)¹¹⁸ and ergosterol (B).¹¹⁹

The non-flammability and full miscibility of supercritical CO_2 with singlet oxygen was extensively explored by our research group. The photooxidation of α -terpinene using 5,10,15,20-tetrakis(pentafluorophenyl) porphyrin (TPFPP) as a photosensitiser in scCO_2 gave ascaridole in quantitative yields (Scheme 3 - A).¹²² This methodology was further employed to other substrates such as 2,3-dimethyl-2-butene (Scheme 3 - B) and 1-methylcyclohexene¹²³ (Scheme 3 - C).



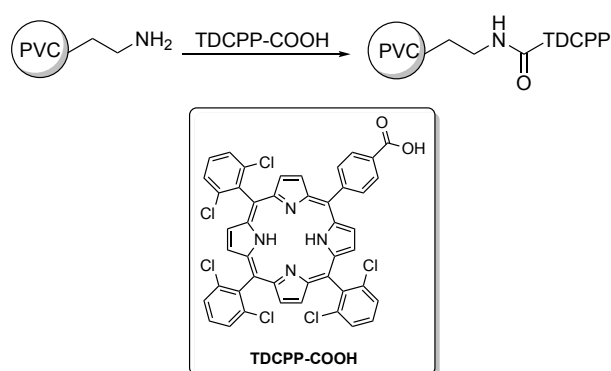
Scheme 3. Scope of batch photooxidations with singlet oxygen in scCO_2 by our research group using α -terpinene (A), 2,3-dimethyl-2-butene (B), and 1-methyl-cyclohexene (C).^{122, 123} The chemical structure of the photosensitiser TPFPP used is highlighted in the scheme.

This methodology was then transferred to a high-pressure continuous flow system, using a sapphire tube reactor (Scheme 4). Photooxidation of α -terpinene resulted in 3000 times scale-up relative to the previous batch results.¹¹⁴ In the same work, the photooxidation of citronellol under similar conditions led to a 9 times improvement of the space-time yield in relation to the experiments carried out in a batch Schlenk reactor.



Scheme 4. Continuous flow system for photooxidation using $^1\text{O}_2$ in scCO_2 . CO_2 is delivered by HPLC pump; O_2 is added via Rheodyne dosage unit; M1 and M2 are the mixers; Subs is the substrate solution containing the photosensitiser; R is the sapphire tube reactor; BPR is the back-pressure regulator; and F is the glassware flask to collect the crude mixture, attached to the condenser C.¹¹⁴

Immobilised photosensitisers were also examined, as these can be easily separated from the reaction mixture, avoiding further purifications. The previous continuous flow setup used was then adapted with a packed sapphire tube.¹²⁴ Eight photosensitisers and four different polymer supports were screened for both photooxidations of citronellol and α -terpinene. The photosensitiser 4-[10,15,20-tris(2,6-dichlorophenyl)-21*H*,23*H*-porphin-5-yl]-benzoic acid (TDCPP-COOH) immobilised in amino polyvinyl chloride (PVC-NH₂) beads (Scheme 5) resulted in the highest space-time yield ($> 100 \text{ mmol}\cdot\text{L}^{-1}\cdot\text{min}^{-1}$) for the model reactions, showing excellent recyclability and stability.



Scheme 5. Synthesis of photosensitiser PVC-TDCPP.¹²⁴

The continuous flow photooxidation of α -terpinene and citronellol was further investigated using a fluorous biphasic catalysis in supercritical CO₂ (Figure 12).¹²⁵ The long-chain modified TPFPP (F8-TPFPP) solution in 3-ethoxyperfluoro(2-methylhexane) (HFE) could be recycled ten times maintaining high activity. This resulted in a 20 times reduction of photocatalyst loading compared to the previous TPFPP/dimethyl carbonate (DMC) system.

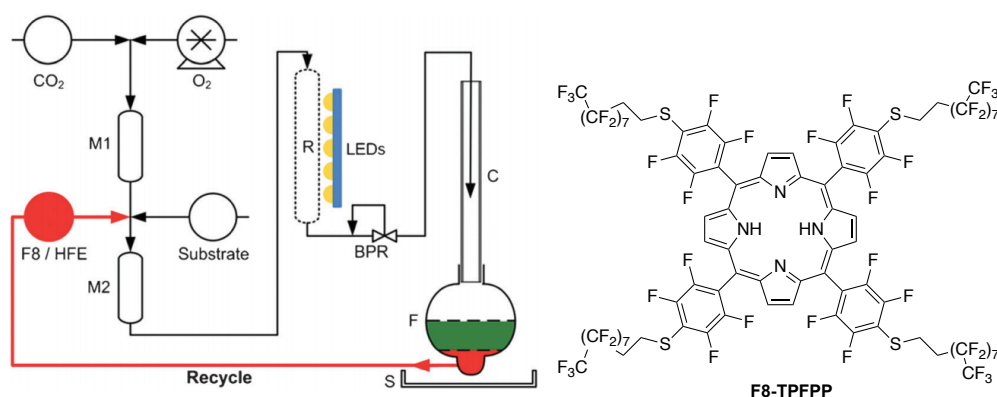
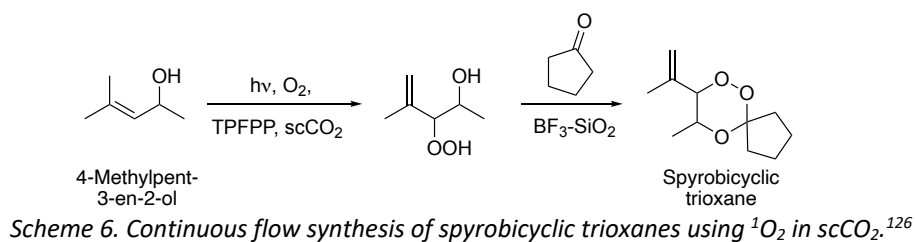


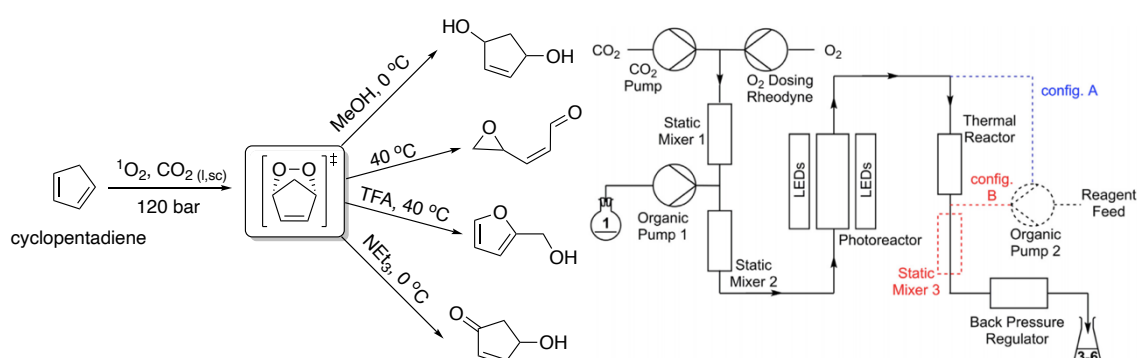
Figure 12. Continuous flow system with fluorous phase recycling for photooxidation using $^1\text{O}_2$ in scCO_2 and structure of photosensitiser F8-TPFPP. CO₂ is delivered by HPLC pump; O₂ is added via Rheodyne dosage unit; M1 and M2 are the mixers; F8-TPFPP/HFE and substrate solution are delivered by HPLC pumps; R is the sapphire tube reactor; BPR is the back-pressure regulator; and F is the glassware flask to collect the crude mixture, attached to the condenser C and immersed in an ultrasonic bath S.¹²⁵

Given the excellent results obtained for the photooxidation α -terpinene and citronellol, our group applied this methodology on the synthesis of antimalarial spirobicyclic trioxanes in continuous flow (Scheme 6).¹²⁶ The photooxidation of 4-methylpent-3-en-2-ol was followed by an acid-catalysed cyclisation using silica/BF₃. The reaction conversion in flow was similar to the equivalent batch method in dichloromethane. However, catalyst leaching was observed, and the conversion decreased after 20 min of reaction.

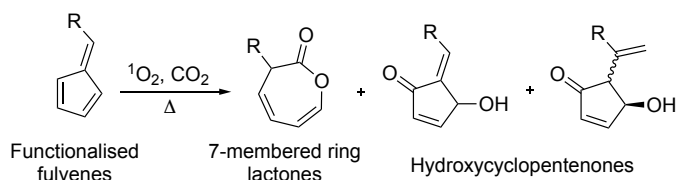


A green alternative production of antimalarial Artemisinin using liquid CO₂ was later published in 2015.¹²⁷ The continuous flow methodology improved process safety when compared to previous methodologies,¹²⁸ as the hydroperoxides are generated *in situ* in a non-flammable solvent. It also enabled the recycling of starting materials and catalyst, which had a positive impact in the overall cost of the process. More details on this reaction will be given in Chapter 4.

In 2018, a continuous photooxidation of cyclopentadiene with singlet oxygen in CO₂ was reported, forming unstable endoperoxide species.¹²⁹ These compounds were further reacted in telescoped synthesis to synthesise four different products with high productivity. The final products were obtained by only altering the temperature or adding quenching reagents downstream (Scheme 7).



The above work on cyclopentadienes was extended to functionalised fulvenes.¹³⁰ This procedure demonstrated a valuable use of these endoperoxides formed *in situ* to form difficult to access 7-membered ring lactones and hydroxycyclopentenones derivatives by tuning the flow rate of CO₂ and co-solvent used (Scheme 8).



Scheme 8. Continuous flow photooxidation of functionalised fulvenes using ¹O₂ in scCO₂.¹³⁰

1.3. Thesis Aims

Flow chemistry is a rapidly growing area of research with increasing interest from both the scientific community and industry, as an enabling tool for the synthesis of chemicals and pharmaceutical compounds. In particular, continuous flow photooxidations using singlet oxygen in supercritical CO₂ have enabled a more efficient, sustainable, and safer utilisation of ¹O₂. This powerful strategy has been applied in the multi-step synthesis of furfuryl alcohol and antimalarial drug Artemisinin. Thus, the design and applications of new photooxidation reactions in flow are highly desirable to promote further implementation of photochemistry in industry, which is still very limited.

The general aim of this thesis is to explore the continuous flow photooxidation of *p*-substituted phenols and its applications in telescoped syntheses of compounds with potential medicinal interest. The photooxidation step is performed using singlet oxygen in supercritical CO₂. Telescoped syntheses are conducted by modifying the continuous flow system according to the reaction needs. The specific aims of this work are:

1. To explore the applications of our custom-built high-pressure continuous flow photooxidation system.
2. To conduct further studies on the photooxidation of *p*-substituted phenols and telescoped synthesis of 1,2,4-trioxanes previously developed in our group.
3. To investigate the applications of photooxidation of *p*-substituted phenols in telescoped syntheses of other molecular scaffolds with potential pharmaceutical interest.

2. Methods and Materials

2.1. High-pressure continuous flow system for photooxidation and telescoped synthesis

The approach described in this Thesis is based on high-pressure flow chemistry. An early study of reactions using high-pressure flow reactors was reported by Peter Köll in the late 70's, initially investigating the intermolecular ene reaction with nonactivated enophiles in high pressure and temperature.¹³¹⁻¹³³ In 1986, a major review by McHugh and Subramaniam¹³⁴ showed applications and advantages of using supercritical fluids in thermal and photochemical reactions, heterogeneous catalysis, and hydrolysis. A growing interest in supercritical fluids then emerged in the 1990s, with numerous studies showing applications in the extraction of analytes, synthesis of particles for drug delivery, polymerisations, and others.^{96, 135-140}

Since 1995, our group has been active in research regarding the design, manufacture, and use of high-pressure continuous flow systems in scCO_2 .¹⁴¹⁻¹⁵⁰ Of particularly relevance to the work carried out in this Thesis are flow reactors that have been designed and modified to enable the photochemical generation of singlet oxygen in scCO_2 using a sapphire tube and LED arrays.^{114, 122, 124-127, 129, 130, 151, 152} The most recent continuous flow system used at the start of this Thesis is shown in Figure 13, and further modifications will be described throughout this Thesis. This versatile high-pressure flow system was built with individual components, and it can be adapted to enable different photooxidation and telescoped synthesis experiments.

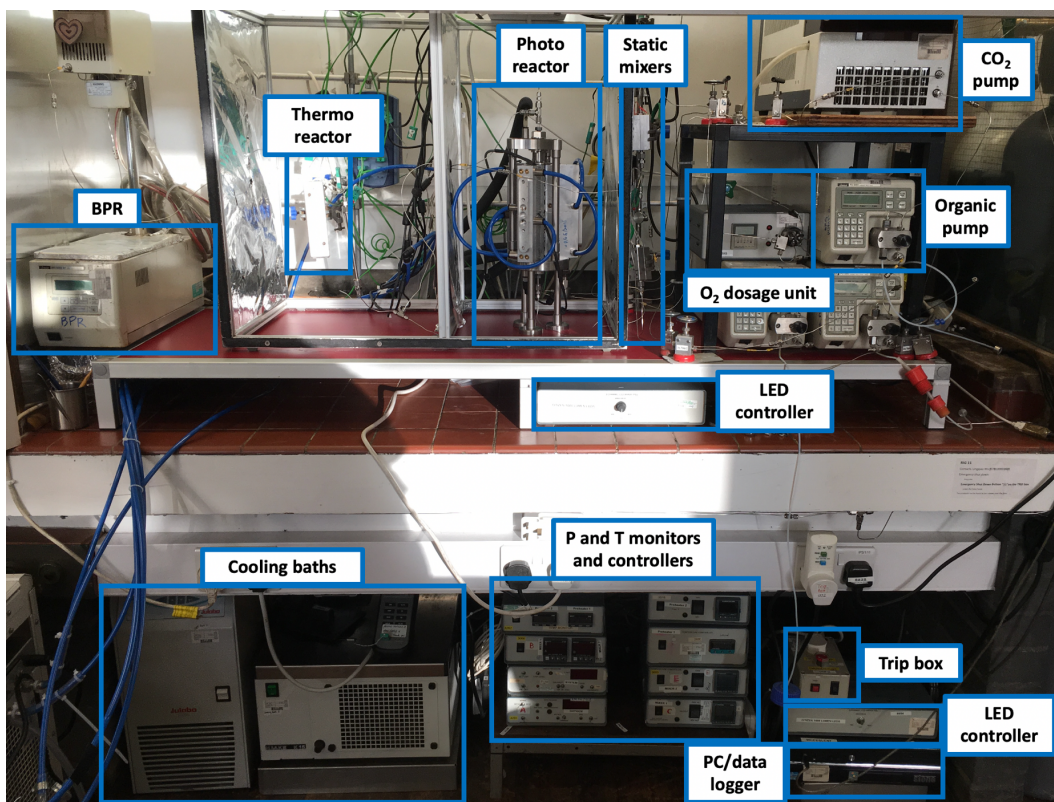


Figure 13. Photograph of the high-pressure flow system for photooxidations using singlet oxygen and supercritical CO₂ and its main components: a Jasco PU-2080-CO₂ pump (**CO₂ pump**); modified Rheodyne 7000L O₂ dosage unit (**O₂ dosage unit**); Jasco PU-980 HPLC pumps (**organic pumps**); (**static mixers**); high-pressure sapphire photo reactor with LED blocks (**photo reactor**); Jasco BP-1580-81 back pressure regulator (**BPR**); Julabo F250 and Haake K15 cooling baths (**cooling baths**); custom-built pressure and temperature monitors, and Eurotherm temperature controllers (**P and T monitors and controllers**); PicoLog data logger (**PC/data logger**); and custom-built trip box (**trip box**). More details are given in Figure 14.

2.1.1. Description of the flow apparatus

A general schematic of the experimental setup is shown in Figure 14. The numbers and letters in grey (X) correspond to each component's code assigned in the high-pressure apparatus and general schematic.

The gaseous streams from Jasco PU-2080-CO₂ HPLC pump (4583) and Rheodyne 7000L O₂ dosage unit (5224) are combined in the first mixer (M1). The gas mixture is then mixed with the Jasco PU-980 HPLC pump (5822) organic stream in the second mixer (M2), which subsequently flows through the high-pressure sapphire tube reactor irradiated by the LED lights (5954 and 5955). After the photo reactor, a second Jasco PU-980 HPLC pump (5821) is added to dilute the organic stream and avoid blockages, flowing through a thermo reactor (only for telescoped processes). Finally, the product is collected after the Jasco BP-1580-81 back pressure regulator (3835) outlet. Each component of the system will be discussed in detail in section 2.1.2.

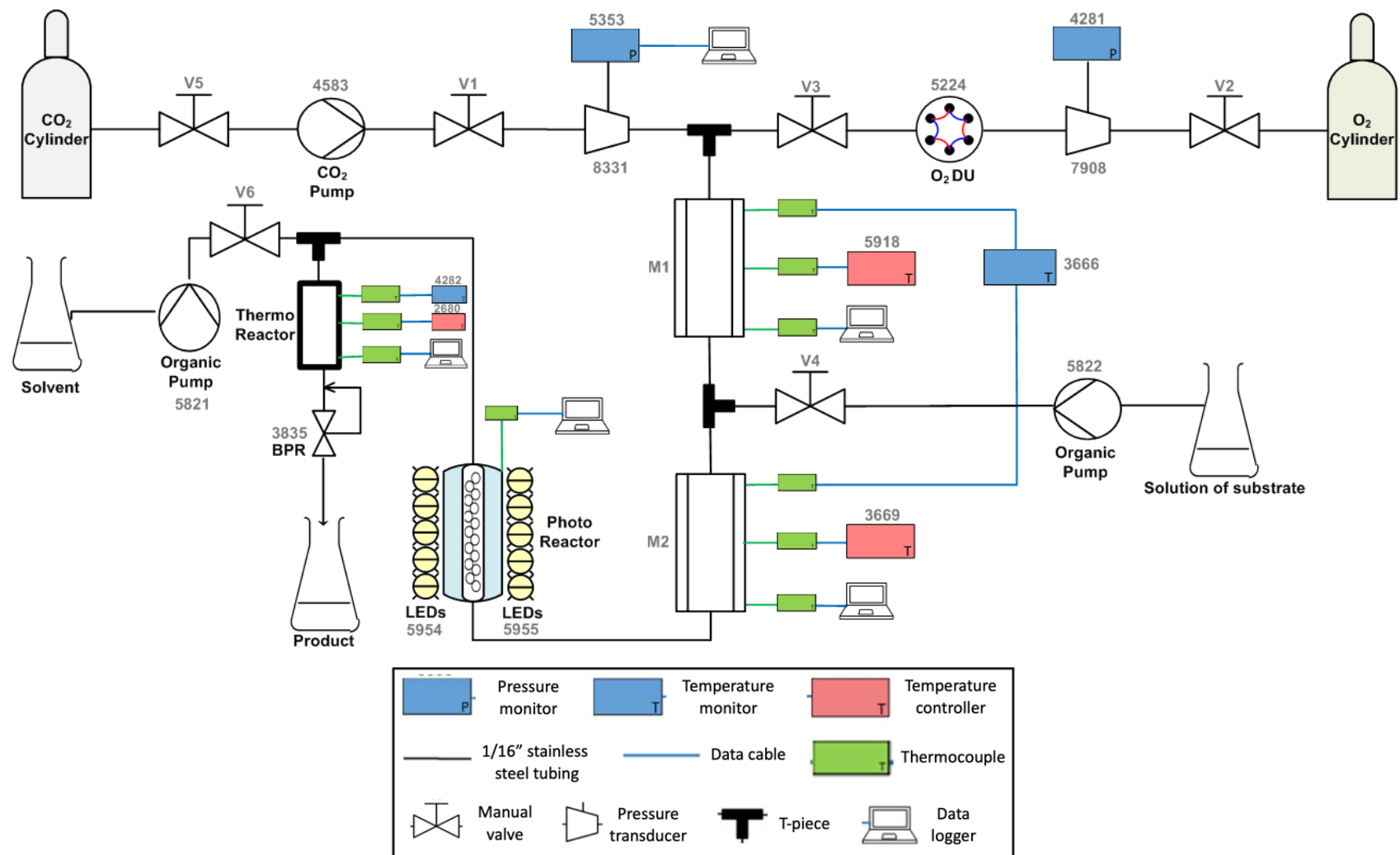


Figure 14. General schematic of the high-pressure flow system with its components. The identification number for each component is showed in grey. The system contains a Jasco PU-2080-CO₂ pump (**CO₂ pump** - 4583); Air Products liquid CO₂ UltraPure cylinder (**CO₂ cylinder**); modified Rheodyne 7000L O₂ dosage unit (**O₂ DU** - 5224); BOC O₂ compressed gas (**O₂ cylinder**); Jasco PU-980 HPLC pumps (**organic pumps** – 5821 and 5822); static mixers (**M1** and **M2**); pressure transducers (8331 and 7908); high-pressure sapphire photo reactor with LED blocks (**photo reactor** and **LEDs** – 5954 and 5955); Jasco BP-1580-81 back pressure regulator (**BPR** - 3835); data logger; thermocouples; pressure monitors (5353 and 4281); temperature monitors (3666 and 4282); temperature controllers (5918, 3669, and 2680); 1/16" stainless steel tubing; data and electric power cables; and manual valves (**VX**), in which X is a number. Cooling baths (1968 and 1969) and trip box (5352) were not represented in this scheme. The gaseous streams from **CO₂ pump** (4583) and **O₂ dosage unit** (**O₂ DU** - 5224) are mixed in static mixer 1 (**M1**). Next, the **solution of substrate** from **organic pump** (5822) is combined with the gas mixture in static mixer 2 (**M2**), flowing through a high-pressure sapphire **photo reactor** with **LED blocks** (5954 and 5955). Another **organic pump** (5821) is added after the photo reactor to dilute the stream with the reaction **solvent**, and the crude is collected after the back-pressure regulator **BPR** (3835). More details of the components are given in the next section.

2.1.2. Components

The high-pressure apparatus used is made of different components, which are shown below. A simplified scheme containing the specific components will be presented for each reaction in the thesis when applicable.

- **Pipes and valves:** 316 stainless steel tubes are used to connect the components in the flow system using Swagelok® fittings, with an outer diameter (o.d.) of 1/16". Leakages might occur due to unreliable metal-to-metal seals, improperly installed tube fittings, or poor tubing handling. Hence, all unions should be tested prior to each experiment using Snoop® liquid to identify any air flow from the fittings. The manual valves are used to stop and start the fluid flow from either the pumps or gas cylinders to the system. They are provided by either the High-Pressure Equipment Company (HiP 15-11AF1, two-way straight valve, 1/16" o.d.), or Scientific Systems, Inc (SSI, 2-way through valve, 1/16" o.d.).
- **CO₂ pump (4583):** the Jasco™ PU-2080-CO₂ HPLC pump delivers and controls the flow rate of liquid CO₂. The gas from a cylinder at room temperature and pressure (*ca.* 58 bar) is liquified by a cooling unit (at -5 °C via an electric cooling method) and pressurised by the pumps via slow suction, quick delivery (SSQD). An in-line filter (stainless steel, 1/8", Swagelok®, 60-micron pore size) was installed after the CO₂ cylinder outlet to avoid any small impurities going to the CO₂ pump. The CO₂ pump was tested regularly using a flow meter to ensure that the flow rate was accurate. Pressure tests were performed before each experiment, pumping CO₂ against a closed valve to ensure that it can build up pressure (over-pressure is set to 200 bar). To avoid any failure from the pump check valves due to a change in temperature and/or pressure, the CO₂ pump should remain on and isolated from the rest of the system by a manual valve.
- **O₂ dosage unit (5224):** a 2-position-6-port switching valve HPLC (modified Rheodyne® 7000L) was used to dose and transfer oxygen from the cylinder (180 bar) to the system (120 bar) through a difference in pressure, as shown in Figure 15.

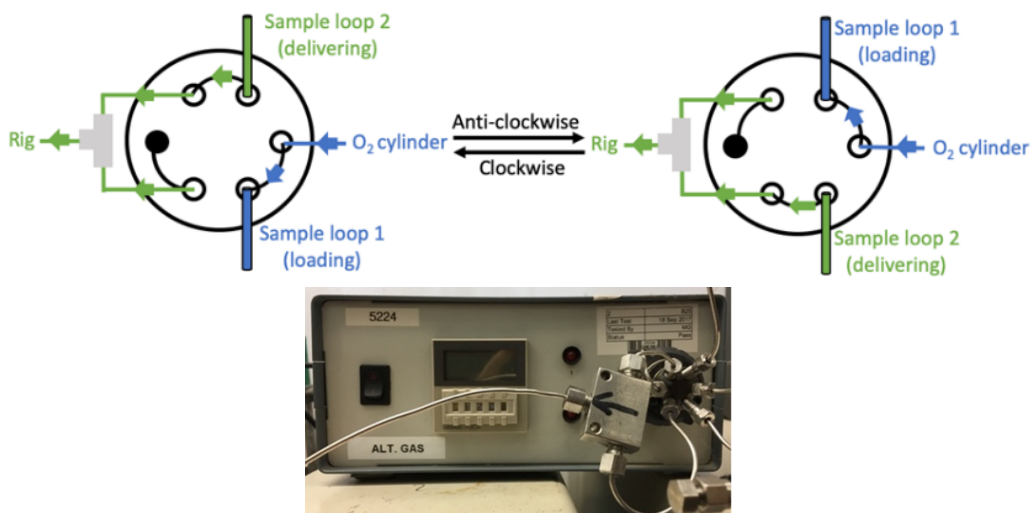


Figure 15. Scheme and photograph of the modified Rheodyne 7000L oxygen dosage unit. There are 3 slots on the rotor which joins the 6 ports, and the sample loops are 10 μL . In the first position (left), sample loop 1 is loaded with O_2 at cylinder pressure (180 bar) whilst previously filled sample loop 2 transfers O_2 through pressure gradient to the system (Rig). When the rotor changes to the second position (right), sample loop 1 delivers O_2 whilst sample loop 2 is filled with O_2 .

This valve has two sample loops (10 μL) containing O_2 at the cylinder pressure and a 3-slot rotor seal that joins the ports in pairs. In the first position (Figure 15: left), while the sample loop 1 is being filled with O_2 from the cylinder, the sample loop 2 is delivering the gas to the flow system due to a pressure gradient. When the rotor switches (Figure 15: right), the sample loop 1, that was previously filled with O_2 , delivers the gas to the system while sample loop 2 is now being filled.

The pressure from the O_2 cylinder should be at least 20 bar above the system pressure. This is because if the O_2 cylinder pressure is lower than the set system pressure, the reaction mixture may back-flow into the oxygen line, which could cause a potential explosion. Regarding the pressure trip setups, the high-pressure system trip is set to be at least 20 bar below the low-pressure trip for the oxygen to avoid any back-flow issues as mentioned above. A one-way check valve is also located between the cylinder and the dosage unit.

The concentration of oxygen must be below the limiting oxygen concentration (LOC) for the solvent in use to avoid any combustion¹⁵³ and, as a general practice, it was kept below 6 % in all cases. To change the concentration of O_2 in the system, the size of the sample loops and the switching time can be altered. If the switching time is too slow or the sample loop is too big, it will create oxygen slugs that causes irregular mixing and spikes in O_2 concentration.¹⁵¹ On the other hand, if the switching time is too fast, lower amounts of oxygen might be transferred per switch and the overall concentration of oxygen will be lower

than calculated. For a specific sample loop, the calculations should consider the pressure difference between the system and O₂ cylinder and the desired O₂: substrate molar ratio, whilst maintaining the overall concentration of oxygen below 6 %. For these reasons, the sample loop used was fixed at 10 µL and the switching time was kept between 4 and 16s.¹⁵⁴ An example of this calculation can be found in 2.1.4.

- **HPLC organic pumps (5821 and 5822):** High-Performance liquid chromatography (HPLC) pumps deliver and control the flow rate of liquids into the system. Provided by Jasco™ (PU-980 Intelligent HPLC pump Module), these pumps had their efficiency tested regularly by pumping for a fixed time into a volumetric flask. Pressure tests were performed before each experiment, as described for the CO₂ pump.
- **Mixers (M1 and M2):** the two mixing chambers are used to pre-heat (40 °C) and ensure efficient mixing between different streams. The mixers are made of a stainless-steel tubing (1/4" o.d., 0.049" wall thickness, 3.1" in length) packed with sand, surrounded by an aluminium heating block.
- **Photo reactor:** the current photo reactor was built by the University of Nottingham's Workshop (Figure 16). It consists of a 316 stainless steel body with connections to the high-pressure system, a sapphire tube (Saint-Gobain Crystals, 10 mm o.d., 1 mm wall thickness, 240 mm long) packed with 6 mm glass beads, and a Lexan™ tube (clear polycarbonate, 18 mm o.d., 2 mm wall thickness and 212 mm length). Both the sapphire and Lexan™ tubes are held by the lower and upper part of the reactor structure. The sapphire tube is sealed to the metal body by two EPDM (ethylene propylene diene monomer) O-rings at each end of the tube to allow any movement caused by thermal expansion of the sapphire, with 1/8" autoclave engineer fittings to connect it to the flow system. The Lexan™ tube surrounds the sapphire cylinder (ca. 2 mm space), creating an additional protection layer while enabling coolant to flow between the two tubes. The small gap between the tubes allows the LED units to be positioned as close as possible to the reactor, enhancing irradiation. Lastly, the versatile design enables the incorporation of different lengths of sapphire and Lexan™ tubes, allowing the reactor volume to be altered.

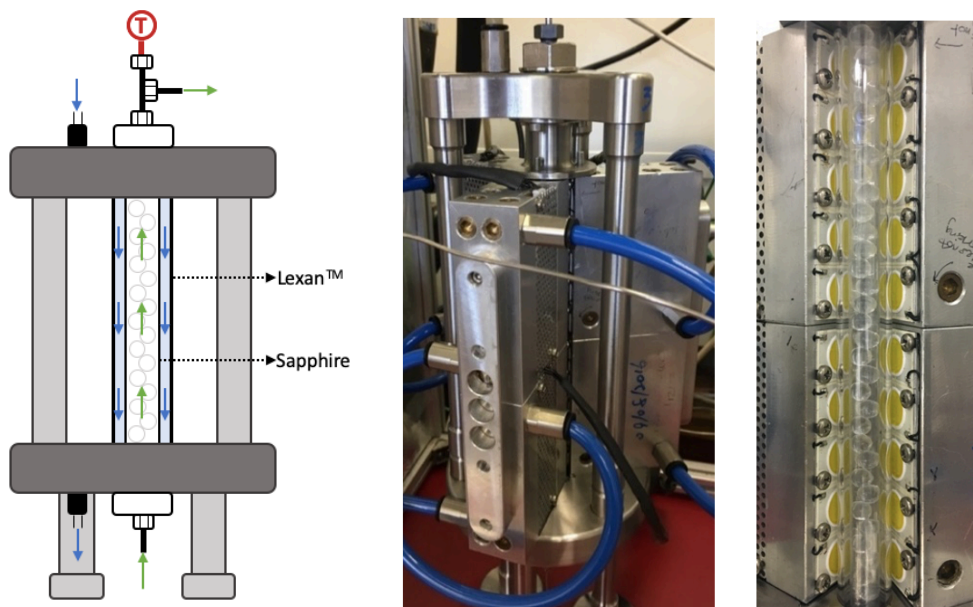


Figure 16. Simplified scheme and photographs of the high-pressure photo reactor. Green arrow: upward reaction flow; Blue arrow: downward reactor cooling flow; T = K-type thermocouple. The two stainless steel plates are screwed to the three struts and the LED units are held to the reactor by grub screws inserted through the top part of the metal body.

- **LED lights and controllers (5954 and 5955):** the photo reactor is surrounded by six blocks of white visible light LEDs, each one containing 5 x Citizen Electronics Co. Ltd 1000 Lumen 12 W LEDs (Figure 17). Their intensities are controlled by two control boxes. To increase the efficiency of the photochemical reaction, the absorption spectrum of the photosensitiser used should overlap with the emission spectrum of the light source.

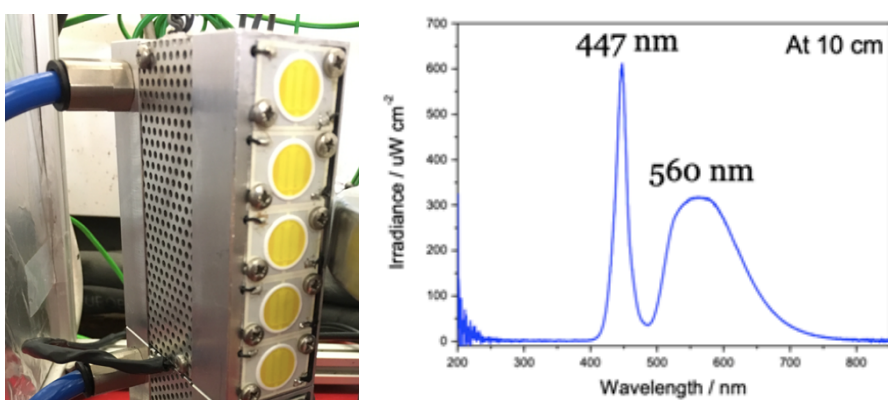


Figure 17. Photograph and the emission spectrum of the Citizen white visible light LED block.

- **Cooling baths (1968 and 1969):** a recirculating cooler Julabo F250 maintains the temperature of the photo reactor by circulating water at 35.5 °C between the sapphire and Lexan™ tubes. In order to prevent over-heating, the LED lights are cooled to - 5 °C

by a refrigerated Haake K15 water bath using a mixture of 1:1 water/glycol. Ethylene glycol works as an antifreeze agent that decreases the freezing point of water.¹⁵⁵

- **Thermo reactor:** the thermo reactor is a tubular reactor (1/4" o.d., 1 mm wall thickness, 156 mm length) surrounded by a heating aluminium block containing two electric cartridges of 100 W each. The tube is packed with 2 mm o.d. glass beads in the bottom and Amberlyst® 15 in the top (Figure 18). The up-flow stream in the thermo reactor firstly passes through the glass beads, which works as a pre-mixer before the mixture reacts with the catalyst. Further modifications of the thermo reactor will be discussed in other chapters.

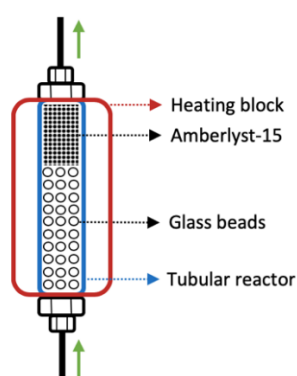


Figure 18. Simplified scheme of the thermo reactor: a tubular reactor (1/4" o.d., 1 mm wall thickness, 156 mm length) filled with glass beads and Amberlyst-15, surrounded by a heating aluminium block containing two electric cartridge of 100 W each. Green arrows: direction of the reaction flow.

- **Back Pressure Regulator 'BPR' (3835):** a Jasco™ BP-1580-81 BPR is used to control the system pressure and is located at the end of the flow system. To avoid potential blockages, the BPR temperature is usually set at 50 °C. If the set pressure is lower than the measured pressure, it could indicate a leak in the system. Conversely, if the measured pressure is higher than the set pressure, it suggests a blockage in the apparatus downstream of the pressure transducer.
- **Temperature controllers (3669, 5918, and 2680):** the heating blocks temperature is controlled by Eurotherm 2216 units through K-type thermocouples.
- **Temperature and pressure monitors (4282, 3666, 4281 and 5353):** West 6700 and 2300 units are used to monitor the mixers temperature as well as the thermo reactor through a K-type thermocouple. For safety reasons, a fail-safe cut off is pre-set at 10 °C above the experimental temperature. The RDP A105 flush diaphragm pressure transducers convert pressure into electrical signal, which is received by the pressure monitors. Pressure monitors (University of Nottingham's Workshop) are used to monitor both the system

and oxygen pressure through two pressure transducers: one located between the oxygen cylinder and the Rheodyne O₂ dosage unit (5224), and the other one immediately after the CO₂ pump (4583). The system monitor has a high limit pre-set value (20 bar above the set pressure) and the oxygen monitor has both a high limit pre-set value (10 bar above the set pressure) and a low limit pre-set value (20 bar below the oxygen set pressure and at least 20 bar above the high limit value for the system pressure) to ensure no back-flow from the system.

- **Trip box (5352):** a safety device built by the University of Nottingham's Workshop (Figure 19). It receives electric signals from the temperature (3666 and 4282) and pressure monitors (5353 and 4281) and cuts off the power supply from the temperature controllers (2680, 3669 and 5918), HPLC pumps (5821 and 5822), Rheodyne O₂ dosage unit (5224) and LED controllers (5954 and 5955). If the measured parameters exceed, fall below the pre-set values, or the red button on the trip box is pressed, the experiment will be safely shut down. When the system is tripped, the CO₂ pump remains on to remove any blockages and the remaining O₂ in the pipes. After the system has tripped, all the components that were shutdown should be switched off and the trip box should be reset. Prior to each experiment, all trips should be tested.

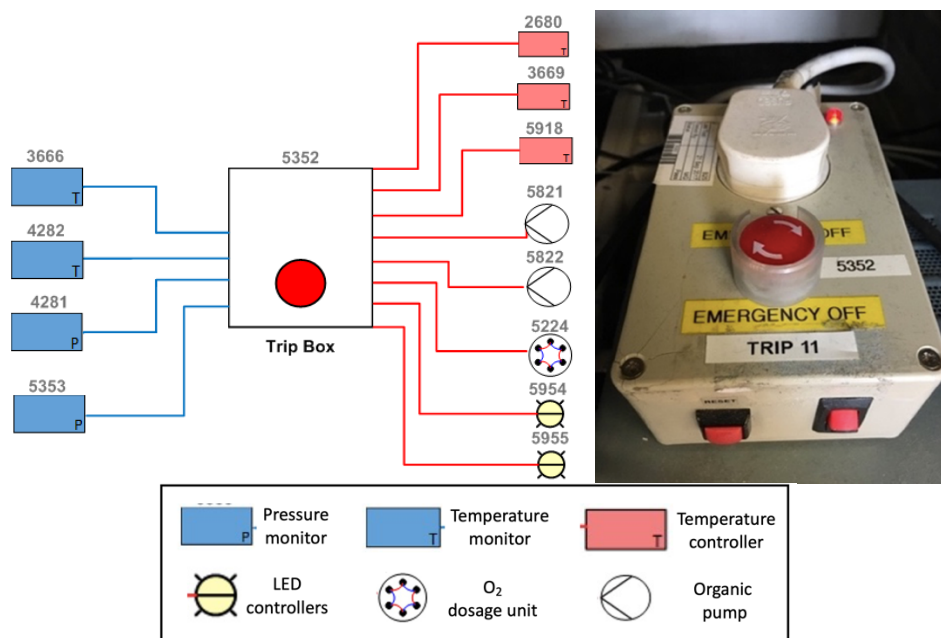


Figure 19. Scheme and photograph of the trip box and its components connected to it. It receives electric signals from pressure and temperature monitors and cuts-off power supply to the temperature controllers, HPLC pumps, O₂ dosage unit and LED controllers. The blue lines represent data cables, and the red lines represent power cables.

- **Data logger:** the Pico® Technology TC-08 thermocouple data logger is connected to a PC *via* USB and relevant data (mixers, thermo reactor, and photo reactor temperatures and system pressure) is recorded using the PicoLog software. This tool is useful to monitor both the system pressure and temperature stabilisation during the initial steps of the standard procedure. It also helps diagnosing the cause of a system trip, showing the time that it happened and any associated data.

2.1.3. Standard Operating Procedures (SOP) for high-pressure continuous flow system

The schematic for all high-pressure flow systems used in this Thesis with its components are shown below. The idle conditions, standard, shutdown, blockage, and emergency procedures are described in detail. The code numbers printed in grey (X) in the SOP correspond to the numbers on the various component in the flow systems schematics (Figures 20 to 23).

Safety Warning: these reactions involve high pressures and require appropriately rated apparatus due to potentially explosive reaction between O₂ and organic compounds. The PhD student gives no undertaking as to the suitability of this equipment when used in other laboratories, particularly because national and local safety regulations may vary between locations. The equipment described is not necessarily the only type that could be used, nor possibly the best available. It is the responsibility of each researcher to check the suitability and safety of their own equipment for such experiments in their laboratories.

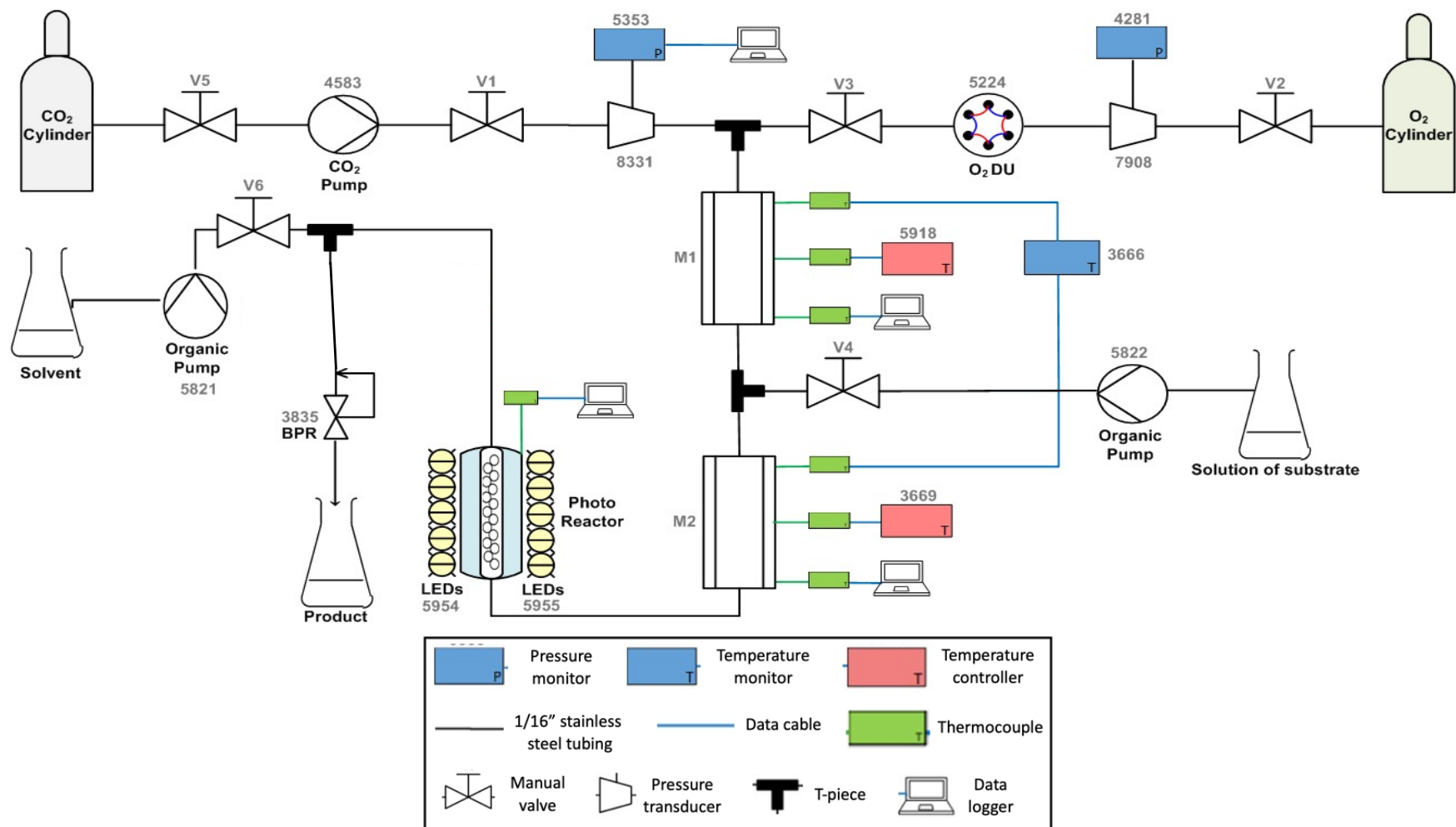


Figure 20. High-pressure continuous flow system schematic with its components (Chapter 3). The identification number for each component is showed in grey. The gaseous streams from **CO₂ pump** (4583) and **O₂ dosage unit (O₂ DU - 5224)** are mixed in static mixer 1 (M1). Next, the **solution of substrate** from **organic pump** (5822) is combined with the gas mixture in static mixer 2 (M2), flowing through a high-pressure sapphire **photo reactor** with **LED blocks** (5954 and 5955). A second **organic pump** (5821) is added after the photo reactor to dilute the stream with the reaction **solvent**, and the crude is collected after the back-pressure regulator **BPR** (3835).

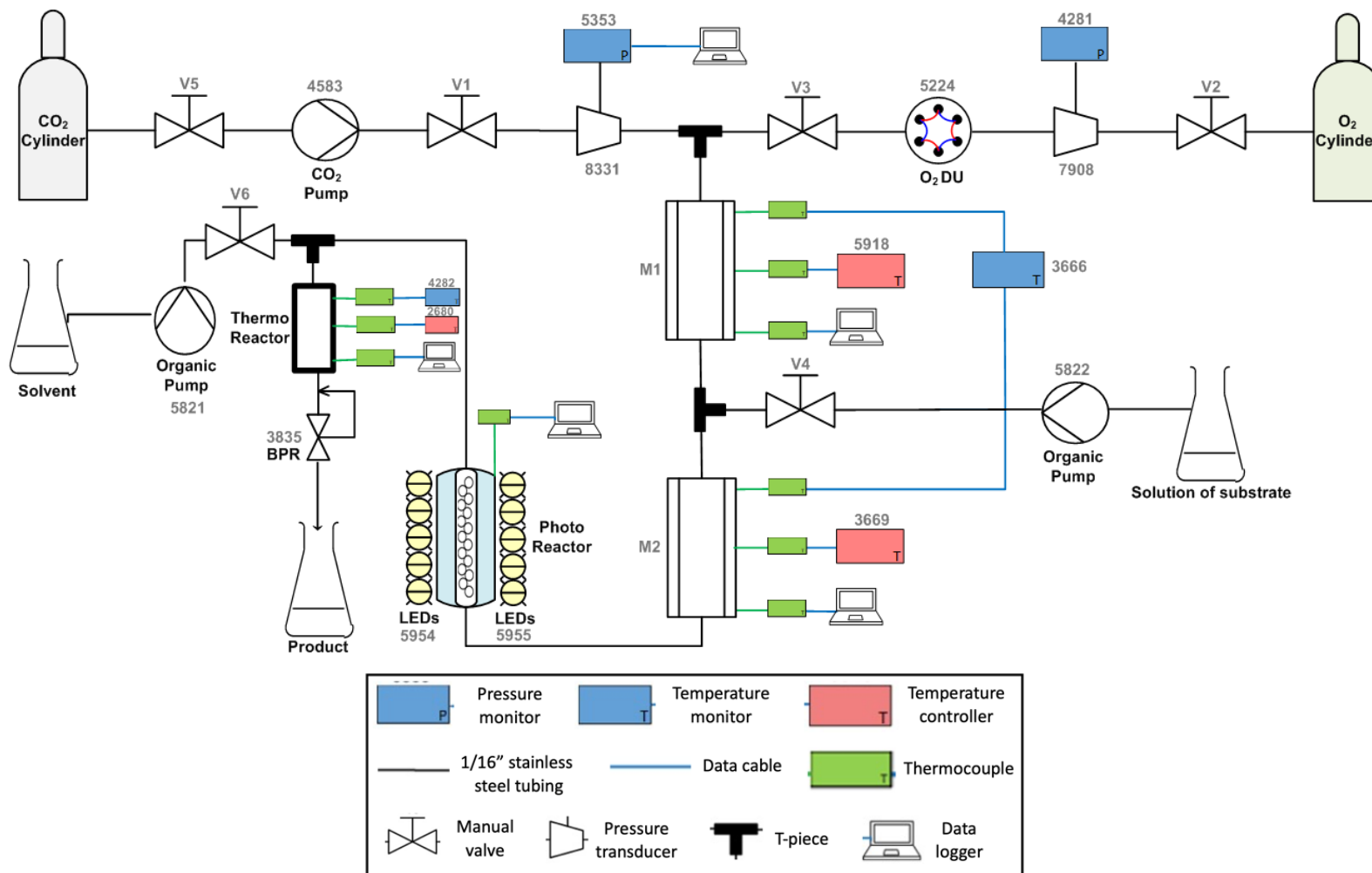


Figure 21. High-pressure continuous flow system schematic with its components (Chapter 4). The identification number for each component is showed in grey. The description is similar to Figure 20, with the addition of **thermo reactor** between **organic pump** (5821) and **BPR** (3835).

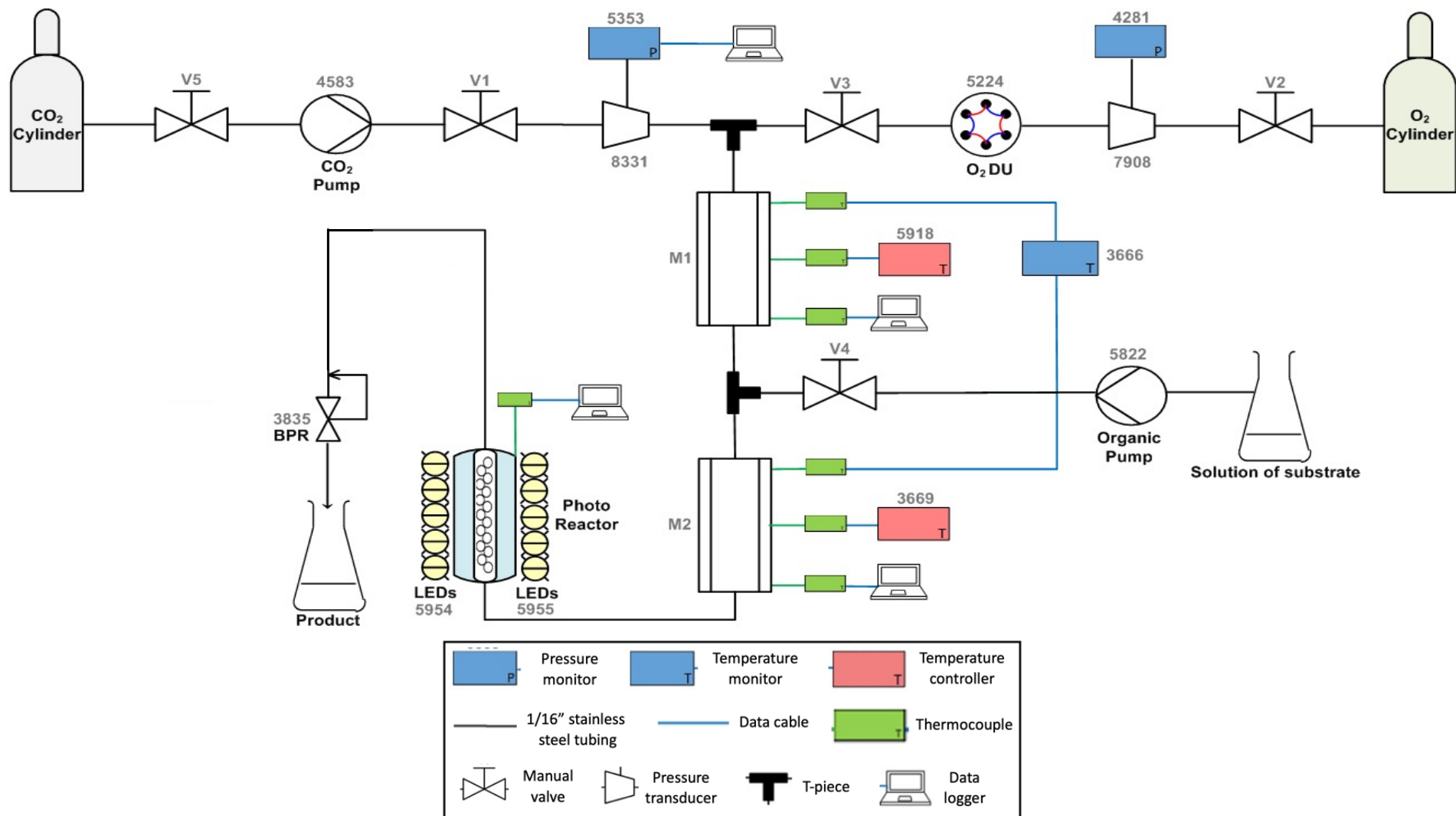


Figure 22. High-pressure continuous flow system schematic with its components (Chapter 5 – Part I). The identification number for each component is showed in grey. The description is similar to Figure 20, without **organic pump** (5821).

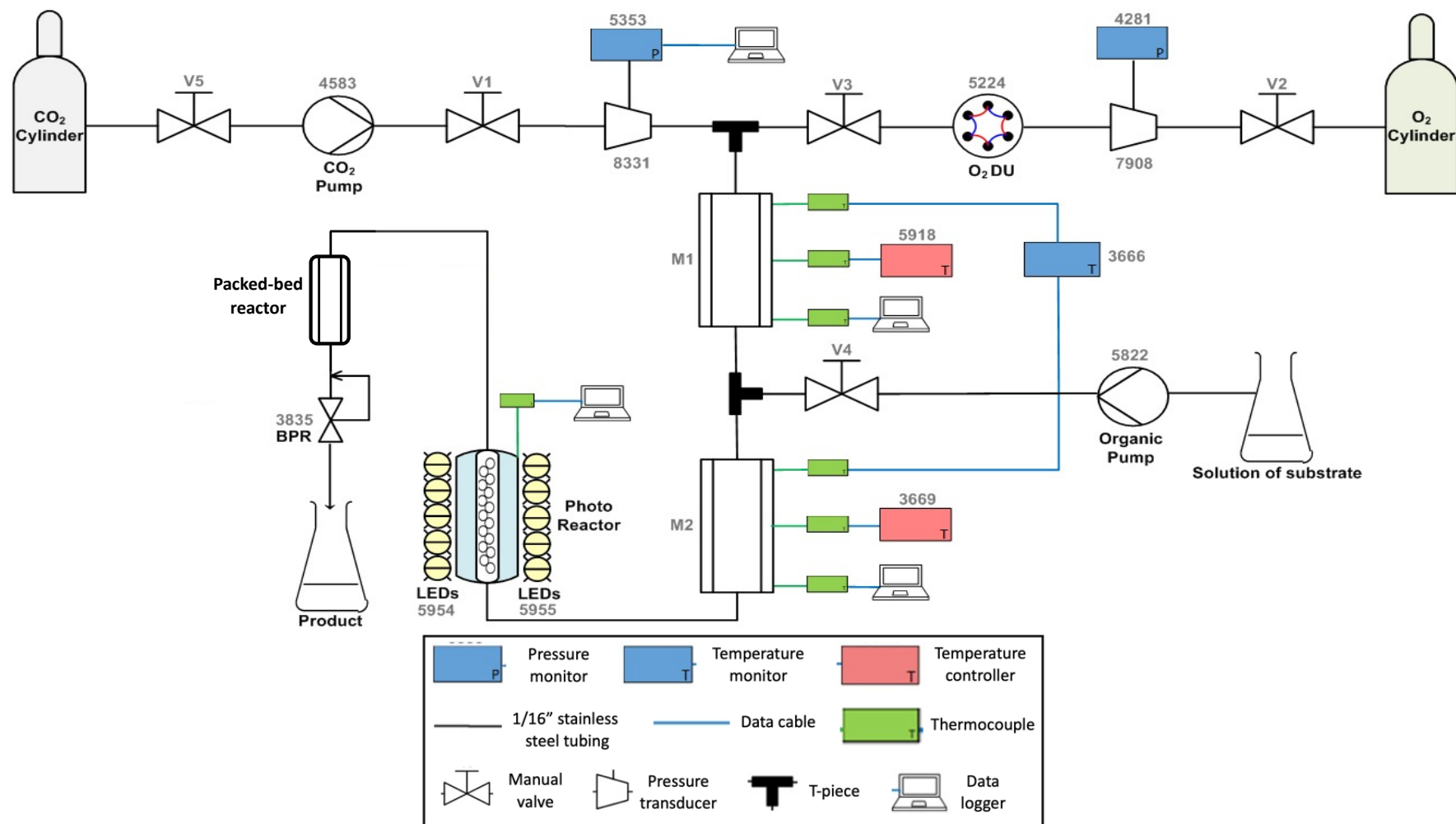


Figure 23. High-pressure continuous flow system schematic with its components (Chapter 5 – Part II). The identification number for each component is showed in grey. The description is similar to Figure 8, without **organic pump** (5821) and with the addition of a **packed bed reactor** between the **photo reactor** and **BPR** (3835).

Idle Conditions

When the system is not being operated, the following procedure should be carried out:

1. All the temperature controllers (5918, 2680 and 3669), cooling baths (1968 and 1969), LED controllers (5954 and 5955), O₂ dosage unit (5224), and organic pumps (5821 and 5822) should be turned off.
2. All the other units should remain turned on, including all the pressure and temperature monitors (4282, 3666, 4281 and 5353), BPR (3835) and CO₂ Pump (4583).
3. Valves V1, V2, V3, V4, and V6 closed and valve V5 open.

Standard Operating Procedure

1. Calculate the required pump flow rates considering its efficiency, O₂ dosage unit switching time, molar ratio substrate: O₂, overall O₂ concentration, and sample loop size for the reaction to be performed.
2. Check if there are any leakages using Snoop liquid on all the couplings, and that all thermocouples are attached, LED lights are working, pressure transducers are calibrated, BPR is holding pressure, and pressure and temperature trips are working and set to the right values.
3. Start the data logger on the PC.
4. Set the trips of the system pressure (5353) and oxygen pressure (4281).
5. Set the BPR (3835) to 120 bar.
6. Set the CO₂ pump (4583) to 2 mL/min and start pumping.
7. Open the valve V1 to allow the CO₂ to enter the system and allow the system to reach the set pressure.
8. Set the CO₂ pump (4583) to the desired flow rate for the reaction and allow the system time to equilibrate (20 min).
9. Meanwhile, set the temperature controllers (5918, 2680 and 3669), and cooling baths (1968 and 1969) to the desired temperatures.
10. 20 min after the CO₂ pump (4583) was started, set the correct switching time on the O₂ dosage unit (5224).
11. Turn on the O₂ cylinder and open the valve V2 to allow the oxygen to fill the O₂ dosage unit (5224).

12. Start the O₂ dosage unit (5224) and open the valve V3 to allow the oxygen to enter the system.
13. Allow the system time to equilibrate (20 min).
14. Meanwhile, prepare the solutions for the reaction and turn on the LED controllers (5954 and 5955).
15. 20 min after the O₂ dosage unit (5224) was started, prime, set flow rates and start the HPLC pumps, pumping the solvent used for the solution (5822 and 5821).
16. Open the valves V4 and V6 to allow the organic solvent to enter the system and allow the system time to equilibrate (20 min).
17. After 20 min since the HPLC pumps (5822 and 5821) were started, pump your desired solutions.
18. The system is now under standard conditions.

Shutdown Procedure

1. Switch off the LED controllers (5954 and 5955).
2. Close the valves V4 and V6 and then stop the HPLC pumps (5822 and 5821).
3. Close the valve V3 and turn off the O₂ dosage unit (5224), as well as the oxygen cylinder.
4. Purge the system with CO₂ at 2 mL/min (20 min).
5. After 20 minutes, turn off the temperature controllers (5918, 2680 and 3669), and cooling baths (1968 and 1969).
6. Prime, open the valves V4 and V6, and start the HPLC pumps (5822 and 5821) pumping pure solvent at 1 mL/min each, together with the CO₂ pump at 1 mL/min (30 min).
7. After 30 min, stop the HPLC pumps (5822 and 5821), close the valves V4 and V6, and allow the system to purge with CO₂ at 2 mL/min (20 min).
8. After 20 min, close the valve V1 and stop the CO₂ pump (4583).
9. Release the pressure slowly by reducing the set pressure at the BPR (3835) to atmospheric pressure in 20 bar increments.

Blockage Procedures

- **Situation 1 (small blockage):** after the system tripped, the system pressure automatically decreases.
1. Close the valves V2, V3, V4 and V6.

2. Turn off the O₂ dosage unit (5224), oxygen cylinder, LED controllers (5954 and 5955), temperature controllers (5918, 2680 and 3669) and cooling baths (1968 and 1969).
3. Keep flushing the system with CO₂ until the pressure stabilises at the set system pressure.
4. Reset the trip box (5352) and flush the system with CO₂ at 2 mL/min, with the temperature controllers (5918, 2680 and 3669) and photo reactor cooling bath (1968) switched on to maintain the supercritical condition and remove any remaining oxygen in the system (30 min).
5. After 30 min, turn off the temperature controllers (5918, 2680 and 3669) and cooling baths (1968 and 1969), open the valves V4 and V6, and start the HPLC pumps at 1 mL/min each (5822 and 5821), as well as the CO₂ at 1 mL/min (30 min).
6. After 30 min, close the valves V4 and V6, stop the HPLC pumps (5822 and 5821), and finally flush the system with CO₂ at 2 mL/min (20 min).
7. After 20 min, close the valve V1 and stop the CO₂ pump (4583).
8. Release the pressure slowly by reducing the set pressure at the BPR (3835) to atmospheric pressure in 20 bar increments.

- **Situation 2 (moderate blockage):** after the system tripped, the system pressure continues to build up.

1. Close the valves V2, V3, V4 and V6.
2. Turn off the O₂ dosage unit (5224), oxygen cylinder, LED controllers (5954 and 5955), temperature controllers (5918, 2680 and 3669) and cooling baths (1968 and 1969).
3. Release the pressure slowly by reducing the set pressure at the BPR (3835) in 20 bar increments until the pressure stabilises. If necessary, close valve V1, stop the CO₂ pump (4583), and release the pressure to the atmospheric pressure following the same procedure.
4. Repeat steps 4-8 from the **Situation 1**.

- **Situation 3 (severe blockage):** after the system tripped, the pressure continues to build up and cannot be released via the BPR.

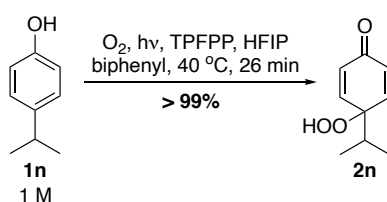
1. Repeat steps 1-3 from the **Situation 2**.
2. If the system is still under pressure after setting the BPR to 0 bar, carefully loosen any unions in which the blockage might have occurred with the fume hood sash as low as possible.
3. Repeat step 4-8 from the **Situation 1**.

Emergency Procedure

In the event of an emergency where the system is not automatically tripped, the following procedure should be followed:

1. Hit the red emergency stop button located on the trip box (5352). This will cut off the power supply from the temperature controllers (5918, 3669 and 2680), HPLC pumps (5821 and 5822), O₂ dosage unit (5224), and LED controllers (5954 and 5955).
2. Close the valves V2, V3, V4 and V6.
3. Turn off the O₂ dosage unit (5224), as well as the oxygen cylinder.
4. Turn off the temperature controllers (5918, 3669 and 2680), HPLC pumps (5821 and 5822), LED controllers (5954 and 5955) and cooling baths (1968 and 1969).
5. The CO₂ pump (4583) will stay on to aid with flushing and cooling the system.
6. The system must be allowed to cool down. Do not remove the blast shield or attempt to release the pressure before the temperature readings are both below 40 °C.
7. Release the pressure slowly by reducing the set pressure at the BPR (3835) in 20 bar increments.
8. When the pressure and temperature hazards have been dealt with, press the square reset button on the side of the trip box (5352) to allow full power back to the system.

2.1.4. Example of excel spreadsheet calculation for high-pressure continuous flow experiments



Scheme 9. Model reaction for calculation: continuous flow photooxidation of 4-isopropylphenol **1n**

Table 1. Calculation of quantity of chemicals for a model starting material solution (1 M) for the photooxidation of 4-isopropylphenol **1n** (Scheme 8).

Chemicals	Equivalents	Mol	M.W (g/mol)	Mass (g)	Density (g/mL)	Volume (mL)
4-isopropylphenol (1.0 M)	1.0	0.0140	136.19	1.9067	-	-
HFIP	-	-	-	-	0.902	14.0
Biphenyl	0.04	0.0006	154.21	0.0864	-	-
TPFPP	0.0005	0.000007	974.55	0.0068	-	-

Table 2. Calculations to obtain CO₂ set flow rate, molar ratio O₂: substrate, O₂ Rheodyne switching time, and O₂ overall concentration for the photooxidation of 4-isopropylphenol **1n** (Scheme 8). The **CO₂ set flow rate** is calculated by dividing the desired flow rate by the CO₂ pump efficiency; The **O₂ Rheodyne switching time** is the ratio of O₂ molar flow rate to mol transferred per switch and is kept between 4 and 16s by adjusting the desired **molar ratio O₂: substrate**; The **O₂ overall concentration** is calculated by dividing the O₂ flow rate by the total flow rate.

KEY			
Values to Edit			
Calculated Values			
Values to be Recorded			
Parameters	Value	Unit	Notes
CO₂			
Desired Flow Rate	0.15	mL/min	-
Pump Efficiency	95.0	%	Table 3 – CO ₂ pump efficiency calculation
Set Flow Rate	0.16	mL/min	Desired Flow Rate/(Pump Efficiency/100)
Mass Flow Rate	0.1463	g/min	Density of CO ₂ (58 bar)*Set Flow Rate
Molar Flow Rate	0.0033	mol/min	Mass Flow Rate/M.W. CO ₂
4-isopropylphenol (1.0 M)			
Molar Concentration of Substrate	0.0010	mol/mL solution	-
Mass Concentration of Substrate	0.1362	g/mL solution	Mass of substrate/Volume of Solution
Mol Required	0.01	mol	Molar Concentration of substrate*Volume of Solution
Mass Required	1.9067	g	Mol substrate*M.W substrate
Mass Flow Rate	0.00681	g/min	Flow Rate Solution*Mass Concentration of substrate
Molar Flow Rate	0.00005	mol/min	Flow Rate Solution*Molar Concentration of substrate
Co-solvent = HFIP			
Molar Concentration of co-solvent	0.01	mol/mL solution	Density of co-solvent/M.W Co-solvent
Molar Ratio co-solvent : Substrate	9.50	:1 mol subs.	Molar concentration co-solvent/molar concentration substrate
Volume of Solution = Volume of co-solvent	14.00	mL	-
Mol Required	0.1330	mol	Mol substrate*Molar Ratio co-solvent:substrate

Mass Required	22.3440	g	Mol co-solvent*M.W. Co-solvent
Flow Rate of Solution = F.R. of co-solvent	0.050	mL/min	-
Mass Flow Rate	0.07980	g/min	Flow Rate Solution*Mass Concentration of co-solvent
Molar Flow Rate	0.00047	mol/min	Flow Rate Solution*Molar Concentration of co-solvent
O₂			
System Pressure	120	bar	-
Set Pressure	180	bar	-
Molar Ratio O₂ : Substrate	2	:1 mol subs.	-
Molar Flow Rate	0.0001	mol/min	Molar Flow Rate Substrate*Molar Ratio O ₂ :Substrate
Mass Flow Rate	0.0031998	g/min	Molar Flow Rate*M.W. O ₂
Density (20 °C, Set Pressure)	0.25237	g/mL	-
Density (20 °C, System Pressure)	0.16745	g/mL	-
Sample Loop Volume	0.01	mL	-
Mol in Sample Loop (20 °C, Set Pressure)	0.000079	mol	Sample Loop Volume*Density at Set Pressure/M.W.
Mol in Sample Loop (20 °C, System Pressure)	0.000052	mol	Sample Loop Volume*Density at System Pressure/M.W.
Mol transferred per switch	0.000027	mol	Mol Sample Loop(Set Pressure)-Mol Sample Loop(Sys. Pressure)
Switching Frequency	3.768017	min ⁻¹	Molar Flow Rate/mol transferred per switch
Conversion 1 min to 0.1 s	600	0.1 s	1 min = 60 seg = 600 0.1s
Switching Time (0.1 s)	159.234952	0.1 s	(1/Switching Frequency)*Conversion to 0.1 s
Switching Time (s)	15.9	s	Conversion 0.1 s to s
Overall concentrations			
Total Molar Flow Rate	0.003948	mol/min	Sum of Molar Flow Rates
CO₂	84.17	mol %	(CO ₂ Flow Rate/Total Flow Rate)*100
4-isopropylphenol (1.0 M)	1.27	mol %	(Substrate Flow Rate/Total Flow Rate)*100
Co-solvent = HFIP	12.03	mol %	(Co-solvent Flow Rate/Total Flow Rate)*100
O₂	2.53	mol %	(O ₂ Flow Rate/Total Flow Rate)*100

Table 3. CO₂ pump efficiency calculation. For a set volume and flow rate of CO₂, the **measured average time** is calculated using a flow meter connected after the BPR. The **measured flow rate** is the ratio of the volume of CO₂ inside the pump (58 bar, -5 °C) to the average time measured using the flow meter. The **CO₂ pump efficiency** is then calculated by dividing the measured flow rate by the set flow rate.

Parameters at 1 bar	
Temperature (°C)	20
Measured Volume CO ₂ (mL)	20
Set Flow Rate (mL.min ⁻¹)	0.15
Measure	Time (s)
1	15.60
2	16.08
3	15.91
4	15.78
5	15.86
6	15.70
7	15.76
8	15.82
9	15.60
10	15.71
Measured Average Time (s)	15.78
Measured Average Time (min)	0.2630

Parameters	Value	Unit	Comment
Mass of CO ₂	0.03660	g	Density of CO ₂ (1 bar, 20 °C)*Volume of CO ₂ (1 bar, 20 °C)
Volume of CO ₂ (58 bar, -5 °C)	0.03754	mL	Mass of CO ₂ /density of CO ₂ (58 bar, -5 °C)
Measured Flow Rate	0.14271	mL.min ⁻¹	Volume of CO ₂ (58 bar, -5 °C)/Average time
CO₂ Pump Efficiency	95	%	Measured flow rate/Set flow rate

2.2. High-pressure view cell

A high-pressure view cell (Figure 24) was employed to test the solubility of the starting material solution in scCO₂ at the set temperature and pressure of the experiments carried out in the high-pressure continuous flow apparatus. If solid particles were observed after the set conditions were reached, that indicates that the starting materials were not soluble in these conditions and could cause blockages in the continuous flow system.

The solubility tests were performed using the high-pressure view cell apparatus built at the University of Nottingham and the training was conducted in collaboration with Ana Patricia Pacheco. For more details about the solubility tests carried out in this Thesis, see Chapter 4.

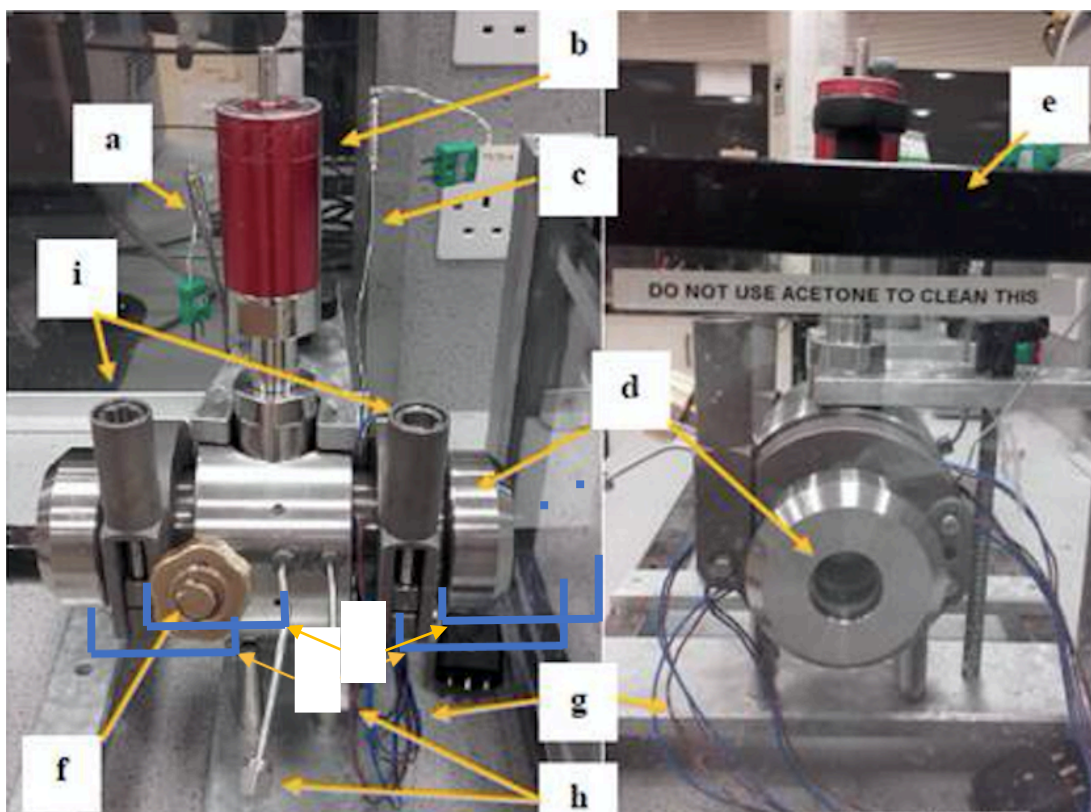


Figure 24. Photograph of the side (left) and front (right) of the high-pressure view cell: (a) internal thermocouple, (b) magnetically overhead stirrer, (c) external thermocouple, (d) view ports with sapphire windows, (e) frame with Lexan™ safety screen, (f) safety key, (g) electrical wires to power heating cartridges, (h) inlet/outlet pipes, (i) sealing clamps and (j) heads. For details of operation see below.

2.2.1. Description of the high-pressure view cell apparatus

A schematic of the high-pressure view cell system (Figure 25) is shown below in detail. The code numbers printed in grey (X) correspond to the numbers on the various components in the high-pressure view cell schematic.

The CO₂ flow is controlled by a valve (V1) and back-flow is prevented by a non-return valve (NRV 1) before V1. The pressure monitor receives information from the pressure transducer (PT1), whereas the temperature controller and monitor, from the thermocouples. The pressure monitor is connected to the trip box, which cuts off the power supply to the temperature controller if the pressure exceeds the pre-set value. The high-pressure view cell (1/8" tubing) is connected to the rest of the system (1/16" tubing) through reducers (R1 and R2), and the second valve (V2) allows the system to be vented to atmosphere.

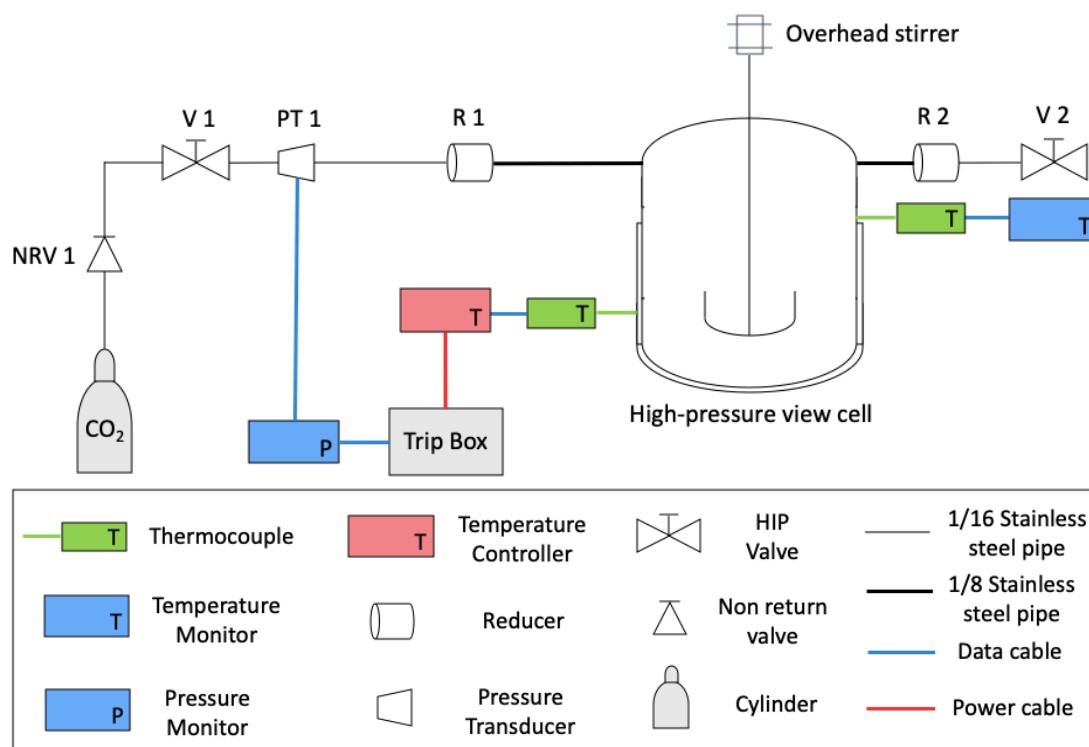


Figure 25. Schematic of the high-pressure view cell system with all its components. The **high-pressure view cell** coupled with an **overhead stirrer** is charged with the reaction reagents, and the system is pressurised with CO₂ by opening the non-return valve V1, whilst V2 is closed. A **pressure monitor** and **temperature controller** are connected to the **trip box**.

The fixed volume (100 mL) high-pressure view cell is made of 316 stainless steel and is equipped with a magnetic stirrer (Figure 26 - h). Sapphire viewing windows (Figure 26 - b) are positioned at each end and are held within the view port (Figure 26 - a) using EPDM O-

rings (Figure 26 - g). These windows allow visualisation of the contents while pressure and temperature parameters are varied. It has a safety key clamp system (Figure 26 - c and f) and is rated for use at pressures up to 34.5 MPa and 300 °C. The view cell is heated by six heating cartridges (Figure 26 - e) which fit into the cylindrical wall of the apparatus.

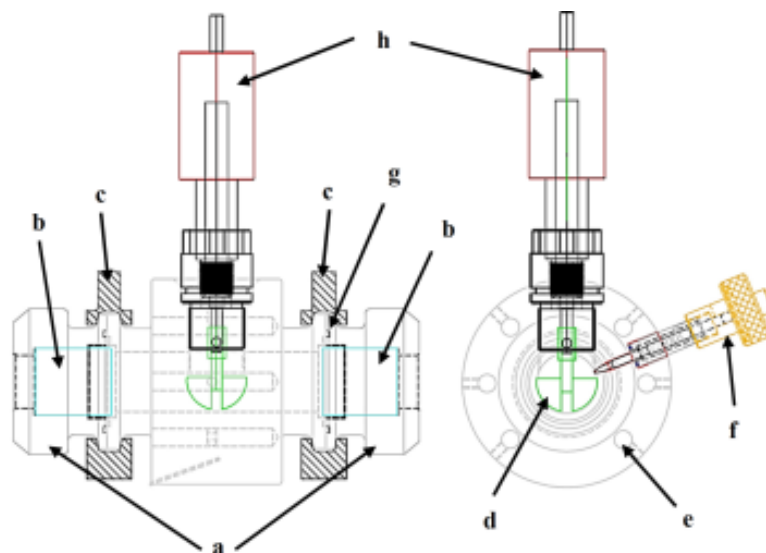


Figure 26. Schematic of the side (left) and front (right) of the high-pressure view cell: (a) view ports, (b) sapphire windows, (c) sealing clamps, (d) stirrer blade, (e) heating cartridges, (f) safety key and needle, (g) EPDM O-ring and (h) magnetically coupled overhead stirrer.

2.2.2. Standard Operating Procedures for high-pressure view cell

Standard Operating Procedure

1. Ensure that the COSHH form is completed and signed.
2. Assemble the two heads: place a Teflon spacer in the groove, fit EPDM O-ring around the sapphire window, lay the head onto a level surface and insert the sapphire window, keeping it straight at all times.
3. Place O-rings at either end of the view cell body.
4. Fit rear head with the clamp and tighten all fittings in the body.
5. Charge the cell with solid reactants *via* the open front end.
6. Check that the stirrer (if needed), heating cartridges, pressure transducer monitor, temperature controller and thermocouples are all connected.
7. Fit the front head, ensuring that the O-ring is in place and clamp it.
8. Ensure that the safety screen is in place before proceeding.
9. Slowly open **V1** until the pressure monitor shows 1500 psi and close **V1**. Check all fittings for leaks with 'Snoop' liquid.

10. If required, vent the cell by closing **V1** and opening **V2**. Adjust any leaking fittings as soon as the system is at atmospheric pressure.
11. Repeat step 7 after adjusting fittings. Vent any remaining gas until the cell is at atmospheric pressure.
12. Open **V1** to purge the view cell with a flow of CO₂ at around 30 psi for 30 min in order to remove residual oxygen.
13. If liquid reactants are required, they should be added by injection through the still open safety valve.
14. Fit and hand tighten the key.
15. Close **V2**, open **V1** to fill the cell with around 800 psi CO₂ and then close **V1** and stir to ensure sufficient mixing for 5 minutes.
16. Set the heaters to the desired temperature.
17. Allow the view cell to reach its final temperature. Monitor the pressure in the vessel constantly throughout this process.
18. Once the temperature has been reached, open **V1** top up the view cell with CO₂ to its final pressure and then close **V1**.
19. Monitor the temperature and pressure throughout the experiment.

Shutdown Procedure

1. After the desired reaction time, set the temperature controller to zero and allow it to cool down to room temperature.
2. Vent CO₂ slowly into the fume hood, opening **V2**. Once at ambient temperature and pressure, remove the key; undo the fittings, followed by the clamp.
3. Open and clean the cell.

2.3. General remarks and analytical methods

2.3.1. *Materials*

Commercially available starting materials and solvents were obtained from Sigma-Aldrich, Alfa Aesar, Acros, Fischer Scientific or Fluorochem, and were used without further purification. The carbon dioxide (liquid UltraPure) and oxygen compressed gas cylinders were supplied by Air Products and BOC, respectively.

2.3.2. *Thin layer chromatography (TLC) and automated flash chromatography*

Experiments were monitored by TLC using pre-coated silica-gel on aluminium plates with fluorescent indicator. The plates were visualised by either UV irradiation ($\lambda = 254$ nm) or *p*-anisaldehyde stain.

Purification of compounds were carried out using a Teledyne Isco CombiFlash® flash chromatography column coupled with UV-vis detector, unless stated otherwise. A suitable RediSep®Rf silica gel column was put in the system and the crude mixture was dry loaded with silica powder into a cartridge, which was then placed in the solid sample position. A separation methodology is then developed, and the system is primed with the eluent system chosen. The fractions are collected by the fraction collector and isolated compounds are obtained after solvent removal.

2.3.3. *Nuclear Magnetic Resonance (NMR) spectroscopy*

NMR spectroscopy spectra were recorded at 20 °C on Bruker AV 400 MHz or AV HD-400 MHz. For quantification purposes, biphenyl was used as internal standard unless stated otherwise.

¹H NMR spectroscopy chemical shifts (δ) are reported in parts per million (ppm) followed by: multiplicity, coupling constants (*J*) in Hz, number of protons, assignment. The values were calculated relative to residual ¹H nuclei in CDCl₃ ($\delta = 7.26$, singlet) or CD₃OD ($\delta = 3.31$, quintet), using MestReNova software. The multiplicity of signals was designated by the following abbreviations: (s) singlet; (bs) broad singlet; (d) doublet; (dd) doublet of doublets; (ddd) doublet of doublets of doublets; (dt) doublet of triplets; (t) triplet; (appt), apparent triplet; (td) triplet of doublets; (q) quartet; (qd) quartet of doublets; (hept) heptet; (heptd) heptet of doublets; and (m) multiplet.

^{13}C NMR spectroscopy spectra were recorded on the spectrometers mentioned above at 101 MHz with ^1H NMR spectroscopy decoupling. Chemical shifts were reported relative to residual ^{13}C nuclei in CDCl_3 ($\delta = 77.16$, triplet) or CD_3OD ($\delta = 49.00$, septet), also using MestReNova.

2.3.4. Ultraviolet-Visible (UV-vis) absorption

UV-vis spectra were recorded on the miniature OceanOptics Flame-S-UV-VIS-ES spectrometer with a Deuterium-Halogen light source and GP400-2-SR fibres in a 1 cm quartz cuvette. The analyses were carried out using an OceanView software.

2.3.5. Electrospray Ionisation Mass Spectrometry (ESI-MS)

Mass spectrometry measurements were conducted using a Bruker MicroTOF mass spectrometer with electrospray ionisation (ESI-MS). Samples were prepared in acetonitrile or methanol for the acquisition.

2.3.6. High-performance liquid chromatography (HPLC)

HPLC calibration curves and quantifications were performed using an Agilent 1200 Liquid Chromatography system with UV detector, Water Nova-Pak C18 column (3.9 x 150 mm, 4 μm diameter particles and 60 Å pores) and Water Nova-Pak C18 pre-column (3.9 x 20 mm, 4 μm diameter particles). Data analyses were conducted using Agilent OpenLab software.

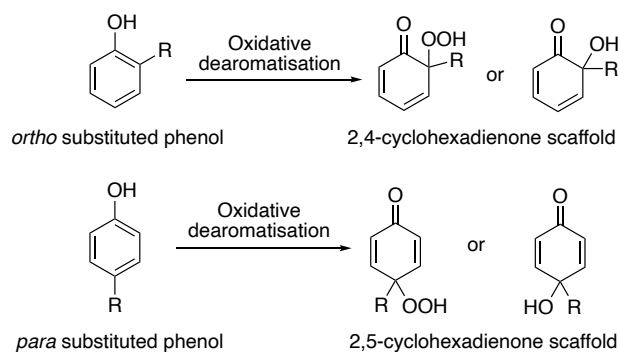
2.3.7. X-ray diffraction (XRD)

XRD structure determinations were performed by Dr. S. Argent at the University of Nottingham using an Agilent SuperNova Atlas S2 diffractometer. Single crystals were put in fomblin film on a micromount and the temperature was kept at 120 K. The structure was solved using the Olex2 software,¹⁵⁶ with the ShelXTstructure solution program using Intrinsic Phasing,¹⁵⁷ and refined with the ShelXL refinement package using Least Squares minimisation.¹⁵⁸

3. Continuous flow dearomatisation of *p*-substituted phenols using singlet oxygen in supercritical CO₂

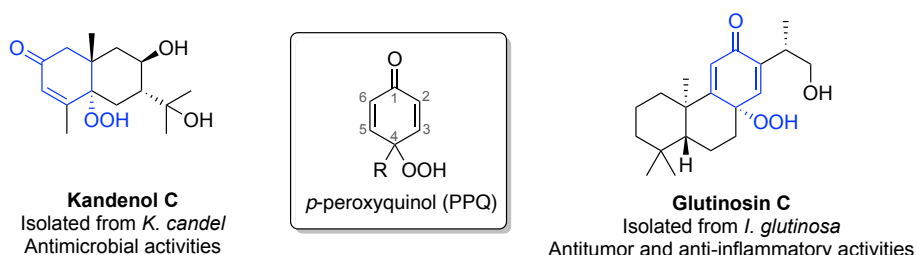
3.1. Introduction

Dearomatisation strategy is a powerful tool to access valuable precursors for organic synthesis, in which aromatic planar structures are transformed into 3D complex architectures.^{159, 160} In particular, the oxidative dearomatisation of phenols is one of the most utilised approaches in the synthesis of complex natural products.¹⁶¹⁻¹⁶⁴ This reaction results in either 2,4- or 2,5-cyclohexadienones products, depending on the reagents and substitution on the aromatic ring (Scheme 10).



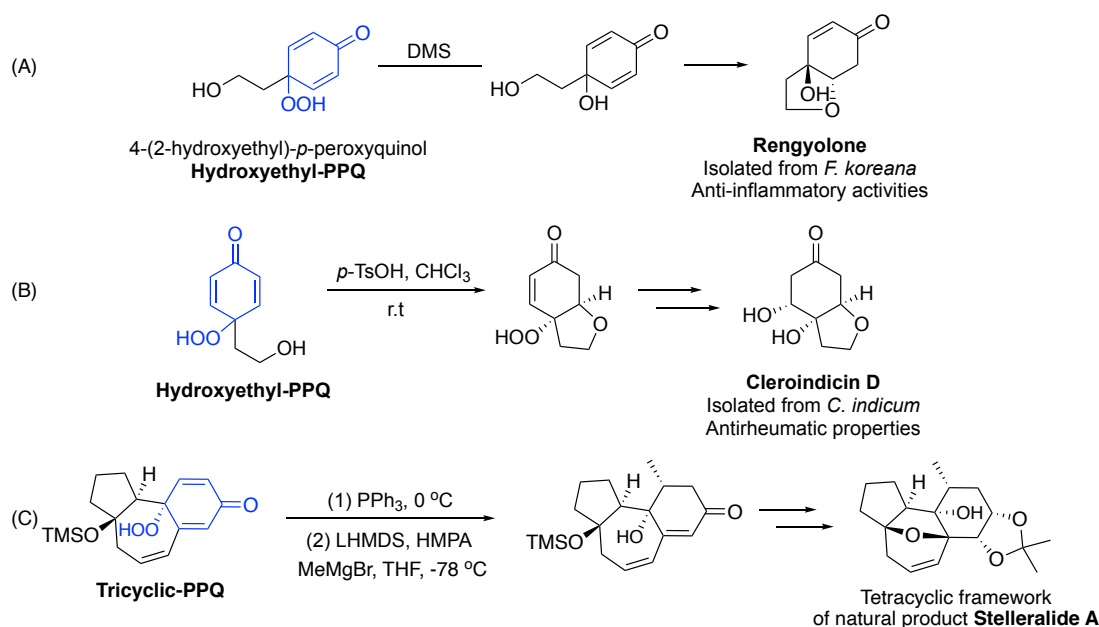
Scheme 10. Oxidative dearomatisation of *ortho* and *para* substituted phenols.

p-Peroxyquinols (PPQs) are one of the products obtained through the dearomatisation of *p*-substituted phenols. Their structure consists in a 2,5-cyclohexadienone ring bearing two *para* substituents, including a hydroperoxyl group. Whilst peroxides are commonly found in natural products such as marine metabolites, terpenes, and steroidal peroxides,¹⁶⁵ PPQs rarely occur in the nature.⁷⁷ For instance, Kandenol C which was isolated from the plant *Kandelia candel*, was reported as an unusual sesquiterpene due to its *p*-peroxyquinol group.¹⁶⁶ (Scheme 11).



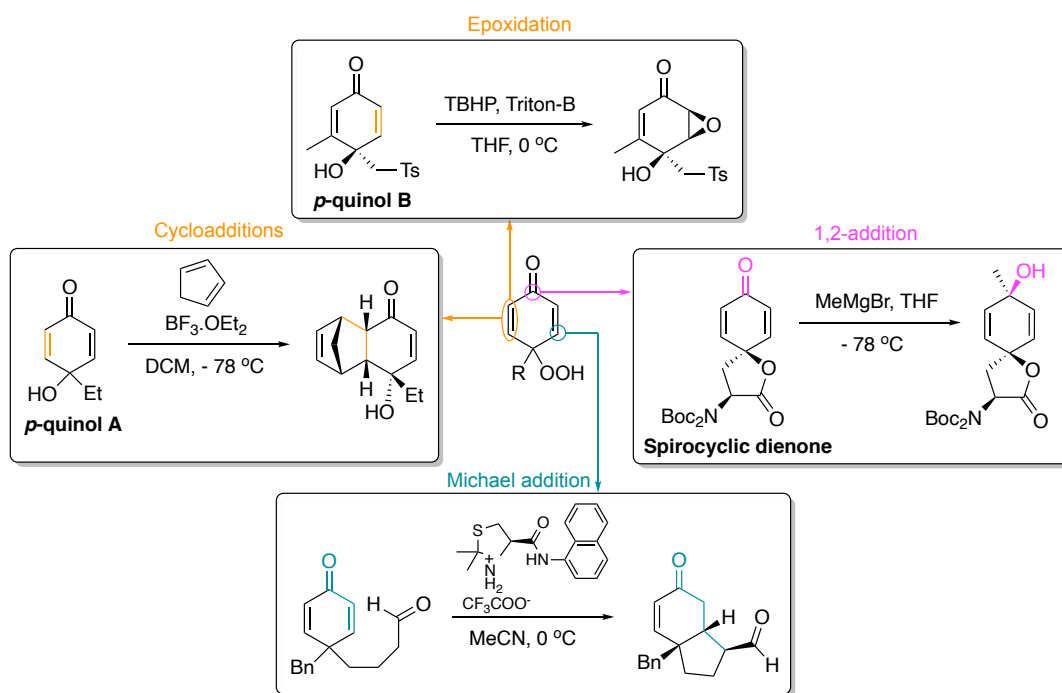
Scheme 11. Structure of *p*-peroxyquinol (PPQ) and examples of naturally occurring PPQs: Kandenol C¹⁶⁶ and Glutinosin C.¹⁶⁷

These compounds are useful building blocks in the total synthesis of natural products (Scheme 12). Rengyolone, isolated from the fruits of *Forsythia koreana*, was found to have anti-inflammatory activities by inhibiting the production of nitric oxide, a biological response regulator.¹⁶⁸ Its synthesis reported by Hikino and co-workers¹⁶⁹ showed that the reduction of 4-(2-hydroxyethyl)-*p*-peroxyquinol (hydroxyethyl-PPQ) followed by spontaneous cyclisation gave rengyolone (Scheme 12 - A). Cleroindicin D, found in the plant *Clerodendrum indicum* which is commonly used in the treatment of rheumatism in India,¹⁷⁰ was also produced via a hydroxyethyl-PPQ (Scheme 12 - B).¹⁷¹ This oxidative dearomatisation strategy was also employed in the synthesis of a tetracyclic framework of a natural product stelleralide A, which is a potent anti-HIV agent (Scheme 12 - C).¹⁷²



Scheme 12. Synthesis of natural products rengyolone¹⁶⁹ and cleroindicin D,¹⁷¹ and tetracyclic framework of stelleralide A¹⁷² using PPQs.

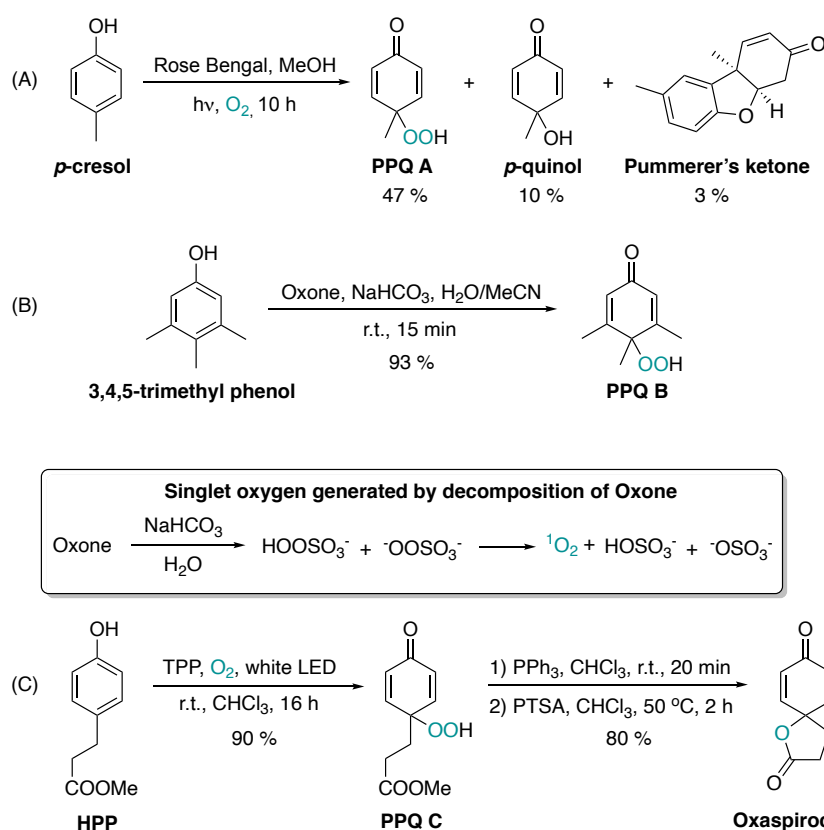
The *p*-peroxyquinol scaffold presents a rich and varied chemistry due to the 2,5-cyclohexadienone structure¹⁷³ (Scheme 13). For example, 1,2-addition of a methyl Grignard reagent to the ketone in a spirocyclic dienone results in a 4,4-disubstituted 2,5-cyclohexadiene bearing an alcohol group (Scheme 13 – 1,2-addition).¹⁷⁴ The electron-poor double bond in *p*-quinol A can participate in Lewis-acid catalysed Diels-Alder cycloaddition with cyclopentadiene to give bicyclic cycloadducts (Scheme 13 - cycloadditions).¹⁷⁵ Another transformation with this reactive double bond was studied by Carreño and co-workers in the epoxidation of *p*-quinol B using *tert*-butyl hydroperoxide (TBHP) and benzyltrimethylammonium hydroxide (Triton-B) (Scheme 13 - epoxidation).¹⁷⁶ Lastly, Hayashi reported an intramolecular Michael addition to the enone, forming a bicyclo[4.3.0]nonene framework (Scheme 13 – Michael addition).¹⁷⁷



Scheme 13. Possible chemical transformations in the 2,5-cyclohexadienone ring of PPQs: 1,2-addition,¹⁷⁴ cycloaddition,¹⁷⁵ epoxidation,¹⁷⁶ and Michael addition.¹⁷⁷

The reported synthetic routes to produce PPQs through oxidative dearomatisation of *p*-substituted phenols use predominantly singlet oxygen. One of the first studies using this strategy was demonstrated by Hikino and co-workers in 1988 (Scheme 14 - A).¹⁶⁹ Irradiation of a solution containing *p*-cresol, oxygen and photosensitiser Rose Bengal for 10 h gave a mixture of PPQ A (45%), *p*-quinol (10%) and Pummerer's ketone (3%). They also investigated the effects of solvent, showing that the best results were achieved in methanol when

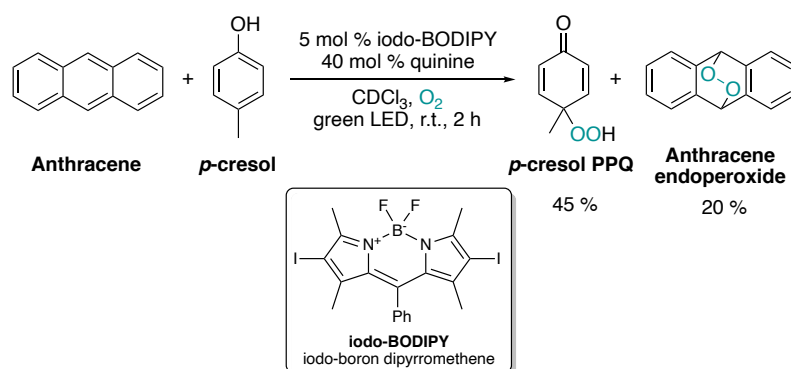
compared to acetone and ethyl acetate. Almost two decades later, Carreño *et al.* developed a more efficient protocol for the synthesis of *p*-peroxyquinols using oxone as the source of singlet oxygen (Scheme 14 - B).⁷⁷ Oxone is a triple salt (2KHSO₅·KHSO₄·K₂SO₄) which decomposes in aqueous basic solution to form singlet oxygen. This protocol was applied to a broad scope of phenols (11 examples) and gave good to excellent yields with reaction times of 15-140 min. In 2013, another photosensitised procedure was reported, using a porphyrinic photosensitiser TPP (Scheme 14 - C).¹⁷⁸ The scope of reaction was mainly focused on phenols bearing an ester group in the chain of the *para*-substituent (4 examples), with subsequent reduction and cyclisation to form oxaspirocycles. For instance, methyl 3-(4-hydroxyphenol) propionate (HPP) was photooxidised in 16 h of reaction yielding 90% of PPQ C.



Scheme 14. Oxidative dearomatisation of phenols via photochemically (rose bengal - A¹⁶⁹ and TPP - C)¹⁷⁸ or chemically (Oxone - B)⁷⁷ generated singlet oxygen.

More recently in 2020, an alternative procedure was developed producing PPQs using a two-module photosensitiser system (Scheme 15). Coeffard and co-workers published a catalytic substrate-selective photooxidation using iodo-boron dipyrromethene (iodo-BODIPY) and quinine as a photosensitiser-catalytic additive system.¹⁷⁹ They stated that BODIPY is responsible for the photo-generation of singlet oxygen and that quinine acts like a

modulator to selectively favour the photooxidation of hydrogen-bond-donor substrates. For instance, when the photooxidation of a mixture of anthracene (non-hydrogen-bond donor) and *p*-cresol (hydrogen-bond donor) was tested in the presence of quinine, 45% of *p*-cresol PPQ was produced along with 20% of anthracene endoperoxide.

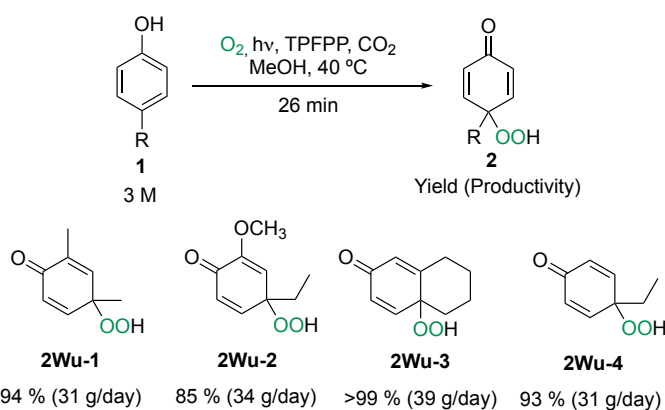


*Scheme 15. Recent procedure on the oxidative dearomatization of phenols: photosensitisation using a quinine-BODIPY system to generate singlet oxygen.*¹⁷⁹

Even though various methodologies for the synthesis of *p*-peroxyquinols from phenols have been described in the literature, they still present some challenges to overcome. For instance, procedures using photochemically generated singlet oxygen frequently have long reaction times (up to 48 h)¹⁷⁸ and high yields are obtained using costly and toxic halogenated solvents.^{178,179} In the case of Carreño's procedure,⁷⁷ the excessive amount of oxidant (5 eq. of Oxone) makes this process less atom efficient, and large quantities of base (15 eq. of NaHCO₃) requires further quenching and extraction, generating more waste. Moreover, the large-scale production of PPQs is often limited by their potential explosive properties – e.g. triacetone triperoxide (TATP)¹⁸⁰ – and instability in oxidisable solvents.¹⁸¹ As a result, this process has rarely been scaled-up beyond 2 g/day.

3.2. Aims and general strategy

Given the ongoing interest in oxidative dearomatisation of phenols^{164, 182} and inspired by the challenges associated with photooxidation of *p*-substituted phenols, our research group developed a different approach. It consists in a continuous flow photooxidation of *p*-substituted phenols **1** using singlet oxygen in supercritical CO₂, using a custom-built high-pressure apparatus¹⁵² (Scheme 16). The photooxidation is mediated by photosensitiser TPFPP and the solutions were prepared in methanol as the co-solvent. To monitor the time to reach the steady-state and to calculate ¹H NMR spectroscopy conversions and yields, biphenyl was used as an internal standard.



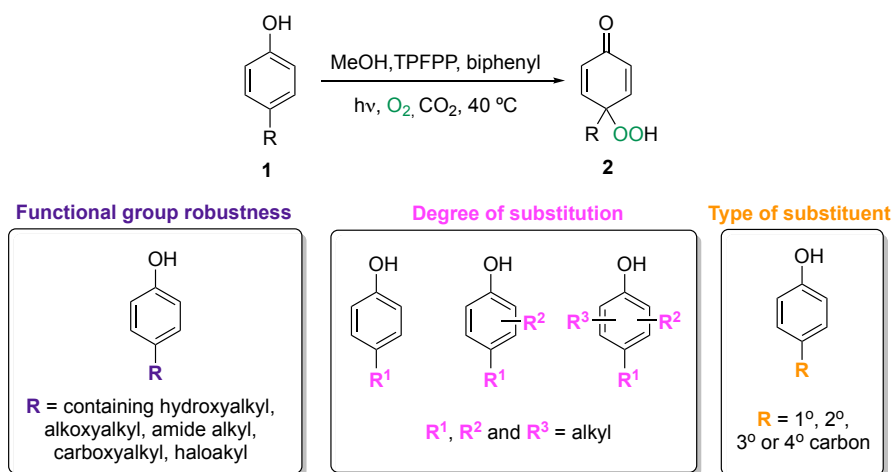
Scheme 16. Summary of previous work on the dearomatisation of *p*-substituted phenol derivatives by Dr. Wu.¹⁵²

Following up this recently developed methodology, the aims for this Chapter were:

- To expand the scope of the high-pressure continuous flow photooxidation of *p*-substituted phenols using singlet oxygen in supercritical CO₂.
- To increase the productivity of the *p*-peroxyquinols **2** using this process.

To address these aims, the following strategies were adopted:

1. The scope of the photooxidation of phenols was investigated, considering functional group robustness, degree of substitution in the aromatic ring and type of substituent at *para* position (Scheme 17).



*Scheme 17. General strategy for expanding the scope of the dearomatization of *p*-substituted phenols **1**.*

2. The productivity of the process was examined considering the concentration of starting materials and flow rates.

3.3. Results and discussion

Given the recent methodology developed by our research group, the scope and scaling up of the reaction was further explored using the apparatus described in the flow diagram depicted in Figure 27.

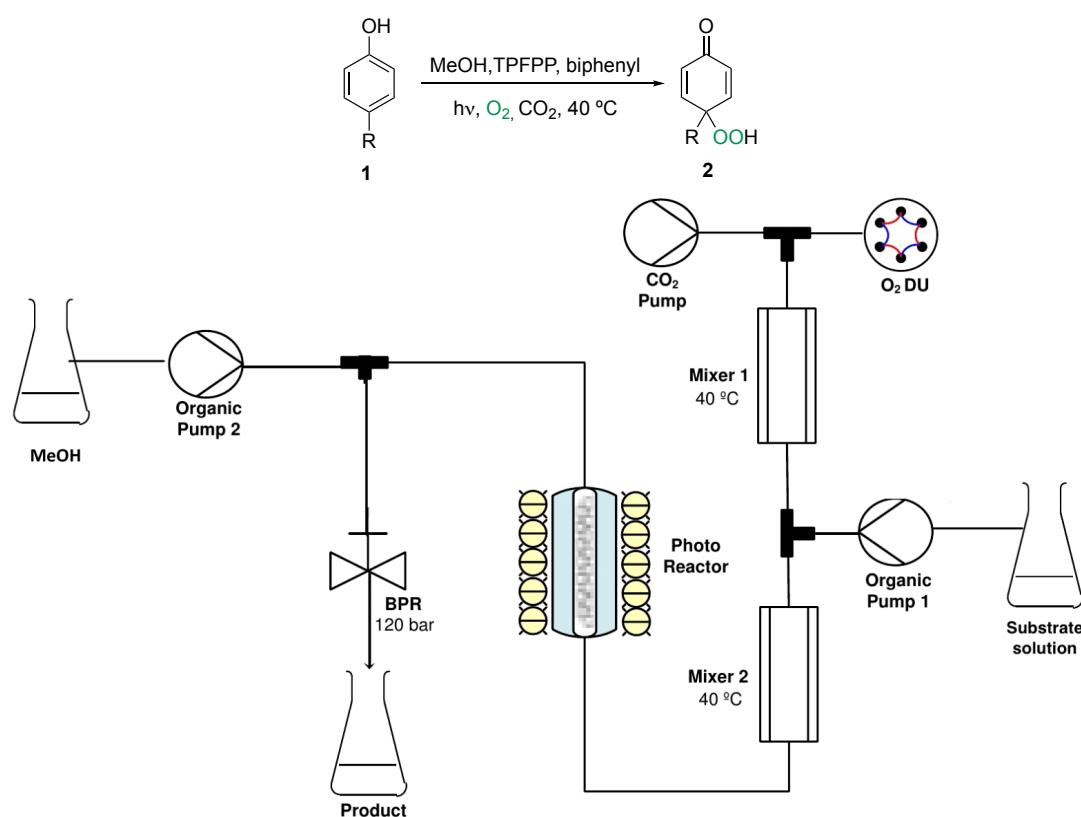


Figure 27. Top: general scheme of the dearomatization of *p*-substituted phenols **1** using ¹O₂ and scCO₂. Bottom: a simplified scheme of the high-pressure flow system used: photo reactor (10 mm outer diameter 'o.d.', 240 mm length, 1 mm wall thickness, effective volume = 5.2 mL, filled with 38 glass beads with 6 mm o.d., at 40 °C); cooling baths (photo reactor = 35.5 °C, LED lights = -5 °C); trips (system set pressure = 120 bar, high trip = 140 bar; oxygen set pressure = 180 bar, high trip = 190 bar, low trip = 160 bar; mixers set temperature = 40 °C, high trip = 50 °C). Flow rates and residence times: (1) CO₂ 0.15 mL/min, HPLC pumps 0.05 mL/min, residence time = 26 min; (2) CO₂ 0.3 mL/min, HPLC pumps 0.1 mL/min, residence time = 13 min. Concentration of TPFPP = 0.05 mol%. Biphenyl used as the internal standard for ¹H NMR spectroscopy quantification.

3.3.1. Reaction Mechanism

The proposed mechanism for the dearomatization of *p*-substituted phenols is initiated by a [4+2] cycloaddition¹⁸³ through a *syn*-addition (suprafacial) of the oxygen to the *p*-substituted phenol. In this pseudo hetero-Diels-Alder reaction, the frontier molecular orbitals illustrate the HOMO-LUMO interaction between the electron-rich *p*-substituted phenol and the electron-deficient singlet oxygen, which is fundamental for the reaction to

occur (Figure 28). Interestingly, the π^* HOMO orbital of singlet oxygen is geometrically orthogonal to the π^* LUMO and it is formed by an out of phase combination of lone pairs orbitals.¹⁸⁴

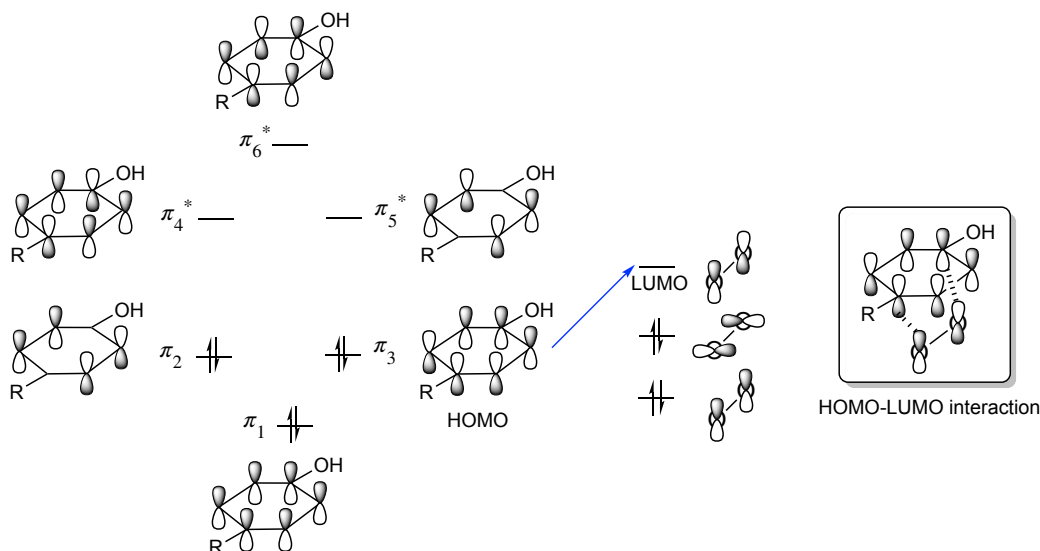
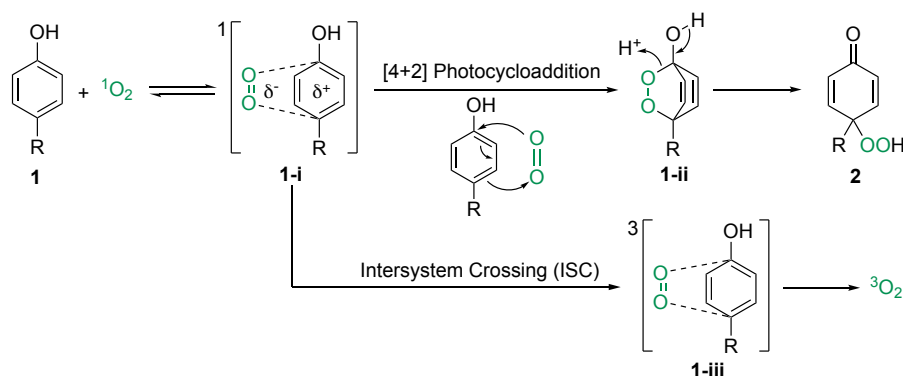


Figure 28. Proposed HOMO-LUMO interactions between the frontier molecular orbitals of a *p*-substituted phenol and singlet oxygen.

It was proposed that the reaction goes through a concerted pathway,¹⁸⁵ starting with the reversible formation of a singlet exciplex transition state **1-i** through a partial charge transfer from the electron-rich aromatic ring on **1** to the singlet oxygen. This exciplex can undergo two different quenching pathways: chemical quenching with the formation of the endoperoxide **1-ii**, which then undergoes a ring-opening to form *p*-peroxyquinol **2**; or physical quenching through a kinetically unfavoured spin-forbidden intersystem crossing to a ground-state complex **1-iii**, regenerating molecular oxygen (Scheme 18).



Scheme 18. Proposed mechanism for the dearomatisation of *p*-substituted phenols **1**.

Lastly, mechanistic and kinetics analysis revealed that the addition of singlet oxygen at the *ipso* and *para* sites of phenol is favoured due to the lower Gibbs activation energy in comparison to the analogous *ortho* and *meta* positions (Figure 29).¹⁸⁶ This is rationalised by the electron distribution in the *p*-substituted phenol, in which the hydroxyl group donates charge to the C2/C6 (*ortho*) and C4 (*para*) carbons, generating a partial positive charge in the COH-*ipso* position. 4-Substituted phenols direct the *ipso-para* regioselectivity of endoperoxide formation, evidenced by electron-donating groups in this site exclusively leading to *p*-peroxyquinols.⁷⁷ The electron-donating groups at *para* position increase the 1,3-diene HOMO energy, enhancing the HOMO-LUMO interaction.

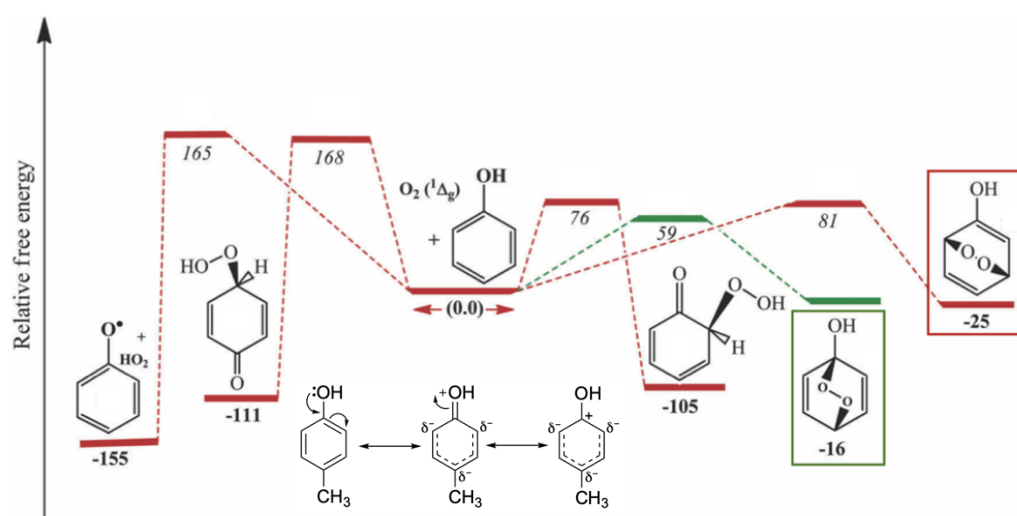
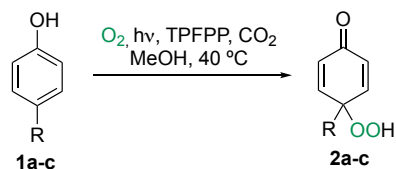


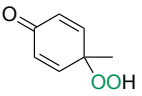
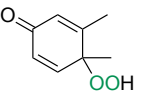
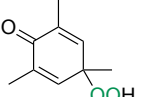
Figure 29. Relative Gibbs energy for the reaction of $^1\text{O}_2$ with phenol. Green box represents the *ipso-para* endoperoxide and the red box represents the *ortho-meta* endoperoxide. The values in bold and italic (kJ/mol) refer to the reaction free energy and the activation energy barrier, respectively.¹⁸⁶

3.3.2. Scope of the dearomatisation of *p*-substituted phenols: Part I

To expand the scope and increase productivity of the production of *p*-peroxyquinols **2**, the dearomatisation strategy was applied to nine other phenols with various substituents at *ortho*, *meta*, and *para* positions. Methanol (MeOH) was chosen as the co-solvent because it is a protic polar solvent, which stabilises the charged transition state and aggregates the reactants through solvation of the exciplex (Scheme 18).¹⁸⁵ In this first part of the discussion, the productivity and degree of substitution on the phenols were investigated (Table 4).

Table 4. Summary of results on the continuous flow dearomatisation of *p*-substituted phenols using $^1\text{O}_2$ in *scCO}_2 (Part I).*



Entry	Product	Concentration (M)	Residence time (min)	NMR conversion of 1 (%)	NMR yield of 2 (%)	Projected productivity (g/day)
1	 2a	1.0	26	> 99	95	10
		3.0	26	> 99	96	29
		3.0	13	83	88	47
2	 2b	3.0	26	> 99	> 99	33
		3.0	13	> 99	> 99	66
3	 2c	1.0	26	> 99	> 99	12

Reactions were carried out in the high-pressure continuous flow apparatus following the guidelines on Figure 27. ^1H NMR spectroscopy yields, and projected productivities were calculated using 0.05 eq. of biphenyl as the internal standard.

The first reaction to be investigated was the dearomatisation of *p*-cresol **1a** (Entry 1 – Table 4). Full conversion and excellent yield (95%) were obtained when the reaction was performed at 1 M. To increase the projected productivity, the reaction was repeated at 3 M, which gave a similar conversion and yield, with a threefold increase in projected productivity (29 g/day) compared to the previous experiment at 1 M. When the residence time was halved, the projected productivity of *p*-peroxyquinol **2a** was higher (47 g/day).

Next, the degree of substitution on the aromatic ring was explored with mono-, di- and tri- substituted phenols. Full conversion and excellent yield (96%) were obtained for *p*-cresol **1a** at 3.0 M concentration and 26 min of reaction, with a slight drop of conversion and yield when the reaction time was halved (Entry 1 – Table 4). For both 3,4-dimethylphenol **1b** (Entry 2 – Table 4) and 2,4,6-trimethylphenol **1c** (Entry 3 – Table 4), full conversion and quantitative yields were achieved. In the case of phenol **1c**, the reaction was performed at 1 M due to solubility issues. These reactions have proven to be easily scalable, with high productivities of up to 66 g/day.

There was no significant difference in yield of *p*-peroxyquinols **2** between mono-, di- and tri- substituted phenols. It was rationalised that *p*-cresol **1a** with just one methyl group makes the aromatic ring sufficiently electron-rich for the [4+2] cycloaddition due to a positive inductive effect (Figure 30). Although the addition of other methyl groups would increase the electron density on the aromatic ring, there was not a significant improvement in the rate of reaction.

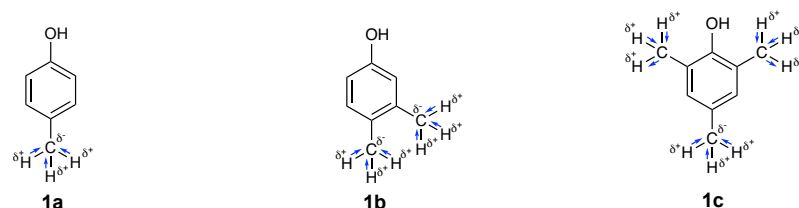
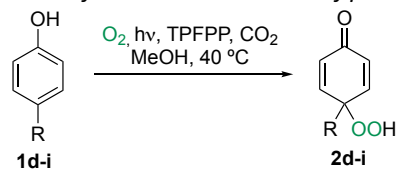


Figure 30. Positive inductive effect (+ I) of the CH₃ group on the aromatic ring for *p*-cresol **1a**, 3,4-dimethylphenol **1b**, and 2,4,6-trimethylphenol **1c**.

3.3.3. Scope of the dearomatisation of *p*-substituted phenols: Part II

After investigating the productivity and the effect of multiple methyl groups on the aromatic ring, a variety of substituents in the alkyl chain of the *para* position of the phenol was studied. These substituents included a tertiary carbon (*t*-Bu), alkyl ether, amino acid, benzylic, protected *O*-benzylic, and electron-withdrawing groups (Table 5).

Table 5. Summary of results on the continuous flow dearomatisation of *p*-substituted phenols using $^1\text{O}_2$ in scCO_2 (Part II).



Entry	Product	Concentration (M)	Residence time (min)	NMR conversion of 1 (%)	NMR yield of 2 (%)	Projected productivity (g/day)
1	 2d	3.0	26	Blockage		
		1.0	26	61	59	8
2	 2e	1.0	26	47	46	6
3	 2f	1.0	26	25	26	6
4	 2g	0.1	26	11	0	0
5	 2h	0.1	26	16	16	0.3
		1.0	26	54	56	11
6	 2i	1	26	0	0	0

The reaction was carried out in the high-pressure continuous flow apparatus following the guidelines on Figure 27. ^1H NMR spectroscopy yields and projected productivities were calculated using 0.05 eq. of biphenyl as the internal standard. ^1H NMR spectroscopy conversion of **1** was calculated as the following: ^1H NMR Conversion of **1** = $100 - X$, where X = ^1H NMR Recovery of **1**.

Dearomatisation of 4-*tert*-butylphenol **1d**

To better understand the effect of bulky substituents, the reaction with 4-*tert*-butylphenol **1d** was examined (Entry 1 – Table 5). When the reaction was performed at 3 M, precipitation of solid caused the flow system to trip. The reaction was then repeated at a lower concentration (1 M). The *tert*-butyl group had a negative effect on the reaction rate when compared to *p*-cresol **1a** under the same conditions (Entry 1 - Table 4), due to steric effects. In addition, although *tert*-butyl is an electron-donating group, it has no $\sigma_{\text{C-H}}$ bond adjacent to the π -orbital on the aromatic ring and therefore, does not donate electron density by hyperconjugation. Even though the yield was moderate, this is the first time that a *p*-peroxyquinol is synthesised with a bulky *tert*-butyl group in *para* position.

Dearomatisation of 4-(2-methoxyethyl)phenol **1e**

The next step was to study the influence of an alkyl ether substituent in 4-(2-methoxyethyl)phenol **1e** (Entry 2 – Table 5). The reaction was carried out at 1.0 M due to solubility issues of the starting material in MeOH. Surprisingly, the yield was much lower (46%) than expected. It was rationalised that the long chain (-CH₂CH₂OCH₃) may cause steric hindrance, with the electrons from the lone pair in the methoxy group repelling the ones from the singlet oxygen (Figure 31). This would make difficult for the oxygen to approach the aromatic ring, as there is a strong electron density around the methoxy group.

To support this, theoretical calculations of an estimator of steric hindrance (E_{st}) or Dynamic Parameter of Steric Hindrance (DPSH) could be performed.^{187, 188} These calculations could predict the contribution of steric effects in the rate of reaction.

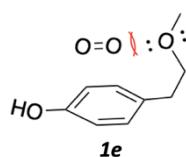
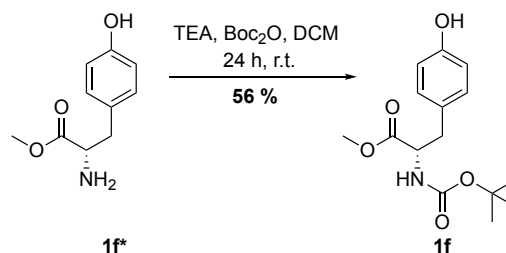


Figure 31. Proposed electronic repulsion of oxygen lone pairs between singlet oxygen and **1e** methoxy group during the [4+2]-cycloaddition.

Dearomatisation of *N*-Boc-*L*-tyrosine methyl ester **1f**

L-tyrosine is an amino acid and precursor for catecholamines such as hormones dopamine and norepinephrine.¹⁸⁹ As this amino acid has a phenol ring in its structure, its reactivity was tested using this new photooxidation methodology. First, both the reactive

amino and carboxylic groups were protected to avoid any side reactions. Starting from the commercially available *L*-tyrosine methyl ester **1f***, the amino group was protected with di-*tert*-butyl dicarbonate (Boc_2O) using triethylamine (TEA) in dichloromethane (DCM)¹⁹⁰ (Scheme 19). Under these conditions, *N*-Boc-*L*-tyrosine methyl ester **1f** was obtained in 56% yield as a white powder.

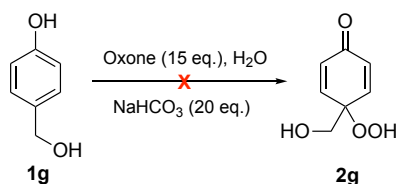


Scheme 19. Protection of *L*-tyrosine methyl ester **1f*** with Boc_2O .

The photooxidation of *N*-Boc-*L*-tyrosine methyl ester **1f** was performed at 1.0 M as the compound was not soluble at higher concentrations (Entry 3 – Table 5). The reaction afforded only 26% yield of **2f**, with projected productivity of 6 g/day. Similarly to 4-(2-methoxyethyl) phenol **1e**, it was hypothesised that the steric hindrance present in **1f** might explain the low conversion and yield observed. The conversion and yield could possibly be increased using a longer residence time, but for means of comparison with other phenols, this parameter was not altered.

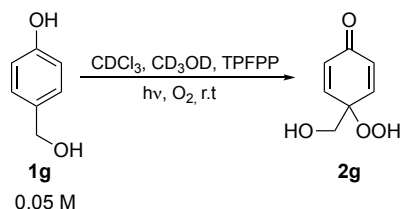
Dearomatisation of 4-(hydroxymethyl) phenol **1g**

The next phenol to be investigated was 4-(hydroxymethyl) phenol **1g** bearing a benzylic alcohol in *para* position. In 2018, Griesbeck's group published the synthesis of a series of *p*-peroxyquinols via dearomatisation of *p*-substituted phenols using Oxone (potassium peroxydisulfate).¹⁹¹ However, their methodology was not suitable for 4-(hydroxymethyl) phenol **1g** and the corresponding *p*-peroxyquinol **2g** was unable to be synthesised (Scheme 20).



Scheme 20. Dearomatisation of 4-(hydroxymethyl) phenol **1g** by Griesbeck.¹⁹¹ **X** represents that no product was observed for the reaction.

To synthesise the desired molecule, the dearomatisation of 4-(hydroxymethyl) phenol **1g** was first performed in batch under similar conditions to those in flow. Deuterated chloroform (CDCl₃) was used as the solvent as it promotes a longer ¹O₂ lifetime and the ¹H NMR spectroscopy analysis could be carried out straightaway. Deuterated methanol (CD₃OD) was added as a polar co-solvent to solubilize 4-(hydroxymethyl) phenol **1g** (Scheme 21).



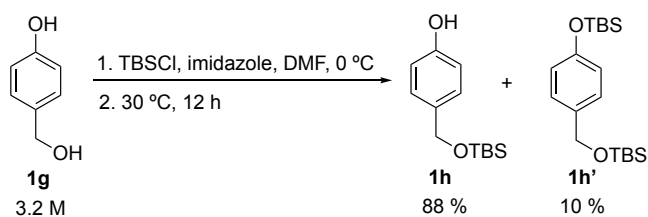
Scheme 21. Batch photooxidation of 4-(hydroxymethyl) phenol **1g**.

The reaction was monitored by ¹H NMR spectroscopy, but after 4 h of reaction, the analysis showed a complex mixture. Nevertheless, the mass spectrometry analysis showed the peak of the product. Additionally, the potassium iodide starch paper test, used to identify the presence of strong oxidants, was positive.

Given the above results, the dearomatisation of 4-(hydroxymethyl) phenol **1g** was carried out in the high-pressure flow system using MeOH as the co-solvent at 0.1 M (Entry 4 – Table 5). Although the KI test was positive during the reaction, the product could not be observed on the ¹H NMR spectroscopy analysis. This may be due to polymerisation of 4-hydroxybenzyl alcohol **1g**, which has been reported to occur in the presence of an oxidising agent.¹⁹² In addition, traces of 4-hydroxybenzaldehyde were identified, possibly because singlet oxygen oxidized the benzylic alcohol to the corresponding aldehyde.¹⁹³

Dearomatisation of 4-((*tert*-butyldimethylsilyloxy)methyl)phenol **1h**

To avoid a possible polymerisation or overoxidation, the benzylic alcohol of 4-(hydroxymethyl) phenol **1g** was protected as a silyl ether with *tert*-butyl(chloro)dimethylsilane (TBSCl) following a procedure published by Fasan *et al.*¹⁹⁴ (Scheme 22).



Scheme 22. Batch hydroxyl protection of 4-hydroxymethyl phenol **1g** using TBSCl and imidazole in DMF.

Phenol **1h** was obtained in 88% isolated yield, as well as a side-product **1h'** in 10% yield. During the course of reaction, the TLC showed an additional spot with a higher retention factor (R_f) relative to the desired product **1h**. A sample was analysed by ^1H NMR spectroscopy and showed that both the phenolic and benzylic hydroxyl groups were protected, forming **1h'**. Even though the reaction was not fully selective for the synthesis of the monoprotected alcohol, excellent isolated yield of the product **1h** was obtained.

With the protected phenol in hand, the reaction was performed in flow (Entry 5 – Table 5). To avoid any blockages caused by a possible polymerisation, the reaction was first carried out at 0.1 M, giving **2h** with a 16% yield. The concentration was increased to 1.0 M, resulting in a 3.5-fold yield increase (56%) and projected productivity of 11 g/day. There were no signs of polymerisation or over oxidation of **1h**, and the silyl ether protecting group remained intact in the reaction conditions. Once again, the steric hindrance caused by the large OTBS group and O -lone pair electron repulsion might explain the moderate yields obtained.

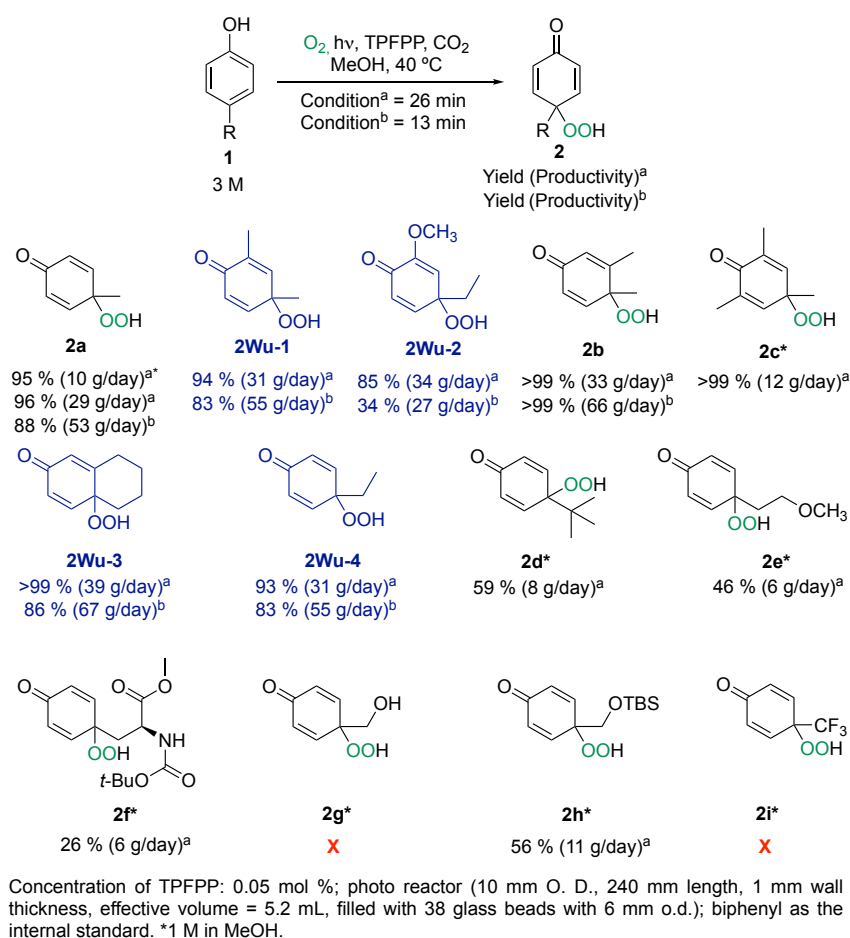
Dearomatisation of 4-hydroxybenzotrifluoride **1i**

To analyse the effect of electron-withdrawing groups, the dearomatisation was attempted with 4-hydroxybenzotrifluoride **1i**, a phenol bearing a CF_3 substituent in the *para* position (Entry 6 – Table 5).

After 3 h of reaction monitored by ^1H NMR spectroscopy, no conversion of **1i** was observed and **2i** could not be synthesised. This phenol structure revealed to be quite stable towards the photooxidation, and not even traces of the product could be identified. The CF_3 substituent has a powerful deactivating effect on the aromatic ring, removing electron density through a negative inductive effect. Consequently, the HOMO orbital energy is decreased and the HOMO-LUMO overlap is unfavoured.

3.4. Conclusions

In this chapter, the high-pressure flow setup was successfully employed in the photooxidation of *p*-substituted phenols using singlet oxygen and supercritical CO₂ (Scheme 23). This methodology provided a platform to access *p*-peroxyquinols with good to excellent yields up to > 99%, easy scaling-up, high projected productivities of up to 67 g/day, and short residence times as low as 13 min. For safety reasons, only small quantities of *p*-peroxyquinols were isolated for characterisation purposes. The continuous flow approach also provides a more effective and safer utilisation of singlet oxygen. The *p*-peroxyquinols are generated continuously, avoiding accumulation of large volumes of potentially explosive compounds, in a non-flammable solvent CO₂. In addition, this reaction utilises a renewable solvent (CO₂) and oxidising reagent (¹O₂). Carbon dioxide is released from the reaction mixture, minimising organic waste and facilitating further purification, whereas singlet oxygen increases high atom efficiency, incorporating both oxygen atoms in the final compound.



Scheme 23. Summary of the dearomatisation of *p*-substituted phenols **2**. Black compounds correspond were synthesised by Abreu and blue compounds were reported by Dr. Wu.¹⁵² X represents compounds that could not be synthesised.

The scope of the dearomatisation of *p*-substituted phenols was expanded from four (synthesised by Dr. Wu) to eleven *p*-peroxyquinols, including three novel compounds, with yields of up to > 99%. The production of some *p*-peroxyquinols was also scaled-up to 67 g/day. *p*-Peroxyquinols **2g** and **2i** could not be produced using this methodology.

The effects of concentration and residence time on the projected productivity, degree of substitution, and the nature of the substituent on the phenol ring were also investigated. High concentrations (3.0 M) and low residence times (13 min) resulted in higher productivities, except for phenol **2Wu-2**. Whilst the yields of *p*-peroxyquinol were similar at 1.0 and 3.0 M concentrations, a decrease in yield was observed when the residence time was doubled, showing that the yield is more affected by the residence time than concentration of starting material. Regarding the degree of substitution, no significant effect on the yield was observed between mono-, di-, and tri- methyl substituted phenols (**2a**, **2Wu-1**, **2b** and **2c**). Concerning the types of substituents, the yield of *p*-peroxyquinol increased depending on the nature of the carbon substituent at *para* position in the order of quaternary (**2d**) < secondary (**2Wu-4**) < primary (**2a**), possibly because of steric hindrance and/or hyperconjugation effects. The negative effect on the yield caused by steric hindrance, EWG removal of electron density of the aromatic ring, or electronic repulsion by *O*-lone pair on the substituent, was also observed in **2e**, **2f** and **2h**. This methodology has proven to be compatible with protecting groups in compounds **2f** and **2h**, as they remained intact in the reaction conditions, avoiding possible side-reactions with their reactive benzylic hydroxyl, carboxylic and amino groups.

The results from this chapter have been recently accepted in the *Organic Process Research & Development* journal:

Wu, L.; **Abreu, B. L.**; Blake, A. J.; Taylor, L. J.; Argent, S. P.; Poliakoff, M.; Boufroua, H.; George, M. W., Multi-gram Synthesis of Trioxanes Enabled by a Supercritical CO₂ Integrated Flow Process. *Org. Process Res. Dev.* **2021**. DOI: <https://doi.org/10.1021/acs.oprd.1c00111>

3.5. Experimental procedures

Continuous flow oxidative dearomatisation of *p*-substituted phenols using singlet oxygen in supercritical CO₂ (general guidelines)

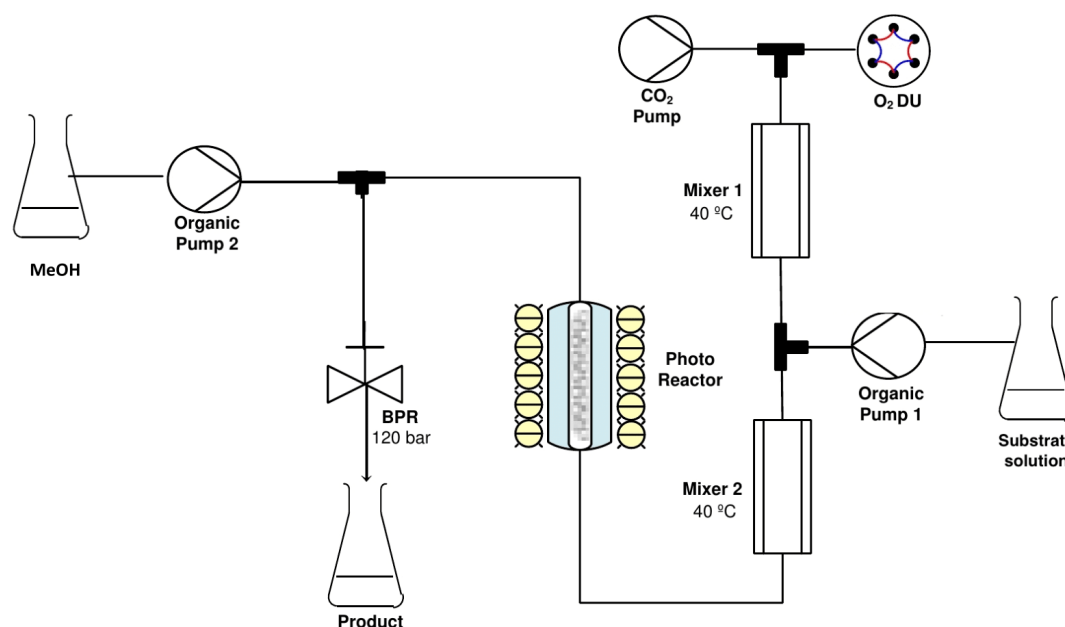


Figure 32. A simplified scheme of the high-pressure flow system for the dearomatisation of *p*-substituted phenols.

System parameters: Photo reactor (10 mm outer diameter (o.d.)), 240 mm length, 1 mm wall thickness, effective volume = 5.2 mL, filled with 38 glass beads with 6 mm o.d., at 40 °C; Cooling baths (photo reactor = 35.5 °C, LED lights = - 5 °C); Trips (System set pressure = 120 bar, high trip = 140 bar; Oxygen set pressure = 180 bar, high trip = 190 bar, low trip = 160 bar; Mixers set temperature = 40 °C, high trip = 50 °C), biphenyl as the internal standard.

Standard procedure parameters for different concentrations and residence times (see Chapter 2, section 2.1.3 for more details)

- **3 M, residence time (RT) = 26 min:** CO₂ (0.15 mL/min and overall [CO₂] = 69%), O₂ (180 bar, sample loop = 10 μL, switching time = 10.6 s, molar ratio O₂: phenol = 1:1 and the overall [O₂] = 3.1 mol%), and HPLC pumps (0.05 mL/min).

- **3 M, RT = 13 min:** CO₂ (0.3 mL/min and overall [CO₂] = 69%), O₂ (180 bar, sample loop = 10 μL, switching time = 5.3 s, molar ratio O₂: phenol = 1:1 and the overall [O₂] = 3.1 mol%), and HPLC pumps (0.1 mL/min).

- **1 M, RT = 26 min:** CO₂ (0.15 mL/min and overall [CO₂] = 71%), O₂ (180 bar, sample loop = 10 μL, switching time = 15.9 s, molar ratio O₂: phenol = 2:1 and the overall [O₂] = 2.1 mol%), and HPLC pumps (0.05 mL/min).

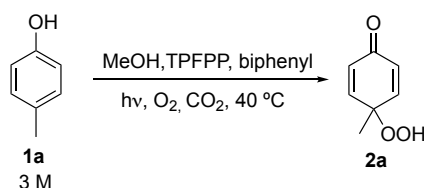
- **0.1 M, RT = 26 min:** CO₂ (0.15 mL/min and overall [CO₂] = 72%, O₂ (180 bar, sample loop = 10 μL, switching time = 15.9 s, molar ratio O₂: phenol = 20:1 and the overall [O₂] = 2.1 mol%), and HPLC pumps (0.05 mL/min).

Reaction procedure: The standard procedure for the flow apparatus is described in Chapter 2, section 2.1.3. In this case, a solution of *p*-substituted phenol, TPFPP and biphenyl in MeOH was prepared and sonicated for 30 min. This solution was pumped into the system, combined with the gaseous mixture (CO₂ and O₂) on Mixer 2 and then passed through the photo reactor. MeOH was pumped after the photo reactor to dilute the mixture and avoid any blockages, and the crude was collected after the BPR. After reaching the steady state, a sample was collected for 3 min, nitrogen blow down for 3 min, and analysed by ¹H NMR spectroscopy. All the remaining peroxides formed were quenched with a saturated solution of thiourea in MeOH.

Reactions were monitored by ¹H NMR spectroscopy analysis of samples taken every 30 min. The steady state time was determined when two consecutive ¹H NMR spectroscopy analysis showed constant conversion and yield values. Samples collected for purification were taken after the steady state was reached. All the remaining reaction mixture was quenched with a saturated solution of thiourea in MeOH. The conversion of *p*-substituted phenols **1** was calculated as the following: ¹H NMR Conversion of **1** = 100 – X, where X = ¹H NMR Recovery of **1**.

Data collected for known compounds is consistent with the literature. Compounds were isolated in small quantities due to potential hazards associated with organic hydroperoxides.

3.5.1. Dearomatisation of *p*-cresol **1a**



Reaction performed under general guidelines for the continuous flow oxidative dearomatisation of *p*-substituted phenols.

- **Reaction 1 (3 M, 26 min):** 12 mL solution of *p*-cresol **1a** (1 eq, 35.9 mmol, 3.89 g, 3 M), TPFPP (0.05 mol%, 18.0 μ mol, 17.5 mg) and biphenyl (0.04 eq, 1.44 mmol, 0.222 g) in MeOH.

Results: The system reached a steady state after 3 h of reaction. ^1H NMR spectroscopy analysis: conversion of **1a** = 99%, yield of **2a** = 96% and projected productivity = 29 g/day.

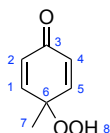
- **Reaction 2 (3 M, 13 min):** 18 mL solution of *p*-cresol **1a** (1 eq, 54.0 mmol, 5.84 g, 3 M), TPFPP (0.05 mol%, 27.0 μ mol, 26.3 mg) and biphenyl (0.04 eq, 2.16 mmol, 0.333 g) in MeOH.

Results: The system reached a steady state after 2 h of reaction. ^1H NMR spectroscopy analysis: conversion of **1a** = 83%, yield of **2a** = 88% and projected productivity = 47 g/day. Another sample was collected for 1.5 h (9 mL), concentrated under reduced pressure and purified by flash chromatography column, eluted with a mixture of EtOAc/Cyclohexane (1:1) to give **2a** (19.3 mmol, 2.71 g, 71%) as an off-white solid.

- **Reaction 3 (1 M, 26 min):** 15 mL solution of *p*-cresol **1a** (1 eq, 15.0 mmol, 1.62 g, 1 M), TPFPP (0.05 mol%, 7.50 μ mol, 7.31 mg) and biphenyl (0.04 eq, 0.600 mmol, 92.5 mg) in MeOH.

Results: The system reached a steady state after 3 h of reaction. ^1H NMR spectroscopy analysis: conversion of **1a** = 99%, yield of **2a** = 95% and projected productivity = 10 g/day.

4-Hydroperoxy-4-methylcyclohexa-2,5-dien-1-one **2a**⁷⁷

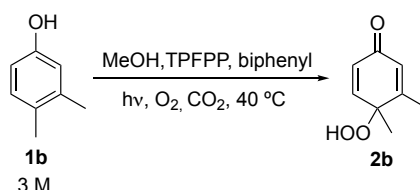


^1H NMR (400 MHz, Chloroform-*d*): δ 8.28 (s, 1H, **8**), 6.90 (d, J = 10.2 Hz, 2H, **1/5**), 6.30 (d, J = 10.2 Hz, 2H, **2/4**), 1.42 (s, 3H, **7**).

^{13}C NMR (101 MHz, Chloroform-*d*): δ 185.5 (**3**), 149.7 (**1/5**), 130.5 (**2/4**), 78.7 (**6**), 22.9 (**7**).

HRMS (ESI) m/z calcd $[\text{C}_7\text{H}_8\text{O}_3\text{Na}]^+$ ($[\text{M} + \text{Na}]^+$): 163.0366, found 163.0363.

3.5.2. Dearomatisation of 3,4-dimethylphenol **1b**



Reaction performed under general guidelines for the continuous flow oxidative dearomatisation of *p*-substituted phenols.

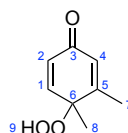
- **Reaction 1 (3 M, 26 min):** 17 mL solution of 3,4-dimethylphenol **1b** (1 eq, 51.0 mmol, 6.23 g, 3 M), TPFPP (0.05 mol%, 25.5 μ mol, 24.9 mg) and biphenyl (0.04 eq, 2.04 mmol, 315 mg) in MeOH.

Results: The system reached a steady state after 1.5 h of reaction. ^1H NMR spectroscopy analysis: conversion of **1b** = > 99%, yield of **2b** = > 99% and projected productivity = 33 g/day. Another sample was collected for 10 min (0.5 mL), concentrated under reduced pressure and purified by flash chromatography column, eluted with a mixture of EtOAc/Cyclohexane (3:7 to 7:3) to give **2b** (1.49 mmol, 229 mg, 99%) as an off-white solid. After that, the CO_2 and organic pumps flow rates, as well as the O_2 switching time were changed for the next reaction accordingly.

- **Reaction 2 (3 M, 13 min):** the solution was the same from reaction 1.

Results: The system reached a steady state after 1.5 h of reaction. ^1H NMR spectroscopy analysis: conversion of **1b** = > 99%, yield of **2b** = > 99% and projected productivity = 66 g/day.

4-Hydroperoxy-3,4-dimethylcyclohexa-2,5-dien-1-one **2b**⁷⁷

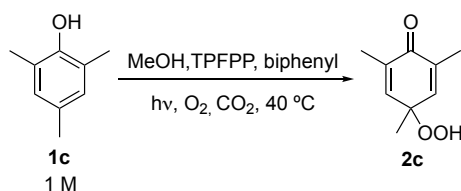


^1H NMR (400 MHz, Chloroform-*d*): δ 9.51 (s, 1H, **9**), 6.93 (d, J = 10.0 Hz, 1H, **1**), 6.22 (dd, J = 10.0 Hz, 2.0 Hz, 1H, **2**), 6.11 (m, 1H, **4**), 2.08 (d, J = 1.4 Hz, 3H, **7**), 1.35 (s, 3H, **8**).

^{13}C NMR (101 MHz, Chloroform-*d*): δ 186.7 (**3**), 161.5 (**5**), 151.9 (**1**), 129.7 (**2**), 128.1 (**4**), 80.5 (**6**), 22.4 (**8**), 18.1 (**7**).

HRMS (ESI) m/z calcd $[\text{C}_8\text{H}_{10}\text{O}_3\text{Na}]^+$ ($[\text{M} + \text{Na}]^+$): 177.0522, found 177.0523.

3.5.3. Dearomatisation of 2,4,6-trimethylphenol **1c**

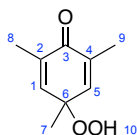


Reaction performed under general guidelines for the continuous flow oxidative dearomatisation of *p*-substituted phenols.

Reaction 1 (1 M, 26 min): 15 mL solution of 2,4,6-trimethylphenol **1c** (1 eq, 15.0 mmol, 2.04 g, 1 M), TPFPP (0.05 mol%, 7.50 μ mol, 7.31 mg) and biphenyl (0.07 eq, 1.05 mmol, 162 mg) in MeOH.

Results: The system reached a steady state after 1.5 h of reaction. ^1H NMR spectroscopy analysis: conversion of **1c** = > 99%, yield of **2c** = > 99% and projected productivity = 12 g/day. Another sample was collected for 1 h (3 mL), concentrated under reduced pressure and purified by flash chromatography column, eluted with a mixture of EtOAc/Cyclohexane (1:1) to give **2c** (2.97 mmol, 500 mg, 99%) as a pale-yellow solid.

4-Hydroperoxy-2,4,6-trimethylcyclohexa-2,5-dien-1-one **2c**⁷⁷

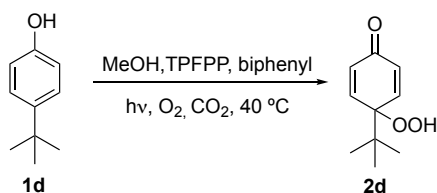


^1H NMR (400 MHz, Chloroform-*d*): δ 8.28 (bs, 1H, **10**), 6.64 (s, 2H, **1/5**), 1.90 (s, 6H, **8/9**), 1.36 (s, 3H, **7**).

^{13}C NMR (101 MHz, Chloroform-*d*): δ 186.9 (**3**), 144.6 (**1/5**), 136.8 (**2/4**), 78.7 (**6**), 23.2 (**7**), 16.1 (**8/9**).

HRMS (ESI) m/z calcd [$\text{C}_9\text{H}_{12}\text{O}_3\text{Na}$]⁺ ($[\text{M} + \text{Na}]^+$): 191.0679, found 191.0683.

3.5.4. Dearomatisation of 4-*tert*-butylphenol **1d**



Reaction performed under general guidelines for the continuous flow oxidative dearomatisation of *p*-substituted phenols.

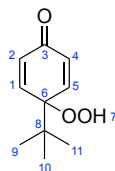
- **Reaction 1 (3 M, 26 min):** 27 mL solution of 4-*tert*-butylphenol **1d** (1 eq, 81.2 mmol, 12.2 g, 3 M), TPFPP (0.05 mol%, 40.6 μ mol, 39.6 mg) and biphenyl (0.04 eq, 3.25 mmol, 501 mg) in MeOH.

Results: After 3 h of reaction, the flow system got tripped due to over pressure caused by solid precipitation.

- **Reaction 2 (1 M, 26 min):** 15 mL solution of 4-*tert*-butylphenol **1d** (1 eq, 15.0 mmol, 2.25 g, 1 M), TPFPP (0.05 mol%, 7.50 μ mol, 7.31 mg) and biphenyl (0.07 eq, 1.05 mmol, 162 mg) in MeOH.

Results: The system reached a steady state after 4 h of reaction. ¹H NMR spectroscopy analysis: conversion of **1d** = 61%, yield of **2d** = 59% and projected productivity = 8 g/day. Another sample was collected for 0.5 h (1.5 mL), concentrated under reduced pressure and purified by flash chromatography column, eluted with a mixture of EtOAc/Cyclohexane (1:1) to give **2d** (0.834 mmol, 152 mg, 55%) as an off-white solid.

4-(*Tert*-butyl)-4-hydroperoxycyclohexa-2,5-dien-1-one **2d** (novel compound)

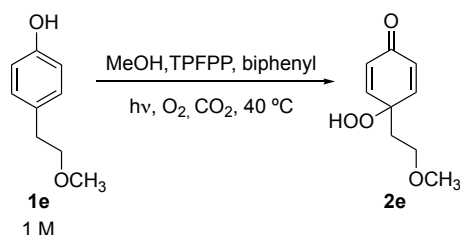


¹H NMR (400 MHz, Chloroform-*d*): δ 8.11 (s, 1H, **7**), 7.06 (d, J = 10.4 Hz, 2H, **1/5**), 6.39 (d, J = 10.4 Hz, 2H, **2/4**), 1.03 (s, 9H, **9/10/11**).

¹³C NMR (101 MHz, Chloroform-*d*): δ 185.3 (**3**), 148.8 (**1/5**), 132.1 (**2/4**), 85.8 (**6**), 39.6 (**8**), 26.0 (**9/10/11**)

HRMS (ESI) m/z calcd [C₁₀H₁₄O₃Na]⁺ ([M + Na]⁺): 205.0835, found 205.0833.

3.5.5. Dearomatisation of 4-(2-methoxyethyl)phenol **1e**

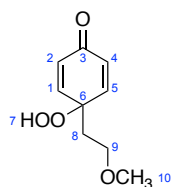


Reaction performed under general guidelines for the continuous flow oxidative dearomatisation of *p*-substituted phenols.

Reaction 1 (1 M, 26 min): 20 mL solution of 4-(2-methoxyethyl)phenol **1e** (1 eq, 20.0 mmol, 3.04 g, 1 M), TPFPP (0.05 mol%, 10.0 μ mol, 9.75 mg) and biphenyl (0.07 eq, 1.40 mmol, 216 mg) in MeOH.

Results: The system reached a steady state after 3 h of reaction. ^1H NMR spectroscopy analysis: conversion of **1e** = 47%, yield of **2e** = 46% and projected productivity = 6 g/day. Another sample was collected for 1 h (3 mL), concentrated under reduced pressure and purified by flash chromatography column, eluted with a mixture of EtOAc/Cyclohexane (1:1) to give **2e** (1.32 mmol, 242 mg, 44%) as a white powder.

4-Hydroperoxy-4-(2-methoxyethyl)cyclohexa-2,5-dien-1-one **2e**¹⁹⁵

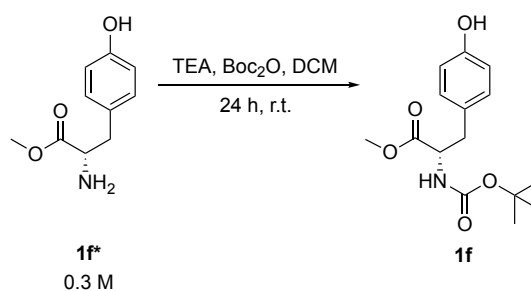


^1H NMR (400 MHz, Chloroform-*d*): δ 9.47 (s, 1H, **7**), 6.96 (d, J = 10.2 Hz, 2H, **1/5**), 6.29 (d, J = 10.2 Hz, 2H, **2/4**), 3.47 (t, J = 5.9 Hz, 2H, **9**), 3.31 (s, 3H, **10**), 2.03 (t, J = 5.9 Hz, 2H, **8**).

^{13}C NMR (101 MHz, Chloroform-*d*): δ 185.8 (**3**), 148.3 (**1/5**), 130.4 (**2/4**), 79.7 (**6**), 67.5 (**9**), 58.9 (**10**), 36.4 (**8**).

HRMS (ESI) m/z calcd $[\text{C}_9\text{H}_{12}\text{O}_4\text{Na}]^+$ ($[\text{M} + \text{Na}]^+$): 207.0628, found 207.0627.

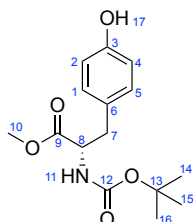
3.5.6. Protection of L-tyrosine methyl ester **1f*** with Boc (Batch)



Procedure: L-tyrosine methyl ester **1f*** (1.0 eq, 50.3 mmol, 9.81 g, 0.3 M) was added to dichloromethane (145 mL), followed by the addition of trimethylamine (2.0 eq, 101 mmol, 13.9 mL). The solution was cooled down to 0 °C with an ice-bath and di-*tert*-butyl dicarbonate (1.1 eq, 55.0 mmol, 12.0 g) was added in portions. After the reaction mixture was stirred for 24 h at room temperature, an acidic extraction using 1 M citric acid (2 x 40 mL), followed by water (40 mL) and brine (2 x 80 mL) was performed, and the organic phase was dried over Na₂SO₄, filtrated and concentrated under vacuum.

Results: The product was purified by flash chromatography column and eluted with a mixture EtOAc/Cyclohexane (3:7) to give **1f** (27.9 mmol, 8.24 g, 56%) as a white solid.

Methyl (*tert*-butoxycarbonyl)-L-tyrosinate **1f**¹⁹⁰

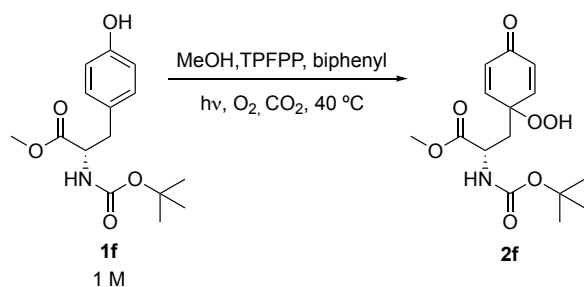


¹H NMR (400 MHz, Chloroform-*d*): δ 6.95 (d, *J* = 8.3 Hz, 2H, **1/5**), 6.72 (d, *J* = 8.3 Hz, 2H, **2/4**), 6.16 (s, 1H, **17**), 5.03 (d, *J* = 8.4 Hz, 1H, **11**), 4.53 (dt, *J* = 8.4, 6.0 Hz, 1H, **8**), 3.71 (s, 3H, **10**), 3.03 (dd, *J* = 14.0, 6.0 Hz, 1H, **7**), 2.95 (dd, *J* = 14.0, 6.0 Hz, 1H, **7'**), 1.41 (s, 9H, **14/15/16**).

¹³C NMR (101 MHz, Chloroform-*d*): δ 172.8 (**9**), 155.5 (**12**), 155.3 (**3**), 130.5 (**1/5**), 127.6 (**6**), 115.6 (**2/4**), 80.4 (**13**), 54.7 (**8**), 52.4 (**10**), 37.7 (**7**), 28.4 (**14/15/16**).

HRMS (ESI) *m/z* calcd [C₁₅H₂₁N₁O₅Na]⁺ ([M + Na]⁺): 318.1312, found 318.1313.

3.5.7. Dearomatisation of *N*-Boc-*L*-tyrosine methyl ester **1f**

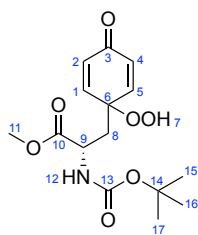


Reaction performed under general guidelines for the continuous flow oxidative dearomatisation of *p*-substituted phenols.

Reaction 1 (1 M, 26 min): 15 mL solution of *N*-Boc-*L*-tyrosine methyl ester **1f** (1 eq, 15.0 mmol, 4.43 g, 1 M), TPFPP (0.05 mol%, 7.50 μmol , 7.31 mg) and biphenyl (0.04 eq, 0.600 mmol, 92.5 mg) in MeOH.

Results: The system reached a steady state after 3.5 h of reaction. ^1H NMR spectroscopy analysis: conversion of **1f** = 25%, yield of **2f** = 26% and projected productivity = 6 g/day. Another sample was collected for 40 min (2 mL), concentrated under reduced pressure and purified by flash chromatography column, eluted with a mixture of EtOAc/Cyclohexane (1:1) to give a novel compound **2f** (0.605 mmol, 198 mg, 30%) as a white solid.

Methyl (*S*)-2-((*tert*-butoxycarbonyl)amino)-3-(1-hydroperoxy-4-oxocyclohexa-2,5-dien-1-yl) propanoate **2f** (novel compound)

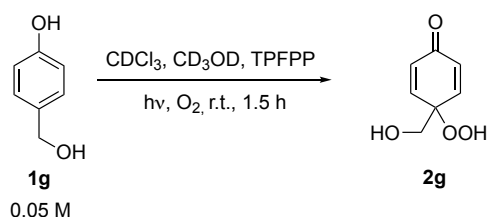


^1H NMR (400 MHz, Methanol- d_4): δ 7.00 – 6.94 (m, 2H, **1/5**), 6.31 (d, $J = 10.0$ Hz, 1H, **2**), 6.22 (d, $J = 10.0$ Hz, 1H, **4**), 4.20 (dd, $J = 10.2, 3.2$ Hz, 1H, **9**), 3.70 (s, 3H, **11**), 2.34 (dd, $J = 14.2, 3.2$ Hz, 1H, **8**), 2.05 (dd, $J = 14.2, 10.2$ Hz, 1H, **8'**), 1.41 (s, 9H, **15/16/17**).

^{13}C NMR (101 MHz, Methanol- d_4): δ 187.4 (**3**), 173.7 (**10**), 157.4 (**13**), 151.1 (**1**), 150.2 (**5**), 132.0 (**2**), 130.7 (**4**), 80.8 (**6**), 80.6 (**14**), 52.9 (**11**), 50.9 (**9**), 39.4 (**8**), 28.7 (**15/16/17**).

HRMS (ESI) m/z calcd [$C_{15}H_{21}N_1O_7Na$] $^+$ ($[M + Na]^+$): 350.1210, found 350.1210.

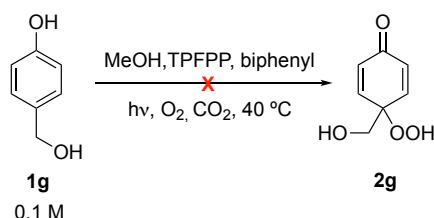
3.5.8. Dearomatisation of 4-(hydroxymethyl)phenol **1g** (Batch)



Procedure: In a sealed vial with a magnetic stir bar and a balloon filled with O_2 , a solution of 4-(hydroxymethyl)phenol **1g** (1 eq, 0.202 mmol, 25.1 mg, 0.05 M) and TPFPP (0.1 mol%, 0.202 μmol , 196 μg) in CDCl_3 (3 mL) and CD_3OD (1 mL) was added at room temperature. The sealed vial was put inside a beaker with water and irradiated by a block of white visible light LEDs (containing 5x 1000 Lumen LEDs). After 1.5 h of reaction, a sample was analysed by ^1H NMR spectroscopy, but the spectra showed a complex mixture. The presence of the desired product was supported by a KI starch paper test and HRMS.

HRMS (ESI) m/z calcd [$\text{C}_7\text{H}_8\text{O}_4$] $^+$ (M^+): 156.1370, found 156.1381.

3.5.9. Dearomatisation of 4-(hydroxymethyl)phenol **1g**

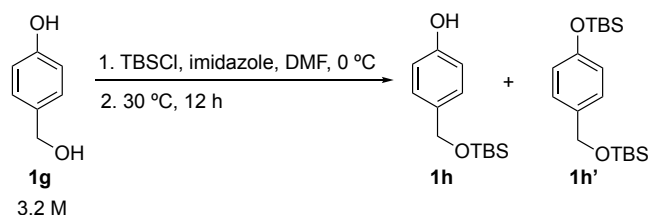


Reaction performed under general guidelines for the continuous flow oxidative dearomatisation of *p*-substituted phenols.

Reaction 1 (0.1 M, 26 min): 15 mL solution of 4-(hydroxymethyl)phenol **1g** (1 eq, 1.50 mmol, 186 mg, 0.1 M), TPFPP (0.05 mol%, 0.750 μmol , 730 μg) and biphenyl (0.07 eq, 0.105 mmol, 16.2 mg) in MeOH.

Results: After 4 h of reaction, the ^1H NMR spectroscopy analysis showed conversion of **1g** = 10%, but no signals of the product **2g**. However, a KI starch paper test detected the presence of *p*-peroxyquinol. Another sample was collected for 50 min (2.5 mL) over a 1.5 M solution of $\text{Na}_2\text{S}_2\text{O}_3$ to quench the *p*-peroxyquinol. The crude was extracted with MeOH, concentrated under vacuum and analysed by ^1H NMR spectroscopy, which only showed peaks of the starting phenol **1g**.

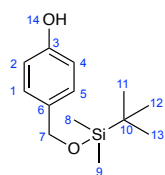
3.5.10. Protection of 4-(hydroxymethyl)phenol **1g** with TBS (Batch)



Procedure: In a sealed 100 mL round-bottom flask with a magnetic stir bar and nitrogen-filled balloon, 4-(hydroxymethyl)phenol **1g** (1.0 eq, 64.5 mmol, 8.00 g, 3.2 M) was added and diluted with dry DMF (20 mL) over an ice bath at 0 °C. After cooling down, imidazole (1.2 eq, 77.4 mmol, 5.27 g) and *tert*-butyldimethylsilyl chloride (1.2 eq, 77.4 mmol, 11.7 g) were added into the solution and the reaction mixture was stirred for 5 min. The reaction was then allowed to warm up under an oil bath at 30 °C and it was kept stirring for 12 h. After completion, the reaction was diluted with Et₂O (200 mL). A saturated solution of NH₄Cl (250 mL) was then added to the mixture, followed by addition of brine (250 mL) during extraction with diethyl ether. The ethereal phase was dried over MgSO₄, filtrated and concentrated under vacuum.

Results: The product was purified by flash chromatography column and eluted with a mixture of EtOAc/Cyclohexane (1:4) to give **1h** (56.9 mmol, 13.6 g, **88%**) as a yellow oil and **1h'** (6.47 mmol, 2.28 g, **10%**) as a colourless liquid.

4-(((*Tert*-butyldimethylsilyl)oxy)methyl)phenol **1h**¹⁹⁶

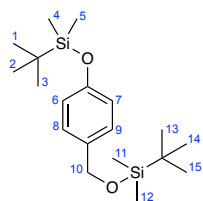


¹H NMR (400 MHz, Chloroform-*d*): δ 7.18 (d, *J* = 8.6 Hz, 2H, **1/5**), 6.77 (d, *J* = 8.6 Hz, 2H, **2/4**), 5.98 (s, 1H, **14**), 4.68 (s, 2H, **7**), 0.96 (s, 9H, **11/12/13**), 0.12 (s, 6H, **8/9**).

¹³C NMR (101 MHz, Chloroform-*d*): δ 154.9 (**3**), 133.2 (**6**), 128.1 (**1/5**), 115.4 (**2/4**), 65.1 (**7**), 26.1 (**11/12/13**), 18.6 (**10**), -5.0 (**8/9**).

HRMS (ESI) *m/z* calcd [C₁₃H₂₂O₂SiNa]⁺ ([M + Na]⁺): 261.1281, found 261.1295.

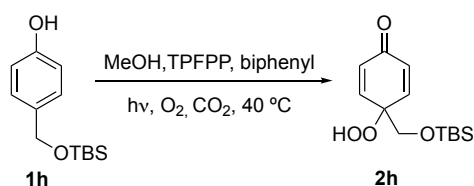
tert-butyl((4-((*tert*-butyldimethylsilyl)oxy)benzyl)oxy)dimethylsilane **1h**¹⁹⁷



¹H NMR (400 MHz, Chloroform-*d*): δ 7.18 (d, J = 8.6 Hz, 2H, **6/7**), 6.81 (d, J = 8.6 Hz, 2H, **8/9**), 4.68 (s, 2H, **10**), 1.00 (s, 9H, **1/2/3**), 0.94 (s, 9H, **13/14/15**), 0.20 (s, 6H, **4/5**), 0.10 (s, 6H, **11/12**).

HRMS (ESI) m/z calcd [C₁₉H₃₆O₂Si₂Na]⁺ ([M + Na]⁺): 375.2146, found 375.2145.

3.5.11. Dearomatisation of 4-((tert-butyldimethylsilyloxy)methyl)phenol **1h**



Reaction performed under general guidelines for the continuous flow oxidative dearomatisation of *p*-substituted phenols.

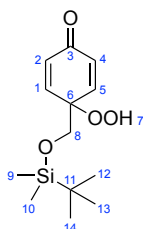
- **Reaction 1 (0.1 M, 26 min):** 20 mL solution of 4-((tert-butyldimethylsilyloxy)methyl)phenol **1h** (1 eq, 2.00 mmol, 476 mg, 0.1 M), TPFPP (0.05 mol%, 1.00 μmol, 975 μg) and biphenyl (0.07 eq, 0.140 mmol, 21.6 mg) in MeOH.

Results: The system reached a steady state after 4 h of reaction. ¹H NMR spectroscopy analysis: conversion of **1h** = 16%, yield of **2h** = 16% and projected productivity = 312 mg/day.

- **Reaction 2 (1 M, 26 min):** 16 mL solution of 4-((tert-butyldimethylsilyloxy)methyl)phenol **1h** (1 eq, 16.0 mmol, 3.81 g, 1 M), TPFPP (0.05 mol%, 8.00 μmol, 0.780 μg) and biphenyl (0.07 eq, 1.12 mmol, 173 mg) in MeOH.

Results: The system reached a steady state after 4 h of reaction. ¹H NMR spectroscopy analysis: conversion of **1h** = 54%, yield of **2h** = 56% and projected productivity = 11 g/day. Another sample was collected for 30 min (1.5 mL), concentrated under reduced pressure and purified by flash chromatography column, eluted with a mixture of EtOAc/Cyclohexane (1:4) to give **2h** (0.673 mmol, 182 mg, **45%**) as a pale-yellow solid. *Even though the ¹³C NMR spectroscopy was too diluted, and the carbonyl signal was missing, it was decided not to isolate this compound again for safety reasons (compound turned black inside the freezer).*

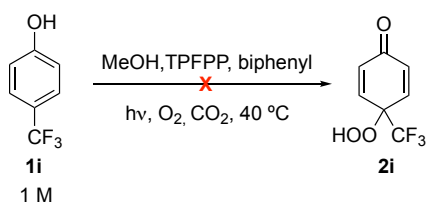
4-(((Tert-butyldimethylsilyl)oxy)methyl)-4-hydroperoxycyclohexa-2,5-dien-1-one **2h** (novel compound)



¹H NMR (400 MHz, Chloroform-*d*): δ 8.16 (s, 1H, **7**), 6.97 (d, *J* = 10.3 Hz, 2H, **1/5**), 6.38 (d, *J* = 10.3 Hz, 2H, **2/4**), 3.76 (s, 2H, **8**), 0.88 (s, 9H, **12/13/14**), 0.06 (s, 6H, **9/10**).

¹³C NMR (101 MHz, Chloroform-*d*): δ 146.2 (**1/5**), 132.0 (**2/4**), 82.0 (**6**), 66.6 (**8**), 25.9 (**12/13/14**), 18.4 (**11**), -5.3 (**9/10**).

3.5.12. Dearomatisation of 4-hydroxybenzotrifluoride **1i**



*Reaction performed under general guidelines for the continuous flow oxidative dearomatisation of *p*-substituted phenols.*

Reaction 1 (1 M, 26 min): 20 mL solution of 4-hydroxybenzotrifluoride **1i** (1 eq, 20.0 mmol, 3.24 g, 1 M), TPFPP (0.05 mol%, 100 μmol , 9.75 mg) and biphenyl (0.07 eq, 1.40 mmol, 216 mg) in MeOH.

Results: Samples were taken and analysed by ^1H NMR spectroscopy every 30 min for 4 h, but no product **2i** was observed. The starting material was fully recovered.

4. Continuous flow telescoped synthesis of 1,2,4-trioxanes

4.1. Introduction

Trioxanes are a class of organic compounds containing a molecular framework consisting of a six-membered heterocyclic ring with three oxygen atoms. The most common isomers found in the literature are 1,2,3-, 1,3,5- and 1,2,4-trioxanes, which will be discussed below (Figure 33).

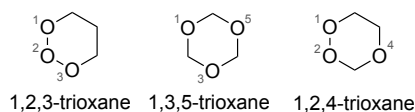


Figure 33. Most common isomers of trioxane: 1,2,3-, 1,2,5- and 1,2,4-trioxane.

This scaffold was discovered by Pratesi in 1885, when paraformaldehyde was heated up with sulfuric acid forming a cyclic trimer called 1,3,5-trioxane.¹⁹⁸ This trioxane is mainly used as an anhydrous source of formaldehyde¹⁹⁹ and has applications in the synthesis of zeolites²⁰⁰ and polyoxometallates (POMs).²⁰¹ In contrast, 1,2,3-trioxanes are scarce in the literature. One of the only examples of this compound was identified as an intermediate in the oxidation of 2,4-didehydroadamantane.²⁰² Among its isomers, 1,2,4-trioxanes are by far the ones with the greatest academic and medicinal interest.

The growing interest in 1,2,4-trioxanes was motivated by the discovery of artemisinin in the 1970s, representing a new potent class of antimalarial drugs.²⁰³ Malaria is a major life-threatening disease (Figure 34) responsible for 229 million infections and 409,000 deaths in 2019.²⁰⁴ This disease is caused by *Plasmodium* parasites and transmitted through *Anopheles* mosquito bites (Figure 34). Although RTS,S is the only approved malaria vaccine,²⁰⁵ it has shown low efficacy (29-36%), encouraging the development of numerous other vaccines which are still in early clinical trials.²⁰⁶ Nevertheless, the most well-established prevention and treatment for malaria are vector control using insecticides, and the use of antimalarial drugs, such as artemisinin.

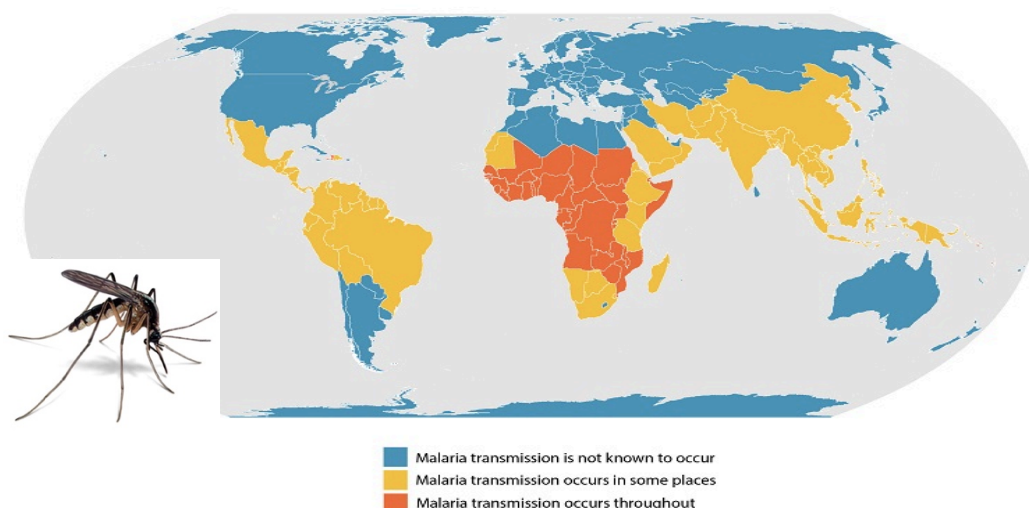


Figure 34. World map of where Malaria occurs²⁰⁷ and photograph of a female *Anopheles* mosquito.²⁰⁸

Artemisinin can be isolated from the extracts of the plant *Artemisia annua* and its structure consists of a sesquiterpene lactone with a unique 1,2,4-trioxane pharmacophore (Figure 35). Its endoperoxide bridge is known to be essential for its pharmacological activity.²⁰⁹



Figure 35. Photograph of the plant *Artemisia annua*²¹⁰ and chemical structure of artemisinin with 1,2,4-trioxane framework highlighted in blue.

Artemisinin-based Combination Therapy (ACT) is currently the most effective and used treatment for malaria worldwide.²¹¹ In addition to its antimalarial properties, its derivatives (e.g. artemether, dihydroartemisinin and artesunate) were found to have numerous medicinal properties (Figure 36). Some of these biological activities include anticancer,²¹² antiviral,²¹³ antibacterial,²¹⁴ antidiabetic,²¹⁵ and more recently, artemisinin has been studied for the treatment of SARS-CoV-2 (COVID-19).^{216, 217} The numerous applications of Artemisinin are related to the varied mechanisms of action, high selectivity and potency, low toxicity, and fast-acting.²¹⁸

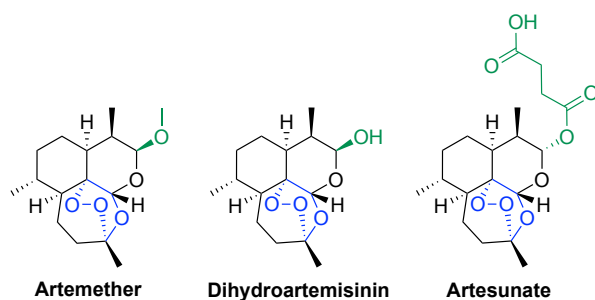
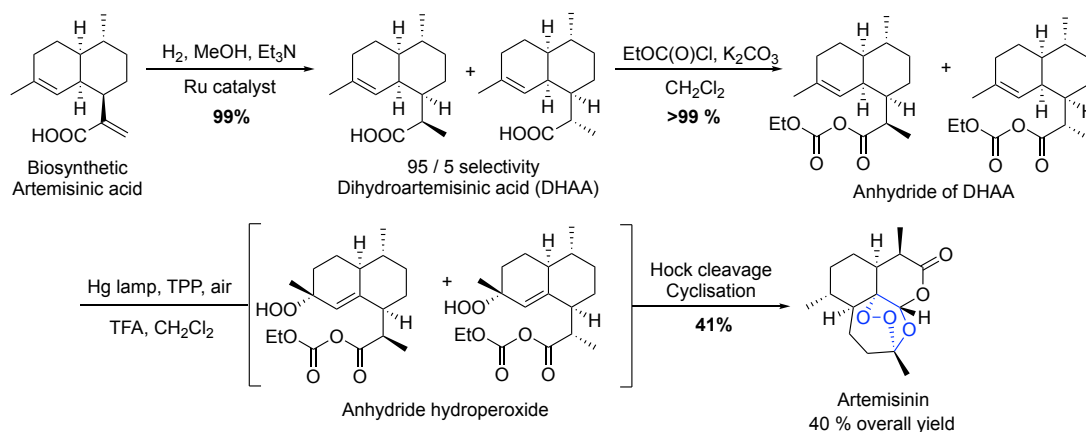
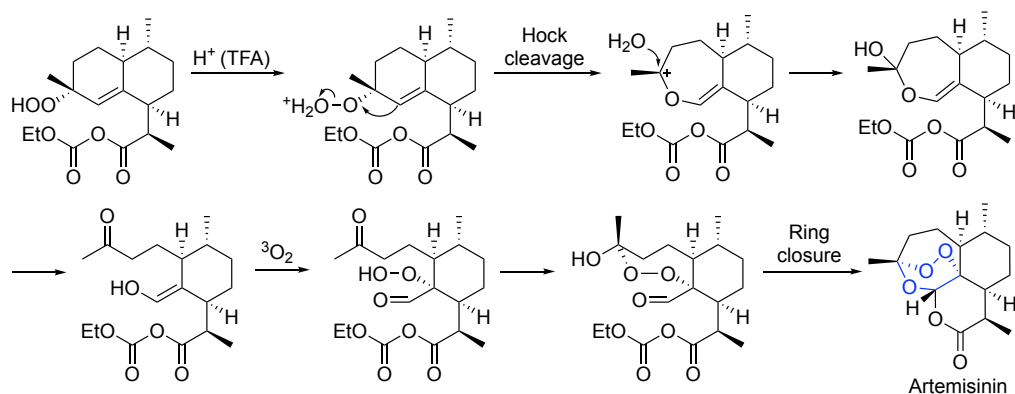


Figure 36. Most common derivatives: artemether, dihydroartemisinin and artesunate. 1,2,4-trioxane scaffold is highlighted in blue and the derivatisation for each compound is shown in green.

However, the main commercial source of artemisinin is still *A. annua*, production of which is limited and unpredictable.²¹⁹ This results in global shortages and consequently price fluctuation. In 2013, Sanofi developed the first industrial semi-synthesis of artemisinin from artemisinic acid.⁵² The synthesis was achieved in four steps with 40% overall yield, producing approximately 60 tonnes of artemisinin per year (Scheme 24). The most challenging step in this transformation was the photooxidation of anhydride of dihydroartemisinic acid (DHAA), followed by Hock cleavage and cyclisation (Scheme 25), because it results in numerous impurities and moderate yield of 41%.



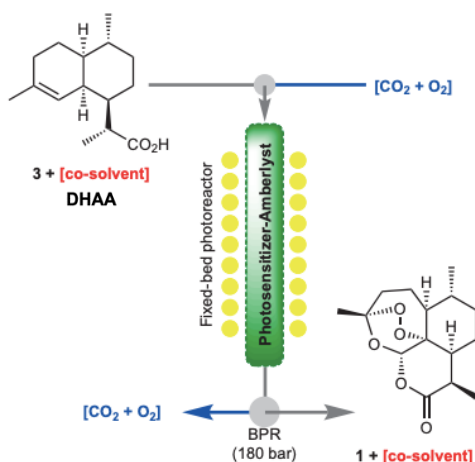
Scheme 24. Industrial semi-synthesis of artemisinin by Sanofi.⁵²



Scheme 25. Hock cleavage followed by ring closure mechanism in the synthesis of Artemisinin by Sanofi.⁵²

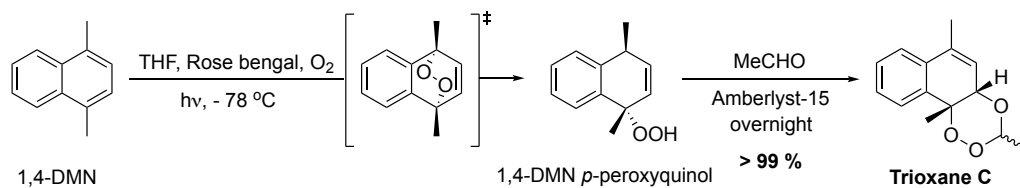
The first continuous flow approach for the semi-synthesis of artemisinin was published by Seeberger, obtaining artemisinin in 46% overall yield.¹²⁸ However, the use of costly halogenated solvent DCM, toxic trifluoroacetic acid (TFA), and inconvenient low temperatures ($-20\text{ }^\circ\text{C}$) for the key photooxidation step are problematic for scale-up. This procedure paved the way for the development of more sustainable continuous flow approaches.

Our research group reported a greener alternative for the continuous flow production of artemisinin from dihydroartemisinic acid using cheap and non-flammable liquid CO_2 .¹²⁷ The reaction was catalysed by Amberlyst-15 with photosensitiser TPP or TPFPP immobilised in the acid catalyst (packed bed), obtaining artemisinin in 39% overall yield (Scheme 26).



Scheme 26. A greener continuous flow semi-synthesis of artemisinin from DHAA using liquid CO_2 .¹²⁷

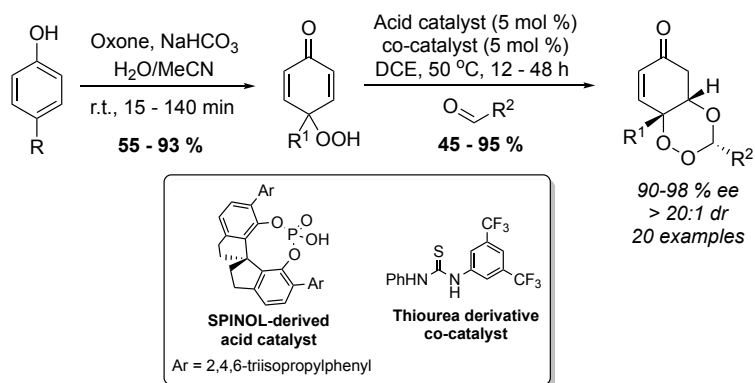
Given the challenges related to artemisinin's production and increasing drug resistance reported in parts of South-East Asia of artemisinin and its derivatives,²²⁰ ongoing research



Scheme 29. Synthesis of 1,2,4-trioxanes through photooxidation of 1,4-DMN.²²⁶

Other examples of syntheses of 1,2,4-trioxanes have also been reported in the literature, including oxidative photocycloaddition of 2H-pyrans,²²⁹ *p*-benzoquinone/cyclooctatetraene,²³⁰ and oxygen mediated reaction between arylamines and aldehydes.²³¹

Inspired by the synthesis of 1,2,4-trioxanes via acetalisation/oxa-Michael cascade,²²⁶ and recent findings on the oxidative dearomatisation of *p*-substituted phenols,⁷⁷ Rovis *et al.* published a novel asymmetric synthesis of 1,2,4-trioxanes combining these two strategies (Scheme 30).¹⁹⁵ The acetalisation/oxa-Michael addition step was catalysed by a chiral 1,1'-spirobiindane-7,7'-diol (SPINOL) derived phosphoric acid and a thiourea derivative as co-catalyst. The scope of the reaction was expanded using different aldehydes and *p*-peroxyquinols, giving twenty 1,2,4-trioxanes with high enantiomeric excess (ee) and diastereomeric ratio (dr), and yields between 45 – 95%.



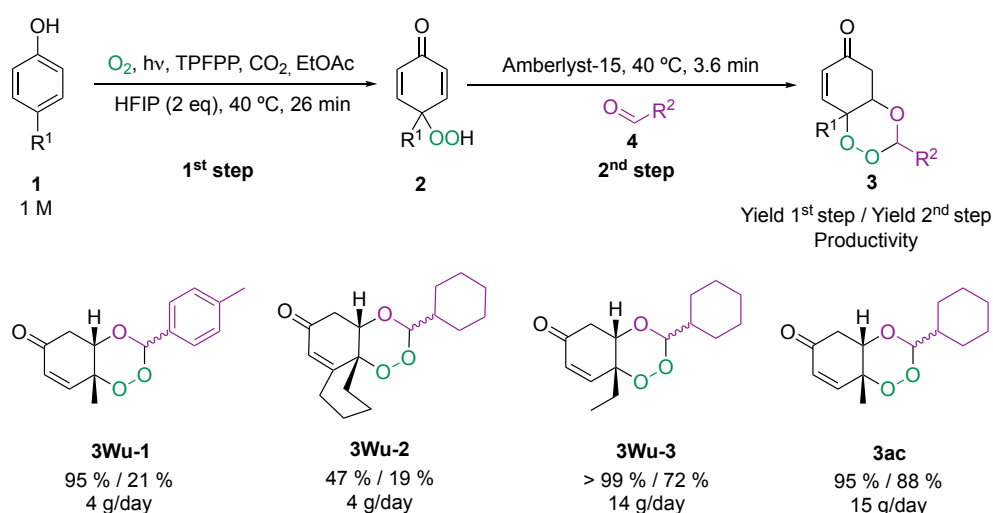
Scheme 30. Synthesis of 1,2,4 trioxanes via oxidative dearomatisation of *p*-alkyl-phenols followed by acetalisation/oxa-Michael cascade.¹⁹⁵

This procedure has proven to be an efficient way to synthesise 1,2,4-trioxanes with high yields, selectivity, and good functional group tolerance. Further applications in the synthesis of other 1,2,4-trioxanes have been reported, including studies on their cytotoxicity and pharmacokinetics.^{232, 233} However, this procedure presents several challenges. The use of costly and toxic halogenated solvent dichloroethane (DCE), long reaction times, and the need to isolate hazardous *p*-peroxyquinols hampers the scalability of this process from a safety,

economical, and environmental point of view. In fact, this procedure has never been scaled-up above 0.1 mmol scale (< 40 mg of trioxane isolated).

4.2. Aims and general strategy

Given the successful results obtained for the continuous flow dearomatisation of *p*-substituted phenols **1** (Chapter 3) combined with the methodology developed by Rovis and co-workers,¹⁹⁵ our research group developed a novel continuous flow telescoped synthesis of 1,2,4-trioxanes **3**. The photooxidation of *p*-substituted phenols **1** using singlet oxygen and supercritical CO₂ was coupled to an acetalisation/oxa-Michael cascade with an aldehyde **4**, catalysed by Amberlyst-15 (Scheme 31). Due to incompatibility for the second step of the process, which will be discussed in the next section, the co-solvent was changed to EtOAc.



Scheme 31. Summary of previous work on the continuous flow telescoped synthesis of 1,2,4-trioxane in our research group.¹⁵²

The aims for this Chapter were:

- To expand the scope of the continuous flow dearomatisation of *p*-substituted phenols **1** using EtOAc as the co-solvent.
- To expand the scope of the continuous flow telescoped synthesis of 1,2,4-trioxanes

The following strategies were considered to address the above aims:

1. The photooxidation of *p*-substituted phenols **1** in EtOAc was first investigated with the compounds previously synthesised in MeOH.
2. Next, the scope was expanded to *p*-substituted phenols **1** bearing other functional groups at *para*-position.

3. Following that, the scope of the telescoped synthesis of 1,2,4-trioxanes **3** was expanded, screening various aldehydes **4** and *p*-peroxyquinols **2**.
4. Different thermo reactor designs were considered and built in an attempt to increase the yield for the cyclisation step.

4.3. Results and discussion

Following the recent work developed by Dr. Wu, the scope of 1,2,4-trioxanes was further explored. In this continuous flow multi-step synthesis, the photooxidation of *p*-substituted phenols **1** using singlet oxygen in supercritical CO₂ was coupled with an acetalisation/oxa-Michael addition between *p*-peroxyquinols **2** and aldehydes **4**. This cyclisation step was undertaken using a packed bed tubular reactor (thermo reactor) filled with an acid catalyst Amberlyst-15 (Figure 37).

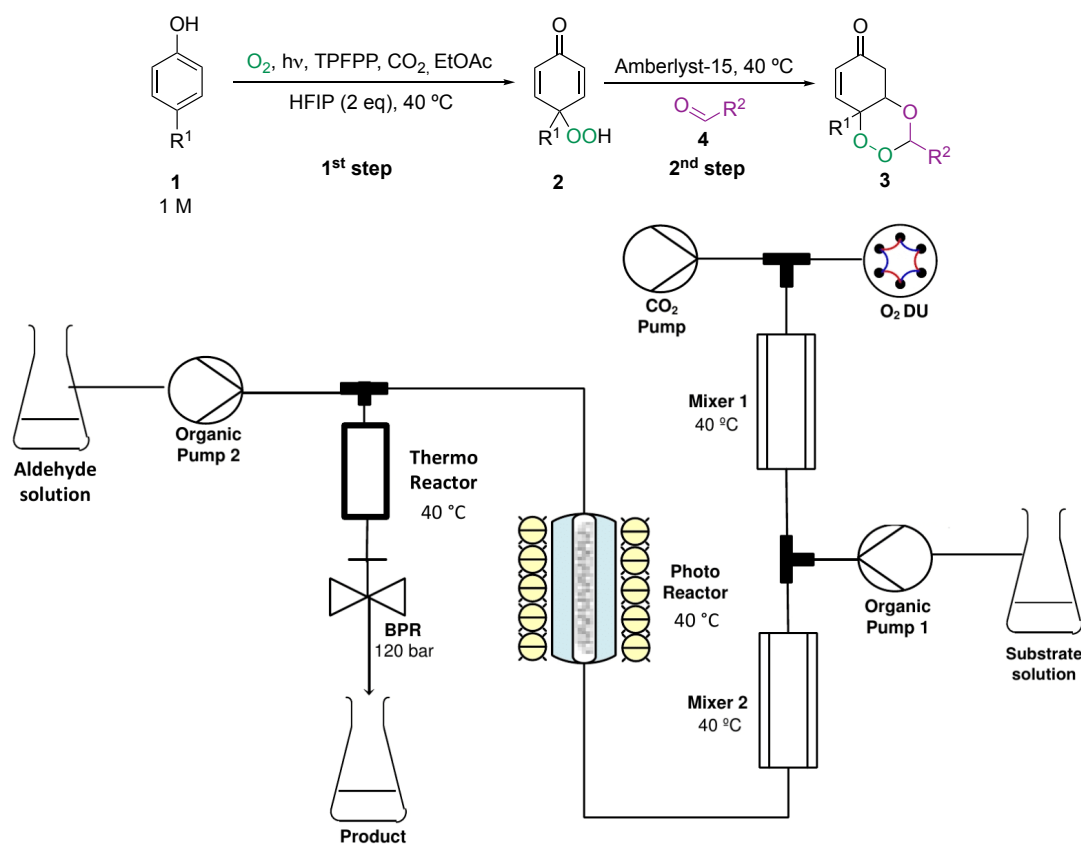
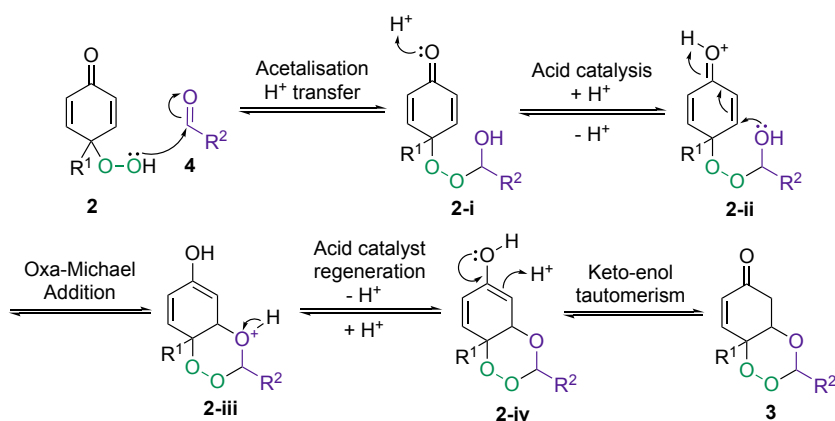


Figure 37. Top: general scheme of the telescoped synthesis of 1,2,4-trioxanes. Bottom: a simplified scheme of the high-pressure flow system used: photo reactor (10 mm outer diameter 'o.d.', 240 mm length, 1 mm wall thickness, effective volume = 5.2 mL, filled with 38 glass beads with 6 mm o.d., at 40 °C); thermo reactor (1/4 inch o.d., 1 mm wall thickness, 15 cm length, loaded with Amberlyst-15 and glass beads at 40 °C, high trip = 50 °C); cooling baths (photo reactor = 35.5 °C, LED lights = - 5 °C); trips (system set pressure = 120 bar, high trip = 140 bar; oxygen set pressure = 180 bar, high trip = 190 bar, low trip = 160 bar; mixers set temperature = 40 °C, high trip = 50 °C). Flow rates and residence times: (1) CO₂ 0.15 mL/min, HPLC pumps 0.05 mL/min, residence time (photo reactor) = 26 min and (thermo reactor) = 3.6 min; (2) CO₂ 0.2 mL/min, HPLC pumps 0.1 mL/min, residence time (photo reactor) = 17 min and (thermo reactor) = 2.3 min. Concentration of TPFPP = 0.3 mol%. Biphenyl used as the internal standard for ¹H NMR spectroscopy quantification.

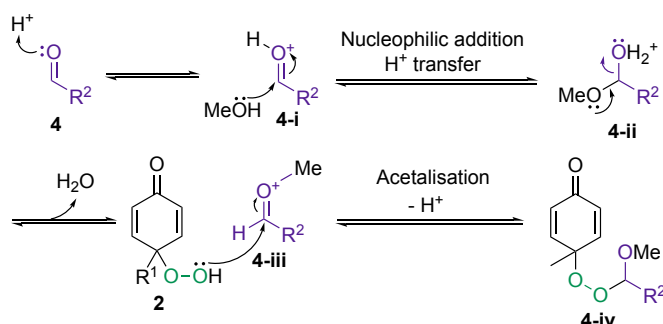
4.3.1. Reaction Mechanism

The proposed mechanism for the cyclisation step starts with the nucleophilic attack of the hydroperoxyl group in *p*-peroxyquinol **2** to the electrophilic site of the aldehyde **4**, leading to peroxyhemiacetal **2-i**. The oxa-Michael addition step is initiated by the activation of the ketone by Amberlyst-15 to form **2-ii**, followed by a 1,4-conjugated addition of the hydroxy group to the cyclohexadienone double bond in **2-iii**. After regeneration of the acid catalyst to form **2-iv**, a keto-enol tautomerisation affords the 1,2,4-trioxane **3** (Scheme 32).



Scheme 32. Proposed mechanism for the formation of 1,2,4-trioxanes **3**.

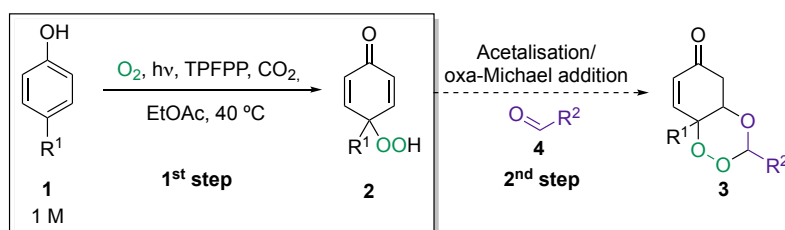
One of the challenges in performing multi-step reactions is to find a suitable co-solvent for both stages of the process, whilst maintaining a homogeneous solution throughout the process to avoid blockages within the flow equipment. In Chapter 3, MeOH was used as the co-solvent for the dearomatisation of *p*-substituted phenols **1**. However, previous studies from Dr. Wu showed that this solvent was not suitable for the oxa-Michael addition step.¹⁵² This is because MeOH is also nucleophilic, and it attacks the protonated aldehyde **4-i**, to form the species **4-ii** (Scheme 33). This tetrahedral intermediate then collapses into **4-iii** through elimination of water. Acetalisation between *p*-peroxyquinol **2** and **4-iii** gives the peroxyacetal **4-iv**, regenerating the acid catalyst. For this reason, the co-solvent was changed to ethyl acetate (EtOAc).



Scheme 33. Proposed mechanism for the side reaction between *p*-peroxyquinol **2** and aldehyde **4**.

4.3.2. Dearomatisation of *p*-substituted phenols **1** using EtOAc as co-solvent

As the dearomatisation of *p*-substituted phenols had been previously carried out using MeOH as a co-solvent, the reactions had to be repeated using an alternative medium to test its suitability (Scheme 34).



Scheme 34. Dearomatisation of *p*-substituted phenols in EtOAc in the proposed telescoped synthesis of 1,2,4-trioxanes.

Previous studies have described good results on the synthesis of 1,2,4-trioxanes in dichloroethane.¹⁹⁵ However, halogenated solvents are not compatible with the high-pressure flow setup used, as there is potential for corrosion of the tubing.²³⁴ Ethyl acetate was chosen as it is considered a recommended solvent²³⁵ and is easily removed from the reaction mixture. In addition, the absorbance spectrum of the photosensitiser TPFPP in EtOAc overlaps with the emission spectrum of the white LED lights used in the system (Figure 38).

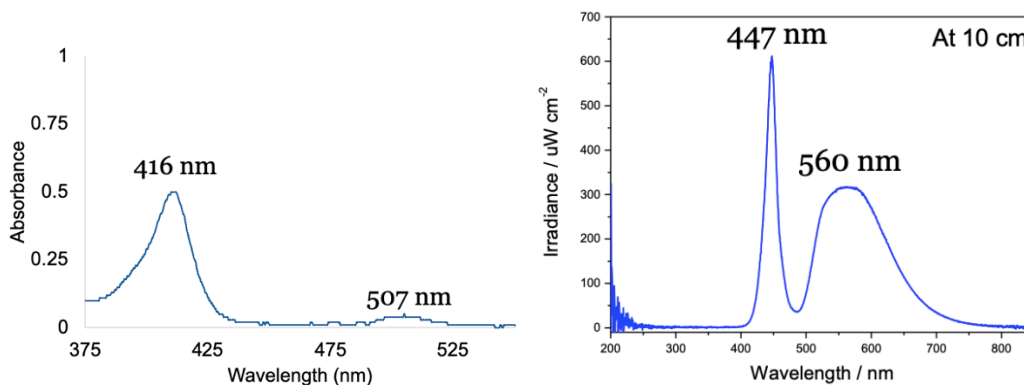
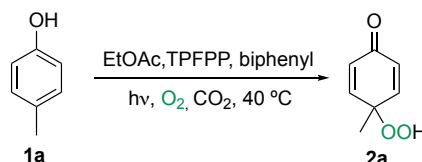


Figure 38. Left: absorbance spectrum of TPFPP in EtOAc (concentration = 0.8 $\mu\text{g/mL}$). Right: emission spectrum of the Citizen LED lights.

The first compound to be tested for the photooxidation of *p*-substituted phenols using EtOAc as the co-solvent was *p*-cresol **1a** (Table 6). In the first experiment (Entry 1 – Table 6), poor conversion (31%) and yield (28%) were obtained in 35 minutes of residence time. To improve the reaction conversion, yield, and productivity, a co-catalyst hexafluoro-2-propanol (HFIP) was added to the starting solution (Entry 2 – Table 6). Even with a shorter residence time of 26 min, the addition of HFIP seemed to be crucial for this reaction, as over a threefold increase in yield (95%) and projected productivity (10 g/day) was observed.

Table 6. Continuous flow dearomatisation of *p*-cresol **1a** in EtOAc.

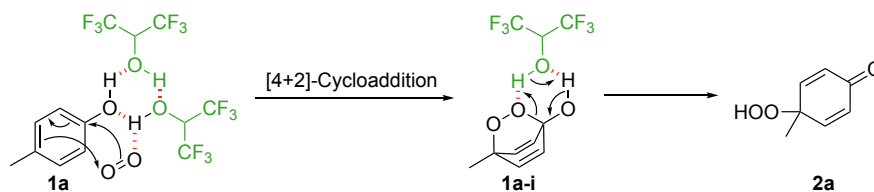


Entry	Residence time (min)	Co-catalyst	Conversion of 1a (%)	Yield of 2a (%)	Projected productivity (g/day)
1	35	-	31	28	3
2	26	HFIP (2 eq.)	95	95	10

High-pressure setup and other reaction parameters are shown in Figure 37. The thermo reactor was not used for this reaction and the aldehyde solution was substituted for EtOAc only.

HFIP is miscible with most organic solvents and has low nucleophilicity compared to other non-fluorinated alcohols. Particularly, HFIP has a strong ability to form hydrogen bonds and to stabilise polarised species.²³⁶ Based on Li and co-workers recent findings on the effect of HFIP in hydride-transfer,²³⁷ a catalytic mechanism was proposed (Scheme 35). It was suggested that two molecules of HFIP could form an aggregate with *p*-cresol **1a** and oxygen

through hydrogen bonding, bringing the reactants closer and assisting the [4+2] cycloaddition. The endoperoxide **1a-i** would then form a second cluster with the co-catalyst, facilitating the hydride-transfer to give *p*-peroxyquinol **2a**.

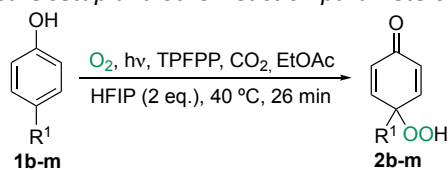


Scheme 35. Proposed catalytic mechanism for the [4+2] cycloaddition assisted by HFIP based on Li and co-workers mechanism.²³⁷

4.3.3. Dearomatisation of *p*-substituted phenols **1** using EtOAc as co-solvent and HFIP as co-catalyst: scope of reaction

The scope of the continuous flow oxidative dearomatisation of *p*-substituted phenols **1** in scCO₂ was explored using EtOAc as the co-solvent and HFIP as the co-catalyst. Eleven *p*-peroxyquinols **2** were synthesised from mono-, di-, and tri- substituted phenols, as well as phenols bearing various substituents in the *para* position, as shown in Table 7.

Table 7. Summary of results on the continuous flow dearomatisation of *p*-substituted phenols **1** in EtOAc/HFIP. High-pressure setup and other reaction parameters are shown in Figure 37.



Entry	Compound	Concentration (M)	NMR Conversion of 1 (%)	NMR yield of 2 (%)	Projected productivity (g/day)
1		1.0	> 99	> 99	11
2		1.0	> 99	> 99	12
3		1.0	Blockage		
		0.5	48	49	3
4		1.0	48	49	6
5		0.5	11	9	1
6		0.1	Blockage		
		0.05	Blockage		
7		1.0	54	50	10
8		1.0	> 99	> 99	12
9		1.0	50	42	8
10		1.0	71	58	9
11		0.5	73	66 (2m : 2m' = 1: 16)	2m = 0.3 2m' = 4

Dearomatisation of phenols 1b, 1c, 1d, 1e, and 1f

The photooxidation of *p*-substituted phenols was first carried out with seven phenols previously tested in Chapter 3, using EtOAc and HFIP. Yields obtained for *p*-peroxyquinols **2b** to **2e** (Entries 1 to 4 – Table 7) in EtOAc/HFIP were similar to the ones in MeOH in Chapter 3 (**2b** = >99%, **2c** = >99%, **2d** = 59%, **2e** = 46%). For phenol **2d** (Entry 3 – Table 7), the concentration had to be lowered to 0.5 M, as the system tripped when the reaction was performed at 1 M. As for phenol **2f** (Entry 5 – Table 7), the yield dropped almost a third in EtOAc/HFIP (9%) when compared to the reaction in MeOH (26%).

Dearomatisation of 4-(hydroxymethyl)phenol 1g and 4-((tert-butyl)dimethylsilyloxy)methyl)phenol 1h

In Chapter 3, the dearomatisation of 4-(hydroxymethyl)phenol **1g** was unsuccessful in MeOH as the high-pressure system tripped during the reaction. The experiment was then repeated in EtOAc/HFIP (Entry 6 – Table 7). At 0.1 M concentration, the system tripped due to a sudden raise in the system pressure after 1 h of reaction. To assess whether the blockage was caused by the starting solution or the *p*-peroxyquinols formed, the same reaction was carried out once again in the same conditions, but with the LED lights turned off to inhibit the formation of $^1\text{O}_2$. The system shut down within the same time frame, concluding that precipitation from the starting solution was causing the blockage. The substrate concentration was then halved, which resulted in the blockage occurring after 2 h of reaction. It was then hypothesised that the precipitation of the highly polar starting material was occurring when the solution was diluted with scCO_2 .

To test this hypothesis, a phase behaviour experiment was performed in a high-pressure static view cell, with a mechanical stirrer. A solution of 4-hydroxymethyl phenol **1g**, HFIP, TPFPP, and biphenyl in EtOAc was put in a vial inside the view cell (Figure 39 - left), pressurised and heated up to mimic the same conditions in flow (120 bar, 40 °C). However, the strong colour of TPFPP made visual analysis difficult and the solid precipitation observed could not be attributed specifically to the phenol **1g** due to the presence of other compounds in the mixture (Figure 39 - right).

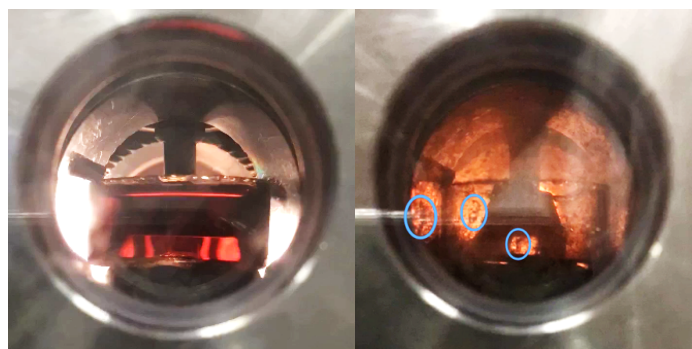


Figure 39. Solubility test in a high-pressure static view cell with a solution of phenol **1g**, HFIP, TPFPP and biphenyl in EtOAc and CO₂. Left: solution inside the view cell at 69 bar, 40 °C; right: view cell at 120 bar, 40 °C. The blue circles correspond to solid precipitation.

A second experiment with only 4-(hydroxymethyl) phenol **1g**, EtOAc and CO₂ was then performed (Figure 40). In the first picture (Figure 40 - A), CO_{2(g)} and EtOAc_(l) are not miscible. The view cell was then heated up to 40 °C and slowly pressurised up to 120 bar. The cloudy state in Figure 40 - B represents the critical point in which the density of CO₂ largely fluctuates, resulting in light scattering (critical opalescence).²³⁸ The supercritical phase is achieved when the temperature and pressure are above the critical point (73.8 bar and 31.1 °C), as shown in Figure 40 - C. From this experiment it was demonstrated that 4-hydroxymethyl phenol **1g** was not soluble in the conditions performed in flow (120 bar and 40 °C) in scCO₂, as shown in Figure 40 - C, which explains the blockage issue that resulted in the system trip.

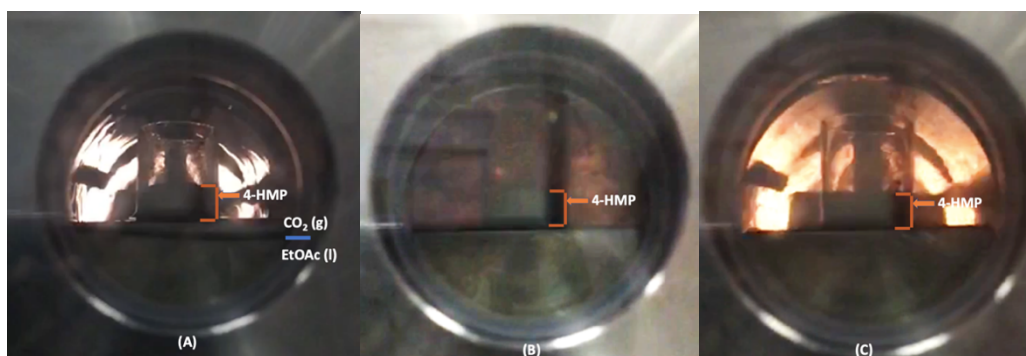


Figure 40. Solubility test in a high-pressure static view cell with 4-(hydroxymethyl)phenol **1g**, EtOAc and CO₂. The orange bars show the amount of 4-(hydroxymethyl)phenol **1g** in the vial, and the blue bar shows the liquid-gas phases. (A) Vial with phenol **1g** inside the view cell, filled with EtOAc_(l) and CO_{2(g)} at 69 bar, 40 °C; (B) critical point, in which CO₂ density largely fluctuates (critical opalescence); (C) Supercritical phase between CO₂ and EtOAc, with most of 4-(hydroxymethyl)phenol **1g** not soluble in solution.

Given the dearomatisation of 4-(hydroxymethyl)phenol **1g** was not possible in these conditions, the photooxidation of 4-((*tert*-butyldimethylsilyloxy)methyl)phenol **1h** with the

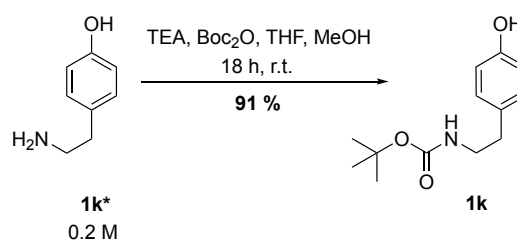
benzyl group protected with *tert*-butyldimethylsilyl was repeated in EtOAc/HFIP (Entry 7 – Table 7). The moderate conversion (54%) and yield (50%) obtained for **2h** were slightly lower when compared to the ones obtained in MeOH (conversion of 54% and yield of 56%).

Dearomatisation of 5-indanol **1j**

After carrying out the dearomatisation of the phenols previously tested in Chapter 3, the scope was expanded to other four *p*-substituted phenols **1**. The photooxidation of 5-indanol **1j**, which is a bicyclic compound with a cyclopentene ring attached to the aromatic ring, was carried out (Entry 8 – Table 7). Although the reaction reached full conversion and quantitative yield of **2j** in 1.5 h, the system over pressured due to solid precipitation in 2 h of reaction.

Dearomatisation of *N*-Boc-tyramine **1k**

Next, we decided to investigate tyramine **1k***, a fermentation product of tyrosine that is formed by a decarboxylation reaction through tyrosine decarboxylase enzymes. To avoid any side reactions, the free amino group in **1k*** was protected with Boc₂O before carrying out the photooxidation²³⁹ (Scheme 36). *N*-Boc-tyramine **1k** was obtained as a white solid in excellent isolated yield of 91%.



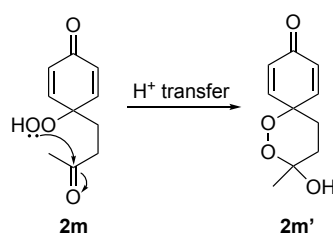
Scheme 36. Protection of tyramine **1k*** with Boc₂O

The dearomatisation of *N*-Boc-tyramine **1k** (Entry 9 – Table 7) gave a moderate yield of 42% and projected productivity of 8 g/day. This represents almost a fivefold increase in yield compared to *N*-Boc-*L*-tyrosine methyl ester **1f**.

Dearomatisation of 3-(4-hydroxyphenyl)propionate **1l** and 4-(4-hydroxyphenyl)-2-butanone **1m**

For the two phenols tested above, the viability of a spontaneous intramolecular cyclisation was investigated with a phenol bearing either an ester **1l** (Entry 10 – Table 7) or a ketone **1m** (Entry 11 – Table 7) in the *para* substituent alkyl chain .

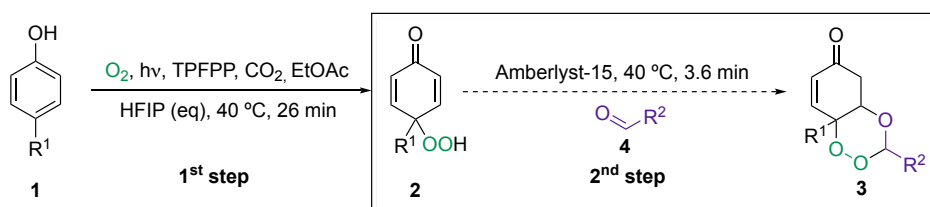
3-(4-Hydroxyphenyl) propionate **1l** gave *p*-peroxyquinol **2l** in moderate yield (58%) and high projected productivity (9 g/day), and the ester functionality remained intact during the photooxidation. However, *p*-peroxyquinol **2m** obtained from 4-(4-hydroxyphenyl)-2-butanone **1m** spontaneously cyclised to give a spirocyclic peroxyhemiacetal **2m'** (62% yield), as shown in Scheme 37. Products **2m** and **2m'** were obtained as a yellow oil containing a ratio of **2m**: **2m'** of 1:6. This inseparable mixture was also reported by Carreño and co-workers with a similar ratio of **2m**: **2m'** of 19:81.²⁴⁰



Scheme 37. Mechanism for the intramolecular acetalisation of *p*-peroxyquinol **2m**.

4.3.4. Continuous flow telescoped synthesis of 1,2,4-trioxanes

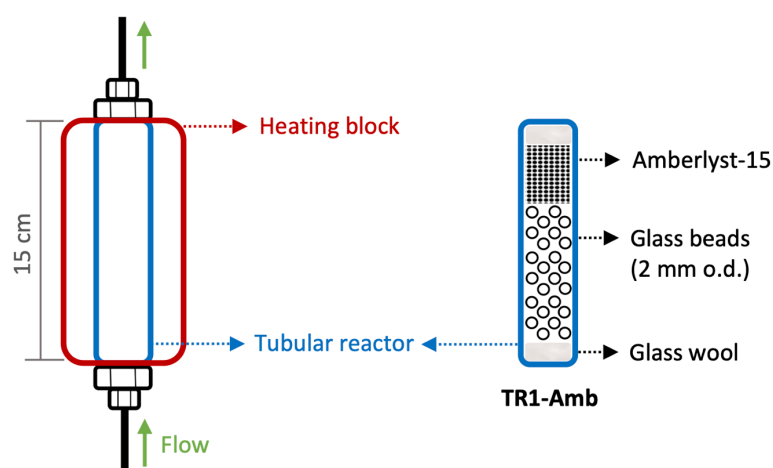
Following the synthesis of eleven *p*-peroxyquinols using EtOAc (co-solvent) and HFIP (co-catalyst) in continuous flow, the scope of the synthesis of 1,2,4-trioxanes was explored using Amberlyst-15 as an acid catalyst (Scheme 38).



Scheme 38. Acetalisation/oxa-Michael addition cascade in the proposed telescoped synthesis of 1,2,4-trioxanes. High-pressure setup and other reaction parameters are shown in Figure 37.

Amberlyst-15 is a robust polymeric acid catalyst which has been reported to facilitate acetalisation/Michael cascade reactions.²⁴¹ It can also be immobilised in packed bed

reactors, simplifying purification, and its porosity enables easy penetration of the solution in supercritical CO₂. For these reasons, a thermo reactor designed by Dr. Wu was added to the high-pressure flow setup.¹⁵² The thermo reactor **TR1-Amb** consists of an electric-heated tubular reactor packed with Amberlyst-15 and glass beads (Scheme 39). Glass beads are added at the bottom of the reactor to enable pre-mixing of the two streams of *p*-peroxyquinol **2** and aldehyde **4** solutions before they come into contact with Amberlyst-15. A layer of glass wool was put at each end of the tubular reactor to prevent the solid catalyst to flow into the system.

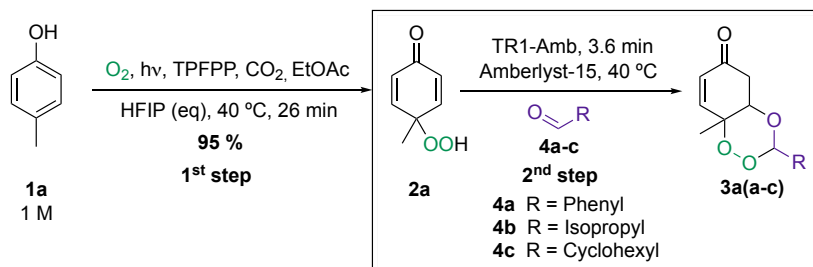


*Scheme 39. Schematic of thermo reactor design **TR1-Amb**: 1/4 inch outer diameter 'o.d.', 1 mm wall thickness, 15 cm length, effective volume = 0.9 mL, loaded with 0.75 g of Amberlyst-15, 0.85 g of glass beads 2 mm o.d. and glass wool layer as each end of the tubular reactor.*

Expanding the scope of 1,2,4-trioxanes using different aldehydes

The phenol derivative chosen for initial investigation was *p*-cresol **1a** as it provided excellent yield of 95% of *p*-peroxyquinol **2a** and the methyl substituent provides low steric hindrance towards the subsequent cyclisation step. Three 1,2,4-trioxanes were synthesised varying the aldehyde counterpart for the acetalisation/oxa-Michael addition step, using Amberlyst-15 at 40 °C (Table 8). 1,2,4-Trioxanes were numbered by combining the codes from the *p*-peroxyquinol **2** and the aldehyde **4** that originated them.

Table 8. Expanding the scope of the continuous flow telescoped synthesis of 1,2,4-trioxanes **3** using different aldehydes **4**. High-pressure setup and reaction parameters are shown in Figure 37.



Entry	Compound	Yield (%)		Overall yield of 3 (%)	Projected productivity (g/day)
		1 st step	2 nd step		
1	 (±)- 3aa	95	36	34	6
2	 (±)- 3ab	95	98	93	14
3a^a	 (±)- 3ac	95	88	84	15
3b^b	 (±)- 3ac	95	62	59	21

These reactions were performed in collaboration with Dr. Wu.^a Reaction performed solely by Dr. Wu.

^b Residence times: 1st step = 17 min and 2nd step = 2.3 min.

The stereochemistry of the 1,2,4-trioxanes obtained was deduced from XRD analyses of 1,2,4-trioxanes synthesised in collaboration with Dr. Wu,¹⁵² ¹H NMR spectroscopy of the crude reactions, and literature data.^{195, 228} The ¹H NMR spectroscopy of all crude reactions showed only signals for one diastereoisomer. In addition, X-ray analysis of 1,2,4-trioxane **3ac** and other examples reported by Jefford²²⁸ and Rovis¹⁹⁵ showed the formation of *cis*-fused 1,2,4-trioxanes with high dr (>20:1) and were isolated as a single diastereoisomer (Figure 41).

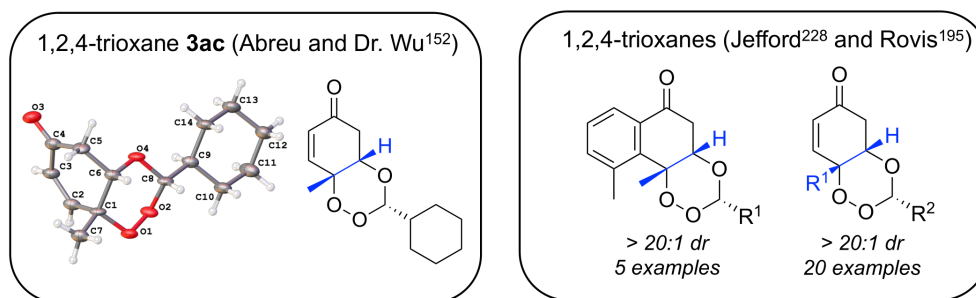
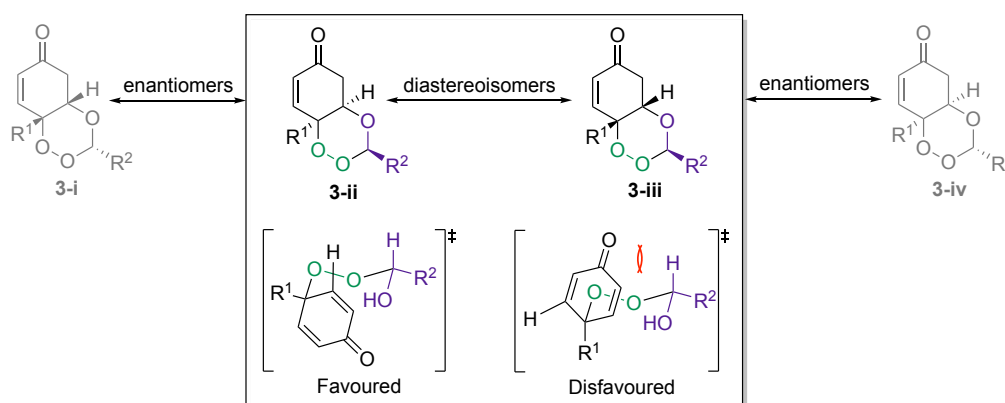


Figure 41. Left: single-crystal XRD and structure of 1,2,4-trioxane **3ac** (Abreu and Dr. Wu¹⁵²). Right: structure of 1,2,4-trioxanes synthesised by Jefford²²⁸ and Rovis.¹⁹⁵ The *cis* stereochemistry on the 1,2,4-trioxanes is highlighted in blue.

The formation of *cis*-fused 1,2,4-trioxanes is kinetically controlled and the high diastereoselectivity arises from the reduced 1,3-diaxial interaction in the cyclisation transition state,²⁴² giving the favoured 1,2,4-trioxanes (pair of enantiomers **3-i** and **3-ii**) as shown in Scheme 40.



Scheme 40. Diastereoselective control on the formation of 1,2,4-trioxanes from the reduced 1,3-diaxial interaction in the cyclisation transition state. One diastereoisomer is obtained as a mixture of enantiomers (**3-i** and **3-ii**).

The poor overall yield of **3aa** (Entry 1 – Table 8) might be explained by the fact that electron-rich aldehydes such as benzaldehyde **4a** lead to a peroxyhemiacetal intermediate which is less thermodynamically favoured.²⁴³

Although the best yield was achieved when isobutyraldehyde **4b** was used (Entry 2 – Table 8), cyclohexanecarboxaldehyde **4c** was chosen for further screening of the reaction (Entry 3a – Table 8). This is because **4c** gave excellent yield (84%) and is less prone to polymerisation compared to **4b**.

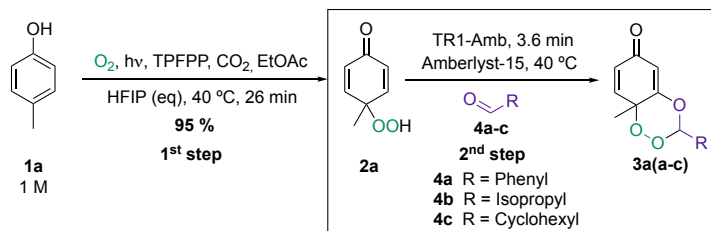
To demonstrate that production of 1,2,4-trioxanes might be further increased, the experiment with **4c** was carried out with shorter residence time (Entry 3b – Table 8).

Although there was a drop in yield from 84% (Entry 3a – Table 8) to 59%, the projected productivity was raised to 21 g/day in comparison to 15g/day in the previous experiment.

Expanding the scope of 1,2,4-trioxanes using different *p*-substituted phenols

After screening different aldehydes for the synthesis of 1,2,4-trioxanes using *p*-cresol **1a**, another nine *p*-substituted phenols **1** were investigated for the acetalisation/oxa-Michael cascade step using cyclohexanecarboxaldehyde **4c** (Table 9).

Table 9. Expanding the scope of the continuous flow telescoped synthesis of 1,2,4-trioxanes **3** using different phenols **1**. High-pressure setup and reaction parameters are shown in Figure 37.

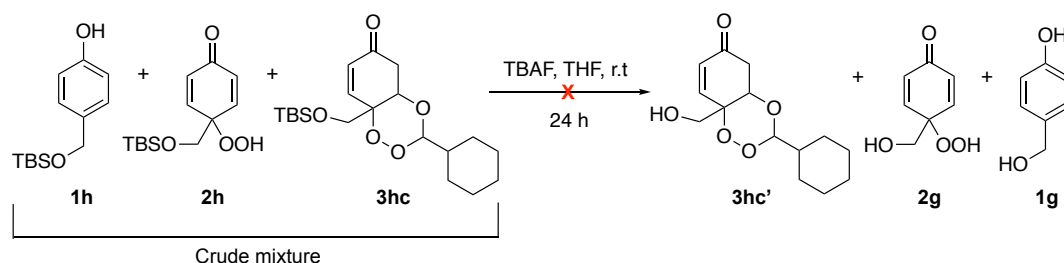


Entry	Compound	Concentration (M)	NMR yield (%)		Overall NMR yield of 3 (%)	Projected productivity (g/day)
			1 st step	2 nd step		
1		1.0	> 99	85	84	16
2		1.0	> 99	0	0	0
3		0.5	49	0	0	0
4		1.0	49	82	40	9
5^a		1.0	42	0	0	0
6^b		1.0	50	56	28	8
7		1.0	58	90	52	12
8		0.5	66	0	0	0

^a Reaction performed by Dr. Wu. ^b Product not isolated.

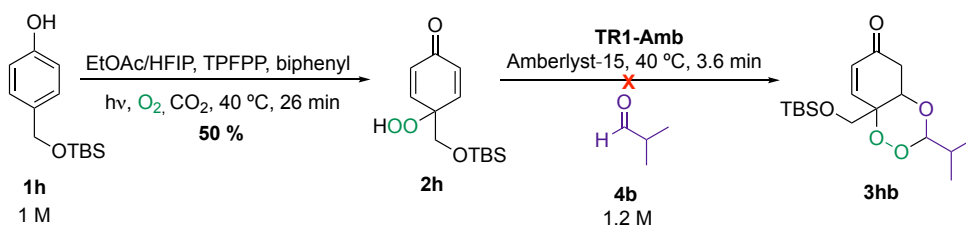
The synthesis of 1,2,4-trioxanes **3bc** (Entry 1 – Table 9), **3ec** (Entry 4 – Table 9) and **3lc** (Entry 7 – Table 9) gave excellent yields for the 2nd step of up to 90%. In particular, 1,2,4-trioxane **3bc** had high overall yield (84%) and projected productivity of 16 g/day (Entry 1 – Table 9) owing to the quantitative yield for the 1st step (> 99%). On the other hand, moderate overall yields of **3ec** (Entry 4 – Table 9) and **3lc** (Entry 7 – Table 9) were achieved as their photooxidation step were not as efficient as **3bc**. Although the overall yields were moderate, the projected productivity of 1,2,4-trioxanes remained excellent (~10 g/day).

Purification challenges arose in the synthesis of 1,2,4-trioxane **3hc** (Entry 6 – Table 9). ¹H NMR spectroscopy and HRMS analyses showed the formation of **3hc**, but the product could not be purified. This compound was found to be unstable on silica during flash chromatography purification, which was confirmed by a 2D thin layer chromatography (TLC) analysis. A sample of the crude mixture was then concentrated under vacuum and a crystallisation with diethyl ether was attempted, but no crystals could be formed. In another crude sample containing the starting phenol **1h**, *p*-peroxyquinol **2h** and 1,2,4-trioxane **3hc**, tetrabutylammonium fluoride 'TBAF' was added to deprotect the silyl ether group²⁴⁴ in an attempt to facilitate purification. However, deprotected trioxane **3hc'** was not identified in the ¹H NMR spectroscopy analysis after 24 h of reaction and a complex mixture was formed (Scheme 41).



Scheme 41. Attempted deprotection of crude mixture containing phenol **1h**, *p*-peroxyquinol **2h** and trioxane **3hc** with TBAF. **X** represents that 1,2,4-trioxane **3hc'** could not be obtained.

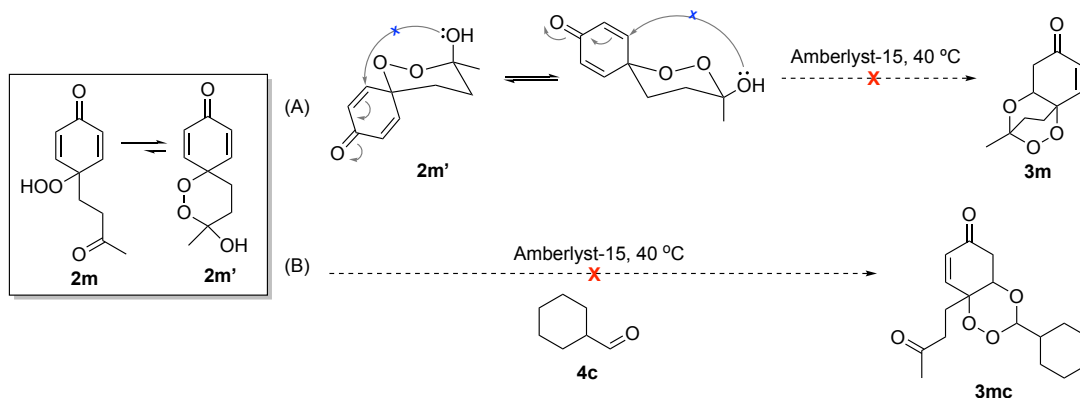
Given the purification of **3hc** was unsuccessful, the synthesis of a similar 1,2,4-trioxane from *p*-peroxyquinol **2h** was attempted, using isobutyraldehyde **4b** instead of cyclohexancarboxaldehyde **4c**. The reaction was monitored by ¹H NMR spectroscopy for 4 h, but no signals for the 1,2,4-trioxane **3hb** were observed (Scheme 42).



Scheme 42. Attempted continuous flow telescoped synthesis of 1,2,4-trioxane **3hb** from *p*-peroxyquinol **2h** and isobutyraldehyde **4b**. **X** represents that product **3hb** could not be obtained.

1,2,4-Trioxanes **3cc** (Entry 2 – Table 9), **3dc** (Entry 3 – Table 9), **3Wu-4** (Entry 5 – Table 9) and **3mc** (Entry 8 – Table 9) could not be obtained using this methodology. The steric hindrance of the *para* substituent in the transition state to form the 1,2,4-trioxanes **3dc** (Entry 3 – Table 9) and **3Wu-4** (Entry 5 – Table 9) might explain the disfavoured formation of the product. The instability of 1,2,4-trioxane **3cc** (Entry 2 – Table 9) combined with steric effects disfavours the formation of this product.

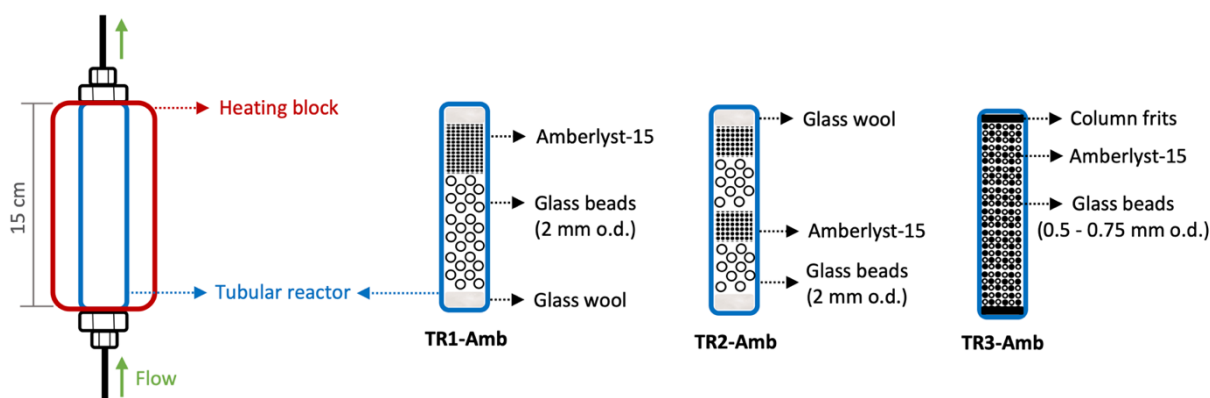
The catalysed intramolecular cyclisation of *p*-peroxyquinol **2m'** to give 1,2,4-trioxane **3m** (Scheme 43 - A) and the acetalisation/oxa-Michael addition between **2m** and **4c** (Scheme 43 - B) were also investigated. The formation of 1,2,4-trioxane **3m** was thought to be hampered by the unfavoured transition state in **2m'**. Then, it was attempted to shift the equilibrium to **2m** by reacting with aldehyde **4c**, but no 1,2,4-trioxane **3mc** was observed (Entry 8 – Table 9). An acid-catalysed aldol reaction between the ketone in **2m** and aldehyde **4c** is a possible side reaction that could occur in these conditions.



Scheme 43. (A) Proposed intramolecular cyclisation of **2m'** to form **3m**; (B) Proposed acetalisation/oxa-Michael addition between **2m** and **4c** to give trioxane **3mc** (B). **X** represents an unfavoured attack of the hydroxyl group and **X** represents that the product could not be formed.

Continuous flow telescoped synthesis of 1,2,4-trioxanes using different thermo reactor designs

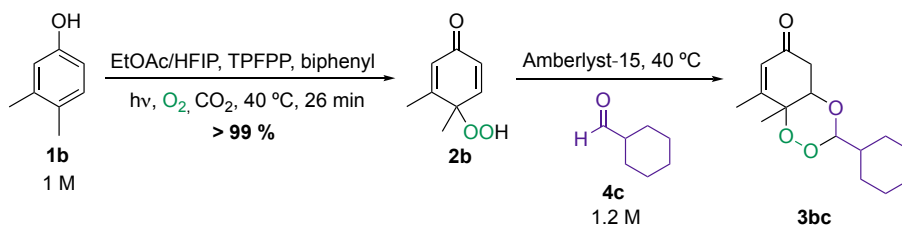
To improve the yields for the second step of the process, different thermo reactor designs were developed and tested (Scheme 44). Based on thermo reactor **TR1-Amb**, 0.75 g of Amberlyst (Amb) and 0.85 g of glass beads were used for design **TR2-Amb**, split in four alternate layers instead of two. In the last design **TR3-Amb**, the tubular reactor was packed with a mixture of 0.75 g Amb and 0.85 g glass beads, but with the outer diameter of glass beads decreased to 0.5 – 0.75 mm.



Scheme 44. Schematic of thermo reactor designs, using a tubular reactor (1/4 inch outer diameter 'o.d.', 1 mm wall thickness, 15 cm length) loaded with glass beads and Amberlyst-15 (Amb): **TR1-Amb**: effective volume = 0.9 mL, bottom layer = glass beads (0.85 g, 2 mm o.d.), top layer = Amb (0.75 g), glass wool layer at each end. **TR2-Amb**: effective volume = 0.9 mL, glass beads = 0.85 g, 2 mm o.d. (two layers), Amb = 0.75 g (two layers), glass wool layer at each end. **TR3-Amb**: effective volume = 1.1 mL, mixture of glass beads (0.85 g, 0.5 – 0.75 mm o.d.) and Amb (0.75 g), column frits at each end.

To test the efficiency of these thermo reactor designs, they were employed in the synthesis of 1,2,4-trioxane **3bc** as a model reaction. The yields and productivities were then compared to the original design **TR1-Amb** (Table 10).

Table 10. Telescoped synthesis of trioxane **3bc** using different thermo reactor designs. High-pressure setup and reaction parameters are shown in Figure 37.



Entry	Type of thermo reactor	Residence time 2 nd step (min)	NMR yield 2 nd step (%)	Overall NMR yield 3bc (%)	Projected productivity 3bc (g/day)
1	TR1-Amb	3.6	85	84	16
2	TR2-Amb	3.6	90	89	17
3	TR3-Amb	4.4	95	94	18

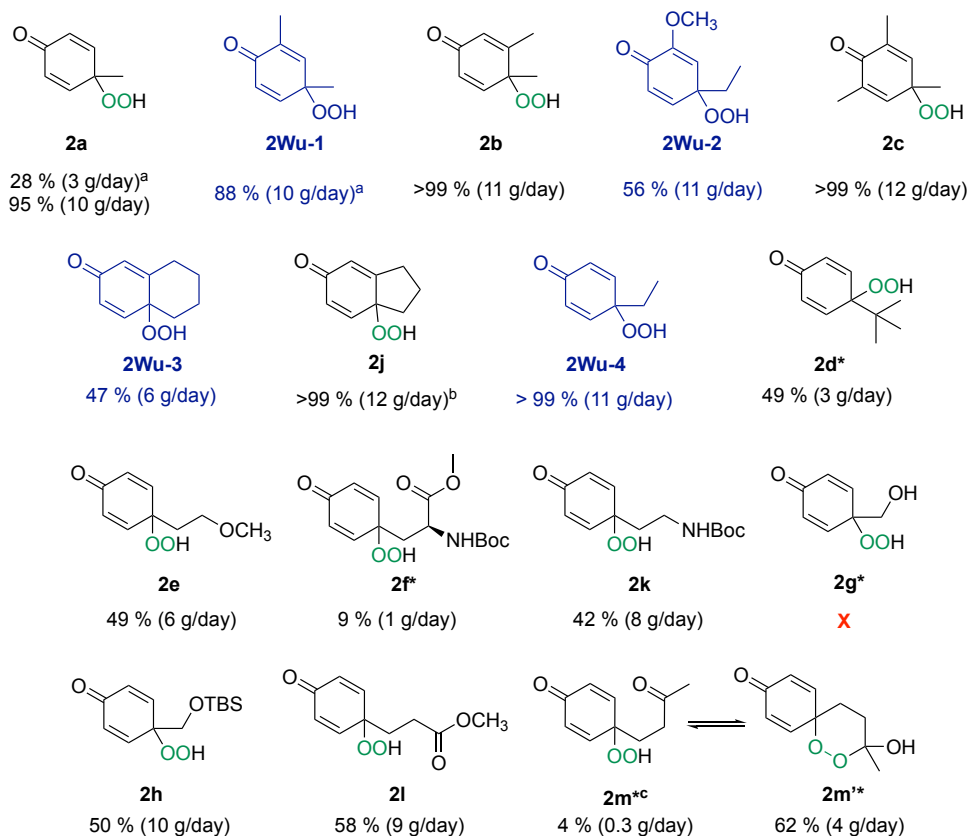
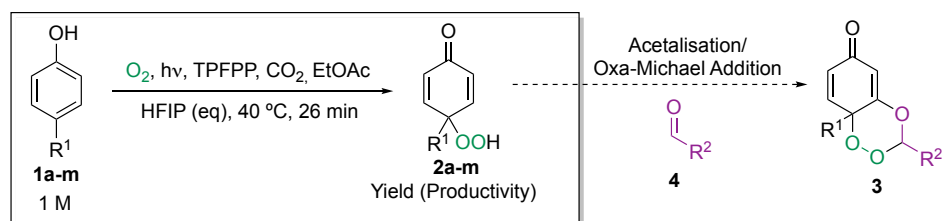
The reaction carried out with **TR2-Amb** resulted in an increase of 5% and 1 g/day in overall yield and projected productivity of **3bc** respectively (Entry 2 – Table 10) when compared to the experiment with **TR1-Amb** (Entry 1 – Table 10). With the design **TR3-Amb** (Entry 3 – Table 10), there was a 10% yield increase when compared to **TR1-Amb** (Entry 1 – Table 10), resulting in a projected productivity of 18 g/day. Although the increase in yield and productivity of the last thermo reactor designed were not significant, these results are promising, and this reactor could be tested with other substrates in the future.

4.4. Conclusions

In this chapter, the previous methodology on photooxidation of *p*-substituted phenols **1** using singlet oxygen in supercritical CO₂ was employed in a telescoped synthesis of 1,2,4-trioxanes **3**.

Due to co-solvent incompatibility for the second step of the process, the photooxidation step had to be re-optimised in an alternative co-solvent EtOAc. Addition of 2 equivalents of HFIP as a co-catalyst gave a threefold yield increase and this optimised condition was used for reaction screening.

The scope of the reaction was expanded from four (synthesised by Dr. Wu) to fifteen *p*-peroxyquinols **2**, with yields of up to > 99% (Scheme 45). From the two novel compounds synthesised, *p*-peroxyquinol **2j** possessing a 5-membered ring substituent gave quantitative yields but caused blockages in the system. On the other hand, tyramine derivative **2k** gave a moderate yield of 42%. No intramolecular cyclisation occurred with **2l** bearing an ester group, whereas **2m** containing a ketone substituent spontaneously cyclised to give **2m'**.



Concentration of TPFPP = 0.3 mol %; photo reactor (10 mm o.d., 240 mm length, 1 mm wall thickness, effective volume = 5.2 mL, filled with 38 glass beads with 6 mm o.d.); biphenyl as the internal standard. *0.5 M concentration. ^aResidence time = 35 min, without HFIP. ^bSystem got tripped after 2 h of reaction. ^c**2m** was spontaneously converted to the hemiacetal **2m'**.

Scheme 45. Summary of the dearomatisation of *p*-substituted phenols scope using EtOAc and 2 equivalents of HFIP. Blue compounds were synthesised by Dr. Wu. X represents compounds that could not be synthesised.

After optimising the photooxidation of *p*-substituted phenols **1** in EtOAc/HFIP, the telescoped synthesis of 1,2,4-trioxanes was performed through an acetalisation/oxa-Michael addition cascade between peroxyquinols **2** and aldehydes **4**, catalysed by Amberlyst-15 (Scheme 46).

First, the scope of reaction was investigated using peroxyquinol **2a** and four aldehydes (**3Wu-1**, **3aa**, **3ab** and **3ac**), with yields from 21% to 98% for the second step. Although the best yield was obtained with isobutyraldehyde **4b**, cyclohexanecarboxaldehyde **4c** was chosen for further screening as it is less prone to polymerisation. To increase productivity,

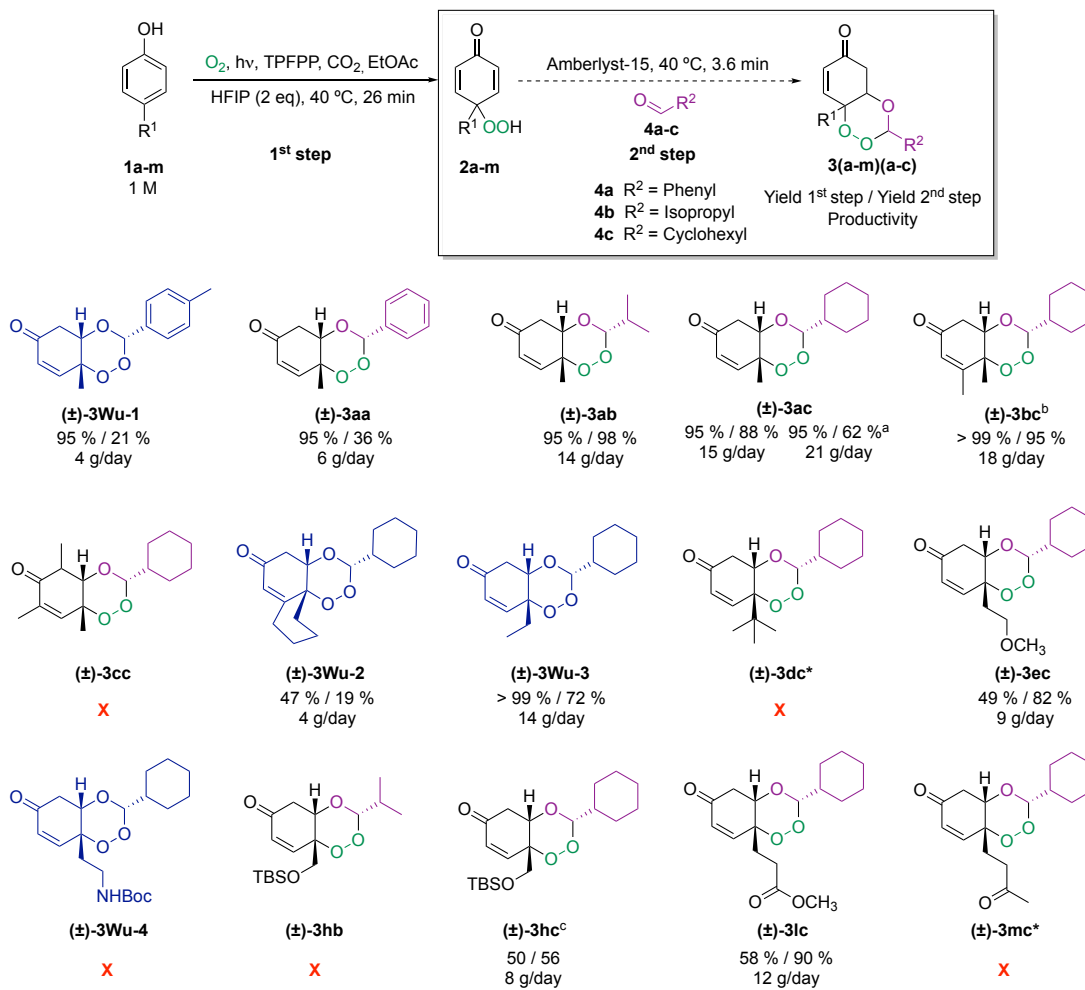
the reaction with **4c** was repeated with a lower residence time, giving 21 g/day of 1,2,4-trioxane **3ac**.

Next, the scope was extended using aldehyde **4c** and six *p*-peroxyquinols **2** with yields (2nd step) and productivities of up to 95% and 18 g/day respectively. 1,2,4-Trioxanes **3cc**, **3dc**, **3Wu-4**, **3hb** and **3mc** could not be obtained using this methodology.

Combining the 1,2,4-trioxanes previously synthesised by Dr. Wu, a total of ten 1,2,4-trioxanes were produced using a continuous flow telescoped approach, including four novel compounds (**3bc**, **3ec**, **3hc** and **3lc**). The methodology has proven to be robust for a variety of aldehydes **4** and mono- and di-substituted *p*-peroxyquinols **2**. This novel continuous flow multi-step process is safer, avoiding the isolation of hazardous *p*-peroxyquinols **2** which are reacted *in situ*. It is also sustainable, using CO₂ as the solvent and small quantities of EtOAc as the co-solvent instead of toxic dichloromethane previously used, minimising organic waste. The use of a catalytic packed bed reactor also facilitates work-up and avoids decomposition of the 1,2,4-trioxanes as they are not exposed to Amberlyst-15 for long periods of time.

The results from this chapter have been accepted in the *Organic Process Research & Development* journal:

Wu, L.; **Abreu, B. L.**; Blake, A. J.; Taylor, L. J.; Argent, S. P.; Poliakoff, M.; Boufroua, H.; George, M. W., Multi-gram Synthesis of Trioxanes Enabled by a Supercritical CO₂ Integrated Flow Process. *Org. Process Res. Dev.* **2021**. DOI: <https://doi.org/10.1021/acs.oprd.1c00111>

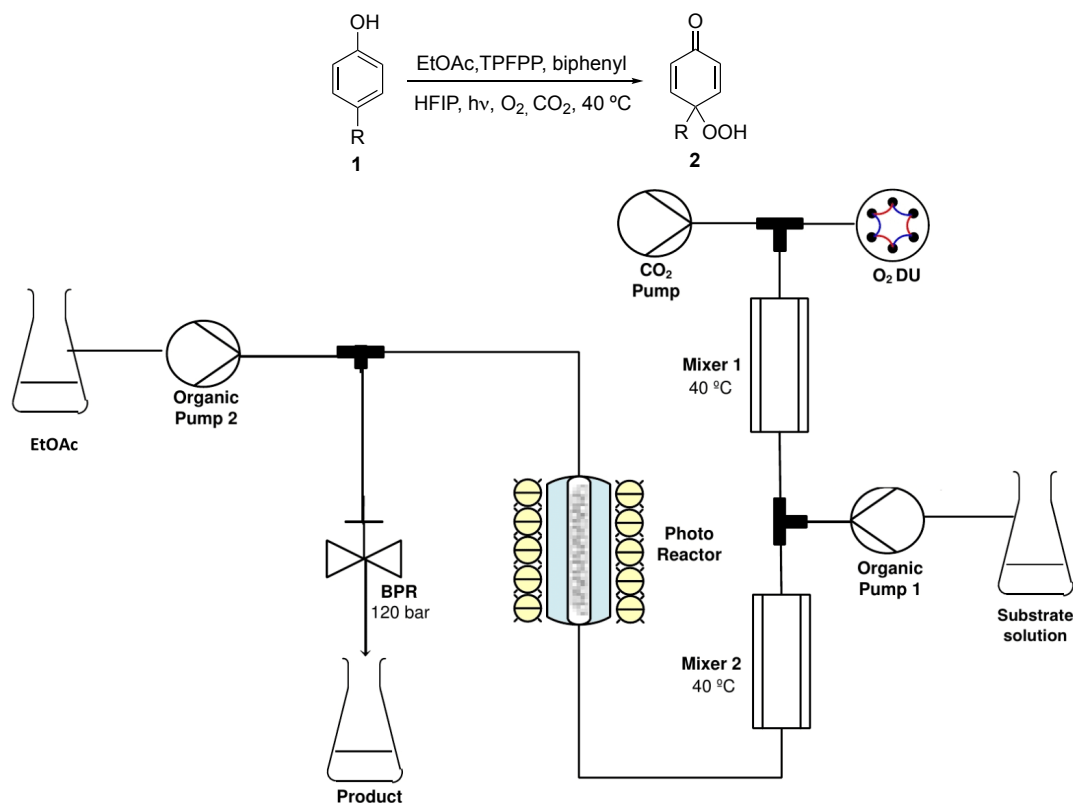


Concentration of TPFPP = 0.3 mol %; photo reactor (10 mm o.d., 240 mm length, 1 mm wall thickness, effective volume = 5.2 mL, filled with 38 glass beads with 6 mm o.d., at 40 °C); thermo reactor **TR1-Amb**: (1/4" o.d., 0.049" wall thickness, 15 cm length, effective volume = 0.9 mL), filled with 0.75 g of Amb-15 and 0.85 g of glass beads (2 mm o.d.); biphenyl as the internal standard. ^a0.5 M concentration. ^a Residence time for the 1st step = 17 min and 2nd step = 2.3 min. ^bDifferent thermo reactor design: **TR3-Amb**: effective volume = 1.1 mL, filled with 0.75 g of Amb-15 and 0.85 g of glass beads (0.5 - 0.75 mm o.d.). ^cProduct not isolated.

Scheme 46. Summary of the telescoped synthesis of 1,2,4-trioxanes 3. Blue compounds were synthesised by Dr. Wu. X represents compounds that could not be synthesised.

4.5. Experimental procedures

Continuous flow oxidative dearomatisation of *p*-substituted phenols using singlet oxygen in supercritical CO₂ (general guidelines)



*A simplified scheme of the high-pressure flow system for the dearomatisation of *p*-substituted phenols.*

System parameters: Photo reactor (10 mm outer diameter (o.d.)), 240 mm length, 1 mm wall thickness, effective volume = 5.2 mL, filled with 38 glass beads with 6 mm o.d., at 40 °C); Cooling baths (photo reactor = 35.5 °C, LED lights = - 5 °C); Trips (System set pressure = 120 bar, high trip = 140 bar; Oxygen set pressure = 180 bar, high trip = 190 bar, low trip = 160 bar; Mixers set temperature = 40 °C, high trip = 50 °C), biphenyl as the internal standard.

Standard procedure (Chapter 2, section 2.1.3) parameters for different concentrations and residence times

- **1 M, residence time = 35 min:** CO₂ (0.10 mL/min and overall [CO₂] = 77%), O₂ (180 bar, sample loop = 10 μL, switching time = 15.9 s, molar ratio O₂: phenol = 2:1 and the overall [O₂] = 3.5 mol%), and HPLC pumps (0.05 mL/min).

- **1 M, residence time = 26 min:** CO₂ (0.15 mL/min and overall [CO₂] = 84%), O₂ (180 bar, sample loop = 10 μL, switching time = 15.9 s, molar ratio O₂: phenol = 2:1 and the overall [O₂] = 2.5 mol%), and HPLC pumps (0.05 mL/min).

- **0.5 M, residence time = 26 min:** CO₂ (0.15 mL/min and overall [CO₂] = 84%), O₂ (180 bar, sample loop = 10 μL, switching time = 15.9 s, molar ratio O₂: phenol = 4:1 and the overall [O₂] = 2.6 mol%), and HPLC pumps (0.05 mL/min).

- **0.1 M residence time = 26 min:** CO₂ (0.15 mL/min and overall [CO₂] = 85%), O₂ (180 bar, sample loop = 10 μL, switching time = 15.9 s, molar ratio O₂: phenol = 20:1 and the overall [O₂] = 2.5 mol%), and HPLC pumps (0.05 mL/min).

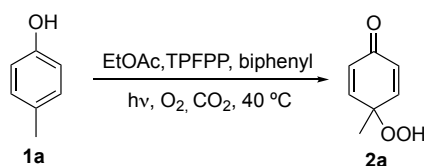
- **0.05 M residence time = 26 min:** CO₂ (0.15 mL/min and overall [CO₂] = 85%), O₂ (180 bar, sample loop = 10 μL, switching time = 15.9 s, molar ratio O₂: phenol = 40:1 and the overall [O₂] = 2.5 mol%), and HPLC pumps (0.05 mL/min).

Reaction procedure: After the standard procedure (**Chapter 2, section 2.1.3**) was performed, a solution of *p*-substituted phenol, HFIP, TPFPP and biphenyl in EtOAc was prepared and sonicated for 30 min, unless stated otherwise. This solution was pumped into the system, combined with the gaseous mixture (CO₂ and O₂) on Mixer 2 and then passed through the photo reactor. EtOAc was pumped after the photo reactor to dilute the mixture and avoid any blockages, and the crude was collected after the BPR. After reaching the steady state, a sample was collected for 3 min, nitrogen blow down for 3 min, and analysed by ¹H NMR spectroscopy. All the remaining *p*-peroxyquinols formed were quenched with a saturated solution of thiourea in MeOH.

Reactions were monitored by ¹H NMR spectroscopy analysis of samples taken every 30 min. The steady state time was determined when two consecutive ¹H NMR spectroscopy analysis showed constant conversion and yield values. Samples collected for purification were taken after the steady state was reached. All the remaining reaction mixture was quenched with a saturated solution of thiourea in MeOH. The conversion of *p*-substituted phenols **1** was calculated as the following: ¹H NMR Conversion of **1** = 100 – X, where X = ¹H NMR Recovery of **1**.

Data collected for known compounds is consistent with the literature. Compounds were isolated in small quantities due to potential hazards associated with organic hydroperoxides and endoperoxides.

4.5.1. Dearomatisation of *p*-cresol **1a**



Reaction performed under general guidelines for the continuous flow oxidative dearomatisation of *p*-substituted phenols

- **Reaction 1 (1 M, 35 min):** 10 mL solution of *p*-cresol **1a** (1 eq, 9.99 mmol, 1.08 g, 1 M), TPFPP (0.3 mol%, 30.0 μmol, 29.2 mg), biphenyl (0.07 eq, 0.699 mmol, 108 mg) in EtOAc.

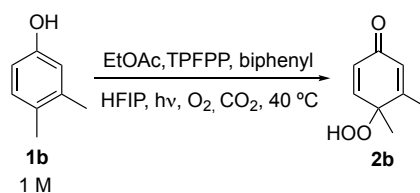
Results: The system reached a steady state after 3 h of reaction. ¹H NMR spectroscopy analysis: conversion of **1a** = 31%, yield of **2a** = 28% and projected productivity = 3 g/day.

- **Reaction 2 (1 M, 26 min):** 10 mL solution of *p*-cresol **1a** (1 eq, 9.99 mmol, 1.08 g, 1 M), TPFPP (0.3 mol%, 30.0 μmol, 29.2 mg), biphenyl (0.07 eq, 0.699 mmol, 108 mg) and HFIP (2 eq, 20.0 mmol, 2.10 mL) in EtOAc.

Results: The system reached a steady state after 3 h of reaction. ¹H NMR spectroscopy analysis: conversion of **1a** = 95%, yield of **2a** = 95% and projected productivity = 10 g/day.

Full characterisation in Chapter 3.

4.5.2. Dearomatisation of 3,4-dimethylphenol **1b**



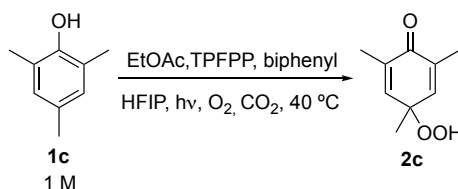
Reaction performed under general guidelines for the continuous flow oxidative dearomatisation of *p*-substituted phenols

- **Reaction (1 M, 26 min):** 15 mL solution of 3,4-dimethylphenol **1b** (1 eq, 15.0 mmol, 1.83 g, 1 M), TPFPP (0.3 mol%, 45.0 μmol, 43.9 mg), HFIP (2 eq, 30.0 mmol, 3.20 mL) and biphenyl (0.07 eq, 1.05 mmol, 162 mg) in EtOAc.

Results: The system reached a steady state after 1.5 h of reaction. ¹H NMR spectroscopy analysis: conversion of **1b** = > 99%, yield of **2b** = > 99% and projected productivity = 11 g/day.

Full characterisation in Chapter 3.

4.5.3. Dearomatisation of 2,4,6-trimethylphenol **1c**



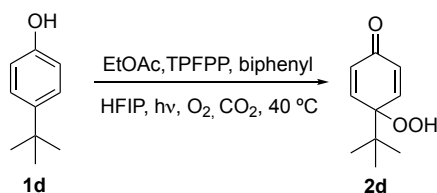
Reaction performed under general guidelines for the continuous flow oxidative dearomatisation of *p*-substituted phenols

Reaction (1 M, 26 min): 15 mL solution of 2,4,6-trimethylphenol **1c** (1 eq, 15.0 mmol, 2.04 g, 1 M), TPFPP (0.3 mol%, 45.0 μmol, 43.9 mg), HFIP (2 eq, 30.0 mmol, 3.20 mL) and biphenyl (0.07 eq, 1.05 mmol, 162 mg) in EtOAc.

Results: The system reached a steady state after 1.5 h of reaction. ¹H NMR spectroscopy analysis: conversion of **1c** = > 99%, yield of **2c** = > 99% and projected productivity = 12 g/day.

Full characterisation in Chapter 3.

4.5.4. Dearomatisation of 4-*tert*-butylphenol **1d**



*Reaction performed under general guidelines for the continuous flow oxidative dearomatisation of *p*-substituted phenols*

- **Reaction (1 M, 26 min):** 20 mL solution of 4-*tert*-butylphenol **1d** (1 eq, 20.0 mmol, 3.00 g, 1 M), TPFPP (0.3 mol%, 60.0 μmol , 58.5 mg), HFIP (2 eq, 40.0 mmol, 4.20 mL) and biphenyl (0.07 eq, 1.40 mmol, 216 mg) in EtOAc.

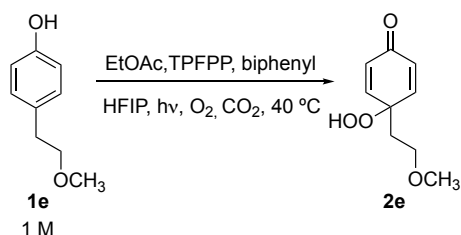
Results: After 2.5 h of reaction, the flow system got tripped due to over pressure caused by solid precipitation.

- **Reaction (0.5 M, 26 min):** 15 mL solution of 4-*tert*-butylphenol **1c** (1 eq, 7.52 mmol, 1.13 g, 0.5 M), TPFPP (0.3 mol%, 22.6 μmol , 22.0 mg), HFIP (2 eq, 15.0 mmol, 1.60 mL) and biphenyl (0.07 eq, 0.526 mmol, 81.2 mg) in EtOAc.

Results: The system reached a steady state after 4 h of reaction. ^1H NMR spectroscopy analysis: conversion of **1d** = 48%, yield of **2d** = 49% and projected productivity = 3 g/day.

Full characterisation in Chapter 3.

4.5.5. Dearomatisation of 4-(2-methoxyethyl)phenol **1e**



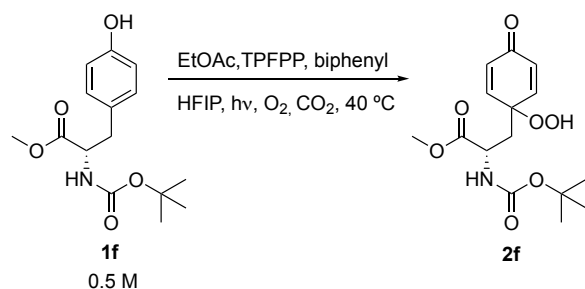
Reaction performed under general guidelines for the continuous flow oxidative dearomatisation of p-substituted phenols

Reaction (1 M, 26 min): 15 mL solution of 4-(2-methoxyethyl)phenol **1e** (1 eq, 14.8 mmol, 2.25 g, 1 M), TPFPP (0.3 mol%, 44.4 μ mol, 43.3 mg), HFIP (2 eq, 29.6 mmol, 3.20 mL) and biphenyl (0.07 eq, 1.04 mmol, 160 mg) in EtOAc.

Results: The system reached a steady state after 3 h of reaction. ^1H NMR spectroscopy analysis: conversion of **1e** = 48%, yield of **2e** = 49% and projected productivity = 6 g/day.

Full characterisation in Chapter 3.

4.5.6. Dearomatisation of *N*-Boc-*L*-tyrosine methyl ester **1f**



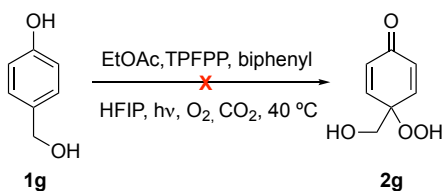
*Reaction performed under general guidelines for the continuous flow oxidative dearomatisation of *p*-substituted phenols*

Reaction (0.5 M, 26 min): 28 mL solution of *N*-Boc-*L*-tyrosine methyl ester **1f** (1 eq, 14.0 mmol, 4.13 g, 0.5 M), TPFPP (0.3 mol%, 42.0 μmol , 40.9 mg), HFIP (2 eq, 28.0 mmol, 2.90 mL) and biphenyl (0.07 eq, 0.980 mmol, 151 mg) in EtOAc.

Results: The system reached a steady state after 4 h of reaction. ^1H NMR spectroscopy analysis: conversion of **1f** = 11%, yield of **2f** = 9% and projected productivity = 1 g/day.

Full characterisation in Chapter 3.

4.5.7. Dearomatisation of 4-(hydroxymethyl)phenol **1g**



*Reaction performed under general guidelines for the continuous flow oxidative dearomatisation of *p*-substituted phenols*

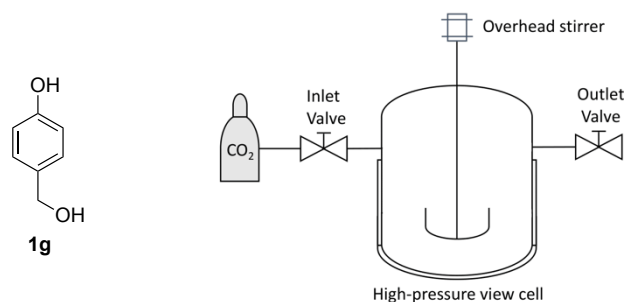
- **Reaction 1 (0.1 M, 26 min):** 15 mL solution of 4-(hydroxymethyl) phenol **1g** (1 eq, 1.50 mmol, 186 mg, 0.1 M), TPFPP (0.3 mol%, 4.50 μ mol, 4.39 mg), biphenyl (0.07 eq, 0.105 mmol, 16.2 mg), and HFIP (2 eq, 3.00 mmol, 315 μ L) in EtOAc.

Results: After 1 h of reaction, the flow system got tripped due to over pressure caused by solid precipitation.

- **Reaction 2 (0.05 M, 26 min):** 15 mL solution of 4-(hydroxymethyl) phenol **1g** (1 eq, 750 μ mol, 93.1 mg, 0.05 M), TPFPP (0.3 mol%, 2.25 μ mol, 2.19 mg), biphenyl (0.07 eq, 52.5 μ mol, 8.10 mg), and HFIP (2 eq, 1.50 mmol, 158 μ L) in EtOAc.

Results: After 2 h of reaction, the flow system got tripped due to over pressure caused by solid precipitation.

4.5.8. Solubility test of 4-(hydroxymethyl)phenol **1g** (high-pressure view cell)



Simple schematic of the high-pressure view cell. More details about this setup can be found in Chapter 2.

The following tests were performed following the standard and shutdown procedures for the high-pressure view cell (see Chapter 2).

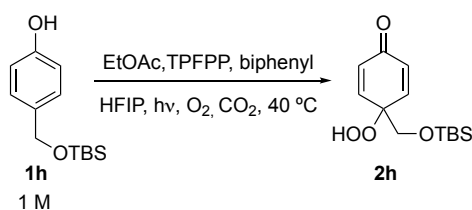
- **Test 1:** A 5 mL solution of 4-(hydroxymethyl)phenol **1g** (1 eq, 501 μmol , 62.2 mg, 0.1 M), TPFPP (0.3 mol%, 1.50 μmol , 1.46 mg), biphenyl (0.07 eq, 35.1 μmol , 5.41 mg), and HFIP (2 eq, 1.00 mmol, 105 μL) was added to a vial and put inside the view cell.

Results: After the system reached supercritical conditions used in the previous flow experiments (120 bar, 40 $^{\circ}\text{C}$), it was observed solid particles on the window of the view cell. To confirm if the solid was the phenol **1g**, another test was carried out.

- **Test 2:** 4-(hydroxymethyl) phenol **1g** (1 eq, 1.50 mmol, 186 mg) was added to a vial and put inside the view cell, followed by the addition of 15 mL of EtOAc, resulting in a 0.1 M solution.

Results: After the system reached the supercritical conditions (120 bar, 40 $^{\circ}\text{C}$), it was observed solid particles of phenol **1g** on the window of the view cell.

4.5.9. Dearomatisation of 4-((*tert*-butyldimethylsilyloxy)methyl)phenol **1h**



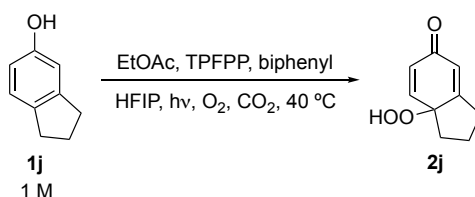
Reaction performed under general guidelines for the continuous flow oxidative dearomatisation of *p*-substituted phenols

- **Reaction (1 M, 26 min):** 12 mL solution of 4-((*tert*-butyldimethylsilyloxy)methyl)phenol **1h** (1 eq, 12.0 mmol, 2.86 g, 1 M), TPFPP (0.3 mol%, 36.0 μ mol, 35.1 mg), HFIP (2 eq, 24.0 mmol, 2.52 mL) and biphenyl (0.07 eq, 0.840 mmol, 130 mg) in EtOAc.

Results: The system reached a steady state after 3.5 h of reaction. ^1H NMR spectroscopy analysis: conversion of **1h** = 54%, yield of **2h** = 50% and projected productivity = 10 g/day.

Full characterisation in Chapter 3.

4.5.10. Dearomatisation of 5-indanol **1j**

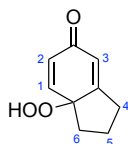


Reaction performed under general guidelines for the continuous flow oxidative dearomatisation of *p*-substituted phenols

Reaction (1 M, 26 min): 15 mL solution of 5-indanol **1j** (1 eq, 15.0 mmol, 2.01 g, 1 M), TPFPP (0.3 mol%, 45.0 μ mol, 43.9 mg), HFIP (2 eq, 30.0 mmol, 3.20 mL) and biphenyl (0.07 eq, 1.05 mmol, 162 mg) in EtOAc.

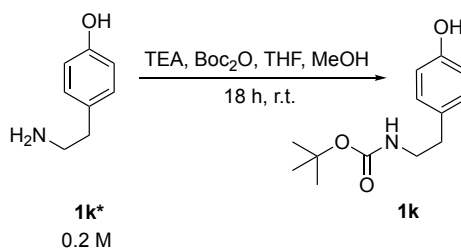
Results: A sample was analysed after 1.5 h of reaction: ^1H NMR spectroscopy conversion of **1j** = > 99%, yield of **2j** = > 99% and projected productivity = 12 g/day. However, after 2 h of reaction, the flow system got tripped due to over pressure caused by solid precipitation. The compound was not isolated as a pure compound, but the ^1H NMR spectroscopy signals could be assigned in the sample.

7a-Hydroperoxy-1,2,3,7a-tetrahydro-5H-inden-5-one **2j** (novel compound)



^1H NMR (400 MHz, Chloroform-*d*): δ 6.93 (d, J = 9.9 Hz, 1H, **1**), 6.26 (dd, J = 9.9, 1.8 Hz, 1H, **2**), 6.15-6.14 (m, 1H, **3**), 2.89-2.80 (m, 1H, **4**), 2.55-2.47 (m, 1H, **4'**), 2.16-2.04 (m, 2H, **6**), 1.98-1.89 (m, 1H, **5**), 1.77-1.67 (m, 1H, **5'**).

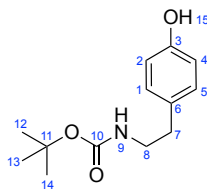
4.5.11. Boc protection of tyramine **1k***



Procedure: In a sealed round-bottom flask with a magnetic stir bar and nitrogen-filled balloon, tyramine **1k*** (1 eq, 58.3 mmol, 8.00 g, 0.2 M) was added to a mixture of dry THF (280 mL) and MeOH (40 mL), followed by the addition of triethylamine (1 eq, 58.3 mmol, 8.12 mL). The solution was cooled down to 0 °C with an ice-bath and di-*tert*-butyl dicarbonate (1 eq, 58.3 mmol, 12.7 g) was added in portions. After the reaction mixture was stirred for 18 h at room temperature, the solvent was removed under vacuum and the crude was diluted with EtOAc (250 mL). An acidic extraction using 1 M HCl (60 mL), followed by water (50 mL) and brine (50 mL) was performed. The organic phase was dried over Na₂SO₄, filtrated and concentrated under vacuum.

Results: The product was purified by flash chromatography column and eluted with a mixture EtOAc/Cyclohexane (1:4 to 3:7) to give **1k** (53.1 mmol, 12.6 g, 91%) as a white solid.

Tert-butyl (4-hydroxyphenethyl)carbamate **1k**²⁴⁵

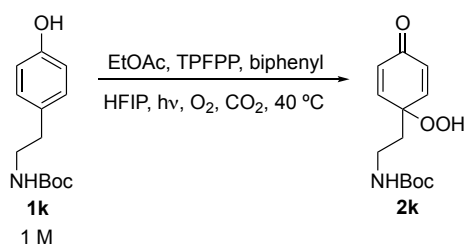


¹H NMR (400 MHz, Chloroform-*d*): δ 7.02 (d, *J* = 8.4 Hz, 2H, **1/5**), 6.81 (d, *J* = 8.4 Hz, 2H, **2/4**), 4.70 (bs, 1H, **9**), 3.36 - 3.34 (m, 2H, **8**), 2.72 (t, *J* = 6.9 Hz, 2H, **7**), 1.47 (s, 9H, **12/13/14**).

¹³C NMR (101 MHz, Chloroform-*d*): δ 156.5 (**10**), 155.0 (**3**), 130.3 (**6**), 129.9 (**1/5**), 115.6 (**2/4**), 79.8 (**11**), 42.2 (**8**), 35.4 (**7**), 28.5 (**12/13/14**).

HRMS (ESI) *m/z* calcd [C₁₃H₂₀NO₃]⁺ ([M + H]⁺): 238.1438, found 238.1441

4.5.12. Dearomatisation of *N*-Boc-tyramine **1k**

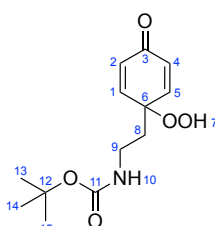


Reaction performed under general guidelines for the continuous flow oxidative dearomatisation of p-substituted phenols

Reaction (1 M, 26 min): 18 mL solution of *N*-Boc-tyramine **1k** (1 eq, 18.0 mmol, 4.27 g, 1 M), TPFPP (0.3 mol%, 54.0 μ mol, 52.6 mg), HFIP (2 eq, 36.0 mmol, 3.81 mL) and biphenyl (0.04 eq, 720 μ mol, 111 mg) in EtOAc.

Results: The system reached a steady state after 4 h of reaction. ^1H NMR spectroscopy analysis: conversion of **1k** = 77%, yield of **2k** = 42% and projected productivity = 8 g/day. Another sample was collected for 30 min (1.5 mL) and concentrated under reduced pressure. Purification was carried out using flash chromatography column, with a mixture of EtOAc/Cyclohexane (1:1) to give **2k** (654 μ mol, 176 mg, 43%) as a colourless oil.

Tert-butyl (2-(1-hydroperoxy-4-oxocyclohexa-2,5-dien-1-yl)ethyl)carbamate **2k** (novel compound)

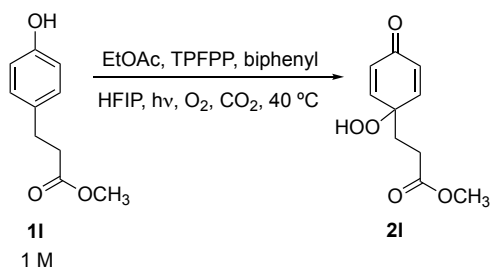


^1H NMR (400 MHz, Chloroform-*d*): δ 10.10 (s, 1H, **7**), 6.94 (d, J = 10.2 Hz, 2H, **1/5**), 6.31 (d, J = 10.2 Hz, 2H, **2/4**), 4.83 (bs, 1H, **10**), 3.20 – 3.15 (m, 2H, **9**), 1.96 – 1.92 (m, 2H, **8**), 1.40 (s, 9H, **13/14/15**).

^{13}C NMR (101 MHz, Chloroform-*d*): δ 185.6 (**3**), 156.3 (**11**), 148.1 (**1/5**), 131.0 (**2/4**), 80.3 (**12**), 80.1 (**6**), 36.7 (**8**), 35.6 (**9**), 28.5 (**13/14/15**).

HRMS (ESI) m/z calcd [$\text{C}_{13}\text{H}_{19}\text{N}_1\text{O}_5\text{Na}$] $^+$ ($[\text{M} + \text{Na}]^+$): 292.1155, found 292.1152.

4.5.13. Dearomatisation of 3-(4-hydroxyphenyl)propionate **1I**

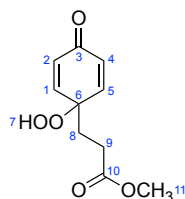


Reaction performed under general guidelines for the continuous flow oxidative dearomatisation of *p*-substituted phenols

Reaction (1 M, 26 min): 18 mL solution of 3-(4-hydroxyphenyl)propionate **1I** (1 eq, 18.0 mmol, 3.24 g, 1 M), TPFPP (0.3 mol%, 54.0 μ mol, 52.6 mg), HFIP (2 eq, 36.0 mmol, 3.81 mL) and biphenyl (0.07 eq, 1.26 mmol, 194 mg) in EtOAc.

Results: The system reached a steady state after 2 h of reaction. ^1H NMR spectroscopy analysis: conversion of **1I** = 71%, yield of **2I** = 58% and projected productivity = 9 g/day. Another sample was collected for 30 min (1.5 mL) and concentrated under reduced pressure. Purification was carried out using flash chromatography column, with a mixture of EtOAc/Cyclohexane (3:7 to 7:3) to give **2I** (763 μ mol, 162 mg, 51%) as an off-white solid.

Methyl 3-(1-hydroperoxy-4-oxocyclohexa-2,5-dien-1-yl)propanoate **1I**¹⁹⁵

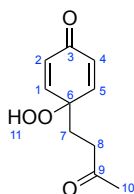


^1H NMR (400 MHz, Chloroform-*d*): δ 9.37 (s, 1H, **7**), 6.88 (d, J = 10.2 Hz, 2H, **1/5**), 6.32 (d, J = 10.2 Hz, 2H, **2/4**), 3.65 (s, 3H, **11**), 2.33 (t, J = 7.7 Hz, 2H, **9**), 2.08 (t, J = 7.7 Hz, 2H, **8**).

^{13}C NMR (101 MHz, Chloroform-*d*): δ 185.7 (**3**), 173.4 (**10**), 148.2 (**1/5**), 131.3 (**2/4**), 80.6 (**6**), 52.2 (**11**), 30.7 (**8**), 28.4 (**9**).

HRMS (ESI) m/z calcd [$\text{C}_{10}\text{H}_{13}\text{O}_5$] $^+$ ($[\text{M} + \text{H}]^+$): 213.0757, found 213.0763.

4-Hydroperoxy-4-(3-oxobutyl)cyclohexa-2,5-dien-1-one **2m**²⁴⁰

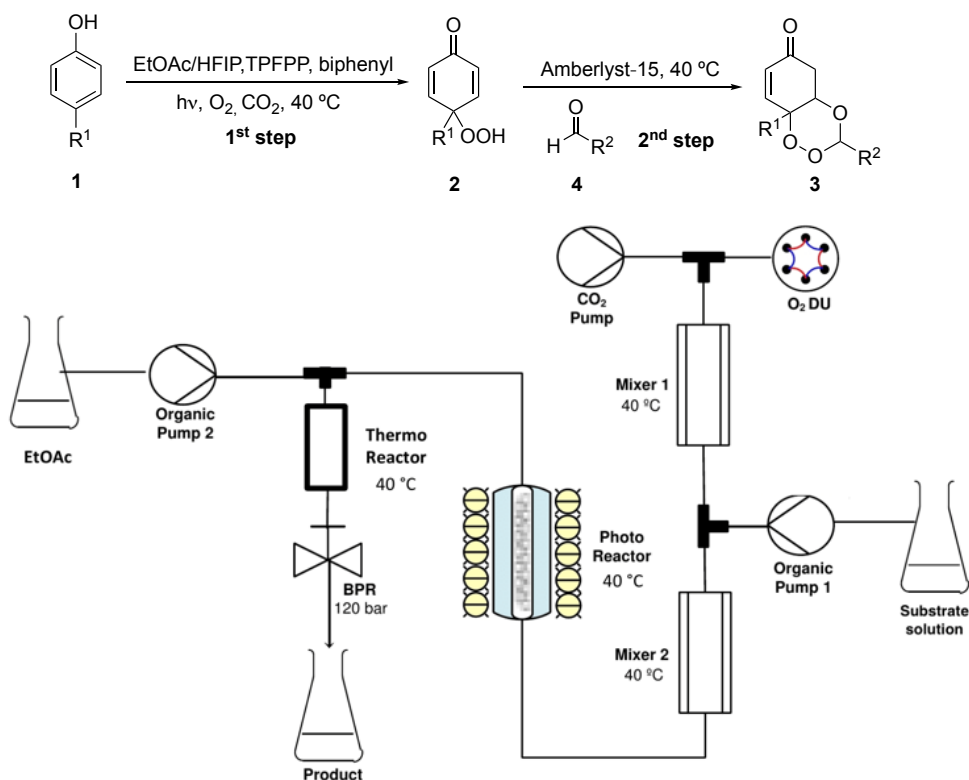


¹H NMR (400 MHz, Chloroform-*d*): δ 9.98 (s, 1H, **11**), 6.85 (d, *J* = 10.3 Hz, 2H, **1/5**), 6.30 (d, *J* = 10.3 Hz, 2H, **2/4**), 2.40 (t, *J* = 7.5 Hz, 2H, **8**), 2.09 (s, 3H, **10**), 1.98 (t, *J* = 7.5 Hz, 2H, **7**).

¹³C NMR (101 MHz, Chloroform-*d*): δ 207.5 (**9**), 185.5 (**3**), 149.0 (**1/5**), 131.0 (**2/4**), 80.7 (**6**), 37.3 (**8**), 30.1 (**10**), 29.1 (**7**).

HRMS (ESI) *m/z* calcd [C₁₀H₁₂O₄Na]⁺ ([M + Na]⁺): 219.0628, found 219.0622.

Continuous flow telescoped synthesis of 1,2,4-trioxanes from photooxidation of *p*-substituted phenols (general guidelines)



A simplified scheme of the high-pressure flow system for the telescoped synthesis of 1,2,4-trioxanes

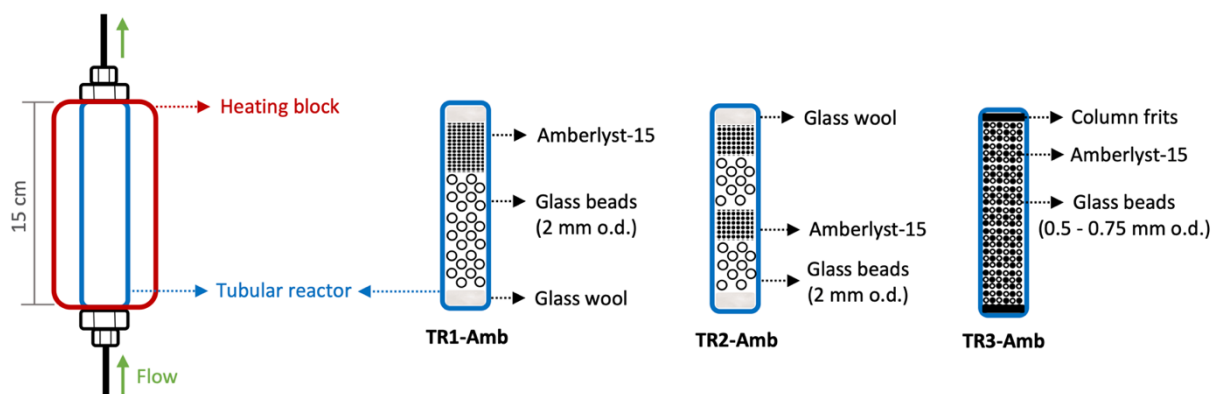
System parameters: Photo reactor (10 mm outer diameter (o.d.)), 240 mm length, 1 mm wall thickness, effective volume = 5.2 mL, filled with 38 glass beads with 6 mm o.d., at $40^\circ C$); Cooling baths (photo reactor = $35.5^\circ C$, LED lights = $-5^\circ C$); Trips (system set pressure = 120 bar, high trip = 140 bar; Oxygen set pressure = 180 bar, high trip = 190 bar, low trip = 160 bar; Mixers set temperature = $40^\circ C$, high trip = $50^\circ C$); thermo reactors (1/4 inch o.d., 1 mm wall thickness, 15 cm length, loaded with Amberlyst-15 and glass beads at $40^\circ C$, high trip = $50^\circ C$), biphenyl as the internal standard for 1H NMR spectroscopy analysis.

Specifications of thermo reactors:

- **TR1-Amb:** effective volume = 0.9 mL, filled with a layer of 0.75 g of Amberlyst-15 and another layer of 0.85 g of glass beads 2 mm o.d. A glass wool layer was put at each end of the tubular reactor.

- **TR2-Amb:** effective volume = 0.9 mL, filled with 0.75 g of Amberlyst-15 (two layers) and 0.85 g of glass beads 2 mm o.d. (two layers). The layers of Amberlyst-15 and glass beads were intercalated, and a glass wool layer was put at each end of the tubular reactor.

- **TR3-Amb:** effective volume = 1.1 mL, filled with a mixture of 0.75 g of Amberlyst-15 and 0.85 g of glass beads 0.5 – 0.75 mm o.d. A column frit was put at each end of the tubular reactor.



A simplified scheme of the thermo reactors used in this chapter.

Standard procedure (Chapter 2, section 2.1.3) parameters for different concentrations:

- **1 M (residence time 1st step = 26 min):** CO₂ (0.15 mL/min and overall [CO₂] = 84%), O₂ (180 bar, sample loop = 10 μL, switching time = 15.9 s, molar ratio O₂: phenol = 2:1 and the overall [O₂] = 2.5 mol%), and HPLC pumps (0.05 mL/min).

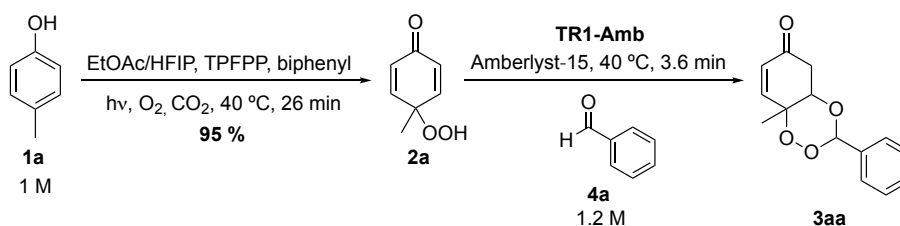
- **0.5 M (residence time 1st step = 26 min):** CO₂ (0.15 mL/min and overall [CO₂] = 84%), O₂ (180 bar, sample loop = 10 μL, switching time = 15.9 s, molar ratio O₂: phenol = 4:1 and the overall [O₂] = 2.6 mol%), and HPLC pumps (0.05 mL/min).

- **1 M (residence time 1st step = 17 min):** CO₂ (0.2 mL/min and overall [CO₂] = 77%), O₂ (180 bar, sample loop = 10 μL, switching time = 8.0 s, molar ratio O₂: phenol = 2:1 and the overall [O₂] = 3.5 mol%), and HPLC pumps (0.1 mL/min).

Reaction procedure: After the standard procedure (**Chapter 2, section 2.1.3**) was performed, a solution of *p*-substituted phenol, HFIP, TPFPP and biphenyl in EtOAc was prepared and sonicated for 30 min. This solution was pumped into the system, combined with the gaseous mixture (CO₂ and O₂) on Mixer 2 and then passed through the photo reactor. A solution of aldehyde in EtOAc was pumped after the photo reactor, the streams were combined and passed through a thermo reactor. The crude was collected after the BPR and all the remaining peroxides were quenched with a saturated solution of thiourea in MeOH. After reaching the steady state, a sample was collected for 3 min, nitrogen blow down for 3 min, and analysed by ¹H NMR spectroscopy.

All 1,2,4-trioxanes were isolated as single diastereoisomers.

4.5.15. 1,2,4-Trioxane **3aa** from *p*-cresol **1a** and benzaldehyde **4a**

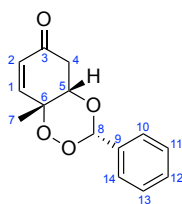


Reaction performed under general guidelines for the continuous flow telescoped synthesis of 1,2,4-trioxanes from photooxidation of *p*-substituted phenols

Reaction (1 M, 26 min): 10 mL starting solution of *p*-cresol **1a** (1.0 eq, 10.0 mmol, 1.08 g, 1.0 M), TPFPP (0.30 mol%, 30.0 μ mol, 29.2 mg), HFIP (2.0 eq, 20.0 mmol, 2.10 mL) and biphenyl (0.070 eq, 700 μ mol, 108 mg) in EtOAc. After 2 h of reaction, a 10 mL benzaldehyde **4a** solution (1.2 eq, 12.0 mmol, 1.22 mL, 1.2 M) was pumped after the photo reactor.

Results: The system reached a steady state after 3.5 h of reaction. ^1H NMR spectroscopy analysis of **3aa**: yield for 2nd step = 36%, overall yield = 34%, projected productivity = 6 g/day. Another sample was collected for 30 min (1.5 mL) and concentrated under reduced pressure. Purification was carried out using flash chromatography column, with a mixture of EtOAc/Cyclohexane (1:4) to give **3aa** (410 μ mol, 101 mg, 27%) as a white solid.

(\pm)-(4*aS*,8*aR*)-8*a*-Methyl-3-phenyl-4*a*,8*a*-dihydrobenzo[*e*][1,2,4]trioxin-6(5*H*)-one **3aa**²³³

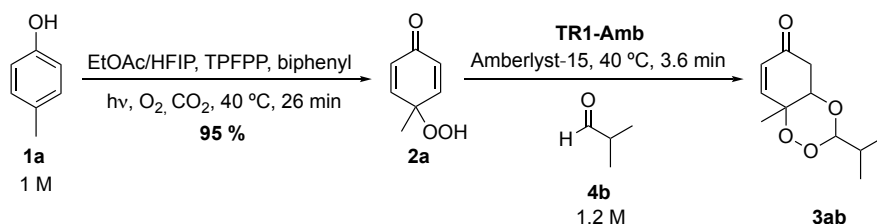


^1H NMR (400 MHz, Chloroform-*d*): δ 7.42 – 7.33 (m, 5H, **10/11/12/13/14**), 6.95 (dd, J = 10.4, 3.0 Hz, 1H, **1**), 6.22 (s, 1H, **8**), 6.17 (dd, J = 10.4, 1.1 Hz, 1H, **2**), 4.41 (q, J = 3.0 Hz, 1H, **5**), 2.84 (ddd, J = 17.5, 3.0, 1.1 Hz, 1H, **4**), 2.79 (dd, J = 17.5, 3.0 Hz, 1H, **4'**), 1.44 (s, 3H, **7**).

^{13}C NMR (101 MHz, Chloroform-*d*): δ 195.0 (**3**), 151.1 (**1**), 133.6 (**9**), 130.4 (**12**), 129.9 (**8**), 128.6 (**11/13**), 127.3 (**10/14**), 103.8 (**8**), 78.1 (**6**), 77.1 (**5**), 41.2 (**4**), 20.8 (**7**).

HRMS (ESI) m/z calcd $[\text{C}_{14}\text{H}_{14}\text{O}_4\text{Na}]^+$ ($[\text{M} + \text{Na}]^+$): 269.0784, found 269.0783.

4.5.16. 1,2,4-Trioxane **3ab** from *p*-cresol **1a** and isobutyraldehyde **4b**

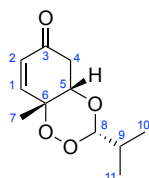


Reaction performed under general guidelines for the continuous flow telescoped synthesis of 1,2,4-trioxanes from photooxidation of *p*-substituted phenols

Reaction (1 M, 26 min): 10 mL starting solution of *p*-cresol (1.0 eq, 10.0 mmol, 1.08 g, 1.0 M), TPFPP (0.30 mol%, 30.0 μ mol, 29.2 mg), HFIP (2.0 eq, 20.0 mmol, 2.10 mL) and biphenyl (0.070 eq, 700 μ mol, 108 mg) in EtOAc. After 2 h of reaction, a 10 mL isobutyraldehyde **4b** solution (1.2 eq, 12.0 mmol, 1.10 mL, 1.2 M) was pumped after the photo reactor.

Results: The system reached a steady state after 3.5 h of reaction. ^1H NMR spectroscopy analysis of **3ab**: yield for 2nd step = 98%, overall yield = 93%, projected productivity = 14 g/day. Another sample was collected for 1 h (3 mL) and concentrated under reduced pressure. Purification was carried out using flash chromatography column, with a mixture of EtOAc/Cyclohexane (1:4) to give **3ab** (1.97 mmol, 418 mg, **66%**) as a pale-yellow solid.

(\pm)-(4*aS*,8*aR*)-3-Isopropyl-8*a*-methyl-4*a*,8*a*-dihydrobenzo[*e*][1,2,4]trioxin-6(5*H*)-one **3ab**²³³

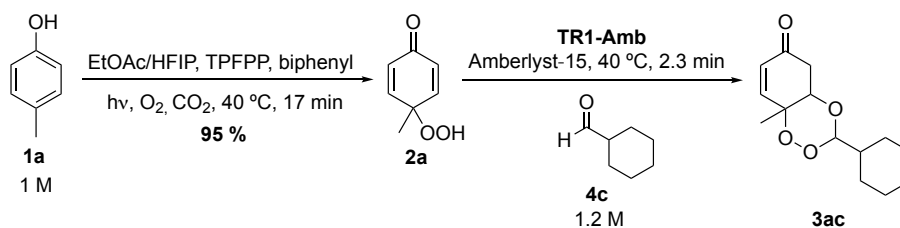


^1H NMR (400 MHz, Chloroform-*d*): δ 6.84 (dd, $J = 10.4, 3.0$ Hz, 1H, **1**), 6.07 (dd, $J = 10.4, 0.9$ Hz, 1H, **2**), 5.01 (d, $J = 5.1$ Hz, 1H, **8**), 4.15 (q, $J = 3.0$ Hz, 1H, **5**), 2.73 (ddd, $J = 17.4, 3.0, 0.9$ Hz, 1H, **4**), 2.70 (dd, $J = 17.4, 3.0$ Hz, 1H, **4'**), 1.77 (septd, $J = 6.9, 5.1$ Hz, 1H, **9**), 1.33 (s, 3H, **7**), 0.89 (d, $J = 6.9$ Hz, 6H, **10/11**).

^{13}C NMR (101 MHz, Chloroform-*d*): δ 195.3 (**3**), 151.2 (**1**), 129.7 (**2**), 107.2 (**8**), 77.9 (**6**), 76.4 (**5**), 41.1 (**4**), 31.0 (**9**), 20.7 (**7**), 16.8 (d, $J = 10.5$ Hz, **10/11**).

HRMS (ESI) m/z calcd $[\text{C}_{11}\text{H}_{16}\text{O}_4\text{Na}]^+$ ($[\text{M} + \text{Na}]^+$): 235.0941, found 235.0934.

4.5.17. 1,2,4-Trioxane **3ac** from *p*-cresol **1a** and cyclohexanecarboxaldehyde **4c**

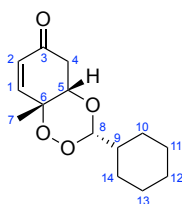


Reaction performed under general guidelines for the continuous flow telescoped synthesis of 1,2,4-trioxanes from photooxidation of *p*-substituted phenols

Reaction (1 M, 17 min): 72 mL solution of *p*-cresol **1a** (1.0 eq, 72.0 mmol, 7.79 g, 1.0 M), TPFPP (0.30 mol%, 216 μ mol, 211 mg), HFIP (2.0 eq, 144 mmol, 15.1 mL) and biphenyl (0.070 eq, 5.04 mmol, 777 mg) in EtOAc. After 1 h of reaction, a 72 mL cyclohexanecarbaldehyde **4c** solution (1.2 eq, 86.4 mmol, 10.5 mL, 1.2 M) was pumped after the photo reactor.

Results: The system reached a steady state after 2 h of reaction. ^1H NMR spectroscopy analysis of **3ac**: yield for 2nd step = 62%, overall yield = 59%, projected productivity = 21 g/day. Another sample was collected for 8.5 h (51 mL) and concentrated under reduced pressure. Purification was carried out using flash chromatography column, with a mixture of EtOAc/Cyclohexane (1:4) to give **3ac** (16.2 mmol, 4.10 g, 31%) as a white solid.

(\pm)-(4a*S*,8a*R*)-3-Cyclohexyl-8a-methyl-4a,8a-dihydrobenzo[*e*][1,2,4]trioxin-6(5*H*)-one **3ac**¹⁹⁵

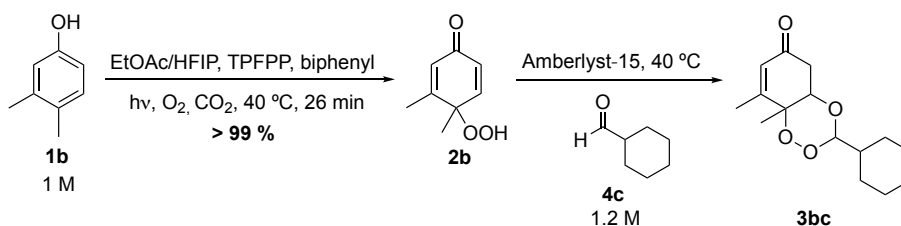


^1H NMR (400 MHz, Chloroform-*d*): δ 6.84 (dd, $J = 10.4, 3.0$ Hz, 1H, **1**), 6.07 (d, $J = 10.4$, 1H, **2**), 5.02 (d, $J = 5.3$ Hz, 1H, **8**), 4.14 (q, $J = 3.0$ Hz, 1H, **5**), 2.73 (dd, $J = 17.4, 3.0$ Hz, 1H, **4**), 2.68 (dd, $J = 17.4, 3.0$ Hz, 1H, **4'**), 1.69 – 1.61 (m, 5H, **10/11/12/13/14**), 1.55 – 1.46 (m, 1H, **9**), 1.33 (s, 3H, **CH₃**), 1.21 – 0.99 (m, 5H, **10'/11'/12'/13'/14'**).

^{13}C NMR (101 MHz, Chloroform-*d*): δ 195.3 (**3**), 151.3 (**1**), 129.7 (**2**), 106.7 (**8**), 78.0 (**6**), 76.5 (**5**), 41.2 (**4**), 40.5 (**9**), 27.0 (**11/13**), 26.3 (**12**), 25.7 (**10/14**), 20.7 (**7**).

HRMS (ESI) m/z calcd $[\text{C}_{14}\text{H}_{21}\text{O}_4]^+$ ($[\text{M} + \text{H}]^+$): 253.1436, found 253.1434.

4.5.18. 1,2,4-Trioxane **3bc** from 3,4-dimethylphenol **1b** and cyclohexanecarboxaldehyde **4c**



Reaction performed under general guidelines for the continuous flow telescoped synthesis of 1,2,4-trioxanes from photooxidation of *p*-substituted phenols

- **Reaction 1 (1 M, 26 min, TR1-Amb):** 15 mL starting solution of 3,4-dimethylphenol **1b** (1.0 eq, 15.0 mmol, 1.83 g, 1.0 M), TPFPP (0.30 mol%, 45.0 μ mol, 43.9 mg), HFIP (2.0 eq, 30.0 mmol, 3.20 mL) and biphenyl (0.070 eq, 1.05 mmol, 162 mg) in EtOAc. Thermo reactor **TR1-Amb** (residence time = 3.6 min). After 1 h of reaction, a 10 mL cyclohexanecarboxaldehyde **4c** solution (1.2 eq, 12.0 mmol, 1.52 mL, 1.2 M) was pumped after the photo reactor.

Results: The system reached a steady state after 2 h of reaction. 1H NMR spectroscopy analysis of **3bc**: yield for 2nd step = 85%, overall yield = 84%, projected productivity = 16 g/day. Another sample was collected for 1 h (3 mL) and concentrated under reduced pressure. Purification was carried out using flash chromatography column, with a mixture of EtOAc/Cyclohexane (3:7) to give **3bc** (2.49 mmol, 663 mg, 83%) as a yellow oil.

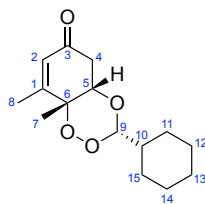
- **Reaction 2 (1 M, 26 min, TR2-Amb):** same as Reaction 1, with thermo reactor **TR2-Amb** (residence time = 3.6 min).

Results: The system reached a steady state after 2 h of reaction. 1H NMR spectroscopy analysis of **3bc**: yield for 2nd step = 90%, overall yield = 89%, projected productivity = 17 g/day.

- **Reaction 3 (1 M, 26 min, TR3-Amb):** same as Reaction 1, with thermo reactor **TR3-Amb** (residence time = 4.4 min).

Results: The system reached a steady state after 2 h of reaction. 1H NMR spectroscopy analysis of **3bc**: yield for 2nd step = 95%, overall yield = 94%, projected productivity = 18 g/day.

(±)-(4a*S*,8a*R*)-3-cyclohexyl-8,8a-dimethyl-4a,8a-dihydrobenzo[*e*][1,2,4]trioxin-6(5*H*)-one
3bc (novel compound)

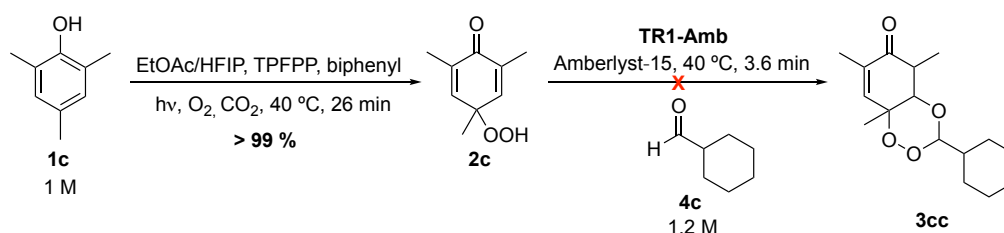


¹H NMR (400 MHz, Chloroform-*d*): δ 5.92 (s, 1H, **2**), 4.99 (d, *J* = 5.3 Hz, 1H, **9**), 4.08 (t, *J* = 2.9 Hz, 1H, **5**), 2.66 (d, *J* = 2.9 Hz, 2H, **4**), 2.01 (s, 3H, **8**), 1.66 – 1.59 (m, 5H, **11/12/13/14/15**), 1.49 – 1.42 (m, 1H, **10**), 1.28 (s, 3H, **7**), 1.18 – 0.97 (m, 5H, **11'/12'/13'/14'/15'**).

¹³C NMR (101 MHz, Chloroform-*d*): δ 194.8 (**3**), 161.3 (**1**), 127.7 (**2**), 106.5 (**9**), 79.7 (**6**), 77.0 (**5**), 41.1 (**4**), 40.3 (**10**), 26.9 (**12/14**), 26.2 (**13**), 25.6 (**11/15**), 20.0 (**7**), 18.3 (**8**).

HRMS (ESI) *m/z* calcd [C₁₅H₂₂O₄Na]⁺ ([M + Na]⁺): 289.1410, found 289.1423.

4.5.19. 1,2,4-Trioxane **3cc** from 2,4,6-trimethylphenol **1c** and cyclohexanecarboxaldehyde **4c**

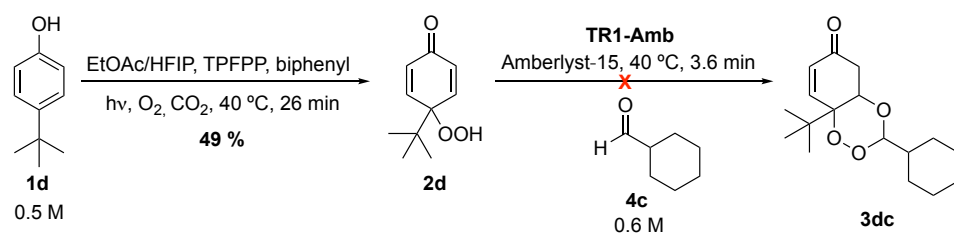


Reaction performed under general guidelines for the continuous flow telescoped synthesis of 1,2,4-trioxanes from photooxidation of *p*-substituted phenols

Reaction (1 M, 26 min): 15 mL starting solution of 2,4,6-trimethylphenol **1c** (1.0 eq, 15.0 mmol, 2.04 g, 1.0 M), TPFPP (0.30 mol%, 45.0 μmol, 43.9 mg), HFIP (2.0 eq, 30.0 mmol, 3.20 mL) and biphenyl (0.07 eq, 1.05 mmol, 162 mg) in EtOAc. After 2 h of reaction, a 10 mL cyclohexanecarboxaldehyde **4c** solution (1.2 eq, 12.0 mmol, 1.52 mL, 1.2 M) was pumped after the photo reactor.

Results: The reaction was carried out for 4 h and monitored by ¹H NMR spectroscopy every 30 min. However, trioxane **3cc** was not identified and a complex mixture was formed.

4.5.20. 1,2,4-Trioxane **3dc** from 4-tert-butylphenol **1d** and cyclohexanecarboxaldehyde **4c**

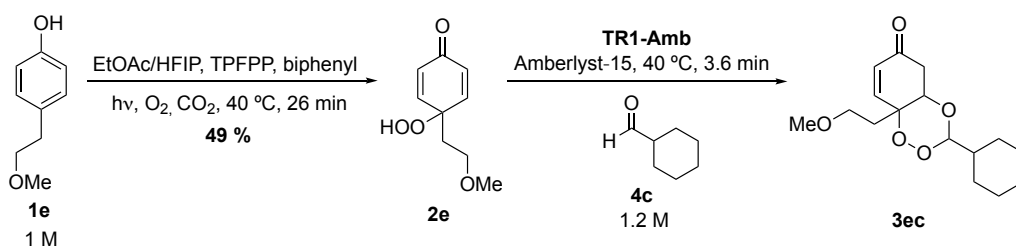


Reaction performed under general guidelines for the continuous flow telescoped synthesis of 1,2,4-trioxanes from photooxidation of *p*-substituted phenols

Reaction (0.5 M, 26 min): 22 mL starting solution of 4-tert-butylphenol **1d** (1.0 eq, 11.0 mmol, 1.65 g, 0.50 M), TPFPP (0.30 mol%, 33.0 μ mol, 32.2 mg), HFIP (2.0 eq, 22.0 mmol, 2.30 mL) and biphenyl (0.070 eq, 770 μ mol, 119 mg) in EtOAc. After 3.5 h of reaction, a 12 mL cyclohexanecarboxaldehyde solution (1.2 eq, 7.20 mmol, 872 μ L, 0.60 M) was pumped after the photo reactor.

Results: The reaction was carried out for 5 h and monitored by 1H NMR spectroscopy every 30 min. However, trioxane **3dc** was not identified and a complex mixture was formed.

4.5.21. 1,2,4-Trioxane **3ec** from 4-(2-methoxyethyl)phenol **1e** and cyclohexanecarboxaldehyde **4c**

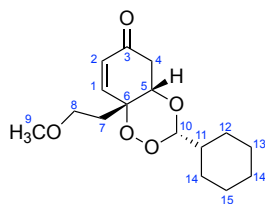


Reaction performed under general guidelines for the continuous flow telescoped synthesis of 1,2,4-trioxanes from photooxidation of *p*-substituted phenols

Reaction (1 M, 26 min): 18 mL solution of 4-(2-methoxyethyl)phenol **1e** (1.0 eq, 18.0 mmol, 2.74 g, 1.0 M), TPFPP (0.30 mol%, 54.0 μ mol, 52.6 mg), HFIP (2.0 eq, 36.0 mmol, 3.81 mL) and biphenyl (0.070 eq, 1.26 mmol, 194 mg) in EtOAc. After 2 h of reaction, a 12 mL cyclohexanecarboxaldehyde solution (1.2 eq, 14.4 mmol, 1.72 mL, 1.2 M) was pumped after the photo reactor.

Results: The system reached a steady state after 3.5 h of reaction. ^1H NMR spectroscopy analysis of **3ec**: yield for 2nd step = 82%, overall yield = 40%, projected productivity = 9 g/day. Another sample was collected for 1 h (3 mL) and concentrated under reduced pressure. Purification was carried out using flash chromatography column, with a mixture of MeOH/DCM (1:20) to give **3ec** (945 μ mol, 280 mg, 32%) as a yellow oil.

(\pm)-(4*aS*,8*aR*)-3-cyclohexyl-8*a*-(2-methoxyethyl)-4*a*,8*a*-dihydrobenzo[*e*][1,2,4]trioxin-6(5*H*)-one **3ec** (novel compound)

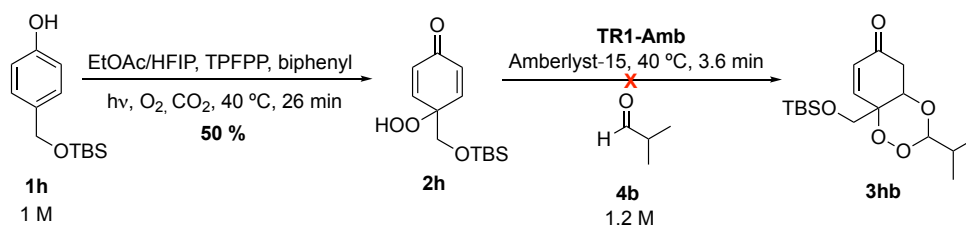


^1H NMR (400 MHz, Chloroform-*d*): δ 6.85 (dd, J = 10.4, 3.0 Hz, 1H, **1**), 6.07 (dd, J = 10.4, 1.2 Hz, 1H, **2**), 4.99 (d, J = 5.4 Hz, 1H, **10**), 4.26 (q, J = 3.0 Hz, 1H, **5**), 3.57 – 3.42 (m, 2H, **8**), 3.29 (s, 3H, **9**), 2.74 (dd, J = 17.6, 3.0 Hz, 1H, **4**), 2.66 (ddd, J = 17.6, 3.0, 1.2 Hz, 1H, **4'**), 2.03 – 1.85 (m, 2H, **7**), 1.76 – 1.59 (m, 5H, **12/13/14/15/16**), 1.52 – 1.44 (m, 1H, **11**), 1.19 – 0.97 (m, 5H, **12'/13'/14'/15'/16'**).

^{13}C NMR (101 MHz, Chloroform-*d*): δ 195.6 (**3**), 150.5 (**1**), 129.8 (**2**), 106.6 (**10**), 79.4 (**6**), 75.3 (**5**), 66.5 (**8**), 58.7 (**9**), 40.9 (**4**), 40.4 (**11**), 35.6 (**7**), 27.0 (**13/15**), 26.2 (**14**), 25.6 (**12/16**).

HRMS (ESI) m/z calcd [$\text{C}_{16}\text{H}_{28}\text{N}_1\text{O}_5$] $^+$ ($[\text{M} + \text{NH}_4]^+$): 314.1962, found 314.1966.

4.5.22. 1,2,4-Trioxane **3hb** from 4-((tert-butyldimethylsilyloxy)methyl)phenol **1h** and isobutyraldehyde **4b**

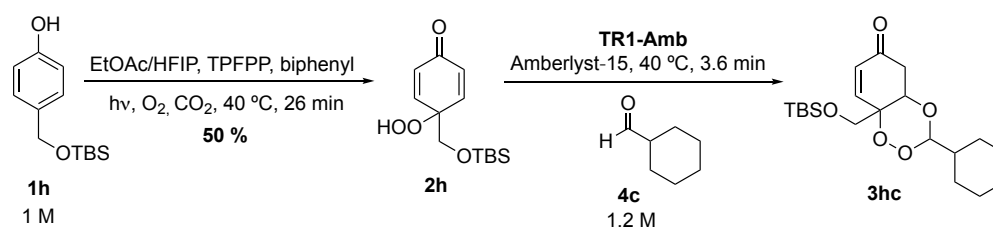


Reaction performed under general guidelines for the continuous flow telescoped synthesis of 1,2,4-trioxanes from photooxidation of *p*-substituted phenols

Reaction (1 M, 26 min): 15 mL starting solution of 4-((tert-butyldimethylsilyloxy)methyl)phenol **1h** (1.0 eq, 15.0 mmol, 3.57 g, 1.0 M), TPFPP (0.30 mol%, 45.0 μmol, 43.9 mg), HFIP (2.0 eq, 30.0 mmol, 3.20 mL) and biphenyl (0.070 eq, 1.05 mmol, 162 mg) in EtOAc. After 2.5 h of reaction, a 15 mL isobutyraldehyde **4b** solution (1.2 eq, 18.0 mmol, 1.12 mL, 1.2 M) was pumped after the photo reactor.

Results: The reaction was carried out for 4 h and monitored by ¹H NMR spectroscopy every 30 min. However, trioxane **3hb** was not identified in any of the analysis.

4.5.23. 1,2,4-Trioxane **3hc** from 4-((tert-butyldimethylsilyloxy)methyl)phenol **1h** and cyclohexanecarboxaldehyde **4c**



Reaction performed under general guidelines for the continuous flow telescoped synthesis of 1,2,4-trioxanes from photooxidation of *p*-substituted phenols

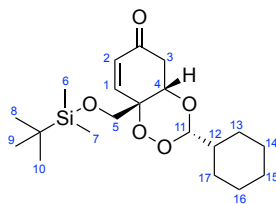
Reaction (1 M, 26 min): 19 mL starting solution of 4-((tert-butyldimethylsilyloxy)methyl)phenol **1h** (1.0 eq, 19.0 mmol, 4.52 g, 1.0 M), TPFPP (0.30 mol%, 57.0 μ mol, 56.2 mg), HFIP (2.0 eq, 38.0 mmol, 4.12 mL) and biphenyl (0.070 eq, 1.26 mmol, 205 mg) in EtOAc. After 2.5 h of reaction, a 10 mL cyclohexanecarboxaldehyde **4c** solution (1.2 eq, 12.0 mmol, 1.22 mL, 1.2 M) was pumped after the photo reactor.

Results: The system reached a steady state after 4.5 h of reaction. 1H NMR spectroscopy analysis of **3hc**: yield for 2nd step = 56%, overall yield = 28%, projected productivity = 8 g/day. Another sample was collected for 1 h (3 mL) and the following purification methods were attempted:

- Flash chromatography column: The product decomposed using this method when eluted with a mixture of EtOAc/Cyclohexane (1:4). A 2D thin layer chromatography (TLC) was then performed and confirmed the decomposition of the product over silica with the same elution used in the flash chromatography column.
- Crystallisation with Et_2O : a sample was concentrated under vacuum to give a dark brown oil. Crystallisation using diethyl ether did not work, even after the solution was put in the freezer for 24 h.

The compound could not be isolated, but the 1H NMR spectroscopy signals could be assigned in the sample and a HRMS was obtained.

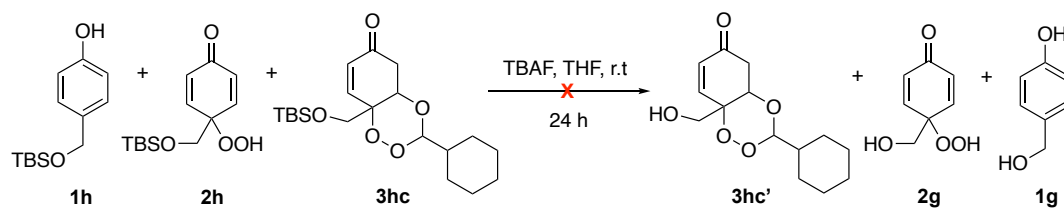
(±)-(4*a*S,8*a*R)-3-cyclohexyl-8*a*-(2-methoxyethyl)-4*a*,8*a*-dihydrobenzo[*e*][1,2,4]trioxin-6(5H)-one **3hc** (novel compound)



$^1\text{H NMR}$ (400 MHz, Chloroform-*d*): δ 6.80 (d, $J = 8.6$ Hz, 1H, **1**), 6.34 (d, $J = 8.6$ Hz, 2H, **2**), 4.94 (d, $J = 6.1$ Hz, 1H, **11**), 4.12 (q, $J = 7.1$ Hz, 1H, **4**), 3.81 (d, $J = 10.6$ Hz, 1H, **5**), 3.76 - 3.74 (m, 2H, **3**), 3.68 (d, $J = 10.6$ Hz, 1H, **5'**), 1.77 - 1.53 (m, 5H, **13/14/15/16/17**), 1.53 - 1.42 (m, 1H, **12**), 1.20 - 0.97 (m, 5H, **13'/14'/15'/16'/17'**), 0.87 (s, 9H, **8/9/10**), 0.05 (s, 6H, **6/7**).

HRMS (ESI) m/z calcd $[\text{C}_{20}\text{H}_{34}\text{O}_5\text{SiNa}]^+$ ($[\text{M} + \text{Na}]^+$): 405.2068, found 405.2047.

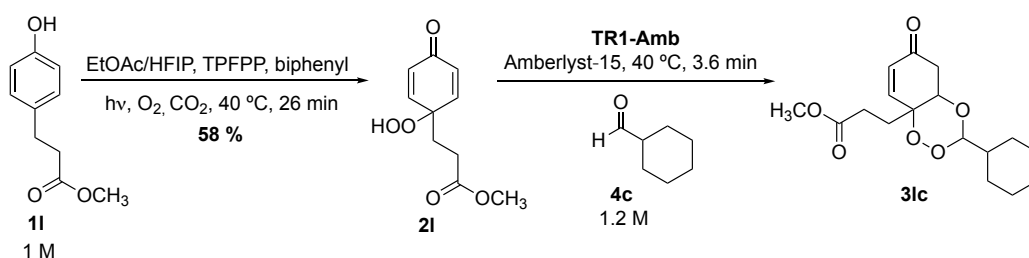
4.5.24. Deprotection of crude mixture of 1,2,4-Trioxane **3hc**, phenol **1h** and *p*-peroxyquinol **2h**



Procedure: An aliquot of 1.5 mL of the crude mixture containing **1h**, **2h** and **3hc** (1.0 eq, 1.50 mmol) from experiment 4.5.23 was concentrated under vacuum and diluted with THF (28 mL) in inert atmosphere, resulting in a red solution. Tetra-butylammonium fluoride 'TBAF' (1.50 eq, 2.25 mmol, 588 mg) was then added to the reaction mixture at room temperature and the brown solution was stirred for 24 h. After that, the solution was quenched with a saturated solution on NH_4Cl (10 mL), followed by extraction with EtOAc (3 x 10 mL). The organic layer was dried over MgSO_4 , filtered and concentrated under vacuum.

Results: a flash chromatography column of the reaction mixture was performed with EtOAc/Cyclohexane (1:4), but trioxane **3hc'** was not observed in any of the fractions in ^1H NMR spectroscopy.

4.5.25. 1,2,4-Trioxane **3c** from 3-(4-hydroxyphenyl)-propionate **1l** and cyclohexanecarboxaldehyde **4c**

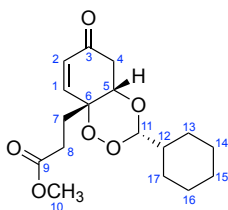


Reaction performed under general guidelines for the continuous flow telescoped synthesis of 1,2,4-trioxanes from photooxidation of p-substituted phenols

Reaction (1 M, 26 min): 18 mL starting solution of 3-(4-hydroxyphenyl)-propionate **1l** (1.0 eq, 18.0 mmol, 3.24 g, 1 M), TPFPP (0.30 mol%, 54.0 μ mol, 52.6 mg), HFIP (2.0 eq, 36.0 mmol, 3.81 mL) and biphenyl (0.070 eq, 1.26 mmol, 194 mg) in EtOAc. After 2 h of reaction, a 10 mL cyclohexanecarboxaldehyde **4c** solution (1.2 eq, 12.0 mmol, 1.52 mL, 1.2 M) was pumped after the photo reactor.

Results: The system reached a steady state after 3.5 h of reaction. ¹H NMR spectroscopy analysis of **3c**: yield for 2nd step = 90%, overall yield = 52%, projected productivity = 12 g/day. Another sample was collected for 27 min (1.35 mL) and concentrated under reduced pressure. Purification was carried out using flash chromatography column, with a mixture of MeOH/DCM (1:20) to give **3c** (469 μ mol, 152 mg, 35%) as a yellow oil.

(±)-Methyl 3-((4*aS*,8*aR*)-3-cyclohexyl-6-oxo-5,6-dihydrobenzo[*e*][1,2,4]trioxin-8*a*(4*aH*)-yl) propanoate **3lc** (novel compound)

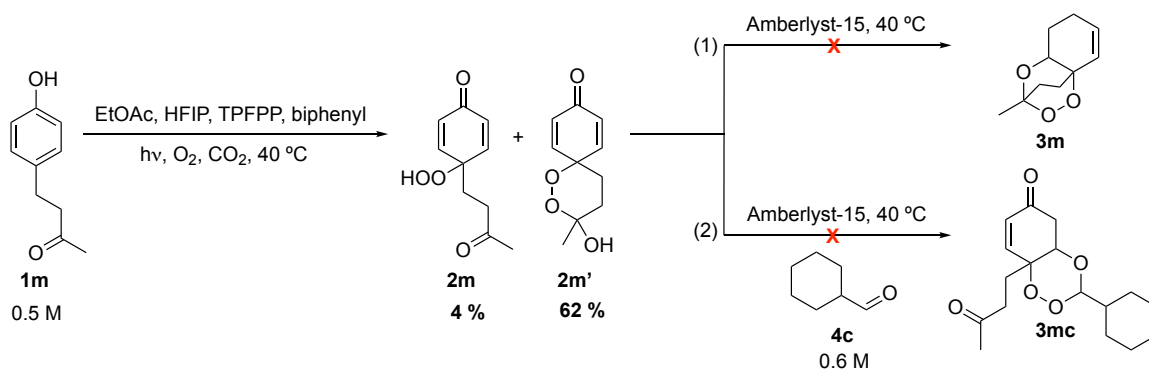


¹H NMR (400 MHz, Chloroform-*d*): δ 6.84 (dd, $J = 10.5, 2.9$ Hz, 1H, **1**), 6.12 (dd, $J = 10.5, 0.9$ Hz, 1H, **2**), 4.99 (d, $J = 5.4$ Hz, 1H, **11**), 4.16 (q, $J = 2.9$ Hz, 1H, **5**), 3.68 (s, 3H, **10**), 2.76 (dd, $J = 17.7, 2.9$ Hz, 1H, **4**), 2.72 (ddd, $J = 17.7, 2.9, 0.9$ Hz, 1H, **4'**), 2.54 (ddd, $J = 16.4, 9.9, 6.2$ Hz, 1H, **8**), 2.42 (ddd, $J = 16.4, 10.0, 6.0$ Hz, 1H, **8'**), 2.10 (ddd, $J = 14.8, 9.9, 6.0$ Hz, 1H, **7**), 2.01 (ddd, $J = 14.8, 10.0, 6.2$ Hz, 1H, **7'**), 1.71 – 1.57 (m, 5H, **13/14/15/16/17**), 1.53 - 1.45 (m, 1H, **12**), 1.21 – 0.98 (m, 5H, **13'/14'/15'/16'/17'**).

¹³C NMR (101 MHz, Chloroform-*d*): δ 195.0 (**3**), 172.9 (**9**), 149.4 (**1**), 130.7 (**2**), 106.7 (**11**), 79.0 (**6**), 75.3 (**5**), 52.1 (**10**), 40.9 (**4**), 40.4 (**12**), 30.5 (**7**), 27.3 (**8**), 27.0 (**14/16**), 26.2 (**15**), 25.7 (**13/17**).

HRMS (ESI) m/z calcd [C₁₇H₂₄O₆Na]⁺ ([M + Na]⁺): 347.1465, found 347.1467.

4.5.26. 1,2,4-Trioxane **3m** and 1,2,4-trioxane **3mc** from 4-(4-hydroxyphenyl)-2-butanone **1m** and cyclohexanecarboxaldehyde **4c**



Reaction performed under general guidelines for the continuous flow telescoped synthesis of 1,2,4-trioxanes from photooxidation of *p*-substituted phenols

- **Reaction 1 (0.5 M, 26 min):** 30 mL starting solution of 4-(4-hydroxyphenyl)-2-butanone **1m** (1.0 eq, 15.0 mmol, 2.46 g, 0.50 M), TPFPP (0.30 mol%, 45.0 μ mol, 43.9 mg), HFIP (2.0 eq, 30.0 mmol, 3.21 mL) and biphenyl (0.070 eq, 1.05 mmol, 162 mg) in EtOAc.

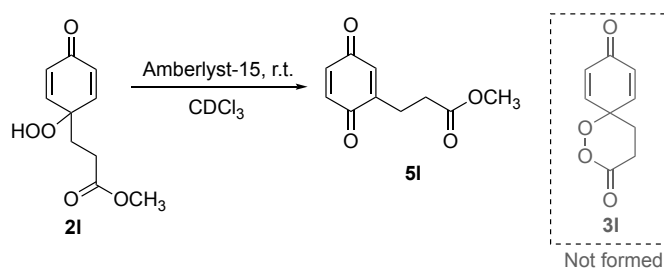
Results: The reaction was carried out for 3.5 h and monitored by 1H NMR spectroscopy every 30 min. However, trioxane **3m** was not identified in any of the analysis.

- **Reaction 2 (0.5 M, 26 min):** after 4h of Reaction 1, a 12 mL cyclohexanecarboxaldehyde **4c** solution (1.2 eq, 7.20 mmol, 872 μ L, 0.60 M) was pumped after the photo reactor.

Results: The reaction was carried out for another 2 h and monitored by 1H NMR spectroscopy every 30 min. However, trioxane **3mc** was not identified and a complex mixture was formed.

5. Continuous flow telescoped synthesis of 2-substituted 1,4-benzoquinones

This project arose from an observation during the scoping investigation of the dearomatisation of *p*-substituted phenols, see Chapter 3. In one reaction performed with an ester *p*-peroxyquinol **2I** in batch in the presence of Amberlyst-15, no cyclisation product **3I** was observed. Instead, an unexpected rearrangement of the *p*-peroxyquinol occurred to form a 1,4-benzoquinone **5I** (Scheme 47).



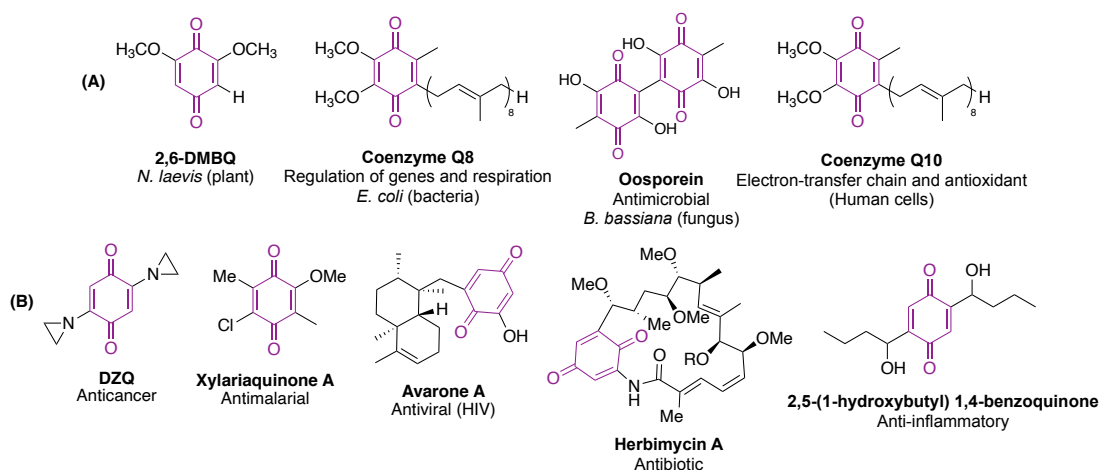
Scheme 47. 1,4-benzoquinone **5I** from methyl 3-(4-hydroxyphenyl) propionate *p*-peroxyquinol **2I**. No cyclisation product **3I** was observed.

5.1. Introduction

Quinones are cyclohexadienediones, a class of compounds that contain two carbonyl groups that are *ortho* or *para* to each other. Natural quinones' core structures are mainly derived from three aromatic rings: benzene, naphthalene or anthracene, and are classified in benzoquinones, naphthoquinones, or anthraquinones, respectively.²⁴⁶ Polyquinones are usually dimers²⁴⁷ or trimers²⁴⁸ of their respective quinones.

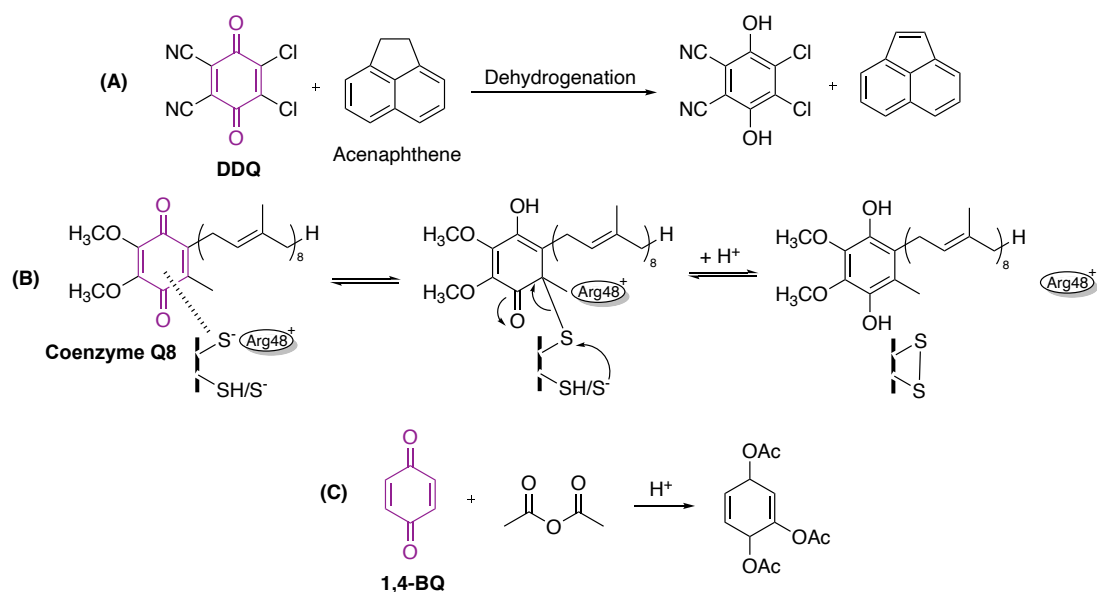
More specifically, 1,4-benzoquinones are found across a variety of living species²⁴⁹ (Scheme 48 - A), and possess a variety of medicinal properties²⁵⁰ (Scheme 48 - B). These compounds have been isolated from, for example, plant *N. laevis* (2,6-Dimethoxy-1,4-benzoquinone);²⁵¹ bacteria *E. coli* (Coenzyme Q8, which is essential for the regulation of genes, respiration, and oxidative stress adaptation);²⁵² fungus *B. bassiana* (Oosporein, which has antimicrobial properties);²⁵³ and humans (Coenzyme Q10, found in every cell of the body, possessing important antioxidant properties).²⁵⁴ CoQ10 also plays a significant role in the electron-transfer respiratory chain, through a redox reaction with Nicotinamide Adenine Dinucleotide (NADH) in the synthesis of Adenosine Triphosphate (ATP), the main compound responsible for the storage and transfer of energy in cells²⁵⁵ (Scheme 48 - A). 1,4-

Benzoquinones have also been reported to have additional pharmacological properties, such as anticancer (2,5-diaziridinyl-1,4-benzoquinone - DZQ),²⁵⁶ antimalarial (Xylariaquinone A),²⁵⁷ antibacterial (Herbimycin A)²⁵⁸, and anti-inflammatory (2,5-(1-hydroxybutyl) 1,4-benzoquinone)²⁵⁹ (Scheme 48 - B).

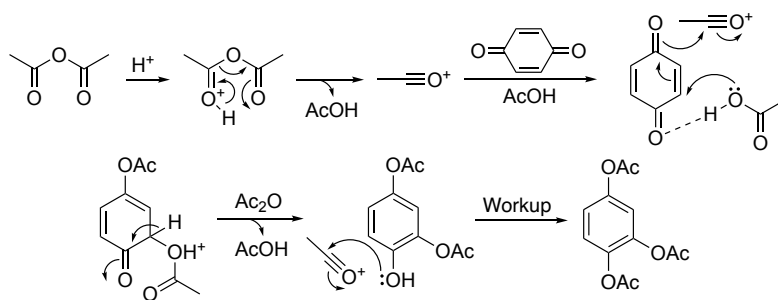


Scheme 48. Naturally occurring 1,4-benzoquinones across different kingdoms (A) and other pharmacological properties (B).

1,4-Benzoquinones, such as 2,3-dichloro-5,6-dicyanobenzoquinone (DDQ) and coenzyme Q8, are known to be oxidants.²⁶⁰ DDQ has been reported to abstract a pair of hydrogen atoms from acenaphthene (Scheme 49 - A).²⁶¹ Coenzyme Q8, on the other hand, participates in a charge transfer complex with thiolate in *de novo* disulfide bond generation (Scheme 49 - B).²⁶² 1,4-Benzoquinone itself can react with acetic anhydride in an acid-catalysed Thiele reaction (Scheme 49 - C).²⁶³ In this type of reaction, acetic anhydride forms acetyl cation in the presence of acid, which then reacts with 1,4-benzoquinone in a conjugated addition with acetic acid. Re-aromatization followed by the nucleophilic attack of the phenol to another acetyl cation gives the final product (Scheme 50).



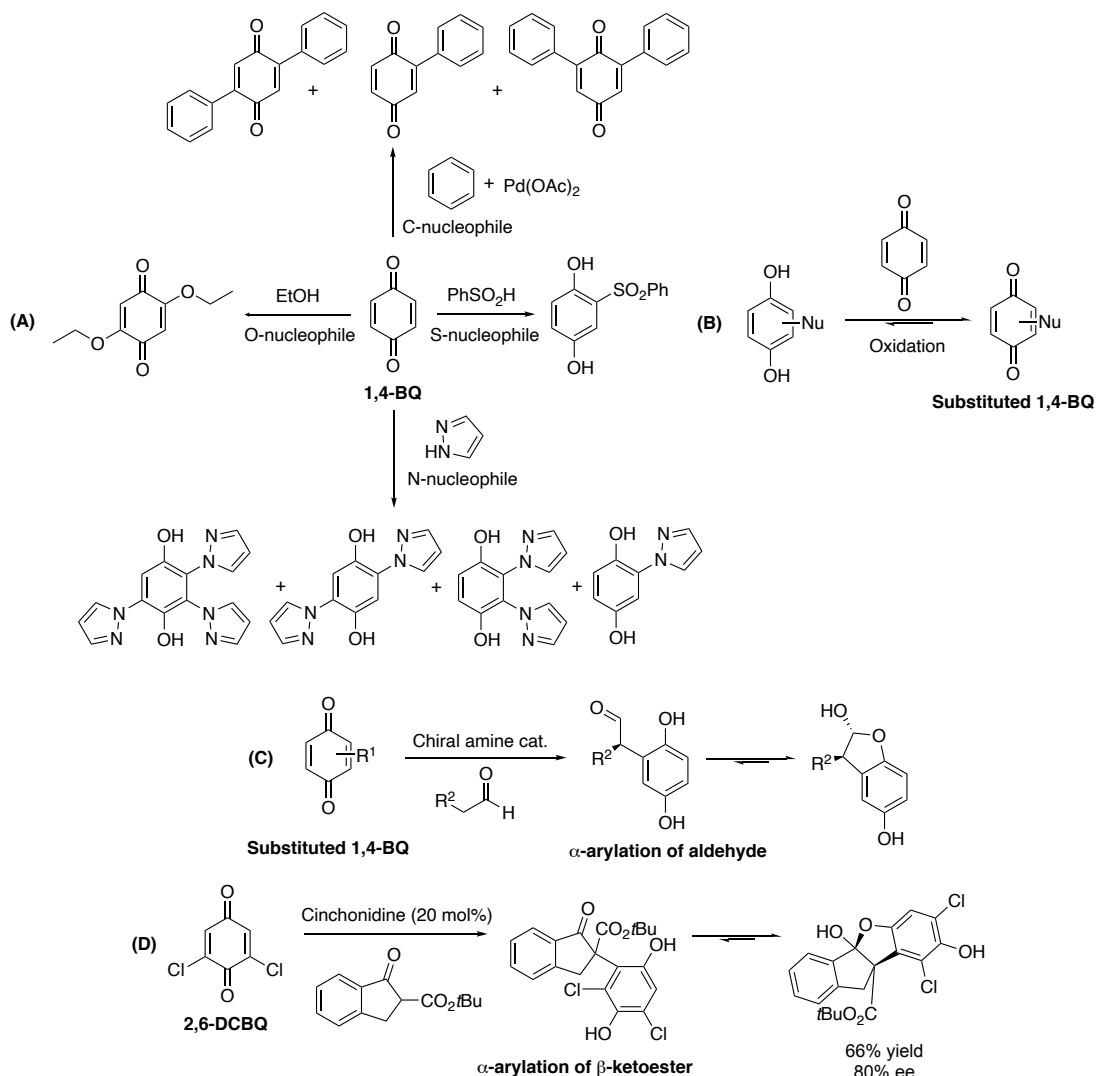
Scheme 49. 1,4-benzoquinones as oxidants: DDQ (A), Coenzyme Q8 (B) and 1,4-BQ (C).



Scheme 50. Thiele reaction mechanism.²⁶³

1,4-Benzoquinones also participate in conjugated nucleophilic addition as Michael acceptors and cycloadditions, which makes this moiety an important and versatile building block in organic syntheses.^{249, 264}

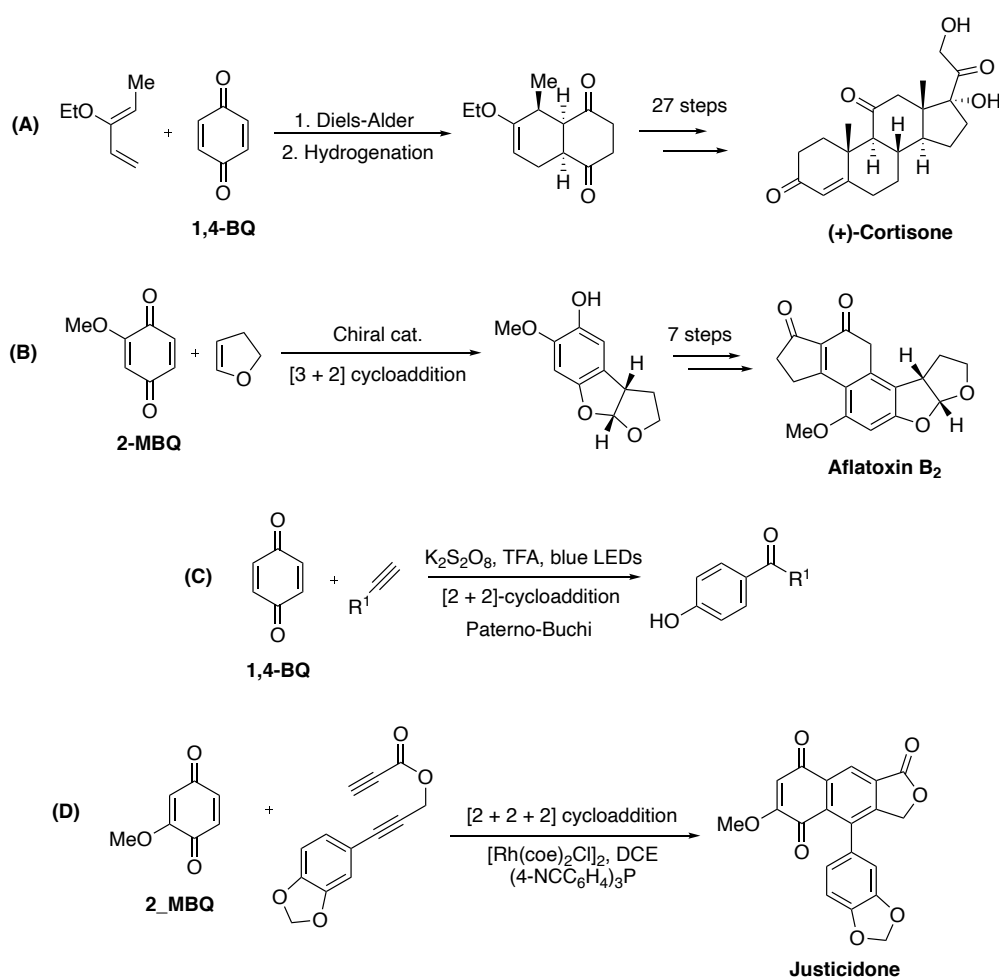
As Michael acceptors, 1,4-benzoquinones can form mono-, di-, or tri- substituted benzoquinones or hydroquinones via conjugated addition of carbon and heteronucleophiles (Scheme 51 - A).²⁶⁵ It was also reported that an excess of benzoquinone can lead to substituted 1,4-benzoquinones (Scheme 51 - B).²⁶⁵ 1,4-Benzoquinones can also participate in arylation reactions to form α -functionalised aldehydes (Scheme 51 - C)²⁶⁶ and β -ketoesters (Scheme 51- D)²⁶⁷. However, the products were isolated as their corresponding cyclic hemiacetals which are more stable.



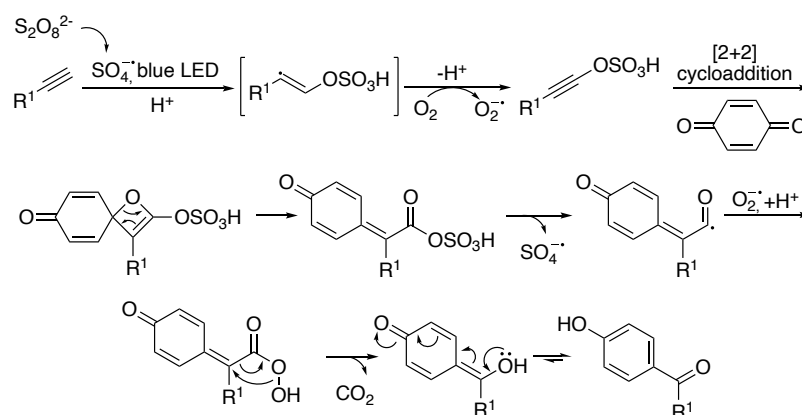
Scheme 51. 1,4-Benzoquinones as Michael-acceptors: Addition of carbon and heteronucleophiles (A), followed by further oxidation to form substituted 1,4-benzoquinones (B); α -arylation of aldehydes (C) and β -ketoesters (D).

Cycloadditions require electron-deficient dienophiles/dipolarophiles such as 1,4-benzoquinones, which are excellent reagents for these types of reaction. They have been employed in numerous total syntheses of natural products,²⁶⁸ such as the enantioselective synthesis of the steroid hormone (+)-cortisone (Scheme 52 **Error! Reference source not found.**- A).²⁶⁹ The mutagen aflatoxin B₂ was synthesised by Corey and Zhou through a [3+2] cycloaddition between 2-methoxy-1,4-benzoquinone (2-MBQ) and 1,3-dihydrofuran (Scheme 52 - B).²⁷⁰ Besides thermal cycloaddition, these benzoquinones can also undergo Paternò-Büchi [2+2]-photocycloadditions in the presence of K₂S₂O₈ and TFA (Scheme 52 - **Error! Reference source not found.**C).²⁷¹ The mechanism for this particular reaction starts with the addition of sulfate radical ion to the alkyne, forming a vinyl radical intermediate,

which then reacts with molecular oxygen to form an organosulfonic species. A [2+2]-cycloaddition with the carbonyl of 1,4-benzoquinone generates an oxetene, which after rearrangement and release of sulfate radical ion, gives an acyl radical intermediate. The following reaction with superoxide anion in the presence of acid, decarboxylation, and keto-enol tautomerism gives the final product observed (Scheme 53). Besides [2+2] cycloadditions, the first metal catalysed [2+2+2] cycloaddition between 2-MBQ and diynes was reported by Bower and co-workers.²⁷² This methodology was then applied in the total synthesis of the anti-leishmanial justicidone (**Error! Reference source not found.** - D).



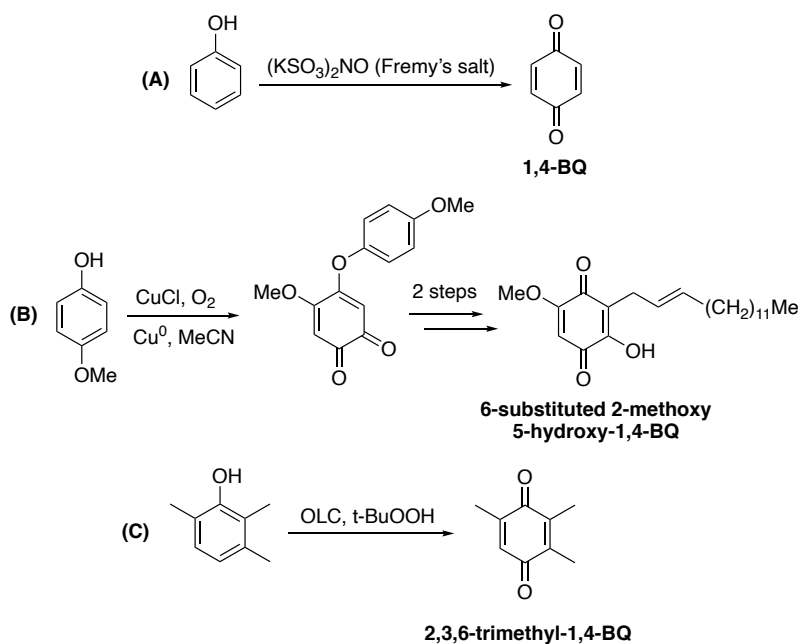
Scheme 52. 1,4-Benzoquinones as dienophiles/dipolarophiles: synthesis of (+)-cortisone (A); aflatoxin B₂ (B); Paternò-Büchi [2+2]-photocycloaddition (C); and synthesis of justicidone (D).



Scheme 53. Mechanism of Patternò-Büchi [2+2]-photocycloaddition between 1,4-benzoquinone and a substituted alkyne.

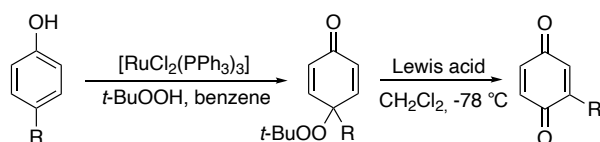
In general, 1,4-benzoquinones can be biosynthesised, for example in the case of Coenzyme Q10,²⁷³ or chemically synthesised from hydroquinones, dimethoxybenzenes, and phenols predominantly. Other chemical pathways and substrates for the synthesis of 1,4-benzoquinones include the oxidation of hydroquinone acetates,²⁷⁴ *N*-arylsulphonamides²⁷⁵ and anilines,²⁷⁶ thermal rearrangement of cyclobutenones,²⁷⁷ and others.^{249, 278}

One of the earliest synthesis of 1,4-benzoquinones from phenols used Fremy's salt [potassium nitrodisulfonate, (KSO₃)₂NO] (Scheme 54 - A).²⁷⁹ Since then, many other oxidants have been used for the oxidation of phenols, including heavy metal oxidants,²⁸⁰⁻²⁸⁵ hydroperoxides,²⁸⁶ nitric acid,²⁸⁷ and ammonium cerium nitrate.²⁸⁸ Alternative strategies have also been employed, such as the Claisen rearrangement of *o*-benzoquinone from the oxidation of 4-methoxyphenol (Scheme 54 - B).²⁸⁴ However, these oxidations can be inefficient due to the lack of selectivity and formation of by-products,^{281, 289} as the initial phenoxy radical intermediates are highly reactive and undergo multiple side reactions. Also, they often require strong oxidants in corrosive conditions and/or toxic, expensive and inconvenient transition metal catalysts, hampering its application at large scale. Only few studies have reported metal-free selective oxidation of phenols, for example, using onion-like carbon (OLC) nanocatalysts (Scheme 54 - C).²⁹⁰ The synthesis of substituted 1,4-benzoquinones from phenols is also economically attractive, as the product is often more expensive than the corresponding phenol.²⁹¹



Scheme 54. Examples of 1,4 benzoquinones from phenols: synthesis using Fremy's salt (A), Claisen rearrangement strategy via *o*-benzoquinones (B) and metal-free selective oxidation of substituted phenols (C).

Given the ongoing synthetic importance of dearomatisation strategies of aromatic compounds,^{292, 293} Murahashi has reported three publications on the synthesis of 2-substituted quinones through oxidative dearomatisation of *p*-substituted phenols (Scheme 55).²⁸¹⁻²⁸³ The cyclohexadienone bearing a *p*-*tert*-butoxide group would then undergo a 1,2-alkyl shift, yielding 2-substituted-1,4-benzoquinone in a selective manner.



Scheme 55. Selective synthesis of 2-substituted-1,4-benzoquinones via dearomatisation of *p*-substituted phenols.

Selective metal catalysed oxidation of phenols appear to have previously been underexploited and limited, in some cases, by bulky substituents in specific positions on the phenol.²⁹⁴⁻²⁹⁶ Murahashi's procedure, therefore, has advantages such as an expanded scope of the reaction, including 1,4-benzoquinones bearing two or three substituents which are challenging to prepare, and selectivity at the 2-position of the cyclohexadienone ring.²⁸² However, this methodology could be further improved to enable a safe and efficient scaling-up. The oxidative dearomatisation step uses an air sensitive catalyst tris(triphenylphosphine)ruthenium(II) dichloride ($RuCl_2(PPh_3)_3$),²⁹⁷ which makes processing

complicated. In addition, *tert*-butyl hydroperoxide could readily cause runaway reactions,²⁹⁸ especially in highly flammable solvents such as benzene. For the second step, an environmentally undesirable solvent (dichloromethane) and acid catalyst (titanium chloride) are used. In addition, the low temperature required (-78 °C) and the use of dichloromethane makes the process expensive and unattractive for scale-up.

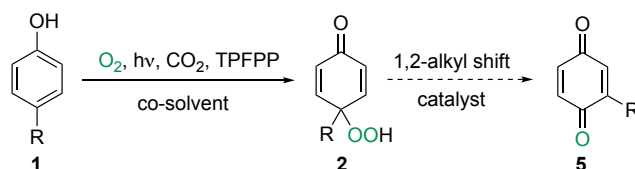
5.2. Aims and general strategy

Even though the literature concerning the synthesis of 1,4-benzoquinones **5** is extensive, new sustainable and selective methodologies for their synthesis are still required.^{299, 300} My recent work on the dearomatisation of *p*-substituted phenols **1** in continuous flow, combined with Murahashi's findings,²⁸¹⁻²⁸³ suggested a new synthetic route for 2-substituted-1,4-benzoquinones. The aims for this Chapter were:

- To explore whether the dearomatisation of *p*-substituted phenols can be used in the synthesis of 2-substituted-1,4-benzoquinones in batch.
- To transfer this batch methodology to a telescoped continuous flow approach.
- To begin expanding the scope of the synthesis of 2-substituted-1,4-benzoquinone.

To address the above aims, the following strategies were put in place:

1. A synthetic route for the telescoped synthesis of 2-substituted-1,4-benzoquinones **5** was developed. It consists of two consecutive steps: continuous flow dearomatisation of *p*-substituted phenols **1** using singlet oxygen in supercritical CO₂, followed by a catalysed 1,2-alkyl shift to form 2-substituted-1,4-benzoquinones **5** (Scheme 56).



Scheme 56. Proposed telescoped synthesis of 2-substituted-1,4-benzoquinones.

2. The reaction was tested in similar conditions previously reported by Murahashi for reproducibility purposes.

3. Then, the second step of the proposed synthesis of 1,4-benzoquinones **5** was investigated in batch, screening different catalysts, concentrations of starting material, catalyst loadings, temperatures, and solvents.

4. Telescoped synthesis was then investigated in continuous flow and this approach was extended to other 1,4-benzoquinones **5**.

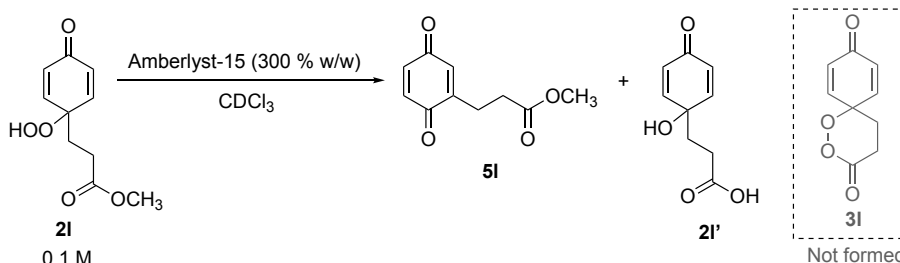
5.3. Results and discussion

5.3.1. Project inspiration: rearrangement of *p*-peroxyquinols to 1,4-benzoquinones

During previous studies on the synthesis of 1,2,4-trioxanes (Chapter 4), an intramolecular cyclisation of *p*-peroxyquinol **2I** was attempted in batch, screening different temperatures and catalyst loading (Table 11). CDCl₃ was used as the solvent so the samples could be taken directly from the reaction mixture and analysed by ¹H NMR spectroscopy.

Surprisingly, 1,4-benzoquinone **5I** was identified instead of the cyclisation product **3I**. The ratio of 1,4-benzoquinone **5I**: *p*-peroxyquinol **2I** increased with reaction time (Entry 1 – Table 11). However, complete decomposition of both compounds occurred after heating up the reaction to 40 °C (Entry 2 – Table 11). The reaction was repeated with less Amberlyst-15 and the product obtained after purification was confirmed to be the 1,4-benzoquinone **5I**, with 8% isolated yield (Entry 3 – Table 11).

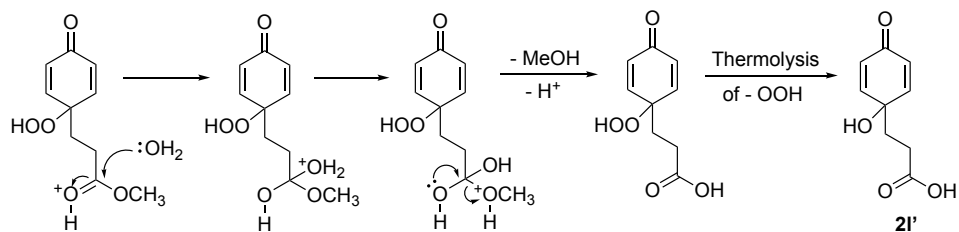
Table 11. Screening of catalyst loading and temperature in the attempted intramolecular cyclisation of methyl 3-(4-hydroxyphenyl) propionate *p*-peroxyquinol **2I**.



Entry	Temperature (°C)	Time (h)	NMR ratio 5I : 2I	NMR ratio 2I' : 2I
1	r.t.	1	1: 4.5	1: 4.9
		2	1: 1.8	1: 3.9
2	40	2	Decomposition	
3^a		2	Isolated yield: 5I (8%), 2I (6%)	

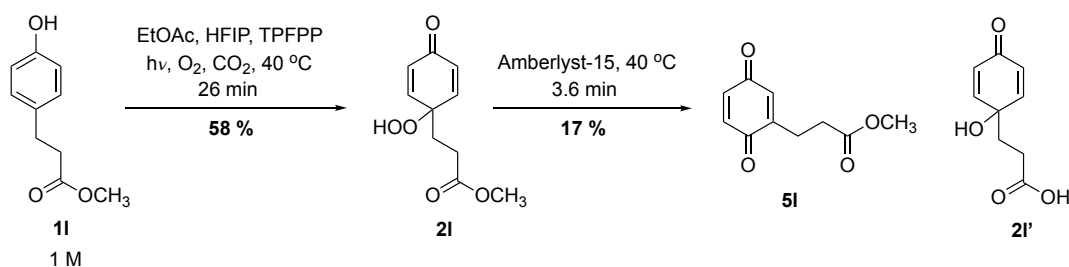
¹H NMR spectroscopy yields were calculated using 0.05 of biphenyl as the internal standard. ^a Amberlyst (100% w/w)

In most experiments, hydrolysis of **2I** occurred, possibly catalysed by Amberlyst-15.³⁰¹ Thermolysis of the *p*-peroxyquinol³⁰² would then occur, resulting in the formation of the compound **2I'** (Scheme 57).



Scheme 57. Possible mechanism for the hydrolysis and thermolysis of **2I** to generate **2I'**.

The reaction was then transferred to flow, under similar conditions used in the telescoped synthesis of 1,2,4 trioxanes (Scheme 58). The overall yield of 1,4-benzoquinone **5I** was 10% (17% for the second step), with a residence time of 3.6 min and productivity of 1 g/day. This result was promising since the reaction had not been yet optimised. Therefore, the 1,2-alkyl shift step became the object of further investigation.

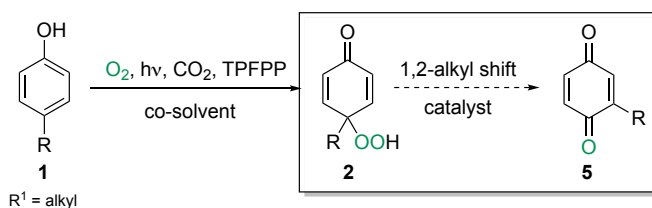


Concentration of TPFPP: 0.3 mol %; 2 equiv. HFIP; 0.75 g Amberlyst-15, biphenyl as the internal standard for NMR yields.

Scheme 58. Telescoped synthesis of 1,4-benzoquinone **5I** in flow under similar conditions for the synthesis of 1,2,4-trioxanes.

5.3.2. 1,2-alkyl shift of *p*-peroxyquinol **2a**: initial studies

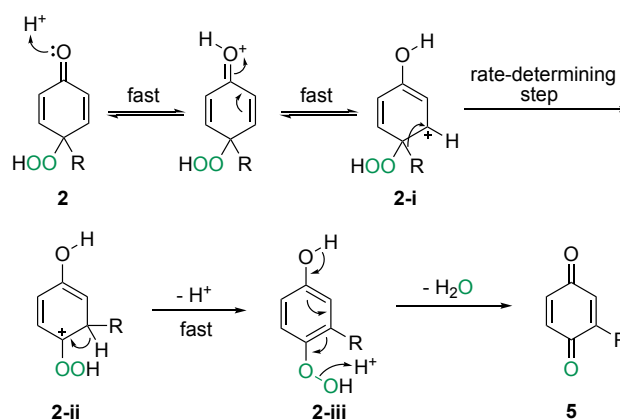
Following up the discovery of the 1,2-alkyl shift of *p*-peroxyquinols **2**, this reaction was further investigated in batch (Scheme 59).



Scheme 59. 1,2-alkyl shift of *p*-peroxyquinols **2** in the proposed telescoped synthesis of 1,4-benzoquinones **5**.

Reaction Mechanism

Based on Murahashi's work,²⁸³ it was hypothesised that the carbonyl of the *p*-peroxyquinol **2** would be activated by acid via a dienone-phenol rearrangement, forming a cation **2-i**. The rate-determining step is the 1,2-shift of the alkyl group in *para* position to form species **2-ii**, which is followed by deprotonation to give **2-iii**. Elimination of water and regeneration of the catalyst would give the 2-substituted-1,4-benzoquinone **5** (Scheme 60).

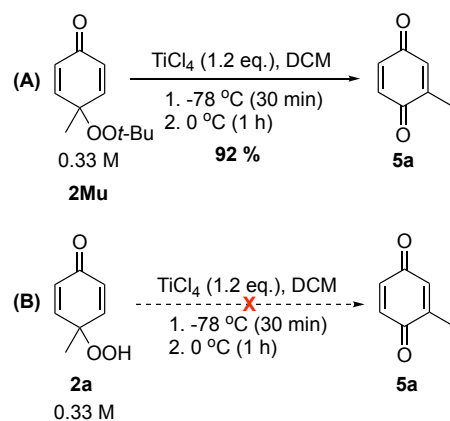


Scheme 60. Proposed mechanism for the synthesis of 2-substituted-1,4-benzoquinones **5**.

The migratory aptitude of the group in *para* position of the phenol has also been studied by Murahashi *et al.*, who concluded that groups which are stabilised by resonance or are electron-donating can undergo the 1,2-alkyl shift more easily, resulting in higher yields.^{283, 303} The migratory aptitude is a result of the ability to stabilise the carbocation and it was ordered as $Ph > iPr > Et > Me$.

Reproducibility test of Murahashi's procedure

To test if the procedure reported by Murahashi was reproducible for an analogous substrate, the reaction was performed under similar conditions²⁸² (Scheme 61 - A), with *p*-peroxyquinol **2a** instead of 4-(*tert*-butylperoxy)-2,5-cyclohexadienone **2Mu** (Scheme 61 - B). It was decided to start with *p*-peroxyquinol **2a** as the methyl migration is the most challenging and the optimised methodology developed would then give better results for other substituents. However, when similar conditions were replicated, no signals of the product were identified in 1H NMR spectroscopy analysis.

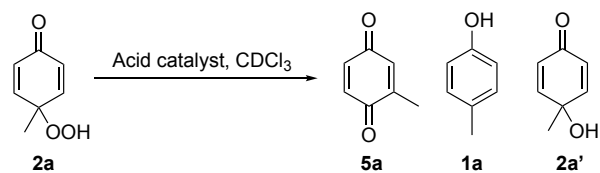


Scheme 61. (A) Synthesis of 2-methyl-1,4-benzoquinone by Murahashi²⁸² and (B) under similar conditions using *p*-peroxyquinol **2a**. X represents that the product could not be formed.

Initial studies in batch

As the conditions reported by Murahashi failed to give the desired product, a series of experiments were designed to try to obtain 1,4-benzoquinone **5a**. To do so, different acid catalysts such as $\text{BF}_3 \cdot \text{OEt}_2$, triflic acid, TFA, PTSA, and Amberlyst-15 were tested. The reactions were performed with different concentrations of *p*-peroxyquinol **2a**, catalyst loadings, and temperatures (Table 12). As these were initial investigations to check if the reaction could work, no internal standard was used. Instead, ^1H NMR spectroscopy ratios of products and by-products to starting material were compared to find a condition suitable for further optimisation.

Table 12. Summary of the initial experiments for the synthesis of 1,4-benzoquinone **5a**.



Entry	Catalyst	Concentration 2a (M)	Catalyst loading	Temperature (°C)	Time (h)	NMR Ratio 5a: 2a	NMR Ratio 1a: 2a	NMR Ratio 2a': 2a
1	BF ₃ .OEt ₂	0.2	1.2 eq.	r.t.	1	Decomposition		
2	TfOH		1.2 eq.	r.t.	1	Decomposition		
3	TFA		1.2 eq.	r.t.	24	No reaction		
4			1.2 eq.	40	24	No reaction		
5			4.8 eq.	40	24	0	0	1: 3.6
6	PTSA		1.2 eq.	40	4	1: 2.4	1: 9.4	0
		1.2 eq.	40	24	Decomposition			
7	Amberlyst-15	0.1	100% w/w	40	2	1: 8.3	1: 45.4	0
				40	4	1: 5.0	1: 28.0	0
				40	24	1: 1.3	1: 9.6	0
8		0.2		40	2	1: 4.9	1: 35.0	0
				40	4	1: 3.0	1: 23.3	0
				40	24	1: 0.6	1: 2.6	0
9		r.t.		24	1: 4.9	1: 45.5	0	
10		1.0		40	2	1: 3.1	1: 9.8	0
				40	4	1: 1.8	1: 6.8	0
	40		24	Decomposition				

Strong acids such as Lewis acid $\text{BF}_3 \cdot \text{OEt}_2$ (Entry 1 – Table 12) and Brønsted acid TfOH ($\text{pK}_a = -15$)³⁰⁴ (Entry 2 – Table 12) led to complete decomposition of the starting material, after only 1 h of reaction at room temperature. Although lower temperatures could have been tested, these acids would be incompatible with the stainless steel of the high-pressure flow system. Therefore, other acids were investigated.

To avoid decomposition of the starting material, a weaker acid TFA ($\text{pK}_a = 0.52$)³⁰⁵ was tested. In the first two experiments, no reaction was observed even when the temperature was increased from room temperature (Entry 3 – Table 12) to 40 °C (Entry 4 – Table 12). Increasing the acid catalyst loading (Entry 5 – Table 12) caused the reduction of *p*-peroxyquinol **2a** to *p*-quinol **2a'**. TFA was likely not strong enough to protonate the carbonyl in the *p*-peroxyquinol **2a**.

When the reaction was carried out with PTSA ($\text{pK}_a = -6.0$),³⁰⁶ a ^1H NMR spectroscopy ratio of 1: 2.4 of 1,4-benzoquinone **5a**: *p*-peroxyquinol **2a** was observed after 4 h, but complete decomposition occurred after 24 h of reaction (Entry 6 – Table 12). Notably, a small conversion of *p*-peroxyquinol **2a** to the corresponding phenol **1a** also occurred. It is possible that PTSA activates **2a'** and facilitates rearomatisation of the ring to give *p*-cresol **1a**.

To investigate the difference between homogeneous and heterogeneous catalysis, Amberlyst-15 ($\text{pK}_a = -6.5$)³⁰⁷ was used as an equivalent polymer-supported acid catalyst to PTSA, as both compounds possess a benzenesulfonic group and have similar pK_a values. Indeed, at 0.2 M similar results were obtained after 4 h of reaction between both catalysts (Entries 6 and 8 – Table 12).

Although few experiments were performed, there was an indication that the concentration of substrate might have an influence on the ratio of **5a**: **2a**. Comparing the values obtained in Entries 7, 8 and 10 on Table 12 after 4 h of reaction, the ratios of 1,4-benzoquinone **5a** increased from 1: 5.0 at 0.1 M (Entry 7 – Table 12) to 1: 1.8 at 1.0 M (Entry 10 – Table 12). However, no ^1H NMR spectroscopy signals for either the *p*-peroxyquinol **2a** or the 1,4-benzoquinone **5a** were detected at 1.0 M after 24 h of reaction (Entry 10 – Table 12). Instead, a complex mixture was formed.

Regarding the effect of temperature, there was a significant increase in ratio of 1,4-benzoquinone **5a** from 1: 4.9 to 1: 0.6 when the reaction was heated up to 40 °C for 24 h (Entry 8 – Table 12) compared to room temperature (Entry 9 – Table 12).

Based on these experiments, two parameters were fixed to carry out the optimisation: The concentration of substrate was fixed at 0.5 M and the reaction time was set at 4 h. As for the solvent system, EtOAc/HFIP was selected because the first step of the proposed telescoped synthesis had previously been carried out in this solvent mixture. After fixing the concentration of **2a**, reaction time and solvent system, other catalysts and temperatures were screened to optimise the reaction.

5.3.3. 1,2-Alkyl shift of p-peroxyquinol 2a: batch optimisation of catalyst and temperature

For the first part of the optimisation, five acid catalysts were tested: diphenylphosphinic acid ($\text{Ph}_2\text{PO}_2\text{H}$), trimethylsilyl trifluoromethanesulfonate (TMSOTf), camphorsulfonic acid (CSA), niobium phosphate (NbOPO_4) and Amberlyst-15. The reaction was also analysed at four different temperatures between $-78\text{ }^\circ\text{C}$ and $60\text{ }^\circ\text{C}$ (Table 13).

To investigate if the removal of water could increase the yield of **5a**, 4Å molecular sieves were added to the reaction (Entry 6 – Table 13), but there was no difference in yield compared to Entry 5.

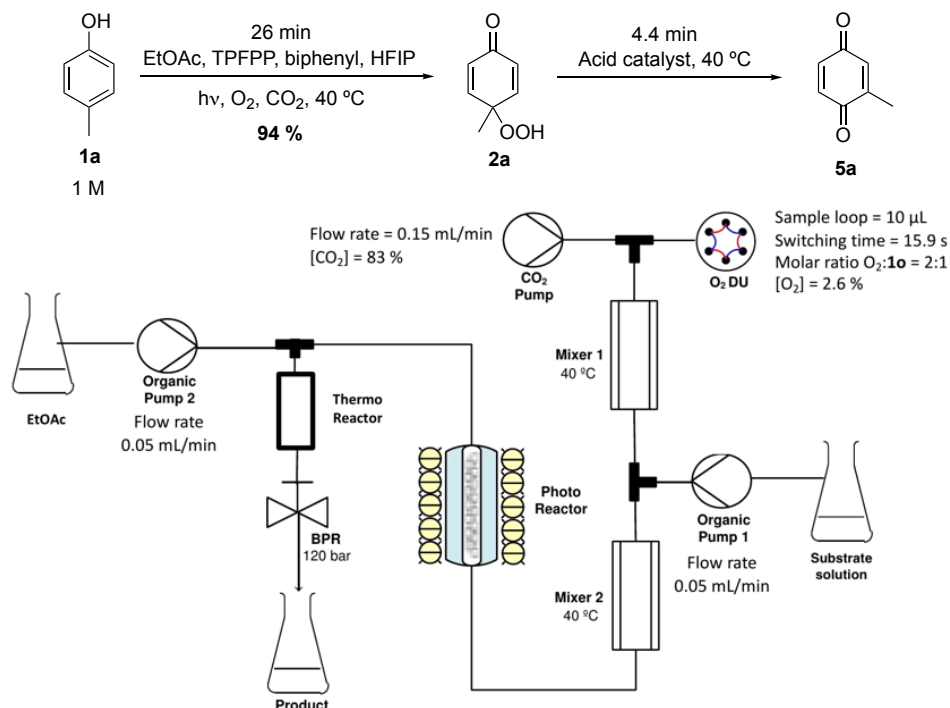
Different temperatures were also tested (Entries 7 to 9 – Table 13). Based on Murahashi's experiments, the reaction was cooled down to – 78 °C (Entry 7 – Table 13), but there was no conversion of starting material. At room temperature (Entry 8 – Table 13), a slightly lower yield of **5a** (3%) was obtained when compared to 40 °C (Entry 5 – Table 13), whereas heating up the reaction to 60 °C led to complete decomposition of **2a** (Entry 9 – Table 13).

In all experiments, moderate to high conversions of substrate were observed, even though the yields obtained of **5a** were very poor. Although ¹H NMR spectroscopy analysis did not show signals for other by-products, it might be that 1,4-benzoquinone **5a** had polymerised in the presence of acid catalyst, as this has been observed for a similar compound 1,4-benzoquinone.³¹¹ As the flow setup proposed would have the catalyst in a packed bed, it was thought that 1,4-benzoquinone **5a** would be exposed to the acid for a shorter period of time and therefore, diminish possible polymerisation.

5.3.4. 1,2-Alkyl shift of p-peroxyquinol 2a: continuous flow test using Amberlyst-15 and NbOPO₄

As the best results obtained were the same for both solid acid catalysts (Amberlyst-15 and NbOPO₄), these reactions were tested in flow and the results were compared (Table 14). More information about the conditions used in these experiments, can be found in the experimental procedures.

Table 14. Comparison between the continuous flow telescoped synthesis of 1,4-benzoquinone **5a** with Amberlyst-15 and NbOPO₄, and simplified scheme of the high-pressure setup used.



Entry	Catalyst	Thermo reactor and catalyst loading	NMR conversion 1a (%)	NMR yield 5a (%)
1	Amberlyst-15	TR3-Amb (0.75 g)	78	4
2	NbOPO ₄	TR3-NbP (0.75 g)	84	1

System specifications: photo reactor (10 mm outer diameter 'o.d.', 240 mm length, 1 mm wall thickness, effective volume = 5.2 mL, filled with 38 glass beads with 6 mm o.d., at 40 °C) and thermo reactor (1/4" o.d., 0.049" wall thickness, 15 cm length, effective volume = 1.1 mL, at 40 °C) was packed with either: **TR3-Amb** = 0.75 g Amberlyst-15 and 0.85 g of 0.5-0.75 mm o.d. glass beads; or **TR3-NbP** = 0.75 g NbOPO₄ and 2.5 g of 1.5 – 2 mm o.d. glass beads. Concentration of TPFPP = 0.3 mol%, and biphenyl (0.05 eq.) was used as internal standard for ¹H NMR spectroscopy analysis.

For the experiment using Amberlyst-15 (Entry 1 – Table 14), the thermo reactor **TR3-Amb** with smaller glass beads (0.5 – 0.75 mm o.d.) was used as it gave better results in Chapter 4. However, as NbOPO₄ (NbP) is a finer powder, different thermo reactor designs had to be made to avoid blockages or leakages (Figure 42).

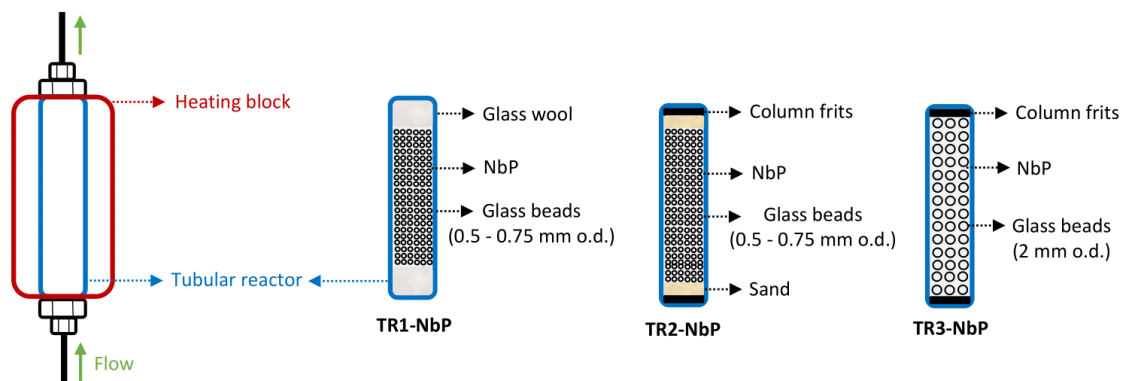


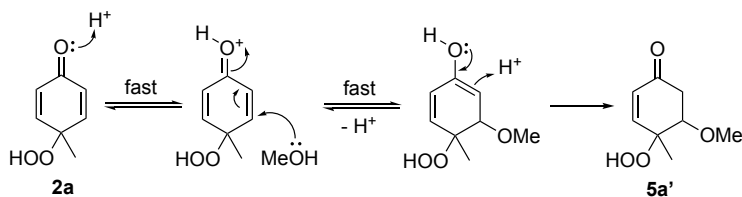
Figure 42. Different niobium phosphate (NbP) packed bed reactor schemes: **TR1-NbP** = 0.75 g NbP + 1.9 g 0.5 – 0.75 mm o.d. glass beads; **TR2-NbP** = 0.75 g NbP + 1.6 g 0.5 – 0.75 mm o.d. glass beads and **TR3-NbP** = 0.75 g NbP + 2.0 g 2 mm o.d. glass beads.

The first design (**TR1-NbP**) failed when the reactor was connected to the nitrogen line and the glass beads and NbP went through the glass wool. To avoid that, a column frit and a layer of sand were installed at each end of the tubular reactor (**TR2-NbP**). However, when the reactor was connected to the flow system and CO₂ flowed through it, the system reached overpressure possibly because NbP was highly compacted. In the last design (**TR3-NbP**), the sand layers were removed, and bigger glass beads were mixed with NbP to avoid overpacking. This reactor was successfully implemented for the reaction in Entry 2 – Table 14.

Although both reactions had very poor yield, Amberlyst-15 was chosen as the acid-catalyst for further batch optimisation.

5.3.5. 1,2-Alkyl shift of *p*-peroxyquinol 2a: batch optimisation of solvent

After studying the influence of concentration on starting material, temperature and catalyst, seven different solvents were tested to improve the yield of 1,4-benzoquinone **5a**: dimethyl carbonate (DMC), EtOAc, 2-Methyltetrahydrofuran (Me-THF), acetonitrile (MeCN), MeOH, toluene/HFIP and CDCl₃, at 0.5 M concentration of peroxyquinol **2a** using Amberlyst-15 at 40 °C (Table 15).



Scheme 62. Mechanism of 1,4-conjugate addition of methanol to peroxyquinol **2a**.

Murahashi published a separate article specifically about the 1,2-alkyl shift of a methyl group, as this migration is very challenging, changing the solvent system to toluene/HFIP 1:3.²⁸³ Compared to the experiment in EtOAc + 2 eq. HFIP (Entry 5 – Table 13), the toluene/HFIP mixture did not show any improvement, resulting in the same 5% yield of **5a** (Entry 6 – Table 15).

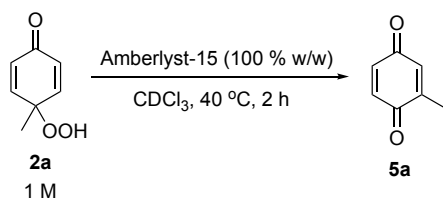
The final solvent tested was CDCl₃, as it was the medium for the initial studies (Table 12). Although the dielectric constant of chloroform is quite low ($\epsilon = 4.8$),³¹⁷ the results were very similar (Entry 7 – Table 15) to the ones with EtOAc/HFIP and toluene/HFIP solvent mixtures.

Optimisation of the concentration of **2a**, temperature, catalyst, and solvent for the 1,2-alkyl shift of peroxyquinol **2a** did not improve the yield significantly, with only 5% of 1,4-benzoquinone **5a** obtained in the best results, using either toluene/HFIP or CDCl₃. The dielectric constant of the solvents was not a good predictor for this reaction, as CDCl₃ and toluene/HFIP gave similar yields of **5a** and have different dielectric constants. It was then hypothesised that instead of the reaction yield being low, that the quantification method was not suitable.

5.3.6. 1,2-alkyl shift of *p*-peroxyquinol **2a**: quantification methods

In previous experiments, ¹H NMR spectroscopy yields were calculated from samples taken directly from the reaction mixture, which were concentrated with nitrogen-blow down and diluted in CDCl₃ for analysis. However, it is possible that 1,4-benzoquinone **5a** co-evaporated in this process, resulting in an “apparent” low yield. To test this hypothesis, volatility tests were undertaken, as shown in Table 16.

Table 16. 1,2-alkyl shift of peroxyquinol **2a**: volatility tests.



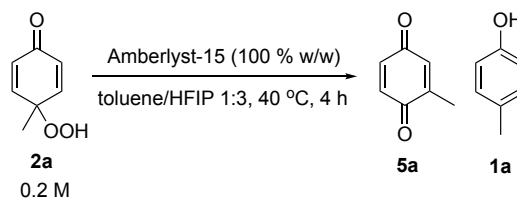
Entry	Method	Duration (min)	Ratio 5a: 2a
1	Original sample	-	1: 3.1
2	Nitrogen blown down	30	1: 3.6
3	Rotary evaporator		1: 4.9
4	Schlenk line		1: 6.1

A sample was taken directly from the reaction mixture, diluted with CDCl_3 and analysed by ^1H NMR spectroscopy as a control experiment (Entry 1 – Table 16). The same sample was then concentrated and analysed subsequently by three different methods: nitrogen blow down (Entry 2 – Table 16), rotary evaporator (Entry 3 – Table 16) and Schlenk line (Entry 4 – Table 16).

The ratio **5a: 2a** decreased by almost half after successive solvent removal techniques, which gave an indication that the yields of 1,4-benzoquinone **2a** obtained previously could have been higher than expected. In fact, 1,4-benzoquinone was found to undergo sublimation.³¹⁸

To find the most suitable quantification method for the synthesis of 1,4-benzoquinone **5a**, a reaction was quantified by ^1H NMR spectroscopy using biphenyl as the internal standard and HPLC calibration curve. For the reaction using biphenyl, two samples were taken: one was concentrated using nitrogen blow down and diluted with CDCl_3 and the other was analysed directly from the reaction mixture and diluted with CDCl_3 to avoid co-evaporation of **5a** (Table 17).

Table 17. 1,2-alkyl shift of peroxyquinol **2a**: quantification methods.



Entry	Quantification method		Conversion (%)	Yield 5a (%)	Yield 1a (%)
1	¹ H NMR yield with internal standard (0.05 eq.)	Biphenyl ^a	45	3	traces
2		Biphenyl	49	11	traces
3	Calibration curve	HPLC	47	11	-

^a Sample was concentrated by nitrogen blow down for 3 min. The ¹H NMR spectroscopy conversion was calculated as the following: ¹H NMR Conversion of **2a** = 100 - X, where X = ¹H NMR Recovery of **2a**.

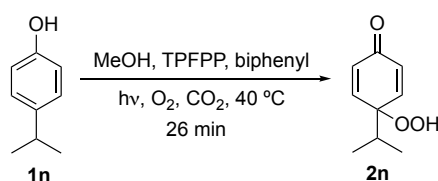
Similar conversions were obtained for all three experiments conducted (Entries 1 to 3 – Table 17). For the first two experiments carried out using biphenyl as the internal standard, there was a significant divergence in the yield of **5a** caused by removal of solvent by nitrogen blow down (Entries 1 and 2 – Table 17). When the experiment was repeated and quantified by HPLC calibration curve (Entry 3 – Table 17), in which the solvent wasn't removed for the analysis, the results were comparable to the ones using biphenyl without solvent removal (Entry 2 – Table 7).

These results showed that using both HPLC calibration curve and biphenyl as the internal standard without solvent removal were appropriate methods to quantify 2-methyl-1,4-benzoquinone **5a**. Although the yields obtained for **5a** using these two methods were higher (Entries 2 and 3 – Table 17) than the previous one with solvent removal (Entry 1 – Table 17), the 1,2-alkyl shift of *p*-peroxyquinol **2a** was still inefficient, giving poor yields of 11%.

5.3.7. Continuous flow telescoped synthesis of 1,4-benzoquinone **5n**: methodology development

Following the challenging optimisation of the synthesis of 1,4-benzoquinone **5a**, another *p*-peroxyquinol with a better migrating group was investigated for the 1,2-alkyl shift reaction. First, *p*-peroxyquinol **2n** had to be prepared (Table 18) to be used in the optimisation reactions in batch.

Table 18. Continuous flow photooxidation of 4-isopropylphenol **1n** using MeOH as the co-solvent.



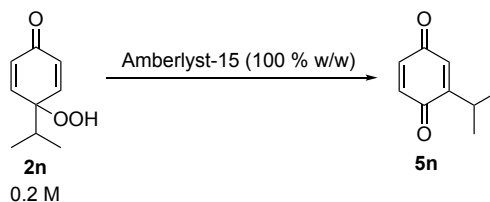
Entry	Concentration 1n (M)	NMR Conversion (%)	NMR yield 2n (%)	Isolated yield 2n (%)
1	1	69	64	61
2	3	89	85	76

System specifications: photo reactor (10 mm outer diameter 'o.d.', 240 mm length, 1 mm wall thickness, effective volume = 5.2 mL, filled with 38 glass beads with 6 mm o.d., at 40 °C) and concentration of TPFPP = 0.3 mol%. Entry 1: overall [CO₂] = 71%, molar ratio O₂:**1n** = 2:1, O₂ switching time = 15.9 s and overall [O₂] = 2.1%; Entry 2: overall [CO₂] = 68%, molar ratio O₂:**1n** = 1:1, O₂ switching time = 10.6 s and overall [O₂] = 3.1%. Biphenyl (0.05 eq.) was used as internal standard for ¹H NMR spectroscopy analysis. The ¹H NMR spectroscopy conversion was calculated as the following: ¹H NMR Conversion of **1n** = 100 - X, where X = ¹H NMR Recovery of **1n**.

The photooxidation of 4-isopropylphenol **1n** gave good yields of **2n** (Entry 1 – Table 18), with an increase of 21% in yield when the concentration was tripled (Entry 2 – Table 18).

Next, the synthesis of 1,4-benzoquinone **5n** was investigated in batch with different solvents and temperatures, using Amberlyst-15 as the acid catalyst. The results for each experiment were presented when maximum conversions were obtained (Table 19).

Table 19. 1,2-Alkyl shift of *p*-peroxyquinol **2n**: optimisation of solvent and temperature.



Entry	Solvent	Temperature (°C)	Time (min)	Conversion (%)	Yield 5n (%)
1	Toluene/HFIP 1:3	40	30	100	55
2^a	Toluene/HFIP 1:3	40	30	-	59
3	EtOAc + 2 eq. HFIP	40	30	86	36
4	EtOAc/HFIP 1:3	40	60	100	47
5	EtOAc/HFIP 1:3	20	120	100	69
6	HFIP	20	20	100	>99
7	HFIP	0	20	100	80

Yields were obtained from ¹H NMR spectroscopy analysis using biphenyl (0.05 eq.) as internal standard. ^a Reaction was performed without biphenyl and the yield **5n** is the isolated yield.

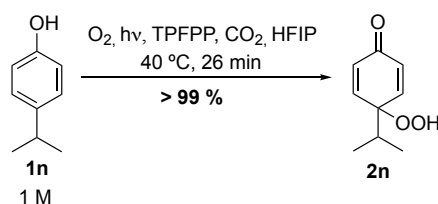
The first condition tested was the one that resulted in the best yield of 1,4-benzoquinone **5a**, with toluene/HFIP 1:3 as the solvent mixture at 40 °C (Entry 1 – Table 19). Surprisingly, the yield of 1,4-benzoquinone **5n** was 55%. When the reaction was repeated without internal standard, an isolated yield of 59% was obtained (Entry 2 – Table 19). However, the gap between conversion and yield was still considerable.

When the reaction was repeated with EtOAc + 2 eq. HFIP (Entry 3 – Table 19), a lower yield of 36% was achieved. Increasing the amount of HFIP (Entry 4 – Table 19), resulted in an increase of 11% in yield compared to Entry 3.

The gap between conversion and yield in these experiments was still quite significant, even though the yields were much higher for **5n** compared to **5a**. This might be due to a selectivity issue, as the carbocation formed during the rearrangement (see Scheme 60) would be very reactive. Then, the experiment was repeated at 20 °C (Entry 5 – Table 19) and 1,4-benzoquinone **5n** was obtained in 69%, an increase of 22% compared to the same experiment at 40 °C in Entry 4.

As the addition of HFIP increased the yield of **5n** (Entries 3 and 4 – Table 19), the reaction was also carried out solely in HFIP (Entry 6 – Table 19). 1,4-Benzoquinone **5n** was then obtained in quantitative yield, with full conversion of the substrate. In fact, HFIP was found to be an excellent solvent to stabilise cationic intermediates due to its high dielectric constant ($\epsilon = 15.7$) and low nucleophilicity.²³⁶ When the experiment was repeated at 0 °C, the yield decreased by 20% (Entry 7 – Table 19), showing that the optimal temperature for this reaction was 20 °C (Entry 6 – Table 19).

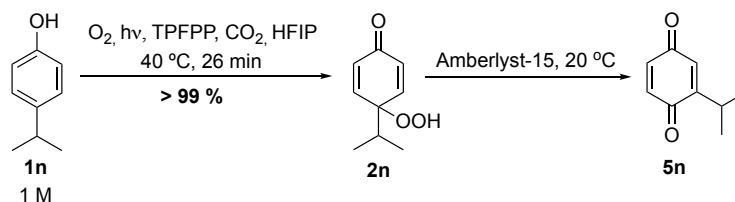
Following the optimisation of the 1,2-alkyl shift of *p*-peroxyquinol **2n**, the reaction was then tested in flow. As the optimal condition has HFIP as the reaction medium, the dearomatisation of **1n** had to be repeated in this co-solvent and quantified before telescoping the two reactions (Scheme 63).



Scheme 63. Continuous flow photooxidation of 4-isopropylphenol in HFIP (same high-pressure setup from Table 18). System specifications: photo reactor (10 mm outer diameter 'o.d.', 240 mm length, 1 mm wall thickness, effective volume = 5.2 mL, filled with 38 glass beads with 6 mm o.d., at 40 °C), overall $[CO_2] = 84\%$, molar ratio $O_2:1n = 2:1$, O_2 switching time = 15.9 s, overall $[O_2] = 2.5\%$ and concentration of TPFPP = 0.05 mol%. Biphenyl (0.05 eq.) was used as internal standard for 1H NMR spectroscopy analysis.

Quantitative yields of **2n** were obtained when the reaction was performed using HFIP as the co-solvent and $scCO_2$ at 1 M: an increase of about 40% when compared with the same reaction in EtOAc/HFIP (Entry 1 - Table 18). The next step was to investigate the continuous flow telescoped synthesis of 1,4-benzoquinone **2n** from 4-isopropylphenol in HFIP (Table 20).

Table 20. Continuous flow telescoped synthesis of 1,4-benzoquinone **2n** using HFIP as the co-solvent.



Entry	Time (h)	Packed bed reactor and catalyst loading / Overall NMR yield					
		TR3-Amb (0.75 g)		TR3-Amb II (0.25 g)		TR4-Amb (1.05 g)	
		2n (%)	5n (%)	2n (%)	5n (%)	2n (%)	5n (%)
1	1	-	-	0	83	0	82
2	1.5	-	-	8	76	0	82
3	2	0	80	20	68	0	82
4	2.5	3	78	28	61	0	82
5	3	7	77	37	52	0	82
6	3.5	9	75	-	-	-	-
7	4	12	72	-	-	-	-

System specifications: photo reactor (10 mm outer diameter 'o.d.', 240 mm length, 1 mm wall thickness, effective volume = 5.2 mL, filled with 38 glass beads with 6 mm o.d.). Thermo reactors (1/4" o.d., 0.049" wall thickness, 15 cm length) were packed with Amberlyst-15 (Amb-15) and 0.5-0.75 mm glass beads (gb) in the following specifications: **TR3-Amb**: 0.75 g Amb-15 + 0.85 g gb, effective volume = 1.1 mL, residence time = 5.5 min; **TR3-Amb II**: 0.25 g Amb-15 + 2.05 g gb, effective volume = 1.4 mL, residence time = 7 min; **TR4-Amb**: 1.05 g Amb-15 only, effective volume = 0.6 mL, residence time = 3.0 min. Concentration of TPFPP = 0.05 mol% and biphenyl (0.05 eq.) was used as internal standard for ¹H NMR spectroscopy analysis.

The packed bed reactor (**TR3-Amb**) filled with 0.75 g Amberlyst-15 was the first one to be tested. The reaction was monitored by ¹H NMR spectroscopy for four hours, in which the overall yield of 1,4-benzoquinone **5n** decreased over time. It was hypothesised that the quantity of Amberlyst-15 might have been the cause for these results.

To investigate if the decrease in yield was affected by the amount of acid catalyst, other two thermo reactors were built and charged with either 0.25 g (**TR3-Amb II**) or 1.05 g (**TR4-Amb**) of Amberlyst-15. All three thermo reactors design schemes can be compared in Figure 43 .

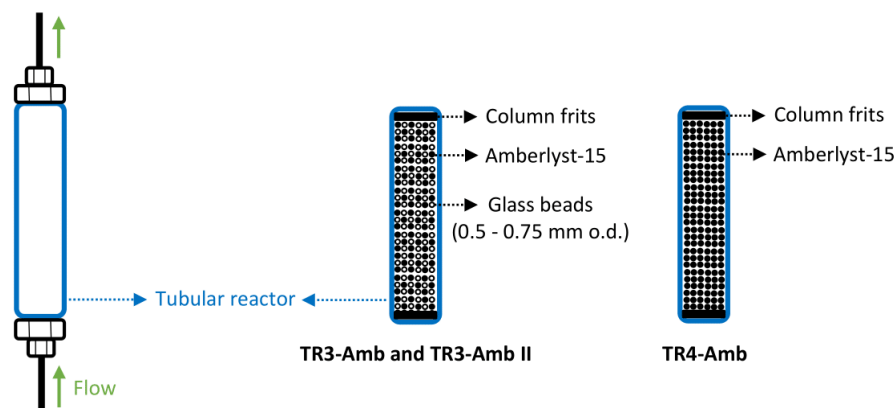


Figure 43. Different Amberlyst-15 (Amb) packed bed reactor schemes: **TR3-Amb** = 0.75 g Amb-15 + 0.85 g 0.5 – 0.75 mm o.d. glass beads; **TR3-Amb II** = 0.25 g Amb-15 + 2.05 g 0.5 – 0.75 mm o.d. glass beads and **TR4-Amb** = 1.05 g Amb-15 with no glass beads

The reaction was then repeated with 0.25 g of Amberlyst-15 using packed bed reactor **TR3-Amb II**. The decrease in yield of **5n** was even more pronounced with less quantity of acid, with an overall drop of 30% over 2h of reaction. On the other hand, when a larger amount of Amberlyst-15 was used (**TR4-Amb**), the overall yield stabilised at 82% (yield for 2nd step = 83%), with productivity of 9 g/day.

The decrease in yield of **5n** was proportional to the appearance of *p*-peroxyquinol **2n** in the first two experiments, with the sum of both yields maintained relatively stable. On the other hand, *p*-peroxyquinol **2n** was not identified when the packed bed reactor was filled with 1.05 g of Amberlyst-15 (Figure 44).

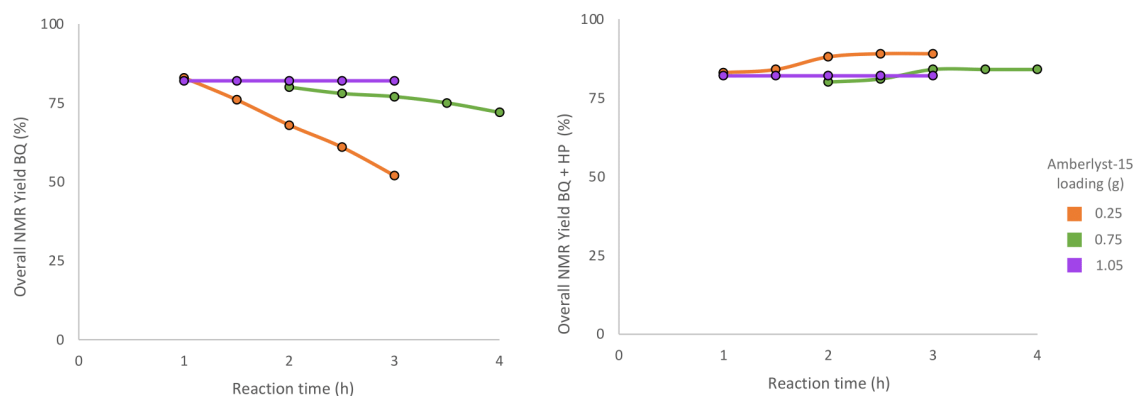


Figure 44. Left: overall ¹H NMR spectroscopy yields of 1,4-benzoquinone **5n** (BQ); right: sum of overall yields of **5n** and *p*-peroxyquinol **2n** (HP) monitored over time for reactions in Table 20.

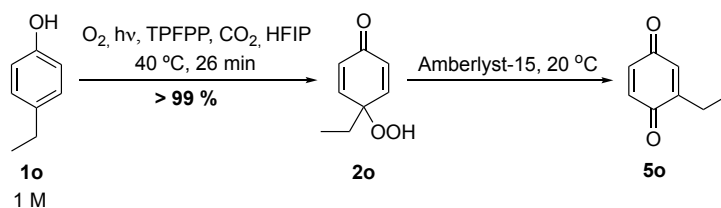
These results suggest that Amberlyst-15 was deactivated over time, with a more drastic effect on the yield of **5n** when lower amounts of catalyst were used. The appearance of *p*-peroxyquinol **2n** could be explained by the fact that less active sites were available to catalyse the 1,2-alkyl shift and, therefore, less *p*-peroxyquinol **2n** was converted into 1,4-benzoquinone **5n** throughout the experiment.

After developing a methodology for the synthesis of 1,4-benzoquinone **5n** using thermo reactor **TR4-Amb**, the next step was to expand the scope to other 1,4-benzoquinones. For each compound, the photooxidation had to be tested first in HFIP and then telescoped with the 1,2-alkyl shift of *p*-peroxyquinols.

5.3.8. Continuous flow telescoped synthesis of 1,4-benzoquinones: scope of reaction

The methodology developed was tested with *p*-peroxyquinol **2o**, bearing an ethyl group at the migrating *para* position. The photooxidation of 4-ethylphenol **1o** was first performed in flow, giving a quantitative yield of *p*-peroxyquinol **2o**. After that, the 1,2-alkyl shift was telescoped with the dearomatisation of *p*-substituted phenol **1o** and the results are shown in Table 21.

Table 21. Continuous flow telescoped synthesis of 1,4-benzoquinone **5o**



Entry	Time (h)	Packed bed reactor and catalyst loading / Overall NMR yield					
		TR4-Amb (1.05 g)		TR4-Amb II (1.92 g)		TR4-Amb III (4.38 g)	
		2o (%)	5o (%)	2o (%)	5o (%)	2o (%)	5o (%)
1	1	6	80	-	-	-	-
2	2	13	71	0	76	0	64
3	2.5	26	60	0	77	0	66
4	3	36	56	0	75	0	69

Same high-pressure setup and system specifications from Table 20, except for thermo reactors. Each thermo reactor (1/4" o.d., 0.049" wall thickness) was packed with Amberlyst-15 (Amb-15) in the following specifications: **TR4-Amb**: length = 15 cm, 1.05 g Amb-15, effective volume = 0.6 mL, residence time = 3 min; **TR4-Amb II**: length = 30 cm, 1.92 g Amb-15, effective volume = 0.9 mL, residence time = 4.5 min; **TR4-Amb III**: length = 70 cm, 4.38 g Amb-15, effective volume = 1.5 mL, residence time = 7.5 min. Yields were obtained from ¹H NMR spectroscopy analysis using biphenyl (0.05 eq.) as internal standard.

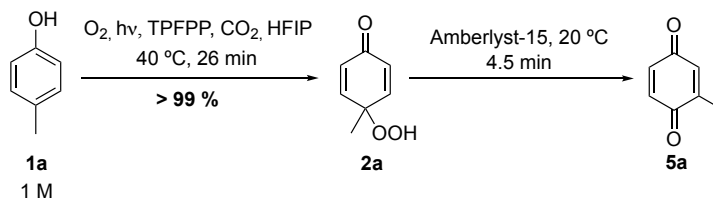
When the reaction was performed with the packed bed reactor **TR4-Amb**, there was a significant drop in yield of 1,4-benzoquinone **5o** over 2 h of reaction. Instead, another packed bed reactor was built (**TR4-Amb II**) with a larger amount of Amberlyst-15 and longer residence time of 4.5 min. The overall yield of **5o** maintained relatively constant at 76% (yield for 2nd step = 77%), with productivity of 7 g/day. However, increasing the amount of catalyst to 4.38 g (**TR4-Amb III**) proved less efficient, resulting in overall 10% less yield of **5o**.

It is not surprising that the formation of 1,4-benzoquinone **5o** was less efficient than the previous 1,4-benzoquinone **5n**, as the ethyl group has a lower migratory aptitude and stabilisation of the intermediate carbocation compared to isopropyl.

This methodology was also applied in the synthesis of 2-methyl-1,4-benzoquinone, the original substrate tested in the beginning of this Chapter, as shown in Table 22. The photooxidation of *p*-cresol **1a** in HFIP gave a quantitative yield, whereas the overall yield of 1,4-benzoquinone **5a** was relatively stable at 13% (yield for 2nd step = 13%), with productivity of 1

g/day. Although this methodology gave good yields for 1,4-benzoquinones **5n** and **5o**, the telescoped synthesis of **5a** is still a challenge to be overcome.

Table 22. Continuous flow telescoped synthesis of 1,4-benzoquinone **5a**



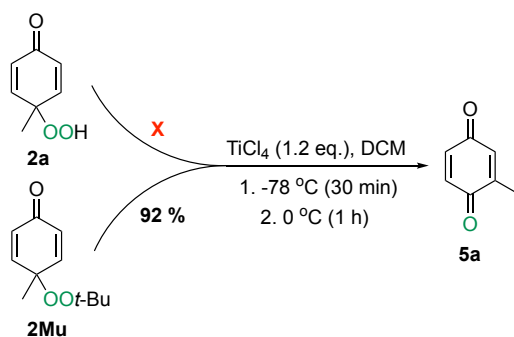
Entry	Time (h)	Overall NMR yield	
		2a (%)	5a (%)
1	1	4	14
2	2	23	14
3	2.5	41	13
4	3	51	12

Same high-pressure setup and system specifications from Table 20, except for thermo reactor. The packed bed reactor **TR4-Amb II** (1/4" o.d., 0.049" wall thickness, 30 cm length) was packed with 1.92 g of Amberlyst-15, with effective volume = 0.9 mL and residence time = 4.5 min. Yields were obtained from ^1H NMR spectroscopy analysis using biphenyl (0.05 eq.) as internal standard.

5.4. Conclusions

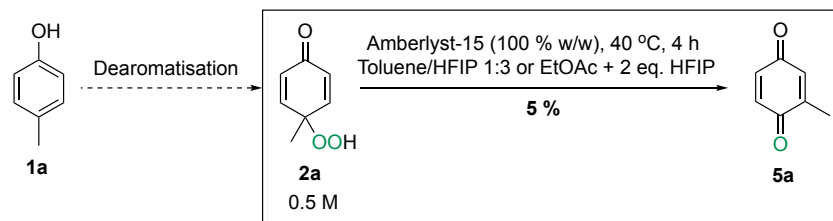
1,2-alkyl shift of *p*-peroxyquinol 2a: initial studies, optimisation, and quantification methods

Following the discovery of a 1,2-alkyl shift of *p*-peroxyquinols during previous studies on the synthesis of 1,2,4-trioxanes, a continuous flow telescoped synthesis of 2-substituted-1,4-benzoquinones was proposed. To test reproducibility, the rearrangement step was carried out with *p*-peroxyquinol **2a** instead of 4-(*tert*-butylperoxy)-2,5-cyclohexadienone **2Mu**, under similar conditions reported by Murahashi²⁸² (Scheme 64). In this study, no product **5a** was obtained and **2a** was mostly decomposed.



Scheme 64. Reproducibility test for the synthesis of 1,4-benzoquinone **5a** (batch) with 2-methyl-1,4-benzoquinone **2a** using Murahashi's procedure.²⁸² **X** represents that the product **5a** was not observed.

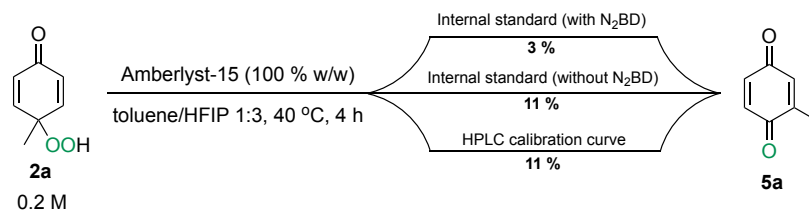
This reaction was then optimised in batch, screening different concentrations of **2a** (0.1, 0.2, 0.5 and 1 M), temperatures (-78 °C, 0 °C, 40 °C, and 60 °C), acid catalysts (BF₃.OEt₂, TfOH, TFA, PTSA, Ph₂PO₂H, CSA, TMSOTf, NbOPO₄ and Amberlyst-15), and solvents (DMC, CDCl₃, Me-THF, MeCN, MeOH, EtOAc, toluene/HFIP and EtOAc/HFIP). The optimal condition gave only 5% yield of product **5a**, using Amberlyst-15 as the acid catalyst at 40 °C in either toluene/HFIP or EtOAc/HFIP solvent mixtures (Scheme 65).



Scheme 65. 1,2-alkyl shift of *p*-peroxyquinol **2a**: best result obtained from the optimisation in batch.

Various parameters were screened to increase the yield of this reaction, but since none gave higher yields than 5%, the quantification method was then investigated. From volatility tests undertaken with a sample of 1,4-benzoquinone **5a**, it was observed that this compound co-evaporates, even with mild solvent removal techniques such as nitrogen blown down (N₂BD).

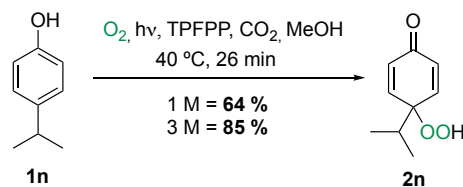
To investigate the validity of the previous quantification method used (internal standard with sample concentrated by N₂BD), a model reaction was analysed using three techniques: internal standard with and without N₂BD, and HPLC calibration curve, as shown in Scheme 66. These experiments showed that solvent removal affected the quantification analysis and that both the internal standard and HPLC methods gave consistent results when the solvent was not removed. However, the yields of **5a** obtained through these two methods were still poor (11%).



Scheme 66. 1,2-alkyl shift of peroxyquinol **2a** quantified by three different methods: internal standard (with N₂BD); internal standard (without N₂BD); and HPLC calibration curve.

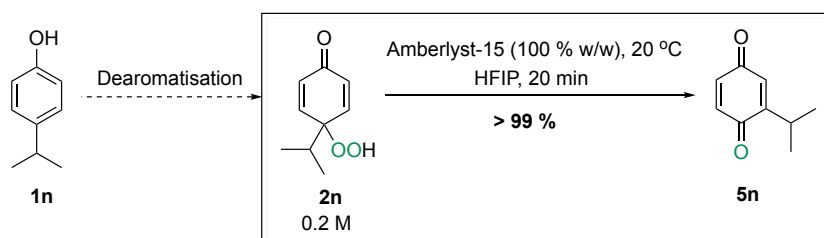
Continuous flow telescoped synthesis of 1,4-benzoquinone **2n**: methodology development

Given the difficulties in improving the yield of 1,4-benzoquinone **5a**, the phenol was substituted for **1n**, which has a better migratory aptitude at the *para* position. First, the starting material was prepared in flow to be used in batch for optimisation tests, giving good yields of 64% and 85% depending on the concentration of **1n**, as shown in Scheme 67.



Scheme 67. Continuous flow photooxidation of 4-isopropylphenol **1n** using 1O_2 in $scCO_2$ and MeOH as the co-solvent.

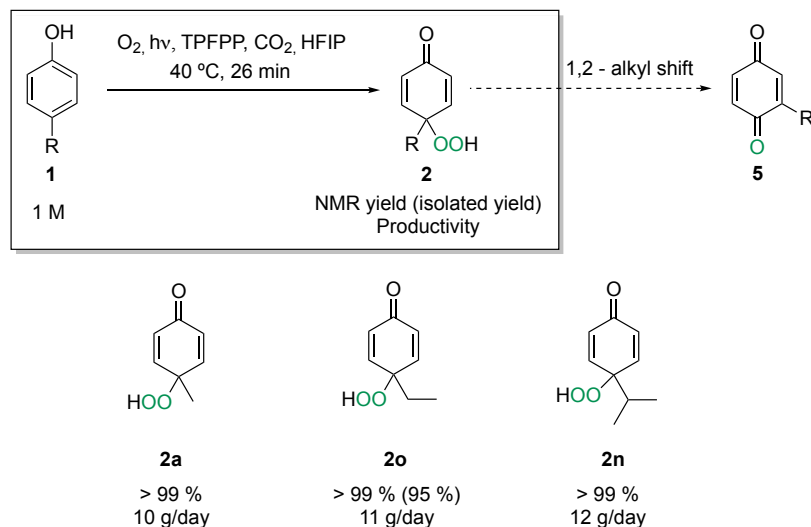
The 1,2-alkyl shift of **2n** was tested in batch and optimised using three different solvent systems (toluene/HFIP, EtOAc/HFIP and HFIP) and three temperatures (0 °C, 20 °C, and 40 °C). The optimal condition found was using Amberlyst-15 (acid catalyst) in HFIP at 20 °C, which gave full conversion and an excellent quantitative yield of 1,4-benzoquinone **5n** in only 20 min (Scheme 68).



Scheme 68. 1,2-alkyl shift of *p*-peroxyquinol **2n**: best result obtained from the optimisation in batch.

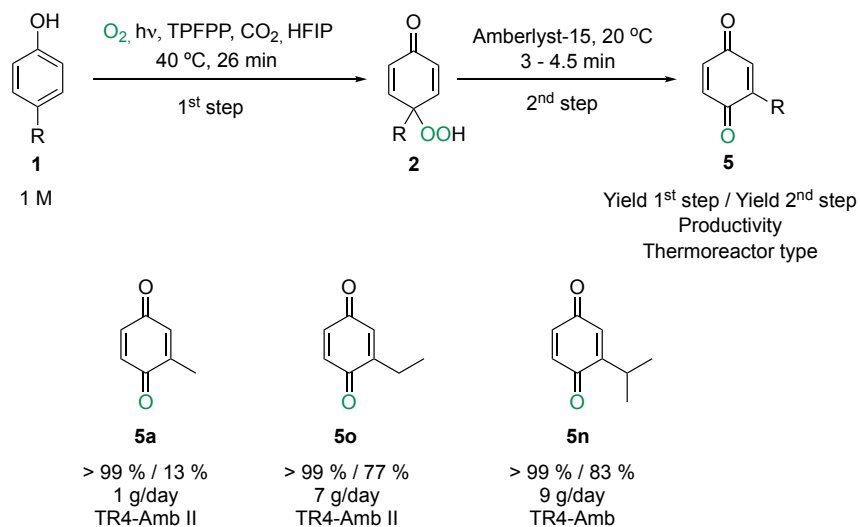
Continuous flow telescoped synthesis of 1,4-benzoquinones: scope of reaction

After developing the methodology in batch, the reaction was transferred to a continuous flow telescoped setup and the scope was expanded to other 1,4-benzoquinones. To start with, the first step of the reaction was carried out in flow with three phenols using HFIP as the co-solvent (Scheme 69). Quantitative yields were obtained for all three *p*-peroxyquinols tested, which are higher than the yields obtained previously in MeOH (Chapter 3).



Scheme 69. Summary of the continuous flow photooxidation of *p*-substituted phenols using $^1\text{O}_2$ in $s\text{CO}_2$ and HFIP as the co-solvent.

Next, the scope of the 1,2-alkyl shift was expanded to three different 1,4-benzoquinones in a continuous flow telescoped approach, as shown in Scheme 70. It was found that the migratory aptitude of the group in *para* position seems to depend on the nature of the carbon and it was ordered Me (**5a**) < Et (**5o**) < *i*Pr (**5n**). In particular, the migration of *i*Pr gave a good overall yield of 83% for **5n** and a productivity of 9 g/day in only 4.5 min of residence time. The *p*-peroxyquinols were reacted *in situ* in a non-flammable solvent CO_2 , enabling safe scaling-up of the synthesis of 1,4-benzoquinones, in short residence times of up to 5 min.



Scheme 70. Continuous flow telescoped synthesis of 1,4-benzoquinones: scope of reaction. Productivities were calculated with the overall yield of 1,4-benzoquinone. All packed bed reactors have 1/4" o.d., 0.049" wall thickness, and were loaded with Amberlyst-15 (Amb-15). **TR4-Amb**: length = 15 cm, effective volume = 0.6 mL, 1.05 g Amb-15, residence time = 3 min; and **TR4-Amb II**: length = 30 cm, effective volume = 0.9 mL, 1.92 g Amb-15, residence time = 4.5 min.

In summary, a methodology for the continuous flow telescoped synthesis of 2-substituted-1,4-benzoquinones was developed, starting from cheap and readily available *p*-substituted phenols at a multi-gram scale. This procedure has proven to be atom efficient and sustainable, as the two atoms of oxygen are incorporated in the resulting *p*-peroxyquinol,⁹³ substituting toxic oxidants (*t*-BuOOH) and corrosive catalysts (TiCl₄). It is also safer, as the *p*-peroxyquinols are generated in scCO₂, which is a non-flammable solvent, and reacted *in situ*. The 1,2-alkyl rearrangement step also was improved when compared to Murahashi's procedure: the reaction was performed at ambient temperature instead of -78 °C, which is inconvenient for the scalability of this process; the solvent was substituted to supercritical CO₂ with small amounts of HFIP as a co-solvent, instead of dichloromethane; and the corrosive/toxic TiCl₄ catalyst was replaced by Amberlyst-15, which is not only non-toxic but also facilitates further purification as it is immobilised in a packed bed reactor.

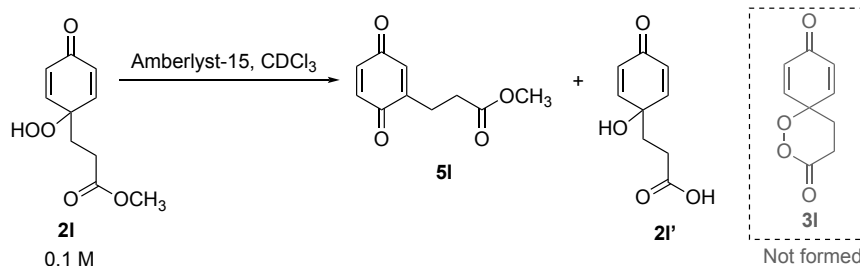
A publication featuring the results from this chapter is to be submitted in the journal *Molecules* for a special issue entitled “singlet oxygen-photooxygenation of organic compounds”

Abreu, B. L.; Boufroua, H.; Moore, J. C.; Poliakoff, M.; George, M. W., Telescoped continuous flow synthesis of 2-substituted-1,4-benzoquinones from *para*-substituted phenols using singlet oxygen in supercritical CO₂.

5.5. Experimental procedures

Data collected for known compounds is consistent with the literature.

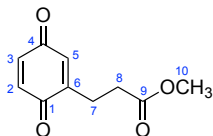
5.5.1. 1,2-alkyl shift of methyl-3-(1-hydroperoxy-4-oxocyclohexa-2,5-dien-1-yl)-propanoate **2I** (Batch)



Standard procedure: Amberlyst-15 was added to a 2 mL solution of methyl-3-(1-hydroperoxy-4-oxocyclohexa-2,5-dien-1-yl)-propanoate **2I** (1.0 eq, 199 μ mol, 42.3 mg) in CDCl₃. The solution was stirred, resulting in a brown reaction mixture. ¹H NMR spectroscopy was recorded from a 0.5 mL sample, taken directly from the reaction mixture.

- **Reaction 1, Test 1:** Amberlyst (300% w/w, 127 mg) at room temperature. After 1 h of reaction: ¹H NMR spectroscopy ratio **5I**: **2I** was 1: 4.5 and ¹H NMR spectroscopy ratio **2I'**: **2I** was 1: 4.9.
 - **Test 2:** After 2 h of reaction, ¹H NMR spectroscopy ratio **5I**: **2I** was 1: 1.8 and ¹H NMR spectroscopy ratio **2I'**: **2I** was 1: 3.9.
 - **Test 3:** The reaction mixture was then heated up to 40 °C. After 2 h of reaction, complete decomposition was observed in the ¹H NMR spectrum.
- **Reaction 2:** Amberlyst (100% w/w, 42 mg) at 40 °C. After 2 h of reaction, Amberlyst-15 was washed with chloroform (3x 5mL), filtered out, and the filtrate was concentrated under vacuum. The product and by-product were purified by flash column chromatography column and eluted with a gradient of 0-50% EtOAc/Hexane to give **5I** (16.1 μ mol, 3.12 mg, 8%) as a yellow oil, and **2I'** (12.2 μ mol, 2.23 mg, 6%) also as a yellow oil.

Methyl 3-(3,6-dioxocyclohexa-1,4-dien-1-yl)propanoate **5I**³¹⁹

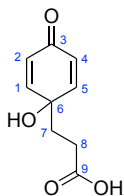


¹H NMR (400 MHz, Chloroform-*d*): δ 6.77 (d, J = 10.1 Hz, 1H, **2**), 6.73 (dd, J = 10.1, 2.4 Hz, 1H, **3**), 6.59 (dt, J = 2.4, 1.4 Hz, 1H, **5**), 3.68 (s, 3H, **10**), 2.76 (td, J = 7.1 Hz, 1.4 Hz, 2H, **7**), 2.58 (t, J = 7.1 Hz, 2H, **8**).

¹³C NMR (101 MHz, Chloroform-*d*): δ 187.6 (**4**), 187.2 (**1**), 172.5 (**9**), 147.6 (**6**), 136.9 (**2**), 136.6 (**3**), 133.2 (**5**), 52.0 (**10**), 32.0 (**8**), 24.7 (**7**).

HRMS (ESI) m/z calcd [$C_{10}H_{10}O_4Na$]⁺ ($[M + Na]^+$): 217.0471, found 217.0471.

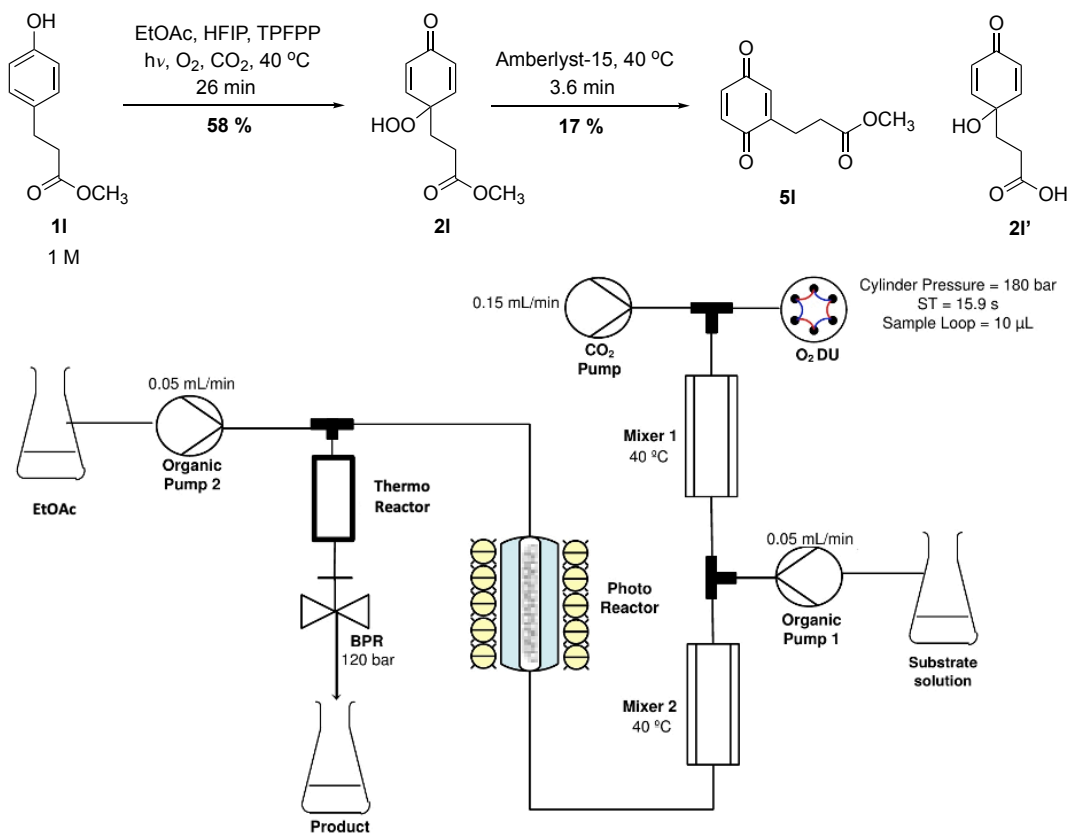
3-(1-Hydroxy-4-oxocyclohexa-2,5-dien-1-yl)propanoic acid **2I'** (novel compound)



¹H NMR (400 MHz, Chloroform-*d*): δ 6.95 (d, J = 10.2 Hz, 2H, **1/5**), 6.35 (d, J = 10.2 Hz, 2H, **2/4**), 2.83 – 2.78 (m, 2H, **8**), 2.37 – 2.31 (m, 2H, **7**).

¹³C NMR (101 MHz, Chloroform-*d*): δ 184.0 (**3**), 175.1 (**9**), 143.0 (**1/5**), 130.0 (**2/4**), 77.2 (**6**), 30.7 (**7**), 25.7 (**8**).

5.5.2. Telescoped synthesis of methyl 3-(3,6-dioxocyclohexa-1,4-dienyl) propanoate **5I** (flow)



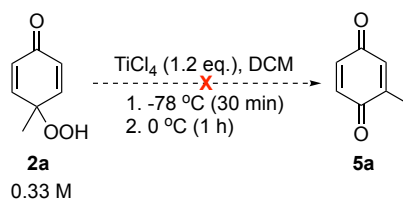
Scheme 71. Simplified schematic diagram of the high-pressure flow system used for the telescoped synthesis of 1,4-benzoquinone **5I'**

System parameters: Photo reactor (10 mm outer diameter (o.d.)), 240 mm length, 1 mm wall thickness, effective volume = 5.2 mL, filled with 38 glass beads with 6 mm o.d., at $40\text{ }^\circ\text{C}$); thermo reactor **TR1-Amb** (1/4" o.d., 0.049" wall thickness, 15 cm length, effective volume = 0.9 mL, loaded with 0.75 g Amberlyst® 15 and 0.85 g of glass beads with 2 mm o.d. at $40\text{ }^\circ\text{C}$, high trip = $50\text{ }^\circ\text{C}$); cooling baths (photo reactor = $35.5\text{ }^\circ\text{C}$, LED lights = $-5\text{ }^\circ\text{C}$); Trips (System set pressure = 120 bar, high trip = 140 bar; Oxygen set pressure = 180 bar, high trip = 190 bar, low trip = 160 bar; Mixers set temperature = $40\text{ }^\circ\text{C}$, high trip = $50\text{ }^\circ\text{C}$), biphenyl as the internal standard. The standard procedure (**Chapter 2, section 2.1.3**) was performed with CO_2 (0.15 mL/min and overall $[CO_2] = 83\%$), O_2 (180 bar, sample loop = $10\ \mu\text{L}$, switching time = 15.9 s, molar ratio O_2 : **1I** = 2:1 and the overall $[O_2] = 2.6\text{ mol}\%$), and HPLC pumps (0.05 mL/min).

Procedure: A starting solution of methyl-3-(4-hydroxyphenyl)-propionate **1I** 1 M (1.0 eq, 18.0 mmol, 3.24 g), TPFPP (0.30 mol%, 0.050 mmol, 52.6 mg), HFIP (2.0 eq, 36.0 mmol, 3.80 mL) and biphenyl (0.070 eq, 1.26 mmol, 194 mg) in EtOAc (18 mL) was prepared and sonicated for 30 min. After performing the standard procedure, starting solution was then pumped into the system at 0.05 mL/min, combined with the gaseous mixture (CO₂ and O₂) on Mixer 2 and then passed through the photo reactor, with a residence time of 26 min. EtOAc was pumped after the photo reactor at 0.05 mL/min and the streams were combined and passed through a thermo reactor, with a residence time of 3.6 min.

Results: The system reached a steady state after 3.5 h of reaction and a sample was collected for 3 min, nitrogen blow down for another 3 min and analysed by ¹H NMR spectroscopy. **5I** was obtained in 10% overall yield (17% for the second step), with productivity of 1 g/day, and **2I'** in 3% overall yield (5% for the second step).

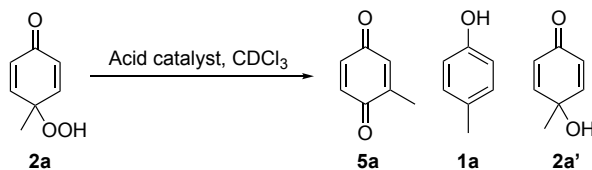
5.5.3. Reproducibility test for the synthesis of 1,4-benzoquinone **5a** (batch)



Procedure: In an oven-dried round bottom flask with a magnetic stirring bar, charged with dry DCM (1 mL), TiCl₄ (1.2 eq, 1.20 mmol, 130 μL) was added under inert atmosphere, turning into a light-yellow solution. The solution was then stirred at -78 °C for 30 min, which turned into purple. *p*-peroxyquinol **2a** (1.0 e, 1.00 mmol, 140 mg) was dissolved in DCM (2mL) and added dropwise into the reaction mixture, resulting in an orange suspension. The reaction was stirred for 1 h at 0 °C, quenched with saturated NaHCO₃ solution (5 mL), diluted with 5 mL of DCM, and stirred for another 30 min. The solution was then filtered over a pad of Celite, extracted with DCM (2 x 10 mL) and dried over MgSO₄. The supernatant was filtered and concentrated under reduced pressure.

Results: ¹H NMR spectroscopy analysis of the crude showed a complex mixture of signals with no product or starting material identified.

5.5.4. 1,2-alkyl shift of *p*-peroxyquinol **2a**: initial studies (batch)



Standard procedure: Acid catalyst was added to a solution of *p*-peroxyquinol **2a** in CDCl_3 . The solution was stirred, resulting in a brown reaction mixture. ^1H NMR spectrum was recorded from a 0.5 mL sample taken directly from the reaction mixture.

SET 1: catalyst $\text{BF}_3 \cdot \text{OEt}_2$

- **Reaction 1:** 2 mL solution (0.2 M) of **2a** (1.0 eq, 0.400 mmol, 56.1 mg) and $\text{BF}_3 \cdot \text{OEt}_2$ (1.2 eq, 0.480 mmol, 60 μL), at room temperature and under inert atmosphere. After 1 h of reaction, complete decomposition was observed in the ^1H NMR spectroscopy.

SET 2: catalyst TfOH

- **Reaction 2:** 2 mL solution (0.2 M) of **2a** (1.0 eq, 0.400 mmol, 56.1 mg), and TfOH (1.2 eq, 0.480 mmol, 40 μL) at room temperature and under inert atmosphere. After 1 h of reaction, complete decomposition was observed in the ^1H NMR spectroscopy.

SET 3: catalyst TFA

- **Reaction 3:** 1 mL solution (0.2 M) of **2a** (1.0 eq, 0.200 mmol, 28.2 mg), TFA (1.2 eq, 0.480 mmol, 40 μL) and biphenyl (0.050 eq, 10 μmol , 2.10 mg) at room temperature. After 24 h of reaction, no reaction occurred.
- **Reaction 4:** similar conditions as Reaction 3, at 40 $^\circ\text{C}$. After 24 h of reaction, no reaction occurred.
- **Reaction 5:** Similar conditions as Reaction 3, at 40 $^\circ\text{C}$ and TFA (4.8 eq, 1.92 mmol, 100 μL). After 24 h reaction, ^1H NMR spectroscopy ratio **2a'**: **2a** was 1: 3.6.

SET 4: catalyst PTSA

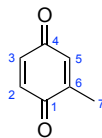
- **Reaction 6, Test 1:** 2 mL solution (0.2 M) of **2a** (1.0 eq, 0.400 mmol, 56.1 mg) and PTSA (1.2 eq, 0.480 mmol, 83.2 mg), at 40 $^\circ\text{C}$. After 4 h of reaction, ^1H NMR spectroscopy ratio **5a**: **2a** was 1: 2.4 and ^1H NMR spectroscopy ratio **1a**: **2a** was 1: 9.4.

- **Test 2:** After 24 h of reaction, complete decomposition was observed in the ^1H NMR spectroscopy.

SET 5: catalyst Amberlyst-15

- **Reaction 7, Test 1:** 2 mL solution (0.1 M) of **2a** (1.0 eq, 0.200 mmol, 28.1 mg) and Amberlyst-15 (100% w/w, 28.1 mg), at 40 °C. After 2 h of reaction, ^1H NMR spectroscopy ratio **5a: 2a** was 1: 8.3 and ^1H NMR spectroscopy ratio **1a: 2a** was 1: 45.4.
 - **Test 2:** After 4 h of reaction, ^1H NMR spectroscopy ratio **5a: 2a** was 1: 5.0 and ^1H NMR spectroscopy ratio **1a: 2a** was 1: 28.0.
 - **Test 3:** After 24 h of reaction, ^1H NMR spectroscopy ratio **5a: 2a** was 1: 1.3 and ^1H NMR spectroscopy ratio **1a: 2a** was 1: 9.6.
- **Reaction 8, Test 1:** 4 mL solution (0.2 M) of **2a** (1.0 eq, 0.800 mmol, 112 mg) and Amberlyst-15 (100% w/w, 112 mg), at 40 °C. After 2 h of reaction: ^1H NMR spectroscopy ratio **5a: 2a** was 1: 4.9 and ^1H NMR spectroscopy ratio **1a: 2a** was 1: 35.0.
 - **Test 2:** After 4 h of reaction, ^1H NMR spectroscopy ratio **5a: 2a** was 1: 3.0 and ^1H NMR spectroscopy ratio **1a: 2a** was 1: 23.3.
 - **Test 3:** After 24 h of reaction, ^1H NMR spectroscopy ratio **5a: 2a** was 1: 0.6 and ^1H NMR spectroscopy ratio **1a: 2a** was 1: 2.6.
- **Reaction 9:** 1 mL solution (0.2 M) of **2a** (1.0 eq, 0.200 mmol, 28.1 mg) and Amberlyst-15 (100% w/w, 28.1 mg), at room temperature. After 24 h of reaction, ^1H NMR spectroscopy ratio **5a: 2a** was 1: 4.9 and ^1H NMR spectroscopy ratio **1a: 2a** was 1: 45.5.
- **Reaction 10, Test 1:** 2 mL solution (1.0 M) of **2a** (1.0 eq, 2.00 mmol, 280 mg) and Amberlyst-15 (100% w/w, 280 mg), at 40 °C. After 2 h of reaction, ^1H NMR spectroscopy ratio **5a: 2a** was 1: 3.1 and ^1H NMR spectroscopy ratio **1a: 2a** was 1: 1: 9.8.
 - **Test 2:** After 4 h of reaction, ^1H NMR spectroscopy ratio **5a: 2a** was 1: 1.8 and ^1H NMR spectroscopy ratio **1a: 2a** was 1: 6.8.
 - **Test 3:** After 24 h of reaction, complete decomposition of **2a** and **5a**.

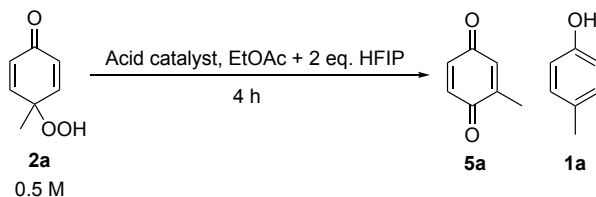
2-Methyl-1,4-benzoquinone **5a**³²⁰



¹H NMR (400 MHz, Chloroform-*d*): δ 6.74 (d, J = 10.1 Hz, 1H, **2**), 6.69 (dd, J = 10.1, 2.3 Hz, 1H, **3**), 6.61 – 6.59 (m, 1H, **5**), 2.04 (s, 3H, **7**).

¹³C NMR (101 MHz, Chloroform-*d*): δ 187.9 (**1**), 187.7 (**4**), 146.0 (**6**), 136.7 (**2**), 136.6 (**3**), 133.5 (**5**), 15.9 (**7**).

5.5.5. 1,2-alkyl shift of *p*-peroxyquinol **2a**: optimisation of catalyst and temperature (batch)



Standard procedure: Acid catalyst (1.2 eq, 1.20 mmol) was added to a 2 mL solution of *p*-peroxyquinol **2a** (1.0 eq, 1.00 mmol, 140 mg) and biphenyl (0.050 eq, 50.0 μ mol, 8.20 mg) in EtOAc (1.8 mL) + HFIP (2.0 eq, 2.00 mmol, 0.2 mL) as the solvent system, unless stated otherwise. The solution was stirred for 4 h, and a ¹H NMR spectroscopy was recorded from a 0.1 mL sample from the reaction mixture, which was then concentrated by nitrogen blow down for 3 min.

SET 1: catalyst Ph₂PO₂H

- **Reaction 1:** Diphenylphosphinic acid (262 mg) at 40 °C. Results from ¹H NMR spectroscopy = no reaction observed.

SET 2: catalyst TMSOTf

- **Reaction 2:** Trimethylsilyl trifluoromethanesulfonate (0.2 mL) at 40 °C. Results from ¹H NMR spectroscopy = complete decomposition of **2a**.

SET 3: catalyst CSA

- **Reaction 3:** (±)-Camphorsulfonic acid (279 mg) at 40 °C. Results from ¹H NMR spectroscopy = conversion **2a** = 23%, yield **5a** = 2% and yield of **1a** = 3%.

SET 3: catalyst NbOPO₄

- **Reaction 4:** Niobium oxide phosphate (245 mg) at 40 °C. Results from ¹H NMR spectroscopy = conversion **2a** = 81% and yield **5a** = 5%.

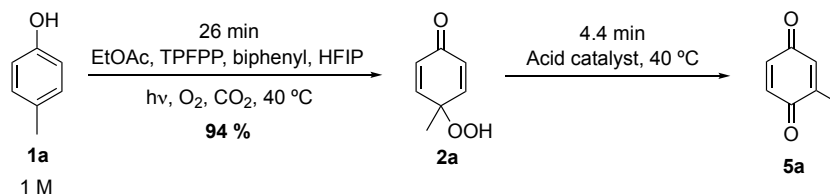
SET 4: catalyst Amberlyst-15

- **Reaction 5:** 4 mL solution of **2a** (1.0 eq, 2.00 mmol, 280 mg), Amberlyst-15 (100% w/w, 280 mg), biphenyl (0.050 eq, 100 μmol, 15.2 mg) in EtOAc (3.6 mL) and HFIP (2.0 eq, 4.00 mmol, 0.4 mL), at 40 °C. Results from ¹H NMR spectroscopy = conversion **2a** = 78%, yield **5a** = 5% and yield of **1a** = 2%.
- **Reaction 6:** similar conditions to Reaction 5, with the addition of 4Å molecular sieves. Results from ¹H NMR spectroscopy = conversion **2a** = 78%, yield **5a** = 5% and yield of **1a** = 2%.

SET 5: catalyst Amberlyst-15 at different temperatures

- **Reaction 7:** similar conditions to Reaction 5, at -78 °C. Results from ¹H NMR spectroscopy = no reaction observed.
- **Reaction 8:** similar conditions to Reaction 5, at room temperature. Results from ¹H NMR spectroscopy = conversion **2a** = 33% and yield **5a** = 3%.
- **Reaction 9:** similar conditions to Reaction 5, at 60 °C. Results from ¹H NMR spectroscopy = conversion **2a** = 94% and complex mixture that could not be analysed.

5.5.6. Telescoped synthesis of 2-methyl-1,4-benzoquinone 5a (flow)



Same flow setup as section 5.5.2

- **Reaction 1:** acid catalyst Amberlyst-15

System parameters: similar as section 5.5.2 with thermo reactor **TR3-Amb** (1/4" o.d., 0.049" wall thickness, 15 cm length, effective volume = 1.1 mL, loaded with 0.75 g Amberlyst® 15 and 0.86 g of glass beads with 0.5 – 0.75 mm o.d.).

Procedure: similar as section 5.5.2, with a starting solution of *p*-cresol 1 M (1.0 eq, 14.0 mmol, 2.52 g), TPFPP (0.30 mol%, 42.0 μmol, 41.3 mg), HFIP (2 eq, 28.0 mmol, 2.90 mL) and biphenyl (0.050 eq, 0.700 mmol, 108 mg) in EtOAc (14 mL), and thermo reactor residence time of 4.4 min.

Results: ¹H NMR spectroscopy overall yield of **5a** = 4% and yield for the second step = 4%.

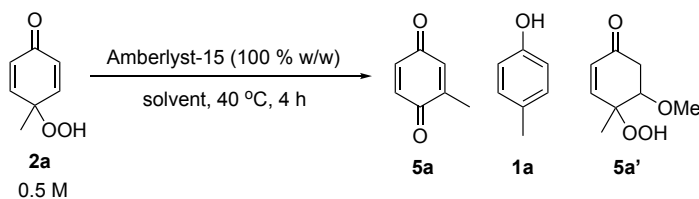
- **Reaction 2:** acid catalyst NbOPO₄

System parameters: similar to section 5.5.2 with thermo reactor **TR1-NbP** (1/4" o.d., 0.049" wall thickness, 15 cm length, effective volume = 1.1 mL, loaded with 0.75 g NbOPO₄ and 2.0 g of glass beads 2 mm o.d.).

Procedure: same as Reaction 1.

Results: ¹H NMR spectroscopy overall yield of **5a** = 1% and yield for the second step = 1%.

5.5.7. 1,2-alkyl shift of *p*-peroxyquinol **2a**: optimisation of solvent (batch)



Standard procedure: Amberlyst-15 (100% w/w, 140 mg) was added to a 2 mL solution of *p*-peroxyquinol **2a** (1.0 eq, 1.00 mmol, 140 mg) and biphenyl (0.050 eq, 50.0 μ mol, 8.10 mg) in various solvents, unless stated otherwise. The solution was stirred for 4 h, and a ^1H NMR spectroscopy was recorded from a 0.1 mL sample from the reaction mixture, which was then concentrated by nitrogen blow down for 3-5 min.

SET 1: solvent DMC

- **Reaction 1:** Dimethyl carbonate (2 mL). Results from ^1H NMR spectroscopy = conversion **2a** = 49%, yield **5a** = 2% and traces of **1a**.

SET 2: solvent EtOAc

- **Reaction 2:** EtOAc (2 mL). Results from ^1H NMR spectroscopy = conversion **2a** = 13%, yield **5a** = 2% and traces of **1a**.

SET 3: solvent Me-THF

- **Reaction 3:** 2-Methyltetrahydrofuran (2 mL). Results from ^1H NMR spectroscopy = no reaction was observed.

SET 4: solvent MeCN

- **Reaction 4:** Acetonitrile (2 mL). Results from ^1H NMR spectroscopy = conversion **2a** = 17%, yield **5a** = 2% and traces of **1a**.

SET 5: solvent MeOH

- **Reaction 5:** Methanol (2mL). The sample was dried over MgSO_4 , filtrated, and concentrated under reduced pressure. As the product has previously decomposed over silica during flash chromatography purification, only a ^1H NMR spectroscopy of the crude could be obtained. Results from ^1H NMR spectroscopy = conversion **2a** = 20%, yield **5a'** = 15%.

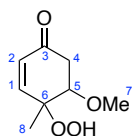
SET 6: solvent toluene/HFIP 1:3

- **Reaction 6:** toluene (0.5 mL) and HFIP (1.5 mL). Results from ^1H NMR spectroscopy = conversion **2a** = 53%, yield **5a** = 5% and traces of **1a**.

SET 7: solvent CDCl_3

- **Reaction 7:** deuterated chloroform (2 mL). Results from ^1H NMR spectroscopy = conversion **2a** = 84%, yield **5a** = 4% and traces of **1a**.

4-Hydroperoxy-5-methoxy-4-methylcyclohex-2-en-1-one **5a'** (novel compound)

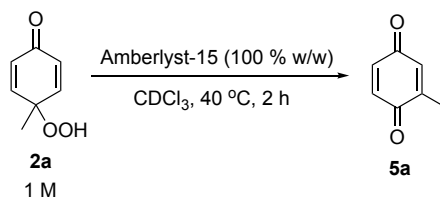


^1H NMR (400 MHz, Chloroform-*d*): δ 6.92 (m, 1H, **1**), 6.01 (dd, $J = 10.2, 1.2$ Hz, 1H, **2**), 4.17 (dd, $J = 11.6, 5.1$ Hz, 1H, **5**), 3.51 (s, 3H, **7**), 2.88 (ddd, $J = 16.8, 5.1, 1.2$ Hz, 1H, **4**), 2.40 (dd, $J = 16.8, 11.6$ Hz, 1H, **4'**), 1.34 (s, 3H, **8**).

^{13}C NMR (101 MHz, Chloroform-*d*): δ 197.8 (**3**), 153.2 (**1**), 129.8 (**2**), 84.9 (**6**), 76.2 (**5**), 58.4 (**7**), 41.1 (**4**), 16.6 (**8**).

HRMS (ESI) m/z calcd $[\text{C}_8\text{H}_{13}\text{O}_4]^+$ ($[\text{M} + \text{H}]^+$): 173.0808, found 173.0793.

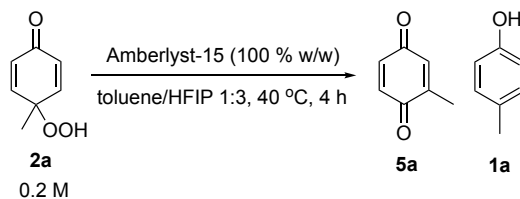
5.5.8. 1,2-Alkyl shift of *p*-peroxyquinol **2a**: volatility tests (batch)



Standard procedure: Amberlyst-15 (100% w/w, 280 mg) was added to a 2 mL solution of *p*-peroxyquinol **2a** (1.0 eq, 2.00 mmol, 280 mg) in CDCl₃. The solution was stirred for 2 h, and volatility tests were undertaken from a 0.1 mL sample from the reaction mixture.

- **Test 1:** a sample was analysed by ¹H NMR spectroscopy, without any solvent removal (ratio **5a: 2a** was 1: 3.1).
- **Test 2:** NMR spectroscopy sample from Test 1 was evaporated by nitrogen blow down for 30 min, diluted with 0.6 mL CDCl₃ and analysed by ¹H NMR spectroscopy (ratio **5a: 2a** was 1: 3.6).
- **Test 3:** NMR spectroscopy sample from Test 2 was put in the rotary evaporator for 30 min, diluted with 0.6 mL CDCl₃ and analysed by ¹H NMR spectroscopy (ratio **5a: 2a** was 1: 4.9).
- **Test 4:** NMR spectroscopy sample from Test 3 was put in the Schlenk line for 30 min, diluted with 0.6 mL CDCl₃ and analysed by ¹H NMR spectroscopy (ratio **5a: 2a** was 1: 6.1).

5.5.9. 1,2-alkyl shift of *p*-peroxyquinol **2a**: quantification methods (batch)



SET 1: internal standard (biphenyl)

Procedure: Amberlyst-15 (100% w/w, 112 mg) was added to a 4 mL solution of *p*-peroxyquinol **2a** (1.0 eq, 0.800 mmol, 112 mg) and biphenyl (0.050 eq, 40.0 μ mol, 6.20 mg) in toluene/HFIP 1:3 (1 mL toluene + 3 mL HFIP). The solution was stirred for 4 h at 40 °C.

- **Test 1:** one sample (0.1 mL) was taken from the reaction mixture, concentrated by nitrogen blow down for 3 min, and diluted with 0.6 mL CDCl₃. Results from ¹H NMR spectroscopy = conversion **2a** = 45%, yield **5a** = 3% and traces of **1a**.
- **Test 2:** another sample (0.1 mL) was taken from the reaction mixture and directly diluted with 0.5 mL CDCl₃. Results from ¹H NMR spectroscopy: conversion **2a** = 49%, yield **5a** = 11% and traces of **1a**.

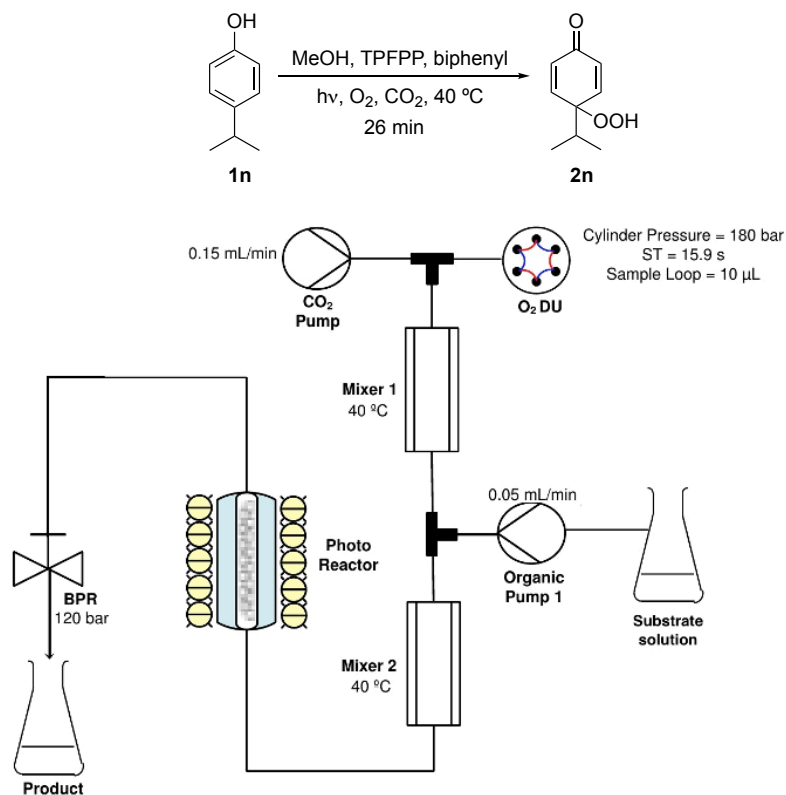
SET 2: HPLC calibration curve

Procedure: Amberlyst-15 (100% w/w, 112 mg) was added to a 4 mL solution of *p*-peroxyquinol **2a** (1.0 eq, 0.800 mmol, 112 mg) in toluene/HFIP 1:3 (1 mL toluene + 3 mL HFIP) and stirred at 40 °C for 24 h. Three samples were collected for HPLC analysis: 0 h, 4 h, and 24 h.

- **Test 1:** after 4 h of reaction, conversion **2a** = 47% and yield **5a** = 11%
- **Test 2:** after 24 h reaction, conversion **2a** = 79% and yield **5a** = 16%

Calibration curves and quantification analysis for both the *p*-peroxyquinol **2a** (PPQ) and 2-methyl-1,4-benzoquinone **5a** (BQ) can be found in section 5.6 (Appendix).

5.5.10. Photooxidation of 4-isopropylphenol **1n** (flow)



Scheme 72. Simplified schematic diagram of the high-pressure flow system used for the photooxidation of 4-isopropylphenol **1n**

- **Reaction 1: concentration of 4-isopropylphenol **1n** = 1 M**

System parameters: Photo reactor (10 mm outer diameter (o.d.)), 240 mm length, 1 mm wall thickness, effective volume = 5.2 mL, filled with 38 glass beads with 6 mm o.d., at $40\text{ }^\circ\text{C}$); cooling baths (photo reactor = $35.5\text{ }^\circ\text{C}$, LED lights = $-5\text{ }^\circ\text{C}$); trips (system set pressure = 120 bar, high trip = 140 bar; oxygen set pressure = 180 bar, high trip = 190 bar, low trip = 160 bar; mixers set temperature = $40\text{ }^\circ\text{C}$, high trip = $50\text{ }^\circ\text{C}$), biphenyl as the internal standard. The standard procedure (**Chapter 2, section 2.1.3**) was performed with CO_2 (0.15 mL/min and overall $[CO_2] = 71\%$), O_2 (180 bar, sample loop = $10\text{ }\mu\text{L}$, switching time = 15.9 s, molar ratio O_2 : phenol = 2:1 and the overall $[O_2] = 2.1\text{ mol}\%$), and HPLC pump (0.05 mL/min), unless stated otherwise.

Procedure: A starting solution of 4-isopropylphenol **1n** (1.0 eq, 18.0 mmol, 2.45 g, 1 M), TPFPP (0.050 mol%, 9.00 μmol , 9.10 mg) and biphenyl (0.050 eq, 0.900 mmol, 139 mg) in MeOH (18 mL) was prepared and sonicated for 30 min. After performing the standard procedure,

starting solution was then pumped into the system at 0.05 mL/min, combined with the gaseous mixture (CO₂ and O₂) on Mixer 2 and then passed through the photo reactor, with a residence time of 26 min.

Results: The system reached a steady state after 3 h of reaction and a sample was collected for 3 min, nitrogen blow down for another 3 min and analysed by ¹H NMR spectroscopy: conversion of **1n** = 69% and yield of **2n** = 64%. Another sample was collected for 2 h (6 mL), concentrated under reduced pressure and purified by flash chromatography column (5% MeOH in DCM), giving **2n** (3.66 mmol, 615 mg, 61%) as a yellow solid.

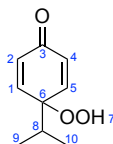
- **Reaction 2: concentration of 4-isopropylphenol **1n** = 3 M**

System parameters: similar to Reaction 1, with overall [CO₂] = 68%) and O₂ (switching time = 10.6 s, molar ratio O₂: phenol = 1:1 and the overall [O₂] = 3.1 mol%).

Procedure: similar to Reaction 1, with a starting solution of 4-isopropylphenol **1n** (1.0 eq, 42.0 mmol, 5.72 g, 3 M), TPFPP (0.050 mol%, 21.0 μmol, 20.1 mg) and biphenyl (0.050 eq, 2.10 mmol, 324 mg) in MeOH (14 mL).

Results: The system reached a steady state after 4 h of reaction and a sample was collected for 3 min, nitrogen blow down for another 3 min and analysed by ¹H NMR spectroscopy: conversion of **1n** = 89% and yield of **2n** = 85%. Another sample was collected for 1 h (3 mL), concentrated under reduced pressure and purified by flash chromatography column (5% MeOH in DCM), giving **2n** (6.84 mmol, 1.15 g, 76%) as a yellow solid.

4-Hydroperoxy-4-isopropylcyclohexa-2,5-dien-1-one **2n** (novel compound)

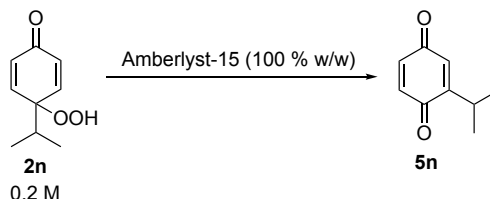


¹H NMR (400 MHz, Chloroform-*d*): δ 8.92 (s, 1H, **7**), 6.89 (d, *J* = 10.3 Hz, 2H, **1/5**), 6.36 (d, *J* = 10.3 Hz, 2H, **2/4**), 2.05 (hept, *J* = 6.9 Hz, 1H, **8**), 0.93 (d, *J* = 6.9 Hz, 6H, **9/10**).

¹³C NMR (101 MHz, Chloroform-*d*): δ 186.4 (**3**), 148.9 (**1/5**), 131.9 (**2/4**), 84.3 (**6**), 34.4 (**8**), 17.3 (**9/10**).

HRMS (ESI) *m/z* calcd [C₉H₁₃O₃]⁺ ([M + H]⁺): 169.0859, found 169.0863.

5.5.11. 1,2-Alkyl shift of *p*-peroxyquinol **2n**: solvent and temperature (batch)



Standard procedure: Amberlyst-15 (100% w/w, 67.2 mg) was added to a 2 mL solution of *p*-peroxyquinol **2n** (1.0 eq, 0.400 mmol, 67.2 mg) and biphenyl (0.050 eq, 20.0 μ mol, 3.10 mg). The solution was stirred, and a ^1H NMR spectroscopy was recorded from a 0.1 mL sample from the reaction mixture, diluted in 0.5 mL CDCl_3 .

SET 1: Temperature = 40 °C

- **Reaction 1:** EtOAc (1.92 mL) and HFIP (2.0 eq, 0.800 mmol, 80.0 μ L). After 30 min reaction, conversion **2n** = 86% and yield **5n** = 36%.
- **Reaction 2:** Toluene (0.5 mL) and HFIP (1.5 mL). After 30 min reaction, conversion **2n** = 100% and yield **5n** = 55%.
- **Reaction 3:** Amberlyst-15 (100% w/w, 168 mg) was added to a 5 mL solution of *p*-peroxyquinol **2n** (1.0 eq, 1.00 mmol, 168 mg) in toluene (1.25 mL) and HFIP (3.75 mL). After the solution was stirred for 4 h, Amberlyst-15 was filtered out and washed with the reaction solvent (3 x 2 mL). The filtrate was concentrated under reduced pressure and the remaining solvent was removed using a Schlenk line, giving **5n** (0.588 mmol, 88.3 mg, 59%) as a dark brown solid.
- **Reaction 4:** EtOAc (0.5 mL) and HFIP (1.5 mL). After 1 h reaction, conversion **2n** = 100% and yield **5n** = 47%.

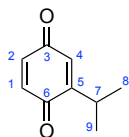
SET 2: Temperature = 20 °C (room temperature)

- **Reaction 5:** EtOAc (0.5 mL) and HFIP (1.5 mL). After 2 h reaction, conversion **2n** = 100% and yield **5n** = 69%.
- **Reaction 6:** HFIP (2 mL). After 20 min reaction, conversion **2n** = 100% and yield **5n** = >99%.

SET 3: Temperature = 0 °C

- **Reaction 7:** HFIP (2 mL). After 20 min reaction, conversion **2n** = 100% and yield **5n** = 80%.

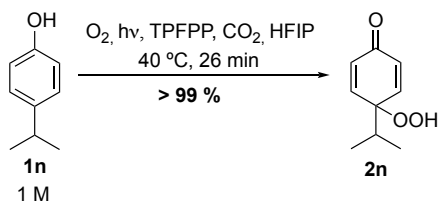
2-Isopropyl-1,4-benzoquinone **5n**²⁸²



¹H NMR (400 MHz, Chloroform-*d*): δ 6.78 (d, J = 10.1 Hz, 1H, **1**), 6.73 (dd, J = 10.1, 2.4 Hz, 1H, **2**), 6.57 (dd, J = 2.4, 1.1 Hz, 1H, **4**), 3.06 (heptd, J = 6.9, 1.1 Hz, 1H, **7**), 1.16 (d, J = 6.9 Hz, 6H, **8/9**).

¹³C NMR (101 MHz, Chloroform-*d*): δ 188.3 (**6**), 187.3 (**3**), 155.2 (**5**), 137.2 (**1**), 136.1 (**2**), 130.5 (**4**), 26.9 (**7**), 21.5 (**8/9**).

5.5.12. Photooxidation of 4-isopropylphenol **1n** – Part II (flow)



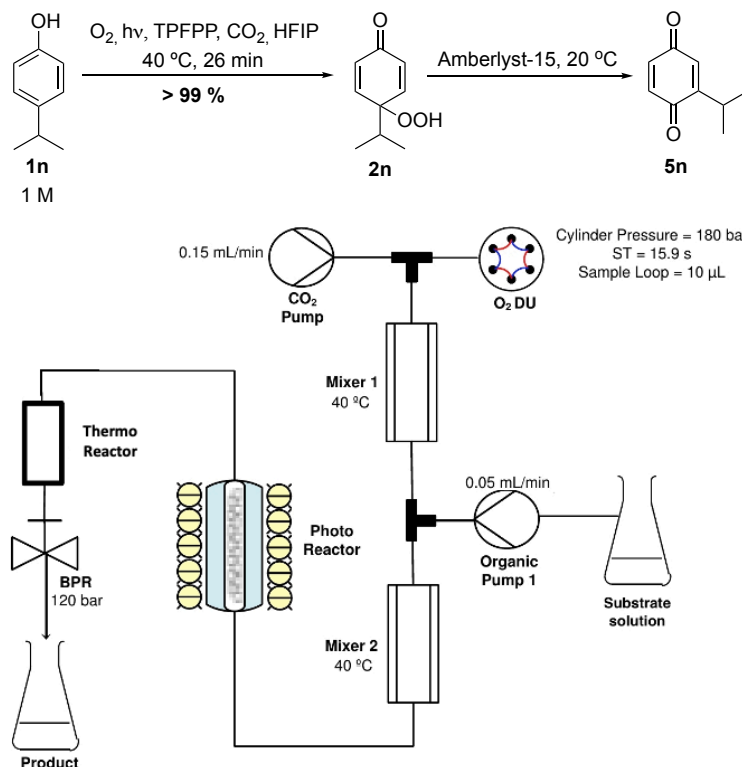
Same high-pressure flow system as section 5.5.10.

System parameters: similar to section 5.5.10, with overall [CO₂] = 84% and overall [O₂] = 2.5 mol%).

Procedure: similar to section 5.5.10, with a starting solution of 4-isopropylphenol **1n** 1 M (1.0 eq, 14.0 mmol, 1.91 g), TPFPP (0.050 mol%, 7.00 μmol, 7.20 mg) and biphenyl (0.040 eq, 0.560 mmol, 86.1 mg) in HFIP (14 mL).

Results: The system reached a steady state after 2.5 h of reaction and a sample was collected for 3 min, diluted with 0.5 mL CDCl₃ and analysed by ¹H NMR spectroscopy: conversion of **1n** = 97% and yield of **2n** = > 99%.

5.5.13. Telescoped synthesis of 2-isopropyl-1,4-benzoquinone 5n (flow)



Scheme 73. Simplified schematic diagram of the high-pressure flow system used for the telescoped synthesis of 2-isopropyl-1,4-benzoquinone 5n

- **Reaction 1: thermo reactor (0.25 g Amberlyst-15, 5.5 min residence time)**

System parameters: photo reactor (10 mm outer diameter (o.d.)), 240 mm length, 1 mm wall thickness, effective volume = 5.2 mL, filled with 38 glass beads with 6 mm o.d., at 40 °C); thermo reactor **TR3-Amb II** (1/4" o.d., 0.049" mm wall thickness, 15 cm length, effective volume = 1.4 mL, loaded with 0.25 g Amberlyst-15 and 2.05 g of glass beads with 0.5 – 0.75 mm o.d, at 20 °C); cooling baths (photo reactor = 35.5 °C, LED lights = -5 °C); trips (system set pressure = 120 bar, high trip = 140 bar; oxygen set pressure = 180 bar, high trip = 190 bar, low trip = 160 bar; mixers set temperature = 40 °C, high trip = 50 °C), biphenyl as the internal standard. The standard procedure (**Chapter 2, section 2.1.3**) was performed with CO₂ (0.15 mL/min and overall [CO₂] = 84%), O₂ (180 bar, sample loop = 10 μL, switching time = 15.9 s, molar ratio O₂: phenol = 2:1 and the overall [O₂] = 2.5 mol%), and HPLC pump (0.05 mL/min), unless stated otherwise.

Procedure: A starting solution of 4-isopropylphenol **1n** 1 M (1.0 eq, 14.0 mmol, 1.91 g), TPFPP (0.050 mol%, 7.00 μ mol, 7.20 mg) and biphenyl (0.040 eq, 0.560 mmol, 86.1 mg) in HFIP (14 mL) was prepared and sonicated for 30 min. After performing the standard procedure, starting solution was pumped into the system at 0.05 mL/min, combined with the gaseous mixture (CO₂ and O₂) on Mixer 2, and then passed through the photo reactor (residence time = 26 min) and thermo reactor (residence time = 7 min).

Results: samples were collected for 2 min, diluted with 0.5 mL CDCl₃ and analysed by ¹H NMR spectroscopy.

- 1 h of reaction, yield of **2n** = 0%, yield of **5n** = 83%, yield of **2n + 5n** = 83%
- 1.5 h of reaction, yield of **2n** = 8%, yield of **5n** = 76%, yield of **2n + 5n** = 84%
- 2 h of reaction, yield of **2n** = 20%, yield of **5n** = 68%, yield of **2n + 5n** = 88%
- 2.5 h of reaction, yield of **2n** = 28%, yield of **5n** = 61%, yield of **2n + 5n** = 89%
- 3 h of reaction, yield of **2n** = 37%, yield of **5n** = 52%, yield of **2n + 5n** = 89%

- **Reaction 2: thermo reactor (0.75 g Amberlyst-15, 5.5 min residence time)**

System parameters: similar to Reaction 1, with thermo reactor **TR3-Amb** (effective volume = 1.1 mL, loaded with 0.75 g Amberlyst-15 and 0.85 g of glass beads with 0.5 – 0.75 mm o.d).

Procedure: similar to Reaction 1, with thermo reactor residence time of 5.5 min.

Results: samples were collected for 2 min, diluted with 0.5 mL CDCl₃ and analysed by ¹H NMR spectroscopy.

- 2 h of reaction, yield of **2n** = 0%, yield of **5n** = 80%, yield of **2n + 5n** = 80%
- 2.5 h of reaction, yield of **2n** = 3%, yield of **5n** = 78%, yield of **2n + 5n** = 81%
- 3 h of reaction, yield of **2n** = 7%, yield of **5n** = 77%, yield of **2n + 5n** = 84%
- 3.5 h of reaction, yield of **2n** = 9%, yield of **5n** = 75%, yield of **2n + 5n** = 84%
- 4 h of reaction, yield of **2n** = 12%, yield of **5n** = 72%, yield of **2n + 5n** = 84%

- **Reaction 3: thermo reactor (1.05 g Amberlyst-15, 3 min residence time)**

System parameters: similar to Reaction 1, with thermo reactor **TR4-Amb** (effective volume = 0.6 mL, loaded with 1.05 g Amberlyst-15).

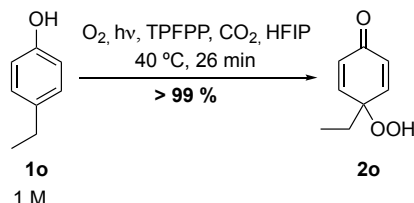
Procedure: similar to Reaction 1, with thermo reactor residence time of 3 min.

Results: samples were collected for 2 min, diluted with 0.5 mL CDCl₃ and analysed by ¹H NMR spectroscopy.

- 1 h of reaction, yield of **2n** = 0%, yield of **5n** = 82%, yield of **2n + 5n** = 82%
- 1.5 h of reaction, yield of **2n** = 0%, yield of **5n** = 82%, yield of **2n + 5n** = 82%
- 2 h of reaction, yield of **2n** = 0%, yield of **5n** = 82%, yield of **2n + 5n** = 82%
- 2.5 h of reaction, yield of **2n** = 0%, yield of **5n** = 82%, yield of **2n + 5n** = 82%
- 3 h of reaction, yield of **2n** = 0%, yield of **5n** = 82%, yield of **2n + 5n** = 82%

This reaction resulted in overall yield of **5n** = 82% (2nd step yield = 83%), and productivity of 9 g/day.

5.5.14. Photooxidation of 4-ethylphenol **1o** (flow)



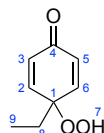
Same high-pressure flow system as section 5.5.10.

System parameters: similar to section 5.5.10, with overall $[\text{CO}_2] = 84\%$ and overall $[\text{O}_2] = 2.5$ mol%).

Procedure: similar to section 5.5.10, with a starting solution of 4-ethylphenol **1o** 1 M (1.0 eq, 14.0 mmol, 1.71 g), TPFPP (0.050 mol%, 7.00 μmol , 7.20 mg) and biphenyl (0.040 eq, 0.560 mmol, 86.1 mg) in HFIP (14 mL).

Results: The system reached a steady state after 1.5 h of reaction and a sample was collected for 3 min, diluted with 0.5 mL CDCl_3 and analysed by ^1H NMR spectroscopy: conversion of **1o** = 97% and yield of **2o** = $> 99\%$. Another sample was collected for 25 min (1.25 mL), concentrated under reduced pressure and purified by flash chromatography column (EtOAc/Hexane 1:1), giving **2o** (1.19 mmol, 183 mg, 95%) as an off-white solid.

4-Ethyl-4-hydroperoxycyclohexa-2,5-dien-1-one **2o**¹⁹⁵

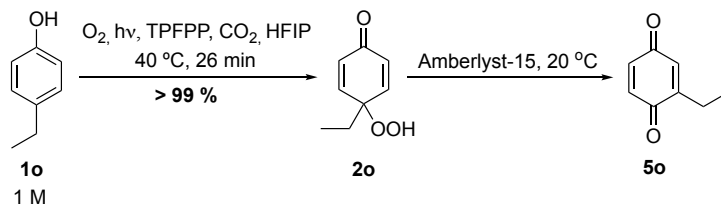


^1H NMR (400 MHz, Chloroform-*d*): δ 9.14 (s, 1H, **7**), 6.87 (d, $J = 10.2$ Hz, 2H, **2/6**), 6.33 (d, $J = 10.2$ Hz, 2H, **3/5**), 1.74 (q, $J = 7.6$ Hz, 2H, **9**), 0.84 (t, $J = 7.6$ Hz, 3H, **9**).

^{13}C NMR (101 MHz, Chloroform-*d*): δ 186.4 (**4**), 149.8 (**2/6**), 131.3 (**3/5**), 82.4 (**1**), 29.0 (**8**), 7.9 (**9**).

HRMS (ESI) m/z calcd $[\text{C}_8\text{H}_{10}\text{O}_3\text{Na}]^+$ ($[\text{M} + \text{Na}]^+$): 177.0522, found 177.0522.

5.5.15. Telescoped synthesis of 2-ethyl-1,4-benzoquinone **5o** (flow)



Same flow setup as section 5.5.13

- **Reaction 1: thermo reactor (1.05 g Amberlyst-15, 3 min residence time)**

System parameters: similar to section 5.5.13, with thermo reactor **TR4-Amb** (1/4" o.d., 0.049" mm wall thickness, 15 cm length, effective volume = 0.6 mL, loaded with 1.05 g Amberlyst-15, at $20\text{ }^\circ\text{C}$).

Procedure: similar to 5.5.13, with a starting solution of 4-ethylphenol **1o** 1 M (1.00 eq, 11.0 mmol, 1.34 g), TPFPP (0.050 mol%, 5.23 μmol , 5.10 mg) and biphenyl (0.040 eq, 0.442 mmol, 68.2 mg) in HFIP (11 mL), and thermo reactor residence time = 3 min.

Results: samples were collected for 2 min, diluted with 0.5 mL CDCl_3 and analysed by ^1H NMR spectroscopy.

- 1 h of reaction, yield of **2o** = 6%, yield of **5o** = 80%, yield of **2o** + **5o** = 86%
- 2 h of reaction, yield of **2o** = 13%, yield of **5o** = 71%, yield of **2o** + **5o** = 84%.

Another sample was collected for 20 min (1 mL), concentrated under reduced pressure and purified by flash chromatography column (EtOAc/Hexane 1:4), giving **5o** (0.706 mmol, 96.1 mg, 71%) as yellow solid.

- 2.5 h of reaction, yield of **2o** = 26%, yield of **5o** = 60%, yield of **2o** + **5o** = 86%
- 3 h of reaction, yield of **2o** = 36%, yield of **5o** = 56%, yield of **2o** + **5o** = 92%

- **Reaction 2: thermo reactor (1.92 g Amberlyst-15, 4.5 min residence time)**

System parameters: similar to Reaction 1, with thermo reactor **TR4-Amb II** (30 cm length, effective volume = 0.9 mL, loaded with 1.92 g Amberlyst-15).

Procedure: similar to Reaction 1, with thermo reactor residence time of 4.5 min.

Results: samples were collected for 2 min, diluted with 0.5 mL CDCl₃ and analysed by ¹H NMR spectroscopy.

- 2 h of reaction, yield of **2o** = 0%, yield of **5o** = 76%, yield of **2o** + **5o** = 76%
- 2.5 h of reaction, yield of **2o** = 0%, yield of **5o** = 77%, yield of **2o** + **5o** = 77%
- 3 h of reaction, yield of **2o** = 0%, yield of **5o** = 75%, yield of **2o** + **5o** = 75%

This reaction resulted in overall yield of **5o** = 76% (2nd step yield = 77%), and productivity of 7 g/day.

- **Reaction 3: thermo reactor (4.38 g Amberlyst-15, 7.5 min residence time)**

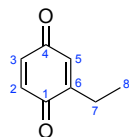
System parameters: similar to Reaction 1, with thermo reactor **TR4-Amb III** (70 cm length, effective volume = 1.5 mL, loaded with 1.92 g Amberlyst-15).

Procedure: similar to Reaction 1, with thermo reactor residence time of 7.5 min.

Results: samples were collected for 2 min, diluted with 0.5 mL CDCl₃ and analysed by ¹H NMR spectroscopy.

- 2 h of reaction, yield of **2o** = 0%, yield of **5o** = 64%, yield of **2o** + **5o** = 64%
- 2.5 h of reaction, yield of **2o** = 0%, yield of **5o** = 66%, yield of **2o** + **5o** = 66%
- 3 h of reaction, yield of **2o** = 0%, yield of **5o** = 69%, yield of **2o** + **5o** = 69%

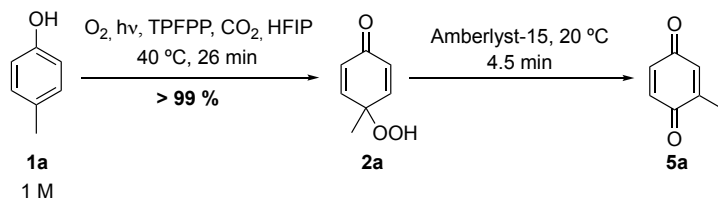
2-Ethyl-1,4-benzoquinone **5o**³²¹



¹H NMR (400 MHz, Chloroform-*d*): δ 6.76 (d, *J* = 10.1 Hz, 1H, **2**), 6.71 (dd, *J* = 10.1, 2.3 Hz, 1H, **3**), 6.57 – 6.56 (m, 1H, **5**), 2.47 (q, *J* = 7.4, 2H, **7**), 1.14 (t, *J* = 7.4 Hz, 3H, **8**).

¹³C NMR (101 MHz, Chloroform-*d*): δ 188.0 (**1**), 187.7 (**4**), 151.0 (**6**), 137.0 (**2**), 136.4 (**3**), 131.8 (**5**), 22.2 (**7**), 11.7 (**8**).

5.5.16. Telescoped synthesis of 2-methyl-1,4-benzoquinone **5a** – Part II (flow)



Same flow setup as section 5.5.10

System parameters: similar to section 5.5.10, with thermo reactor **TR4-Amb II** (1/4" o.d., 0.049" mm wall thickness, 30 cm length, effective volume = 0.9 mL, loaded with 1.92 g Amberlyst-15, at 20 °C).

Procedure: similar to section 5.5.10, with a starting solution of p-cresol **1a** 1 M (1.0 eq, 11.0 mmol, 1.19 g), TPFPP (0.050 mol%, 5.34 μ mol, 5.20 mg) and biphenyl (0.040 eq, 0.443 mmol, 68.3 mg) in HFIP (11 mL), and thermo reactor residence time = 4.5 min.

Results: samples were collected for 2 min, diluted with 0.5 mL $CDCl_3$ and analysed by 1H NMR spectroscopy.

- 1 h of reaction, yield of **2a** = 14%, yield of **5a** = 4%, yield of **2a** + **5a** = 18%
- 2 h of reaction, yield of **2a** = 14%, yield of **5a** = 23%, yield of **2a** + **5a** = 37%.
- 2.5 h of reaction, yield of **2a** = 13%, yield of **5a** = 41%, yield of **2a** + **5a** = 54%.
- 3 h of reaction, yield of **2a** = 12%, yield of **5a** = 51%, yield of **2a** + **5a** = 63%.

This reaction resulted in overall yield of **5a** = 13% (2nd step yield = 13%), and productivity of 1 g/day.

5.6. Appendix

HPLC calibration curve for 1,2-alkyl shift of *p*-peroxyquinol **2a**

(a) System specifications

Jasco 3080 PU X-LC Ultra High-Pressure Pump system with UV detector, Phenomenex Luna C18 column (4.6 x 250 mm, 5 μm diameter particles and 100 \AA pores) and Water Nova-Pak C18 pre-column (3.9 x 20 mm, 4 μm diameter particles).

Table 23. HPLC methodology parameters for calibration curve for 1,2-alkyl shift of *p*-peroxyquinol **2a**

Flow rate	1.0 ml.min ⁻¹
Column oven temperature	26 °C
UV wavelength	254 nm
Time	8 min
Injection volume	5 μL (PPQ) and 1 μL (BQ)
Retention time	3.2 min (PPQ) and 5.2 (BQ)
Pressure	176 bar
Solvent system	50 % deionised water + 50 % acetonitrile

PPQ = *p*-peroxyquinol **2a** and BQ = 2-methyl-1,4-benzoquinone **5a**

(b) Sample preparation – *p*-peroxyquinol **2a**

A 50 mM stock solution of *p*-peroxyquinol **2a** (0.25 mmol, 35 mg) was prepared in chloroform (5 mL). Solutions with different concentrations were prepared from the stock solution, as shown below (Table 24).

Table 24. Sample preparation calculations for *p*-peroxyquinol **2a**

Entry	Volume from stock solution (mL)	Final volume (mL)	Dilution factor	Final concentration (mM)
1	1	10	10	5
2	1	20	20	2.5
3	1	50	50	1
4	1	100	100	0.5

(c) Sample preparation – 2-methyl-1,4-benzoquinone 5a

A 20 mM stock solution of 2-methyl-1,4-benzoquinone **5a** (0.5 mmol, 61 mg) was prepared in chloroform (25 mL). Diluted solutions were prepared as it follows (Table 25).

Table 25. Sample preparation calculations for 2-methyl-1,4-benzoquinone 5a

Volume from stock solution (mL)	Final volume (mL)	Dilution factor	Final concentration (mM)
0.50	2	4	5
0.25	2	8	2.5
0.25	5	20	1
0.25	10	40	0.5

(d) Calibration curve and chromatogram – p-peroxyquinol 2a

An aliquot of 2 mL was taken from each concentration solution and transferred to an HPLC vial to be analysed (Table 26). Each concentration point was performed in triplicate. The calibration curve (Figure 45) and HPLC chromatogram (Figure 46) are shown below.

Table 26. HPLC data collection for p-peroxyquinol 2a calibration curve.

Concentration (mM)	Area (mAU.s)		
	1	2	3
5.0	1296878	1313701	1326329
2.5	739100	714909	722901
1.0	269930	267086	267086
0.5	139606	138602	141043

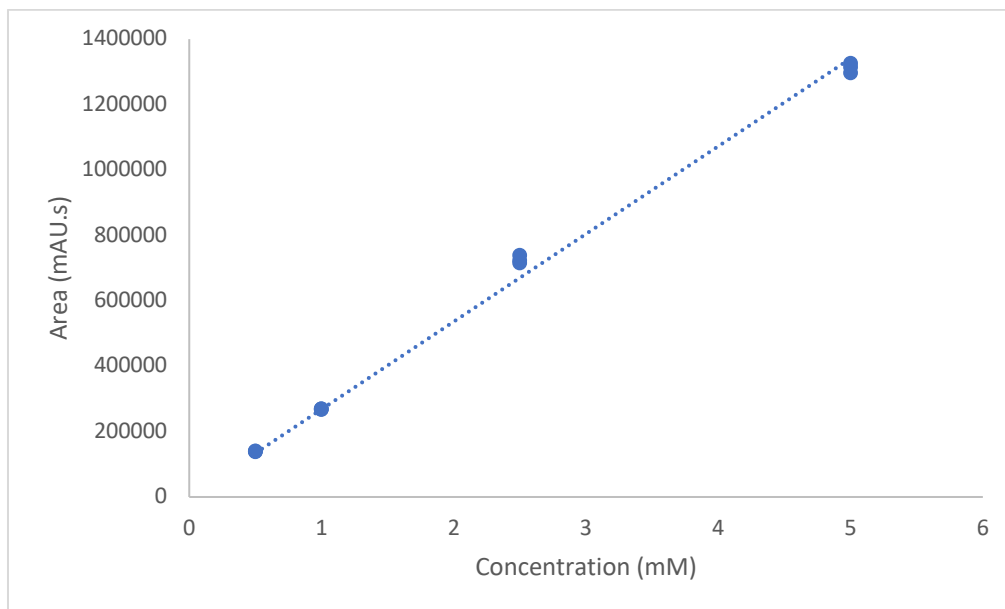


Figure 45. Calibration curve for *p*-peroxyquinol **2a**. The linear equation is $\text{Area} = 268142 \times \text{Concentration}$ with $R^2 = 0.9982$.

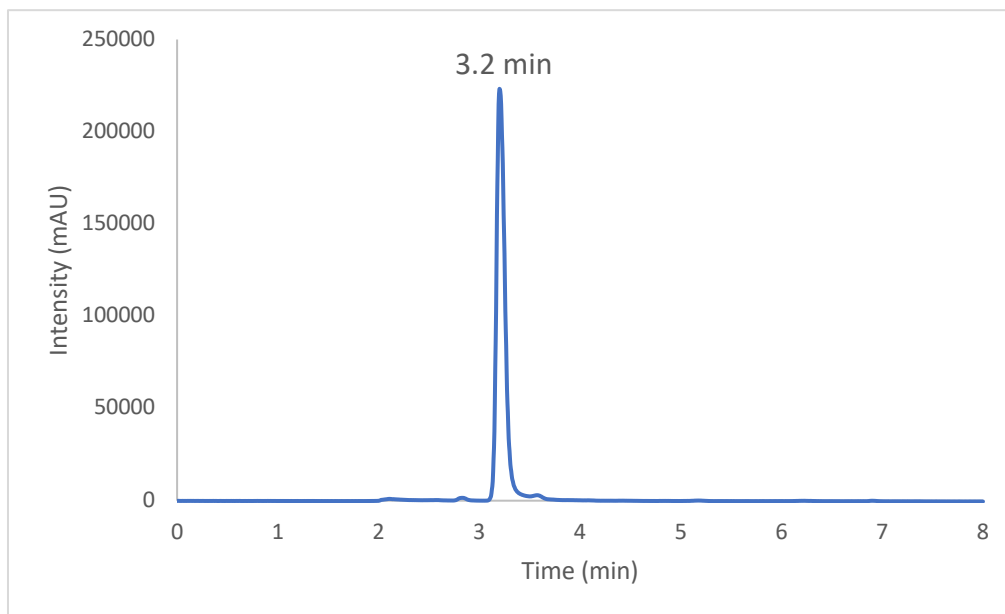


Figure 46. HPLC chromatogram of *p*-peroxyquinol **2a** (5 mM)

(e) Calibration curve and chromatogram – 2-methyl-1,4-benzoquinone 5a

An aliquot of 2 mL was taken from each concentration solution and transferred to an HPLC vial to be analysed (Table 27). Each concentration point was performed in triplicate. The calibration curve (Figure 47) and HPLC chromatogram (Figure 48) are shown below.

Table 27. HPLC data collection for 2-methyl-1,4-benzoquinone 5a calibration curve. Each concentration point was performed in triplicate.

Concentration (mM)	Area (mAU.s)		
	1	2	3
5.0	2193938	2013670	2013670
2.5	1220113	1143126	1150269
1.0	437203	426275	399712
0.5	189828	185255	181099

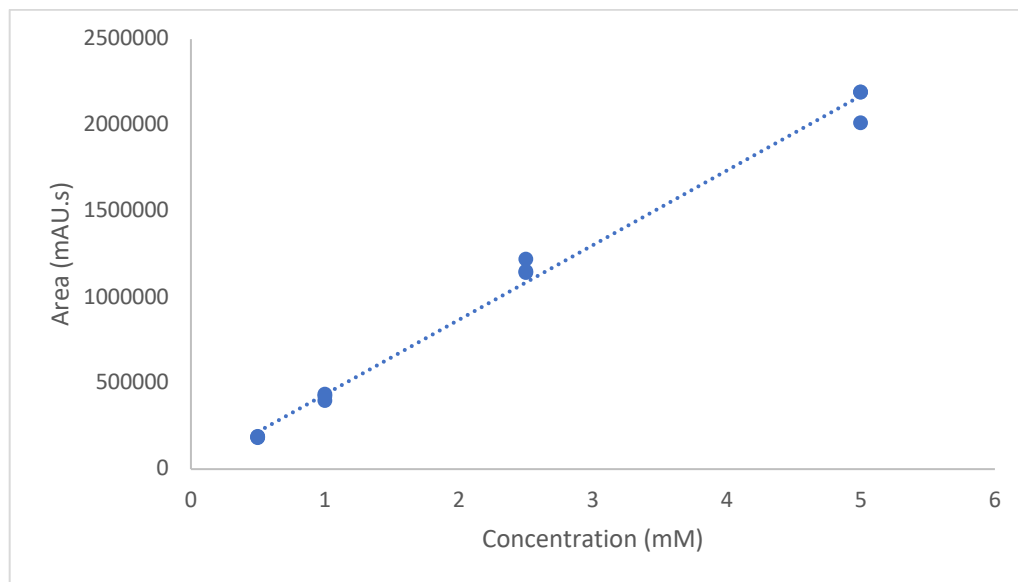


Figure 47. Calibration curve for 2-methyl-1,4-benzoquinone **5a**. The linear equation is $\text{Area} = 434097 \times \text{Concentration}$ with $R^2 = 0.992$.

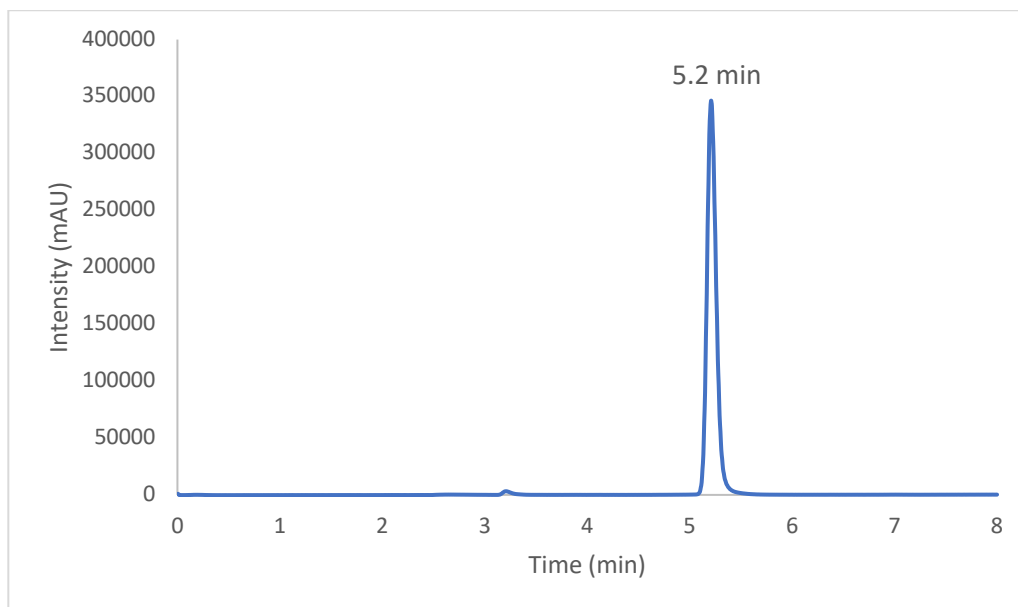


Figure 48. HPLC chromatogram of 2-methyl-1,4-benzoquinone **5a** (5 mM)

HPLC quantification of 1,2-alkyl shift of *p*-peroxyquinol **2a (section 5.5.9)**

Each sample was taken directly from the reaction mixture and diluted for HPLC quantification using the reaction solvent system (toluene/HFIP 1:3), as show in Table 28. An aliquot of 2 mL was then transferred to a HPLC vial and then analysed (Table 29).

Table 28. Sample preparation for HPLC quantification of 1,2-alkyl shift of *p*-peroxyquinol **2a**

Reaction concentration (M)	Sample from reaction (mL)	Final volume (mL)	Dilution factor	HPLC sample concentration (M)
0.2	0.125	5	40	0.005 (5 mM)

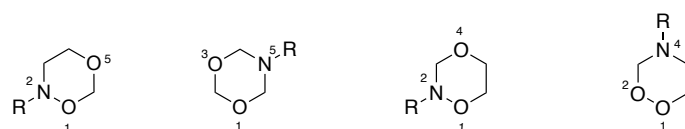
Table 29. HPLC quantification for the 1,2-alkyl shift of *p*-peroxyquinol **2a** (section 5.5.9 in toluene/HFIP 1:3)

Reaction time (h)	Compound	Area (mAU.s)	HPLC sample concentration (mM)	Reaction concentration (M)	Average reaction concentration (M)	Conversion PPQ 2a (%)	Yield BQ 5a(%)
0	PPQ	1261004	4.70	0.19	0.19	-	-
		1260981	4.70	0.19			
4	PPQ	672223	2.51	0.10	0.10	47	-
		669028	2.50	0.10			
	BQ	177811	0.41	0.02	0.02	-	11
		180197	0.42	0.02			
24	PPQ	275015	1.03	0.04	0.04	79	-
		275713	1.03	0.04			
	BQ	276111	0.65	0.03	0.03	-	16
		282679	0.65	0.03			

6. Continuous flow telescoped synthesis of 1,2,4-dioxazinanes

6.1. Introduction

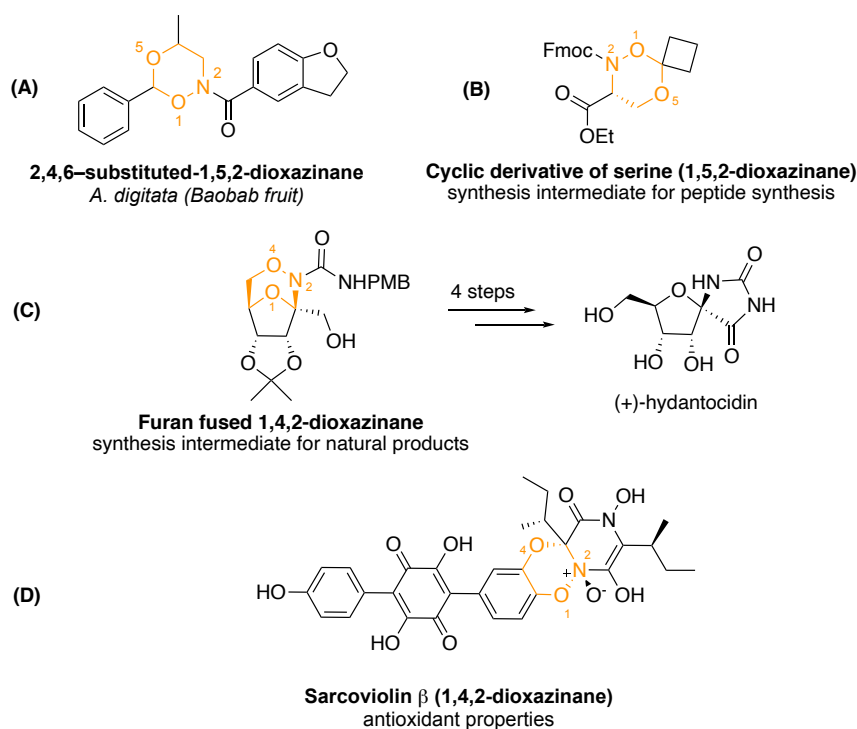
Dioxazinanes are 6-membered saturated heterocyclic rings containing two oxygen and one nitrogen atoms. They are named according to the disposition of the heteroatoms in the ring, commonly occurring as 1,5,2-, 1,3,5-, 1,4,2- and 1,2,4-dioxazinanes (Figure 49).



1,5,2-dioxazinane 1,3,5-dioxazinane 1,4,2-dioxazinane 1,2,4-dioxazinane

Figure 49. Different types of dioxazinanes: 1,5,2-, 1,3,5-, 1,4,2-, and 1,2,4-dioxazinane.

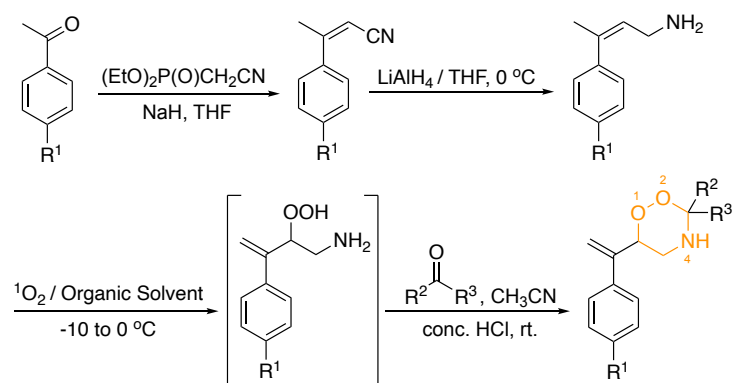
This scaffold is found in extracts from natural products such as Baobab fruit³²² and Carqueja plant³²³ (Scheme 74 - A). Dioxazinanes are potential synthetic intermediates in peptide synthesis, since these compounds have been reported in α -ketoacid-hydroxylamine (KAHA) ligation.³²⁴ They are useful intermediates in the synthesis of spironucleoside (+)-hydantocidin, a chiral substituted furan which possesses herbicidal activities (Scheme 74 - B).³²⁵ The dioxazinane moiety is also found in Sarcoviolin β , an extract from the mushroom *S. leucopus* which is reported to have antioxidant properties (Scheme 74 - C).³²⁶



Scheme 74. Dioxazinanes reported in the literature: extracts from natural products (A), synthetic intermediates (B), and antioxidant properties (C).

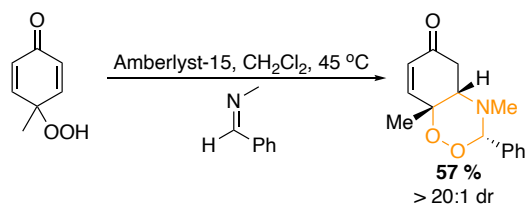
The most common dioxazinanes reported in the literature are 1,4,2-,³²⁷⁻³³² 1,5,2-³³³⁻³³⁵ and 1,3,5-dioxazinanes.^{336, 337} 1,2,4-Dioxazinanes, on the other hand, are largely underexploited with only two examples in the literature regarding their synthesis, and no natural products or drugs were reported to have this moiety.^{242, 338}

In 2018, Tokala³³⁸ investigated the synthesis of 3,6-substituted-1,2,4-dioxazinanes as potential antimalarial/anticancer drug candidates, in a four-step synthesis from acetophenone derivatives (Scheme 75). However, the experimental procedures in this publication were not described in detail, lacking crucial information such as yields, characterisation, reaction times, and discussion of selectivity.



$R^1 = \text{H, Me, F, Cl, Br, CF}_3, \text{OMe, OH, OCH}_2\text{CH}_2\text{OH}$
 $R^2R^3 = \text{acetone, clopentanone, cyclohexanone, and 2-adamantanone}$
 Scheme 75. Synthesis of 3,6-substituted-1,2,4-dioxazinanes by Tokala.³³⁸

In the second published example, a 1,2,4-dioxazinane was synthesised from *p*-peroxyquinol and an imine, using Amberlyst-15 as the acid catalyst (Scheme 76).²⁴² Although the compound was obtained with high diastereoselectivity, the procedure was limited in scope (only one example) and it was not enantioselective.



Scheme 76. Synthesis of 1,2,4-dioxazinane by Rubush²⁴²

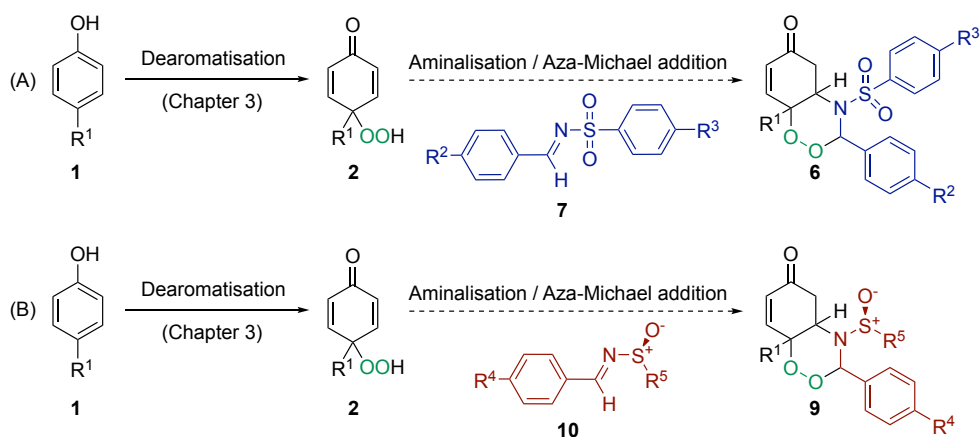
6.2. Aims and general strategy

The synthesis of 1,2,4-dioxazinanes, which as can be seen from above is largely unexplored, could lead to the discovery of new drug candidates for the treatment of malaria and cancer. Particularly, the endoperoxide bridge, present in the 1,2,4-dioxazinane structure, is believed to be essential for the anti-cancer and anti-malarial properties of artemisinin.³³⁹ Indeed, one example of 1,2,4-dioxazinane reported in a thesis demonstrated activity against all of D17 canine osteosarcoma, M21 human melanoma, lung, and prostate carcinoma cells. The asymmetric synthesis of such compounds has never been reported. Thus, the specific aims for this Chapter were:

- To explore the synthesis of 1,2,4-dioxazinanes using $^1\text{O}_2$ and dearomatisation strategy.
- To extend this approach for the racemic and asymmetric synthesis of 1,2,4-dioxazinanes.
- To use the newly developed methodology for telescoped continuous flow processes from *p*-substituted phenols.

The following strategy was used to address these aims:

1. A methodology was proposed for the telescoped synthesis of 1,2,4-dioxazinanes (**6** and **9**) from *p*-substituted phenols **1** (Scheme 77). This was based on the literature^{242, 338} and previous protocols developed in this Thesis (Chapters 3 and 4). The intention was to facilitate safe scale-up, as the hazardous *p*-peroxyquinols **2** are synthesised and reacted *in situ* in a non-flammable solvent (CO_2). This synthetic route starts from the dearomatisation of *p*-substituted phenols **1** in supercritical CO_2 using singlet oxygen, followed by amination/aza-Michael addition of *p*-peroxyquinol **2** to either *N*-sulfonyl imine **7** (racemic synthesis) or *N*-sulfinyl imine **10** (asymmetric synthesis).



Scheme 77. Proposed continuous flow telescoped synthesis of 1,2,4-dioxazines (**6** and **9**) from *p*-substituted phenols **1** using *N*-sulfonyl imines **7** (A) or *N*-sulfinyl imines **10** (B).

2. The racemic synthesis was the first to be investigated in batch to save the cost of using chiral reagents in the early stages. Different *N*-sulfonyl imines **7** were synthesised, bearing either an electron-withdrawing or electron-donating groups attached to their aromatic rings.

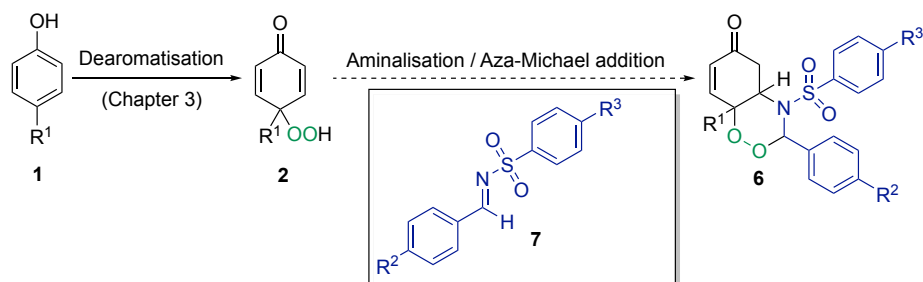
3. The second step of the proposed racemic synthesis of 1,2,4-dioxazines **6** was tested in batch with different *N*-sulfonyl imines **7**.

4. Then, the asymmetric version of 1,2,4-dioxazine **9** was investigated, using *p*-peroxyquinol **2** and *N*-sulfinyl imines **10** in batch, while screening different temperatures, catalysts, and equivalents of *N*-sulfinyl imine **10**.

6.3. Results and discussion

6.3.1. Synthesis of *N*-sulfonyl imines

The racemic synthesis of 1,2,4-dioxazinanes **6** was initially investigated. To examine the amination/Aza-Michael addition step, *N*-sulfonyl imines **7** had to be synthesised first (Scheme 78).

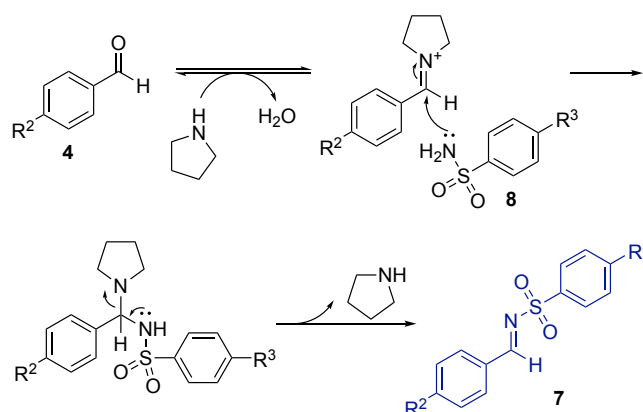


Scheme 78. Synthesis of *N*-sulfonyl imines **7** in the proposed racemic synthesis of 1,2,4-dioxazinanes **6**.

N-sulfonyl imines **7** were chosen because imines bearing an arenesulfonyl group at the nitrogen atom are commonly used in the literature due to their enhanced stability and cheap preparation compared to their aliphatic equivalents.³⁴⁰ Their synthesis was based on a protocol reported by Cid,³⁴¹ which consists on the condensation of sulfonamides and aldehydes, catalysed by pyrrolidine.

Reaction Mechanism

The reaction mechanism starts with the activation of the aromatic aldehyde **4** by nucleophilic attack of the catalyst pyrrolidine to form an iminium reactive species. The attack of sulfonamide **8** on the iminium reactive species, followed by regeneration of pyrrolidine, gives *N*-sulfonyl imine **7** (Scheme 79).

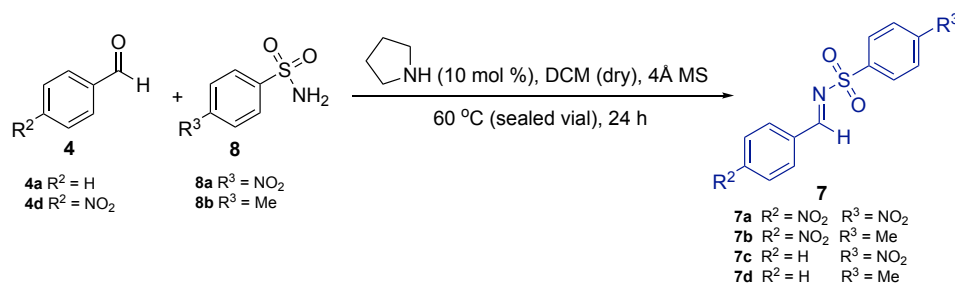


Scheme 79. Mechanism for the pyrrolidine catalysed formation of *N*-sulfonyl imines **7** from aldehydes **4** and sulfonamides **8**.

Synthesis of *N*-sulfonyl imines in batch

To study how the electronic effects would influence the subsequent amination, *N*-sulfonyl imines **7** possessing electron-donating (EDG) or electron-withdrawing (EWG) substituents, as well as unsubstituted aromatic rings were made (Table 30).

Table 30. Summary of results for the synthesis of *N*-sulfonyl imines **7**.



Entry	<i>N</i> -sulfonyl imine	R ²	R ³	¹ H NMR ratio 7 : 8	Isolated Yield of 7 (%)
1	7a	NO ₂	NO ₂	0	0
2	7b	NO ₂	Me	1: 0.3	0
3	7c	H	NO ₂	1: 0.1	77
4	7d	H	Me	1: 0.2	83

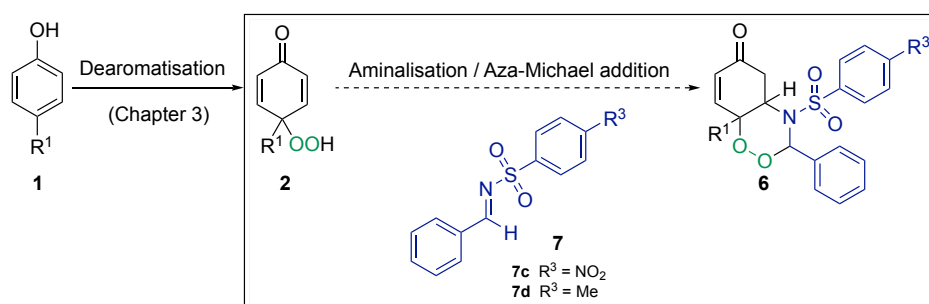
Initially, two *N*-sulfonyl imines (**7a** and **7b**) bearing a strong EWG (-NO₂) in the *N*-benzylidene ring (R²) were synthesised (Entries 1 and 2 – Table 30). A complex mixture was formed when both substituents had an electron-withdrawing group (Entry 1 – Table 30), possibly because the resulting *N*-sulfonyl imine **7a** was too reactive and could undergo side-

reactions. When R³ was changed to an electron-donating group, ¹H NMR spectroscopy analysis showed a high ratio of *N*-sulfonyl imine **7b** to sulfonamide **8b** of 1: 0.3 before purification (Entry 2 – Table 30). However, recrystallisation proved challenging and an attempted flash chromatography resulted in complete hydrolysis of **7b**.

N-sulfonyl imines **7c** and **7d** bearing an unsubstituted aromatic ring at R² were successfully obtained after recrystallisation (Entries 3 and 4 – Table 30). As expected, higher yields of **7d** (Entry 4 – Table 30) were achieved compared to **7c** (Entry 3 – Table 30) as the EDG at R³ increases the nucleophilicity of the *N*-sulfonamide **8b** for the nucleophilic attack on to aldehyde **4a**.

6.3.2. Racemic synthesis of 1,2,4-dioxazinanes with *N*-sulfonyl imines

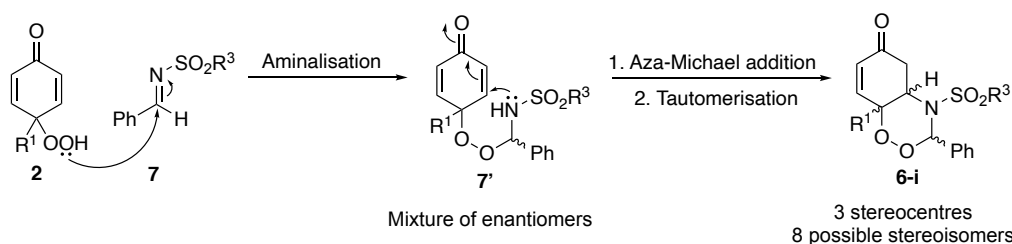
After accomplishing the synthesis of two *N*-sulfonyl imines (**7c** and **7d**), the final step of the synthesis of 1,2,4-dioxazinanes **6** was investigated in batch, as show in Scheme 80.



Scheme 80. Aminalisation/Aza-Michael addition in the proposed racemic synthesis of 1,2,4-dioxazinanes **6**.

Proposed Reaction Mechanism

The proposed mechanism for this reaction (Scheme 81) was based on work developed by Rubush and co-workers.²⁴² The nucleophilic attack of *p*-peroxyquinol **2** to *N*-sulfonyl imine **7**, would form a racemic mixture of peroxyaminal **7'**. Each enantiomer can undergo an aza-Michael addition, in which the attack of *N*-peroxyaminal can happen in either of the double bonds, resulting in different diastereoisomers. Then, tautomerisation of their corresponding enolate gives 1,2,4-dioxazinane **6-i** with three stereocentres and eight possible stereoisomers. If the reaction occurs under kinetic control as the formation of 1,2,4-trioxanes, *cis*-fused 1,2,4-dioxazinanes would be formed, reducing the number of possible stereoisomers to four.

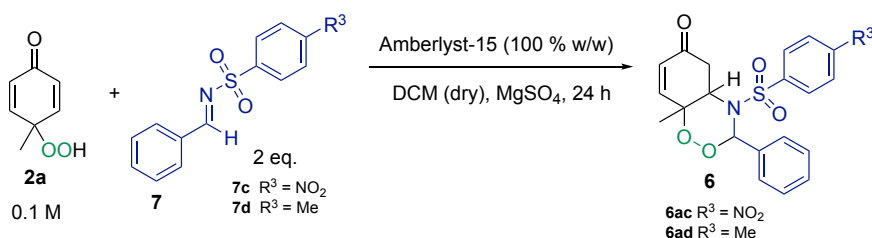


Scheme 81. Proposed mechanism for the racemic synthesis of 1,2,4-dioxazinanes **6-I** possessing three stereocentres and eight possible stereoisomers.

Attempted racemic synthesis of 1,2,4-dioxazinanes in batch

The cyclisation step between *p*-peroxyquinol **2a** and *N*-sulfonyl imines **7** was initially tested in batch under similar conditions based on Rubush's findings²⁴² (Scheme 76), as shown in Table 31.

Table 31. Summary of results for the synthesis of 1,2,4-dioxazinanes **6** from *p*-peroxyquinol **2a** and *N*-sulfonyl imines **7**.

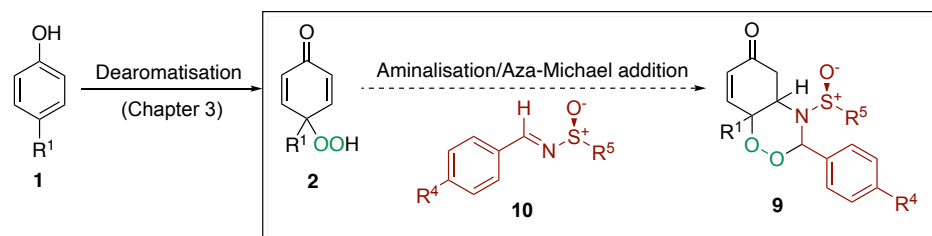


Entry	<i>N</i> -sulfonyl imine	1,2,4-dioxazinane	R ³	Temperature (°C)	Results from ¹ H NMR of the crude mixture
1	7c	6ac	NO ₂	r.t.	6ac not identified
2	7d	6ad	Me	reflux	6ad not identified

N-sulfonyl imine **7c** bearing an electron-deficient sulfonyl group was the first to be tested (Entry 1 – Table 31). ¹H NMR spectroscopy analysis of the crude mixture showed no signals for 1,2,4-dioxazinane **6ac**. However, the starting materials and hydrolysis of *N*-sulfonyl imine **7c** were observed in the same analysis. The reaction was then tested with *N*-sulfonyl imine **7d**, under reflux conditions (Entry 2 – Table 31). Analysis of the crude by ¹H NMR spectroscopy showed similar results: 1,2,4-dioxazinane **6ad** was not identified, and starting materials and hydrolysis of **7d** were observed.

6.3.3. Asymmetric synthesis of 1,2,4-dioxazinanes with *N*-sulfinyl imines

After the disappointing results obtained for the racemic synthesis of 1,2,4-dioxazinanes **6**, an asymmetric variant of this reaction was tested using *p*-peroxyquinols **2**, derived from the dearomatisation of *p*-substituted phenols **1**, and chiral *N*-sulfinyl imines **10** (Scheme 82).



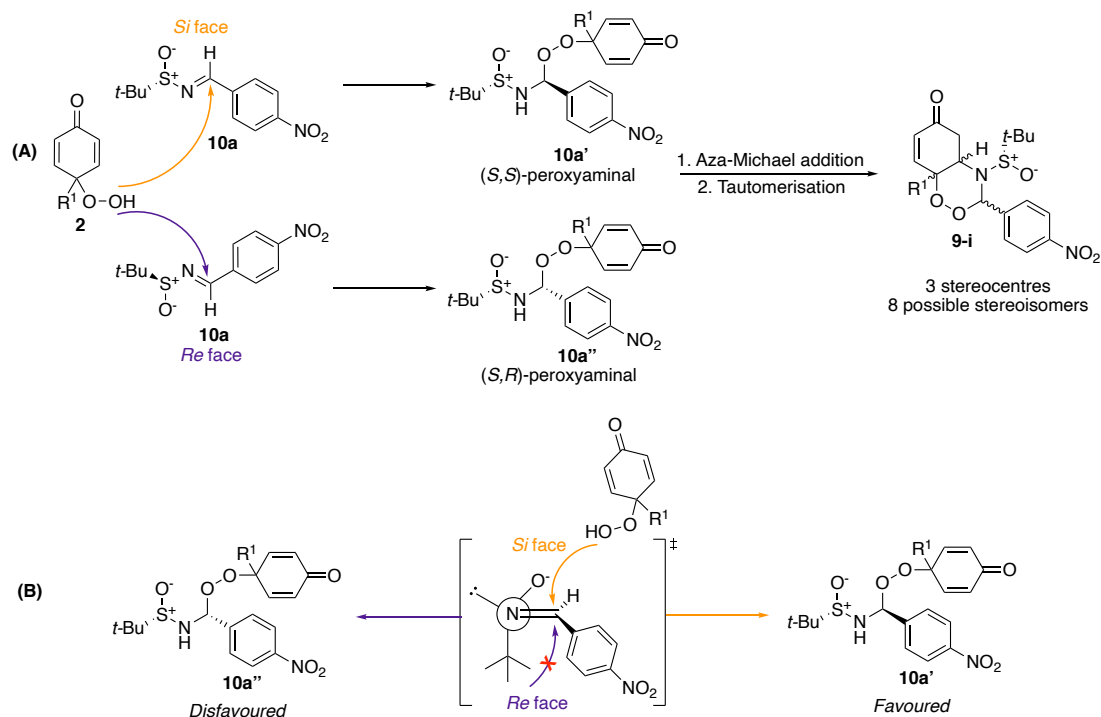
Scheme 82. Amination/Aza-Michael addition in the proposed asymmetric synthesis of 1,2,4-dioxazinanes **9**.

Proposed Reaction Mechanism

The reaction mechanism would be very similar to the racemic synthesis presented in Scheme 81. In this proposed asymmetric synthesis, the nucleophilic attack of *p*-peroxyquinol **2** could happen in either of the *Re* or *Si* faces of the *N*-sulfinyl imine **10a**, forming peroxyaminals **10a'** and **10a''**. Aza-Michael addition followed by tautomerisation would lead to 1,2,4-dioxazinane **9-i** with three stereocentres and eight possible stereoisomers (Scheme 83 - A). If the reaction is under kinetic control, only *cis*-fused 1,2,4-dioxazinanes are formed, and as it is for 1,2,4-trioxanes, the number of possible stereoisomers is reduced to four.

However, based on diastereofacial selectivity studies of *N*-sulfinyl imines,³⁴²⁻³⁴⁴ it was proposed that the nucleophilic attack of *p*-peroxyquinol **2** would be favoured on the *Si* face of *N*-sulfinyl imine **10a**, forming predominantly (*S,S*)-peroxyaminal **10a'**. This is because by using the open non-chelation controlled model, the attack on the *Re* face is disfavoured due to steric hindrance of the bulky *tert*-butyl group (Scheme 83 - B).

It is worth mentioning that the models to predict the stereochemical outcome of additions to *N*-sulfinyl imines are still under debate and stereoinduction is generally considered unpredictable.³⁴² This is due to the fact that other parameters such as solvent and chelation to metals can change the diastereofacial selectivity.



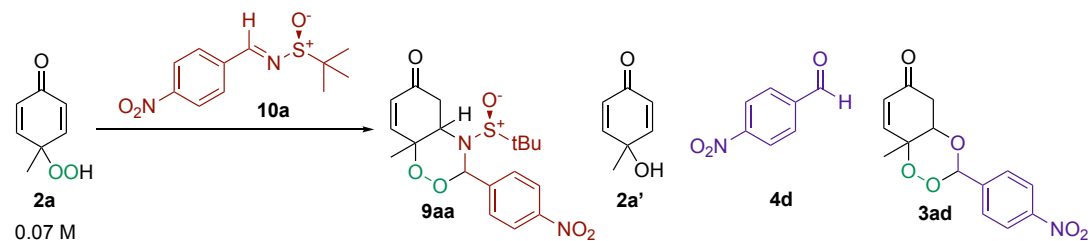
Scheme 83. (A) Proposed mechanism for the asymmetric synthesis of 1,2,4-dioxazine **9-i**. (B) Proposed open non-chelation model to predict the diastereofacial selectivity in the nucleophilic addition to *N*-sulfinyl imine **10a**, forming predominantly (*S,S*)-peroxyaminal **10a'**.

Chiral *N*-sulfinyl imines would be ideal reagents for the amination step as they form aminals enantioselectively, which are often challenging to prepare due to their inherent reversibility and racemisation.³⁴⁵ The sulfinyl group can be easily removed in mild conditions,³⁴⁶ enabling further functionalisation of the amine if necessary.

Attempted asymmetric synthesis of 1,2,4-dioxazines in batch

The synthesis of 1,2,4-dioxazines **9** was first attempted in batch, starting with *p*-peroxyquinol **2a** and *N*-sulfinyl imine **10a**. In this initial study, different catalysts, catalyst loadings, reaction times, and temperatures were screened (Table 32).

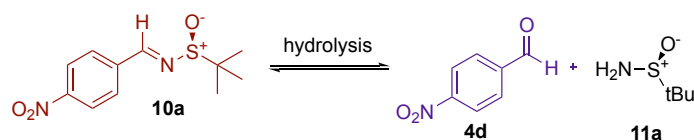
Table 32. Initial studies on the synthesis of 1,2,4-dioxazinanes **9aa** from *p*-peroxyquinol **2a** and *N*-sulfinyl imine **10a**.



Entry	Solvent	Catalyst	Catalyst loading	Temperature (°C)	Time (h)	NMR ratio 9aa: 2a	NMR ratio 2a': 2a	NMR ratio 4d: 10a	NMR ratio 3ad: 2a
1	CDCl ₃	-	-	r.t	24	0	No reaction		
		-	-	50		0	No reaction		
2	Benzene- <i>d</i> 6	-	-	75		0	1: 3.1	0	0
3	CDCl ₃	MsOH	0.15 eq.	50	24	0	No reaction		
4		Amberlyst-15	60% w/w	50	5	0	-	1: 7.1	1: 3.8
5			300% w/w			0	-	1: 1.5	1: 0.3

Initially, this reaction was carried out without catalyst at three temperatures (Entries 1 and 2 – Table 32). No reaction occurred up to 50 °C (Entry 1– Table 32), and the only product identified in the ^1H NMR spectroscopy at 75 °C was the reduced *p*-peroxyquinol **2a'**, due to a possible thermolysis of *p*-peroxyquinol **2a** (Entry 2 – Table 32).

Next, the addition of acid catalyst was tested (Entries 3 to 5 – Table 32). Methanesulfonic acid (MsOH) did not result in any reaction at 50 °C after 24 h (Entry 3 – Table 32). Amberlyst-15 was then screened at different catalyst loadings (Entries 4 and 5 – Table 32). In both reactions, hydrolysis of *N*-sulfinyl imine **10a** (Scheme 84) and a cyclisation product were observed.



Scheme 84. Hydrolysis of the *N*-sulfinyl imine **10a**.

The XRD analysis (Figure 50), as well as ^1H and ^{13}C NMR spectroscopy spectra of the cyclisation product matched with 1,2,4-trioxane **3ad** (synthesised in batch) instead of the expected 1,2,4-dioxazinane **9aa'** (Scheme 85). It was rationalised that 1,2,4-dioxazinane **3ad** was not formed because aldehyde **4d** has a carbonyl that is more electrophilic and, thus, more reactive towards the nucleophilic addition of *p*-peroxyquinol **2a**, relative to *N*-sulfinyl imine **10a**. Increased formation of 1,2,4-trioxane **3ad** over time shifts the hydrolysis equilibrium towards the aldehyde **4d**, driving this cyclisation further. Finally, the increase of catalyst loading resulted in the formation of more 1,2,4-trioxane **3ad**, and consequently more hydrolysis of *N*-sulfinyl imine **10a** (cf Entries 4 and 5 – Table 32).

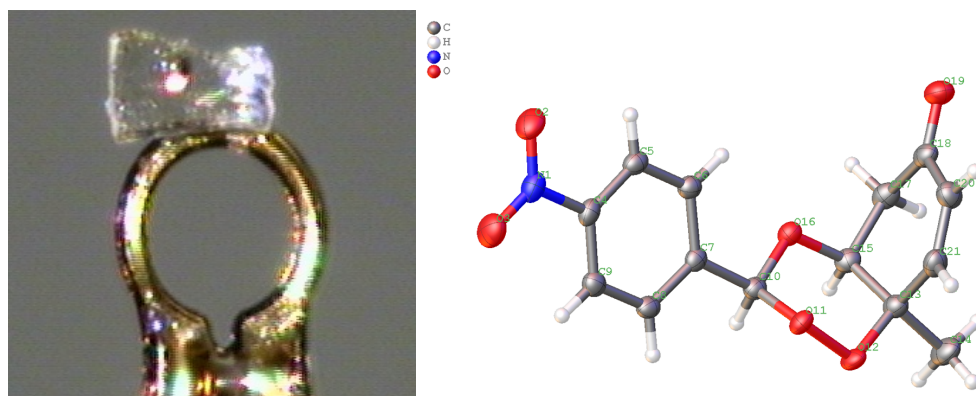
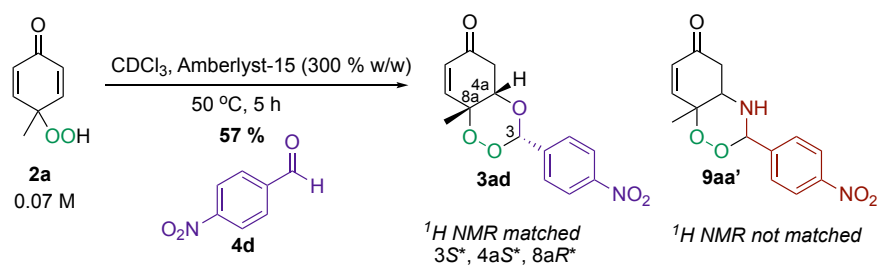


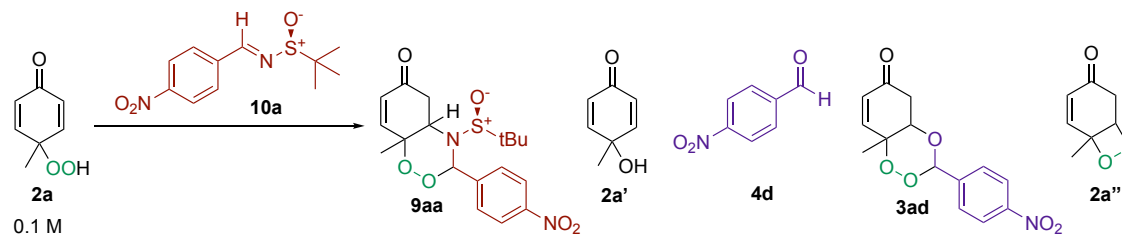
Figure 50. Left: picture of the analysed crystal of **3ad**; Right: XRD structure for **3ad** synthesised by B. Abreu and analysed by Dr. S. Argent.



Scheme 85. Cyclisation product identified to be 1,2,4-trioxane **3ad** instead of 1,2,4-dioxazinane **9aa'**. The structure was also confirmed by XRD analysis.

Following the challenges highlighted by initial studies, another set of experiments was designed using biphenyl as an internal standard for ¹H NMR spectroscopy quantification (Table 33).

Table 33. Summary of results for the asymmetric synthesis of 1,2,4-dioxazinanes **9aa** from *p*-peroxyquinol **2a** and *N*-sulfinyl imine **10a**.



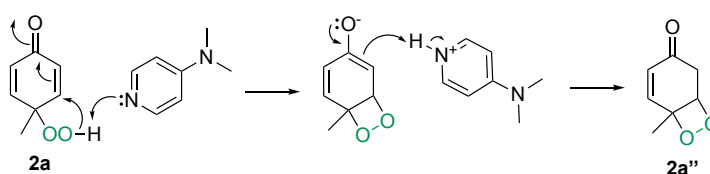
Entry	Solvent	Catalyst	Catalyst Loading	Temperature (°C)	Time (h)	NMR conversion 2a (%)	NMR yield 2a' (%)	NMR yield 4d (%)	NMR yield 3ad (%)	NMR yield 2a'' (%)
1	Dry DCM	Amberlyst-15	300% w/w	40	24	-	0	22	10	0
2^a				r.t.	24	-	0	4	0	0
3^b				r.t.	24	-	0	17	35	0
4				Ph ₂ PO ₂ H	r.t.	24	-	0	0	0
5	CDCl ₃	DMAP	0.15 eq.	r.t.	4	22	22	0	0	0
				r.t.	24	35	34	0	0	0
				r.t.	48	37	36	0	0	0
6				40	48	56	44	0	0	0
7^c				r.t.	72	92	27	0	0	22
8				DABCO	r.t.	24	51	23	0	0

¹H NMR spectroscopy conversions and yields were obtained using 0.05 eq. biphenyl as the internal standard. Reactions in which *p*-peroxyquinol **2a** decomposed or did not have a clear signal on ¹H NMR spectroscopy due to overlap with impurities, could not have their conversion calculated and are represented by -. ^a Addition of MgSO₄; ^b 2 eq. of *N*-sulfinyl imine **10a**; ^c The reaction was performed without the addition of *N*-sulfinyl imine **10a**. The desired product **9aa** was not included in the table as it was unable to be synthesised in these conditions.

Initially, conditions for the aza-Michael addition similar to those described in Rubush's dissertation (Scheme 76) were tested (Entries 1 to 3 – Table 33). In the first experiment, only hydrolysis of the *N*-sulfinyl imine **10a** into aldehyde **4d**, along with the formation of 1,2,4-trioxane **3ad** were observed (Entry 1 – Table 33). To suppress hydrolysis, the reaction was repeated at room temperature with the addition of MgSO₄ as a water scavenger (Entry 2 – Table 33). Although hydrolysis was partially suppressed, 1,2,4-dioxazinane **9aa** was not formed. As the 1,2-addition of *p*-peroxyquinol **2a** is an equilibrium reaction, it was then investigated the addition of 2 equivalents of *N*-sulfinyl imine **10a** at room temperature to favour the formation of the hemiaminal and subsequent cyclisation (Entry 3 – Table 33). However, not only **10a** was hydrolysed but the formation of 1,2,4-trioxane **3ad** increased.

An alternative acid catalyst Ph₂PO₂H was then tested (Entry 4 – Table 33), as this compound has been reported to catalyse similar reactions such as acetalisations,²⁴¹ but no reaction occurred.

Finally, based on Carreño's publication on amination catalysed by dimethylaminopyridine (DMAP) and 4-diazabicyclo[2.2.2]octane (DABCO),³⁰⁸ these two catalysts were used in the last experiments (Entries 5 to 8 – Table 33). The addition of DMAP at room temperature led to the reduction of the *p*-peroxyquinol **2a** into **2a'**, which increased with reaction time (Entry 5 – Table 33) and temperature (Entry 6 – Table 33). To understand if the reduction was occurring due to DMAP or the *N*-sulfinyl imine **10a**, a reaction was performed without **10a** (Entry 7 – Table 33). Not only was the *p*-peroxyquinol **2a** reduced to the *p*-quinol **2a'**, but also an endoperoxide species **2a''** was identified, likely due to an intramolecular Michael addition on the *p*-peroxyquinol **2a** (Scheme 86).



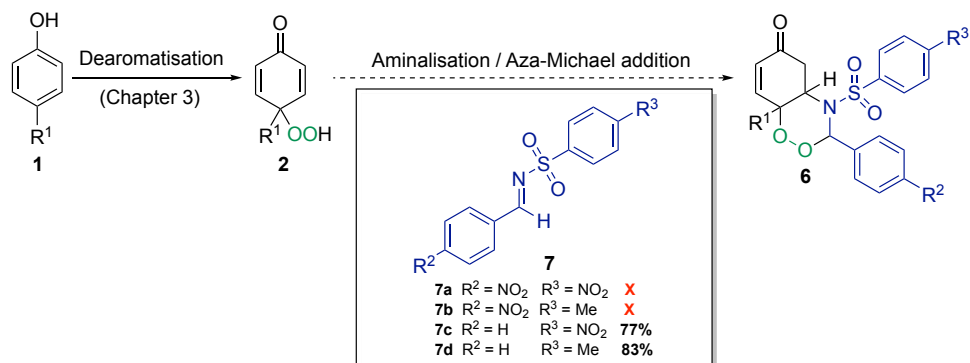
Scheme 86. Proposed mechanism for the intramolecular Michael addition on *p*-peroxyquinol **2a**.

To avoid reduction of *p*-peroxyquinol **2a**, DABCO was used (Entry 8 – Table 33) as it is less basic than DMAP.³⁴⁷ However, only *p*-quinol **2a'** was observed on ¹H NMR spectroscopy analysis.

6.4. Conclusions

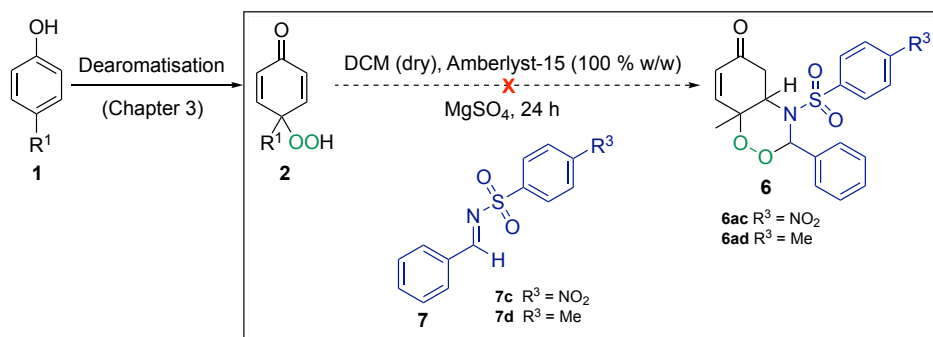
Racemic synthesis of 1,2,4-dioxazinanes with N-sulfonyl imines

Following the strategy proposed for the synthesis of 1,2,4-dioxazinanes from *p*-substituted phenols, the racemic version was the first one to be explored. Different *N*-sulfonyl imines were synthesised to be further used in the investigation of the amination/Aza-Michael addition, which is the second step of the reaction. Although two *N*-sulfonyl imines could not be obtained either because of decomposition (**7a**) or purification issues (**7b**), the other two *N*-sulfonyl imines (**7c** and **7d**) were produced in high isolated yields (Scheme 87).



Scheme 87. Summary of the synthesis of *N*-sulfonyl imines **7**. **X** represents that the product was not formed or could not be purified.

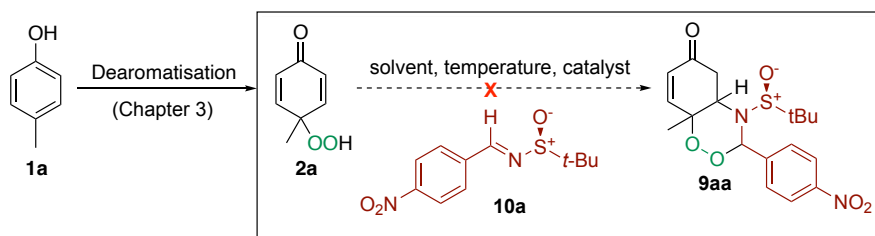
Two *N*-sulfonyl imines (**7c** and **7d**) were tested for the racemic synthesis of 1,2,4-dioxazinanes **6** (Scheme 88), under similar conditions reported by Rubush.²⁴² However, no product was formed in both reactions.



Scheme 88. Summary of the racemic synthesis of 1,2,4-dioxazinanes **6** with *N*-sulfonyl imines **7**. **X** represents that the product could not be synthesised.

Asymmetric synthesis of 1,2,4-dioxazinanes with *N*-sulfinyl imines

Similarly to the previous strategy for the synthesis of 1,2,4-dioxazinanes **6**, the second step of the proposed asymmetric route was first investigated in batch (Scheme 89). The cyclisation was carried out using *N*-sulfinyl imine **10a**.



Scheme 89. Summary of the asymmetric synthesis of 1,2,4-dioxazine **9aa**. **X** represents that the product could not be synthesised.

In preliminary studies, both temperature and addition of catalyst were screened. Non-catalysed reactions resulted in no conversion of starting material and increase in temperature caused reduction of *p*-peroxyquinol **2a**. Only starting materials were observed with the addition of MsOH as an acid catalyst. When the reaction was carried out with Amberlyst-15, hydrolysis of *N*-sulfinyl imine **10a** was identified, as well as the formation of 1,2,4-trioxane **3ad**.

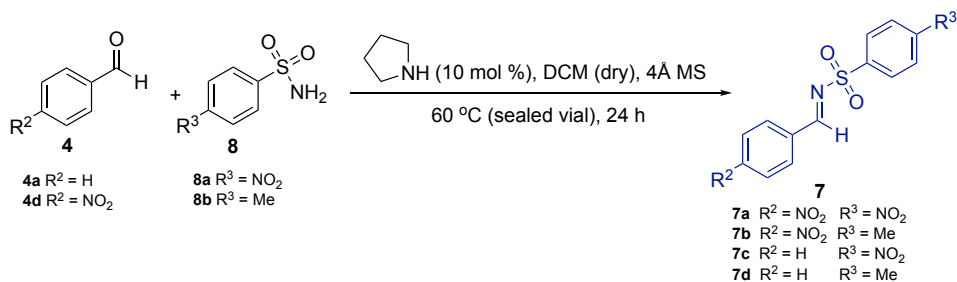
The reaction was also carried out in similar conditions to the ones reported by Rubush.²⁴² Temperature, addition of MgSO₄, and equivalents of *N*-sulfinyl imine **10a** were screened with two acid catalysts (Amberlyst-15 and diphenylphosphinic acid), which resulted in either hydrolysis of **10a** and formation of 1,2,4-trioxane **3ad** (Amberlyst-15), or no reaction (Ph₂PO₂H). It is possible that hydrolysis was caused by adsorbed water present in Amberlyst-15.

Regarding the use of base catalysts, DMAP and DABCO were tested at different temperatures, but only reduction of *p*-peroxyquinol **2a** was identified in both cases. An endoperoxide species **2a''** was also identified in the ¹H NMR spectroscopy analysis when the reaction with DMAP was carried out without *N*-sulfinyl imine **10a**.

6.5. Experimental procedures

Data collected for known compounds is consistent with the literature.

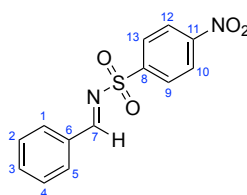
6.5.1. Synthesis of *N*-sulfonyl imines



General procedure: In a microwave sealed vial, sulfonamide **8** (1.0 eq, 1.40 mmol) was added in dry DCM (4 mL), followed by the addition of 4Å molecular sieves (1.40 g), aldehyde **4** (1.0 eq, 1.40 mmol) and pyrrolidine (10 mol%, 0.140 mmol, 12.0 μL). The reaction mixture was then stirred at 60 °C for 24 h, resulting in a yellow solution. The solution was filtered through a short pad of Celite and concentrated under reduced pressure.

- **Reaction 1 (R² = NO₂ and R³ = NO₂):** *p*-nitrobenzenesulfonamide **8a** (283 mg) and *p*-nitrobenzaldehyde **4d** (212 mg). ¹H NMR spectroscopy showed a complex mixture with no signals of the product **7a**.
- **Reaction 2 (R² = NO₂ and R³ = CH₃):** *p*-toluenesulfonamide **8b** (240 mg) and *p*-nitrobenzaldehyde **4d** (212 mg). ¹H NMR spectroscopy showed a ratio **7b**: **8b** = 1: 0.3 (77%). Purification of product **7b** was attempted by recrystallisation, but with no success. Flash column chromatography purification (EtOAc/Hexane 1:3) resulted in full hydrolysis of **7b** over silica.
- **Reaction 3 (R² = H and R³ = NO₂):** *p*-nitrobenzenesulfonamide **8a** (283 mg) and benzaldehyde **4a** (1.2 eq, 1.7 mmol, 0.2 mL). ¹H NMR spectroscopy showed a ratio **7c**: **8a** = 1: 0.1 (91%). The product **7c** was obtained as a yellow powder (1.08 mmol, 314 mg, **77%**) after recrystallisation from pentane.
- **Reaction 4 (R² = H and R³ = CH₃):** *p*-toluenesulfonamide **8b** (240 mg) and benzaldehyde **4a** (1.2 eq, 1.7 mmol, 0.2 mL). ¹H NMR spectroscopy showed a ratio **7d**: **8b** = 1: 0.2 (83%). The product **7d** was obtained as a white solid (1.16 mmol, 300 mg, **83%**) after recrystallisation from diethyl ether.

(*E*)-*N*-Benzylidene-4-nitrobenzenesulfonamide **7c**³⁴⁸

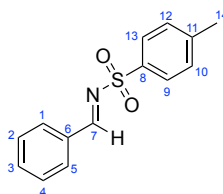


¹H NMR (400 MHz, Chloroform-*d*): δ 9.13 (s, 1H, **7**), 8.39 (d, *J* = 9.0 Hz, 2H, **10/12**), 8.22 (d, *J* = 9.0 Hz, 2H, **9/13**), 7.96 (d, *J* = 6.9 Hz, 2H, **1/5**), 7.68 (t, *J* = 7.5 Hz, 1H, **3**), 7.53 (appt, *J* = 7.7 Hz, 2H, **2/4**).

¹³C NMR (101 MHz, Chloroform-*d*): δ 172.5 (**7**), 150.8 (**8**), 144.3 (**11**), 135.9 (**3**), 132.1 (**6**), 131.8 (**1/5**), 129.5 (**9/13**), 129.5 (**2/4**), 124.5 (**10/12**).

HRMS (ESI) *m/z* calcd [C₁₃H₁₁N₂O₄S]⁺ ([M + H]⁺): 291.0434, found 291.0443.

(*E*)-*N*-Benzylidene-4-methylbenzenesulfonamide **7d**³⁴⁹



¹H NMR (400 MHz, Chloroform-*d*): δ 9.03 (s, 1H, **7**), 7.93 (d, *J* = 7.1 Hz, 2H, **1/5**), 7.89 (d, *J* = 8.3 Hz, 2H, **9/13**), 7.62 (t, *J* = 7.4 Hz, 1H, **3**), 7.49 (appt, *J* = 7.7 Hz, 2H, **2/4**), 7.35 (d, *J* = 8.3 Hz, 2H, **10/12**), 2.44 (s, 3H, **14**).

¹³C NMR (101 MHz, Chloroform-*d*): δ 170.1 (**7**), 144.6 (**11**), 135.2 (**8**), 134.9 (**3**), 132.4 (**6**), 131.3 (**1/5**), 129.8 (**10/12**), 129.2 (**2/4**), 128.1 (**9/13**), 21.7 (**14**).

HRMS (ESI) *m/z* calcd [C₁₄H₁₄NO₂S]⁺ ([M + H]⁺): 260.0740, found 260.0740.

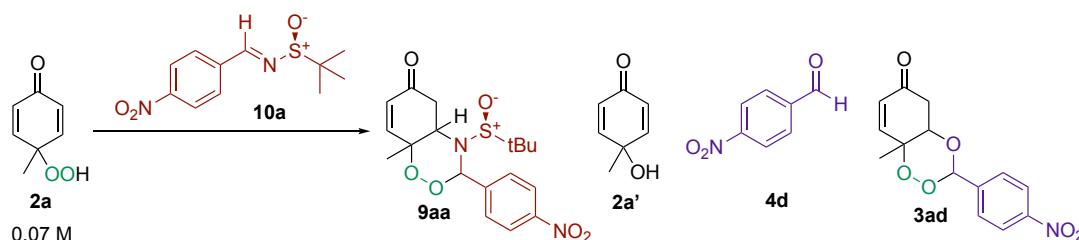
6.5.2. Synthesis of 1,2,4-dioxazinanes **6** from *p*-peroxyquinol **2a** and *N*-sulfonyl imines **7**



General procedure: *N*-sulfonyl imine **7** (2.0 eq, 0.403 mmol), Amberlyst-15 (100% w/w, 28.1 mg), and MgSO₄ (100 mg) were added to a 2 mL solution of *p*-peroxyquinol **2a** (1.0 eq, 0.201 mmol, 28.1 mg, 0.1 M) in dry DCM under inert atmosphere. The solution was stirred for 24 h and ¹H NMR spectroscopy was recorded from a 0.1 mL sample from the reaction mixture after filtration to remove MgSO₄, which was then concentrated by nitrogen blow down for 3 min.

- **Reaction 1 (R³ = NO₂):** (*E*)-*N*-benzylidene-4-nitrobenzenesulfonamide **7c** (116 mg) at room temperature. Results from crude ¹H NMR spectroscopy = 1,2,4-dioxazinane **6ac** was not identified.
- **Reaction 1 (R³ = CH₃):** (*E*)-*N*-benzylidene-4-methylbenzenesulfonamide **7d** (104 mg) under reflux. Results from crude ¹H NMR spectroscopy = 1,2,4-dioxazinane **6ad** was not identified.

6.5.3. Synthesis of 1,2,4-dioxazinanes **9** from *p*-peroxyquinol **2a** and *N*-sulfinyl imine **10a** (initial studies)



General procedure: *N*-[*tert*-butyl-sulfinyl]-*p*-nitrobenzaldimine **10a** was added to a 0.5 mL solution of *p*-peroxyquinol **2a** in CDCl₃. The solution was stirred, resulting in a yellow reaction mixture. ¹H NMR spectroscopy was recorded from a 0.5 mL sample taken directly from the reaction mixture.

SET 1: No addition of catalyst

- **Reaction 1, Test 1:** **2a** (1.0 eq, 36.4 μmol, 5.10 mg) and **10a** (1.1 eq, 40.0 μmol, 10.2 mg), at room temperature. After 24 h of reaction, only starting materials were observed in the ¹H NMR spectroscopy.
 - **Test 2:** The reaction mixture was then heated up to 50 °C. After 24 h of reaction, only starting materials were observed in the ¹H NMR spectroscopy.
- **Reaction 2:** **2a** (1.0 eq, 36.4 μmol, 5.10 mg) and **10a** (1.1 eq, 40.0 μmol, 10.2 mg), at 75 °C in benzene-*d*₆. After 24 h of reaction, ¹H NMR spectroscopy ratio **2a'**: **2a** was 1: 3.1.

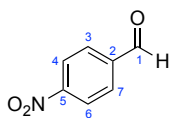
SET 2: acid catalyst MsOH

- **Reaction 3:** **2a** (1.0 eq, 36.4 μmol, 5.10 mg), **10a** (1.1 eq, 40.0 μmol, 10.2 mg) and MsOH (0.15 eq, 5.46 μmol, 0.5 mg), at 50 °C. After 24 h of reaction, only starting materials were observed in the ¹H NMR spectroscopy.

SET 3: acid catalyst Amberlyst-15

- **Reaction 4:** **2a** (1.0 eq, 36.4 μmol, 5.10 mg), **10a** (1.1 eq, 40.0 μmol, 10.2 mg) and Amberlyst-15 (60% w/w, 3.10 mg) at 50 °C. After 5 h of reaction, ¹H NMR spectroscopy ratio **4d**: **10a** was 1: 7.1 and **3ad**: **2a** was 1: 3.8.
- **Reaction 5:** **2a** (1.0 eq, 36.4 μmol, 5.10 mg), **10a** (1.1 eq, 40.0 μmol, 10.2 mg) and Amberlyst-15 (300% w/w, 15.3 mg) at 50 °C. After 5 h of reaction, ¹H NMR spectroscopy ratio **4d**: **10a** was 1: 1.5 and **3ad**: **2a** was 1: 0.3.

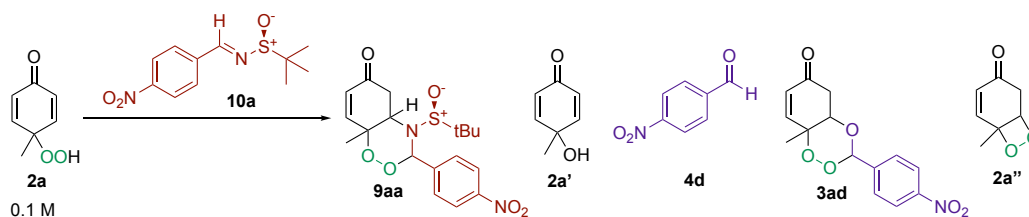
4-Nitrobenzaldehyde **4d**³⁵⁰



¹H NMR (400 MHz, Chloroform-*d*): δ 10.16 (s, 1H, **1**), 8.40 (d, $J = 8.7$ Hz, 2H, **4/6**), 8.08 (d, $J = 8.7$ Hz, 2H, **3/7**).

¹³C NMR (101 MHz, Chloroform-*d*): δ 190.4 (**1**), 151.3 (**5**), 140.2 (**2**), 130.6 (**3/7**), 124.5 (**4/6**).

6.5.4. Synthesis of 1,2,4-dioxazinanes **9** from *p*-peroxyquinol **2a** and *N*-sulfinyl imine **10a**



General procedure: *N*-[*tert*-butyl-sulfinyl]-*p*-nitrobenzaldehyde imine **10a** (1.0 eq, 0.201 mmol, 51.2 mg), catalyst (0.15 eq, 30.2 μ mol) and biphenyl (0.050 eq, 10.1 μ mol, 1.50 mg) were added to a 2 mL solution of *p*-peroxyquinol **2a** (1.0 eq, 0.200 mmol, 28.0 mg) in dry DCM under inert atmosphere, unless stated otherwise. The solution was stirred and ^1H NMR spectroscopy was recorded from a 0.1 mL sample from the reaction mixture, which was then concentrated by nitrogen blow-down for 3 min.

SET 1: acid catalyst Amberlyst-15

- **Reaction 1 (40 °C):** (300% w/w, 84.0 mg) and 40 °C. Results from ^1H NMR spectroscopy = 10% yield of **3ad**, and 22% yield of **4d**.
- **Reaction 2 (20 °C, MgSO_4):** Amberlyst-15 (300% w/w, 84.0 mg), MgSO_4 (200% w/w, 102 mg) at room temperature. Results from ^1H NMR spectroscopy = 4% yield of **4d**.
- **Reaction 3 (20 °C, 2 eq. *N*-sulfinyl imine **10a**):** Amberlyst-15 (300% w/w, 84.0 mg), **10a** (2.0 eq, 0.400 mmol, 102 mg), and room temperature. Results from ^1H NMR spectroscopy = 35% yield of **3ad**, and 17% yield of **4d**.

SET 2: acid catalyst $\text{Ph}_2\text{PO}_2\text{H}$

- **Reaction 4 (20 °C):** Diphenylphosphinic acid (7.00 mg) and room temperature. Results from ^1H NMR spectroscopy = no reaction occurred. Only signals from the starting material were observed.

SET 3: base catalyst DMAP

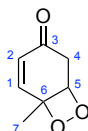
- **Reaction 5, Test 1:** 0.6 mL solution of **2a** (1.0 eq, 0.301 mmol, 42.1 mg), **10a** (1.0 eq, 0.300 mmol, 76.3 mg), DMAP (0.15 eq, 45.0 μ mol, 5.50 mg) and biphenyl (0.050 eq, 14.9 μ mol, 2.30 mg) in CDCl_3 , at room temperature. After 4 h of reaction, ^1H NMR spectroscopy 22% conversion of **2a**, and 22% yield of **2a'**.
 - **Test 2:** After 24 h of reaction, ^1H NMR spectroscopy 35% conversion of **2a**, and 34% yield of **2a'**.

- **Test 3:** After 48 h of reaction, ^1H NMR spectroscopy 37% conversion of **2a**, and 36% yield of **2a'**.
- **Reaction 6:** Same quantities as Reaction 5, but at 40 °C. After 48 h of reaction, ^1H NMR spectroscopy 56% conversion of **2a**, and 44% yield of **2a'**.
- **Reaction 7:** Same quantities as Reaction 5, but *N*-sulfinyl imine **10a** was not added to this reaction. After 72 h of reaction, ^1H NMR spectroscopy 92% conversion of **2a**, 27% yield of **2a'**, and 22% yield of **2a''**.

SET 4: base catalyst DABCO

- **Reaction 8 (r.t.):** 1,4-diazabicyclo[2.2.2]octane (3.00 mg) in CDCl_3 at room temperature. Results from ^1H NMR spectroscopy = 51% conversion of **2a**, 23% yield of **2a'**.

6-Methyl-7,8-dioxabicyclo[4.2.0]oct-4-en-3-one **2a''** (novel compound)

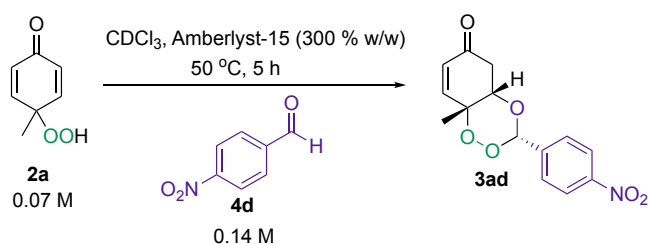


^1H NMR (400 MHz, Chloroform-*d*): δ 6.75 (dd, $J = 10.3, 2.4$ Hz, 1H, **1**), 6.02 (dd, $J = 10.3, 1.1$ Hz, 1H, **2**), 4.47 (m, 1H, **5**), 3.01 (ddd, $J = 17.8, 2.6, 1.1$ Hz, 1H, **4**), 2.70 (dd, $J = 17.8, 3.4$ Hz, 1H, **4'**), 1.63 (s, 3H, **7**).

^{13}C NMR (101 MHz, Chloroform-*d*): δ 194.0 (**3**), 149.3 (**1**), 127.7 (**2**), 81.0 (**5**), 78.5 (**6**), 37.9 (**4**), 21.8 (**7**).

Further analysis should be carried out to confirm the structure above, such as IR spectroscopy and HRMS.

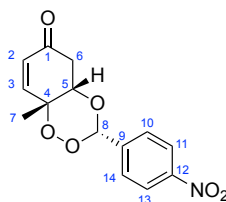
6.5.5. Synthesis of 1,2,4-trioxane **3ad**



General procedure: In a 10 mL solution of *p*-peroxyquinol **2a** (1.0 eq, 0.714 mmol, 100 mg) in chloroform, 4-nitrobenzaldehyde **4d** (2.0 eq, 1.45 mmol, 219 mg) and Amberlyst-15 (300% w/w, 300 mg) were added at $40\text{ }^\circ\text{C}$. The solution was stirred for 5 h, resulting in a brown reaction mixture. Amberlyst was filtered out of the solution, and the filtrate was concentrated under vacuum.

Results: The product was purified by flash column chromatography column and eluted with a gradient of 0-30% EtOAc/hexane to give **3ad** (0.412 mmol, 120 mg, 58%) as a yellow crystalline material.

(3*S*,4*aS*,8*aR*)-8*a*-Methyl-3-(4-nitrophenyl)-4*a*,8*a*-dihydrobenzo[*e*][1,2,4]trioxin-6(5*H*)-one **3ad**²³²



^1H NMR (400 MHz, Chloroform-*d*): δ 8.21 (d, $J = 8.8$ Hz, 2H, **11/13**), 7.59 (d, $J = 8.8$ Hz, 2H, **10/14**), 6.92 (dd, $J = 10.4, 2.9$ Hz, 1H, **3**), 6.30 (s, 1H, **8**), 6.17 (dd, $J = 10.4, 1.0$ Hz, 1H, **2**), 4.45 (q, $J = 2.9$ Hz, 1H, **5**), 2.87 (ddd, $J = 17.7, 2.9, 1.0$ Hz, 1H, **6**), 2.82 (dd, $J = 17.7, 2.9$ Hz, 1H, **6'**), 1.46 (s, 3H, **7**).

^{13}C NMR (101 MHz, Chloroform-*d*): δ 194.5 (**1**), 150.5 (**3**), 149.1 (**12**), 139.8 (**9**), 130.1 (**2**), 128.3 (**10/14**), 123.8 (**11/13**), 102.2 (**8**), 78.5 (**4**), 77.2 (**5**), 41.0 (**6**), 20.7 (**7**).

HRMS (ESI) m/z calcd $[\text{C}_{14}\text{H}_{13}\text{N}_1\text{O}_6\text{Na}]^+$ ($[\text{M} + \text{Na}]^+$): 314.0635, found 314.0628.

^1H and ^{13}C NMR spectroscopy data was found in only one publication in the literature (Ref 233), but the chemical shifts are not consistent with the data reported in this Thesis. However, the ^1H NMR spectroscopy values reported don't match with the structure, no XRD analysis was given, and name of the compound was incorrect.

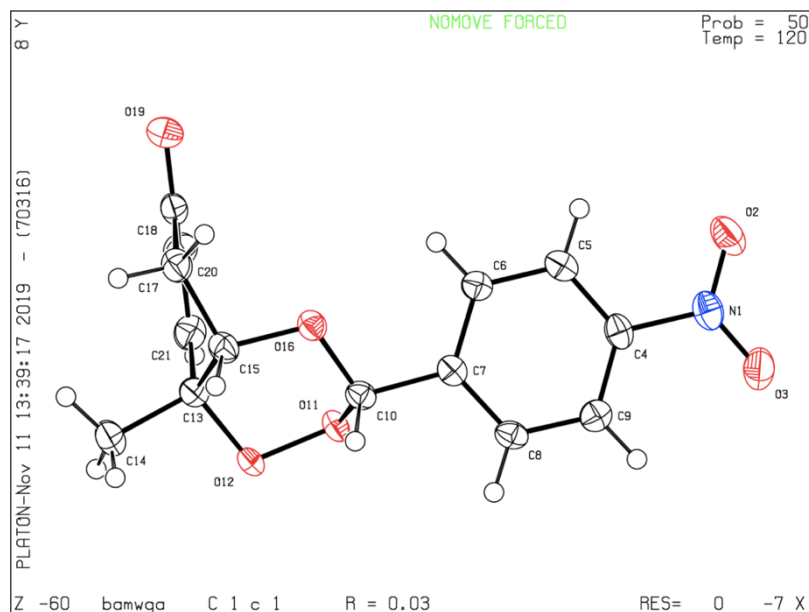
6.6. Appendix

Experimental procedure

Single crystals of $C_{14}H_{13}NO_6$ **3ad** were submitted to Dr. S. Argent for XRD analysis at the University of Nottingham. A suitable crystal was put in fomblin film on a micromount on a SuperNova Atlas S2 diffractometer. The temperature was kept at 120(2) K. Using the software Olex2,¹⁵⁶ the structure was solved with the ShelXTstructure solution program using Intrinsic Phasing¹⁵⁷ and refined with the ShelXL refinement package using Least Squares minimisation.¹⁵⁸

Crystal data and structure refinement

Empirical formula	$C_{14}H_{13}NO_6$	Index ranges	$-8 \leq h \leq 8, -31 \leq k \leq 31,$ $-8 \leq l \leq 8$
Formula weight	291.25	Reflections collected	9834
Temperature/K	120(2)	Independent reflections	2358 [$R_{int} = 0.0203,$ $R_{sigma} = 0.0139$]
Crystal system	monoclinic	Data/restraints/parameters	2358/2/191
Space group	Cc	Goodness-of-fit on F^2	1.045
a/Å	7.2011(2)	Final R indexes [$I \geq 2\sigma(I)$]	$R_1 = 0.0259, wR_2 = 0.0680$
b/Å	25.7849(8)	Final R indexes [all data]	$R_1 = 0.0262, wR_2 = 0.0684$
c/Å	7.1727(3)	Largest diff. peak/hole / $e \text{ Å}^{-3}$	0.15/-0.18
$\alpha/^\circ$	90	Flack parameter	0.05(5)
$\beta/^\circ$	95.776(3)		
$\gamma/^\circ$	90		
Volume/Å³	1325.06(8)		
Z	4		
ρ_{calc}/cm^3	1.460		
μ/mm^{-1}	0.985		
F (000)	608.0		
Crystal size/mm³	0.222 × 0.123 × 0.033		
Radiation	CuK α ($\lambda = 1.54184$)		
2θ range for data collection/°	6.856 to 146.846		



Crystal data: $C_{14}H_{13}NO_6$ ($M = 291.25$ g/mol): monoclinic, space group Cc (no. 9), $a = 7.2011(2)$ Å, $b = 25.7849(8)$ Å, $c = 7.1727(3)$ Å, $\beta = 95.776(3)^\circ$, $V = 1325.06(8)$ Å³, $Z = 4$, $T = 120(2)$ K, $\mu(\text{CuK}\alpha) = 0.985$ mm⁻¹, $D_{\text{calc}} = 1.460$ g/cm³, 9834 reflections measured ($6.856^\circ \leq 2\theta \leq 146.846^\circ$), 2358 unique ($R_{\text{int}} = 0.0203$, $R_{\text{sigma}} = 0.0139$) which were used in all calculations. The final R_1 was 0.0259 ($I > 2\sigma(I)$) and wR_2 was 0.0684.

Refinement model description

Number of restraints: 2; number of constraints: unknown. Details:

1. Fixed Uiso. At 1.2 times of All C(H) groups, All C(H,H) groups; At 1.5 times of: All C(H,H,H) groups
- 2.a. Ternary CH refined with riding coordinates: C10(H10), C15(H15)
- 2.b. Secondary CH2 refined with riding coordinates: C17(H17A,H17B)
- 2.c. Aromatic/amide H refined with riding coordinates: C5(H5), C6(H6), C8(H8), C9(H9), C20(H20), C21(H21)
- 2.d. Idealised Me refined as rotating group: C14(H14A,H14B,H14C)

Fractional Atomic Coordinates ($\times 10^4$) and Equivalent Isotropic Displacement Parameters ($\text{\AA}^2 \times 10^3$) for 3ad. U_{eq} is defined as 1/3 of the trace of the orthogonalised U_{ij} tensor.

Atom	x	y	z	U(eq)
N1	8654(2)	4015.5(7)	5239(2)	29.9(4)
O2	10217(2)	4127.7(6)	4828(2)	38.2(4)
O3	8107(2)	3568.1(6)	5372(3)	42.3(4)
C4	7368(3)	4439.1(7)	5591(3)	23.9(4)
C5	7997(2)	4946.5(7)	5485(3)	24.0(4)
C6	6760(2)	5345.2(7)	5765(3)	22.9(3)
C7	4943(2)	5227.6(7)	6147(2)	20.7(3)
C8	4368(2)	4715.2(7)	6268(2)	23.0(4)
C9	5584(3)	4313.2(7)	5990(3)	24.8(4)
C10	3537(2)	5647.3(7)	6407(3)	21.9(4)
O11	2266.2(16)	5632.9(5)	4745.9(18)	22.7(3)
O12	743.1(15)	5988.3(5)	5112(2)	25.9(3)
C13	1500(2)	6509.6(7)	5203(3)	24.9(4)
C14	-194(3)	6828.3(8)	5603(4)	36.3(5)
C15	3076(3)	6540.0(7)	6798(3)	24.5(4)
O16	4411.9(16)	6130.6(5)	6596.1(17)	23.0(3)
C17	4157(3)	7044.6(7)	6759(3)	27.5(4)
C18	4755(2)	7173.4(7)	4852(3)	26.0(4)
O19	6092.8(18)	7452.7(6)	4677(2)	34.4(3)
C20	3625(3)	6960.8(7)	3204(3)	28.9(4)
C21	2157(3)	6657.3(7)	3361(3)	27.8(4)

Anisotropic Displacement Parameters ($\text{\AA}^2 \times 10^3$) for 3ad. The Anisotropic displacement factor exponent takes the form: $-2\pi^2[h^2a^*2U_{11}+2hka^*b^*U_{12}+\dots]$.

Atom	U_{11}	U_{22}	U_{33}	U_{23}	U_{13}	U_{12}
N1	29.8(8)	32.7(8)	26.8(9)	0.5(7)	0.3(7)	9.1(6)
O2	30.6(7)	46.0(8)	39.7(9)	4.2(7)	12.1(6)	12.5(6)
O3	40.0(8)	28.6(7)	57.5(11)	-2.2(7)	1.0(7)	8.2(6)
C4	24.3(8)	27.9(8)	19.1(9)	0.9(7)	-0.1(7)	7.6(7)
C5	19.7(7)	32.6(9)	19.6(9)	1.1(7)	1.4(7)	1.2(6)
C6	21.2(8)	26.5(8)	20.9(9)	1.2(6)	1.4(6)	-0.5(7)
C7	20.8(8)	26.0(8)	14.9(8)	1.5(6)	0.7(6)	2.5(6)
C8	20.3(8)	29.6(9)	19.2(9)	3.3(7)	2.7(6)	-1.0(6)
C9	26.2(8)	26.3(8)	21.4(10)	2.0(7)	0.2(7)	-0.2(7)
C10	20.0(8)	25.8(8)	20.0(9)	1.7(6)	2.5(7)	0.4(6)
O11	17.3(5)	25.6(6)	25.0(7)	-2.3(5)	0.6(5)	4.9(4)
O12	14.6(5)	24.2(6)	39.1(8)	-0.8(6)	4.3(5)	3.1(4)
C13	21.0(8)	23.3(8)	30.5(10)	-1.6(7)	2.9(7)	0.7(6)
C14	23.9(9)	31.9(10)	53.0(14)	-4.5(9)	4.3(9)	7.0(7)
C15	22.7(8)	26.7(8)	24.6(10)	-3.2(7)	4.9(7)	1.7(7)
O16	20.3(6)	24.1(6)	24.3(7)	-1.4(5)	0.9(5)	2.0(5)
C17	25.1(8)	26.4(8)	30.3(10)	-7.4(7)	-0.4(7)	0.8(7)
C18	20.1(8)	22.5(7)	35.1(11)	-1.9(7)	1.4(7)	3.2(6)
O19	23.4(7)	34.7(7)	44.9(9)	0.8(6)	2.1(6)	-3.3(5)
C20	31.2(9)	29.1(8)	26.3(10)	3.5(7)	2.8(7)	-1.0(7)
C21	28.4(9)	27.3(9)	26.2(10)	0.5(7)	-4.9(7)	1.0(7)

Bond Lengths for 3ad

Atom	Atom	Length/ \AA	Atom	Atom	Length/ \AA
N1	O2	1.226(2)	O11	O12	1.4728(15)
N1	O3	1.226(2)	O12	C13	1.450(2)
N1	C4	1.470(2)	C13	C14	1.522(2)
C4	C5	1.389(3)	C13	C15	1.530(3)
C4	C9	1.383(3)	C13	C21	1.497(3)
C5	C6	1.388(2)	C15	O16	1.445(2)
C6	C7	1.397(2)	C15	C17	1.518(2)
C7	C8	1.390(2)	C17	C18	1.511(3)
C7	C10	1.507(2)	C18	O19	1.219(2)
C8	C9	1.384(3)	C18	C20	1.472(3)
C10	O11	1.427(2)	C20	C21	1.329(3)
C10	O16	1.397(2)			

Bond Angles for 3ad

Atom	Atom	Atom	Angle/°	Atom	Atom	Atom	Angle/°
O2	N1	O3	123.41(17)	C13	O12	O11	107.56(11)
O2	N1	C4	118.38(16)	O12	C13	C14	101.80(14)
O3	N1	C4	118.21(16)	O12	C13	C15	109.18(14)
C5	C4	N1	118.43(16)	O12	C13	C21	110.28(15)
C9	C4	N1	118.40(16)	C14	C13	C15	112.30(16)
C9	C4	C5	123.16(16)	C21	C13	C14	111.07(17)
C6	C5	C4	118.21(16)	C21	C13	C15	111.76(15)
C5	C6	C7	119.65(16)	O16	C15	C13	109.80(14)
C6	C7	C10	121.53(15)	O16	C15	C17	106.03(13)
C8	C7	C6	120.64(15)	C17	C15	C13	111.91(15)
C8	C7	C10	117.82(15)	C10	O16	C15	111.27(12)
C9	C8	C7	120.39(16)	C18	C17	C15	113.50(15)
C4	C9	C8	117.94(16)	O19	C18	C17	121.56(18)
O11	C10	C7	105.10(14)	O19	C18	C20	121.04(18)
O16	C10	C7	110.51(14)	C20	C18	C17	117.38(15)
O16	C10	O11	110.45(14)	C21	C20	C18	122.10(18)
C10	O11	O12	105.15(12)	C20	C21	C13	123.31(18)

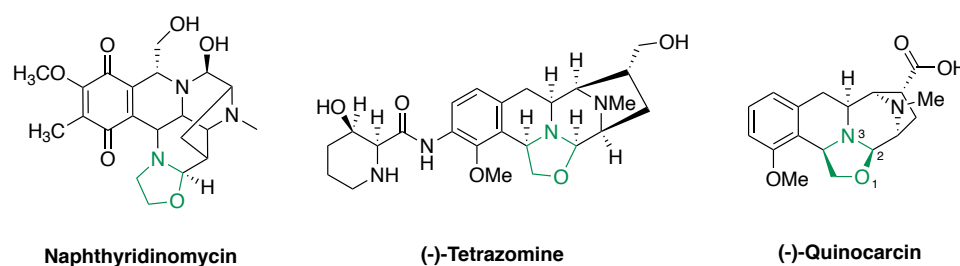
Hydrogen Atom Coordinates ($\text{\AA}\times 10^4$) and Isotropic Displacement Parameters ($\text{\AA}^2\times 10^3$) for 3ad

Atom	x	y	z	U(eq)
H5	9213.17	5017.12	5234.06	29
H6	7139.18	5688.94	5697.69	27
H8	3158.63	4642.03	6536.79	28
H9	5212.42	3969.17	6068.55	30
H10	2877.67	5573.22	7507.35	26
H14A	-1177.3	6778.07	4613.05	54
H14B	138.7	7188.79	5678.2	54
H14C	-611.08	6719.09	6770.75	54
H15	2559.01	6504.86	8004.77	29
H17A	3386.97	7324.72	7152.86	33
H17B	5257.63	7022.29	7653.38	33
H20	3947.78	7041.56	2014.58	35
H21	1504.76	6530.17	2270.96	33

7. Continuous flow telescoped synthesis of 1,3-oxazolidines

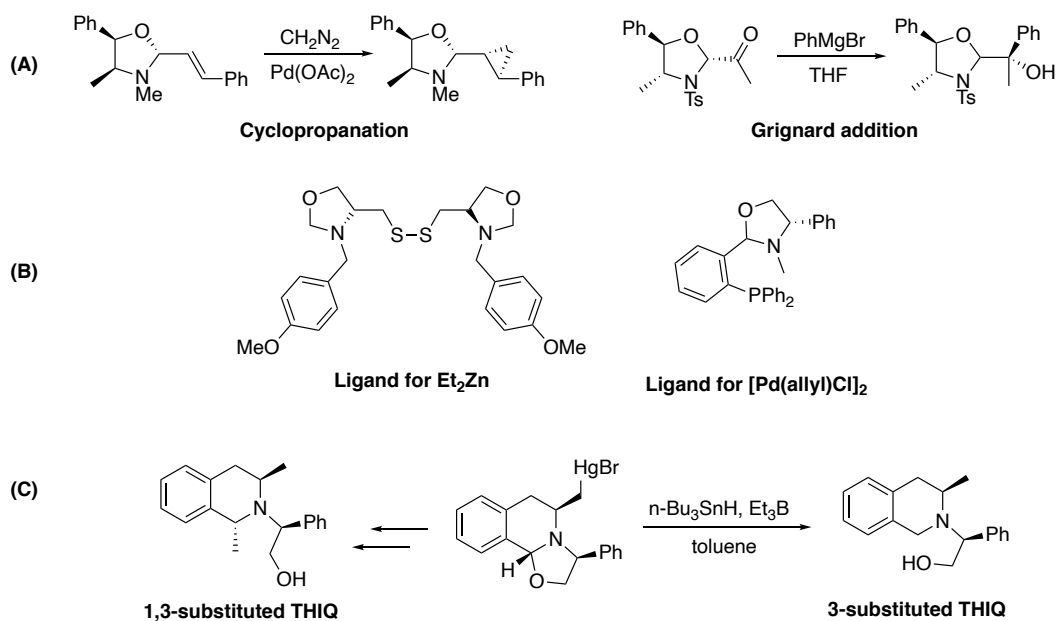
7.1. Introduction

Oxazolidines are saturated five-membered heterocyclic compounds, with nitrogen and oxygen atoms in the 1 and 3 positions. They are found in a variety of natural products with potent antibacterial and antitumor properties, mainly in the tetrahydroisoquinoline alkaloids (TAAs) family.³⁵¹ The naphthyridinomycin and quinocarcin families are subgroups of TAAs containing oxazolidine rings: Naphthyridinomycins inhibits DNA, RNA, and protein synthesis in bacteria;³⁵² Tetrazomine has increased cytotoxicity against P388 leukemia and both Gram-positive and Gram-negative bacteria;³⁵³ and quinocarcin has shown activity against leukaemia, lung cancer, and adenocarcinoma (Scheme 90).³⁵⁴ Other compounds in these families also possess similar biological activities.^{355, 356}



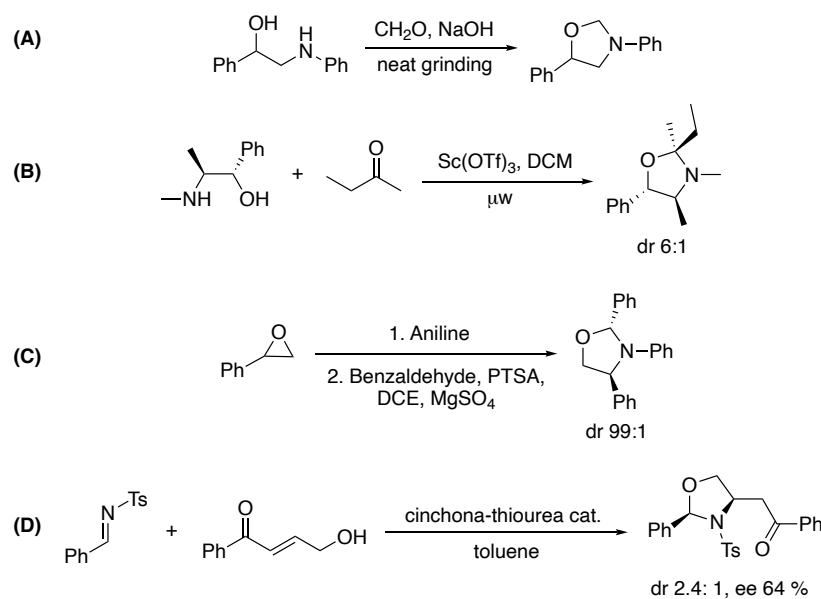
Naphthyridinomycin **(-)-Tetrazomine** **(-)-Quinocarcin**
Scheme 90. Oxazolidines found in natural products: Naphthyridinomycin, (-)-tetrazomine and (-)-quinocarcin.

The use of oxazolidines as chiral auxiliaries has been reported in various reactions (Scheme 91 - A),³⁵⁷ including cyclopropanation of alkenes,³⁵⁸ reduction of ketones to alcohols,³⁵⁹ Grignard addition to ketones,³⁶⁰ aziridinations,³⁶¹ and others.³⁶²⁻³⁶⁵ They can also be used as chiral ligands for transition metal catalysts³⁶⁶ (Scheme 91 - B), such as the disulfide oxazolidine ligand used for ethylation of aldehydes with organozinc Et₂Zn³⁶⁷ and in palladium-catalysed allylic alkylation using phosphinooxazolidine ligands.³⁶⁸ Finally, a few oxazolidines have been used as synthetic intermediates (Scheme 91 - C), as in the formation of 3-substituted and 1,3-disubstituted tetrahydroisoquinolines (THIQs),³⁶⁹ and in an oxazolidine thermal rearrangement yielding 1,5,2-dioxazinanes.³³³



Scheme 91. 1,3-oxazolidines applications: (A) Chiral auxiliaries, (B) chiral ligands for transition metal catalysts, and (C) synthetic intermediates.

Historically, 1,3-oxazolidines have been synthesised through condensation of amino alcohols and aldehydes or ketones,³⁶⁶ but often required harsh conditions such as high temperatures and strong acids, and give poor stereoselectivity.³⁷⁰ For this reason, different techniques under milder conditions have been developed such as mortar-pestle grinding (Scheme 92 - A),³⁷¹ and a diastereoselective synthesis variant was also reported (Scheme 92 - B).³⁷² Other methods using different substrates have also been developed,^{373, 374} including ring-opening cyclisation of epoxides with amines and aldehydes (Scheme 92 - C),³⁷⁵ Pd-catalysed Aza-Wacker reaction between amino alcohols and electron-deficient alkenes,³⁷⁶ and intramolecular Aza-Michael addition of γ -hydroxy- α,β -unsaturated carbonyls to imines (Scheme 92 - D).³⁷⁷

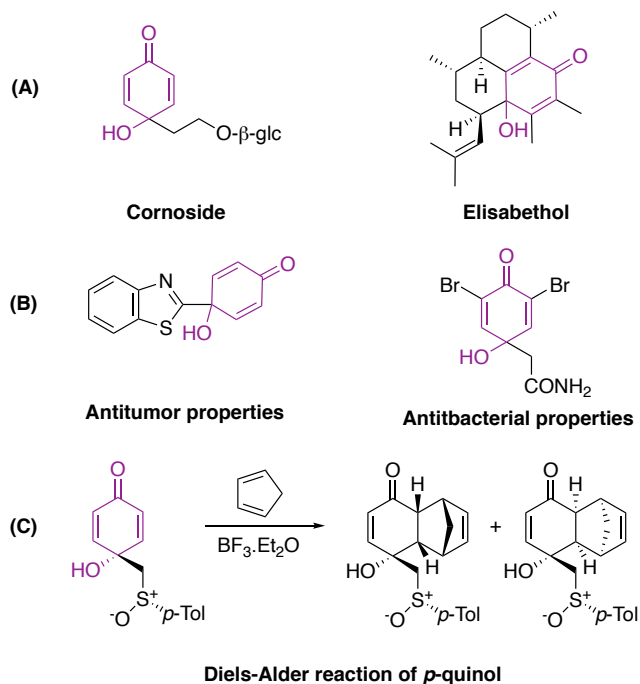


Scheme 92. Synthesis of 1,3-oxazolidines: condensation of amino alcohols and aldehydes/ketones by (A) grinding or (B) microwave, (C) epoxide ring-opening cyclisation, and (D) Aza-Michael addition of imines and γ -hydroxy- α , β -unsaturated carbonyls.

The synthesis of 1,3-oxazolidines via Aza-Michael addition³⁷⁷ paved the way for new stereoselective methodologies, as this approach had poor stereoselectivity. The inherent reversibility of the formation of hemiaminals/aminals, makes the asymmetric synthesis of oxazolidines challenging. The first catalytic enantioselective synthesis of aminals was only reported in 2008 by Antilla and co-workers,³⁷⁸ and the literature in this field is still underdeveloped.³⁷⁹

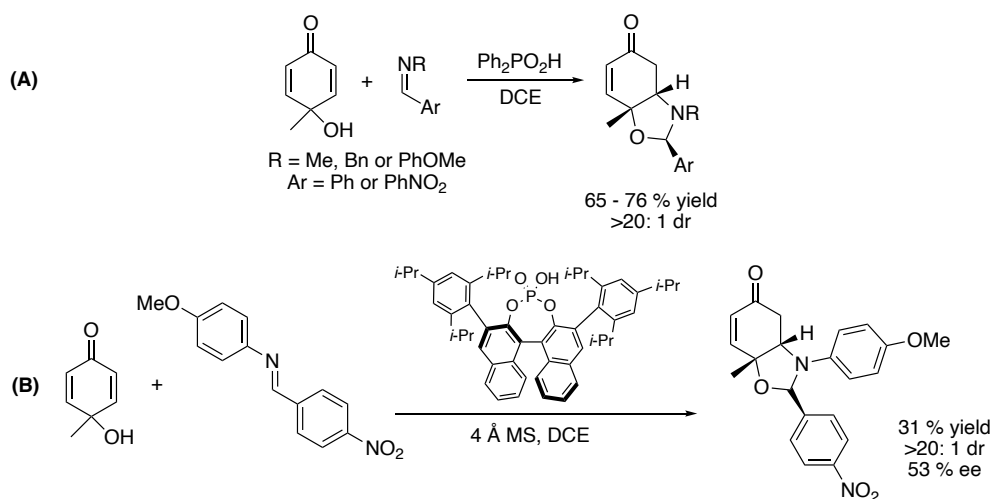
Given current interest in the desymmetrisation of *p*-quinols,^{380, 381} and the need for new methodologies to synthesise oxazolidines in a stereoselective manner, researchers have developed alternative synthetic routes from substituted imines and *p*-quinols.^{241, 308}

p-Quinols are important scaffolds found in natural products (Scheme 93 - A) including cornoside³⁸² (*T. capensis*) and elisabethol³⁸³ (*P. elisabethae*). Some of these compounds have biological activities such as antitumor³⁸⁴ and antibiotic³⁸⁵ (Scheme 93 - B). Finally, they are also versatile building blocks³⁸⁶ for the synthesis of *p*-quinones³⁸⁷ and can undergo [4+2]-cycloadditions³⁸⁸ (Scheme 93 - C). This multifunctional scaffold is rich in its chemistry, possessing two double bonds that are 1,4-Michael acceptors, a carbonyl that can undergo 1,2-substitution and a nucleophilic hydroxy group on the C-4 position. It is not surprising that the desymmetrisation of *p*-quinols has been an important area of study,^{380, 381} as it can lead to highly functionalised molecules that are not easily synthesised.



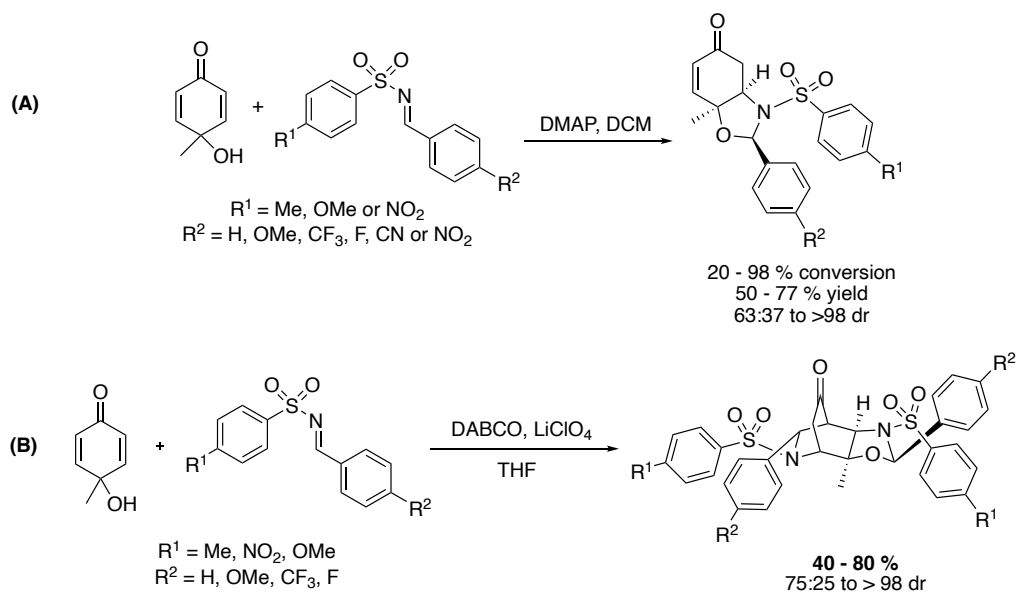
Scheme 93. *p*-quinols found in natural products (A), compounds with biological activity (B), and applications in organic synthesis (C).

In 2014, Rubush reported a stereoselective synthesis of 1,3-oxazolidines from *p*-substituted quinols and imines.²⁴¹ These reactions had high diastereoselectivity and good yields when Ph₂PO₂H was used as the acid catalyst (Scheme 94 - A). It was also reported an enantioselective synthesis variant using a chiral TRIP phosphoric acid catalyst ((*R*)-3,3'-bis(2,4,6-triisopropylphenyl)-1,1'-binaphthyl-2,2'-diyl hydrogenphosphate), at high diastereoselectivity but modest enantiomeric excess and low yield were obtained (Scheme 94 - B). Furthermore, the reaction scope was limited to *N*-alkyl and *N*-aryl imines, and unsuccessful results were obtained when *N*-sulfonyl imines, *O*-methyl oximes or tosylhydrazones were employed.



Scheme 94. Acid-catalysed synthesis of 1,3-oxazolidines using Ph₂PO₂H (A) and chiral TRIP phosphoric acid (B) catalysts by Rovis and Rubush.²⁴¹

In the same year, Carreño and co-workers published a base-catalysed synthesis of 1,3-oxazolidines³⁰⁸ using a similar approach to Rubush and co-workers. Moderate to good yields along with high diastereoselective ratios were obtained when the reaction was performed with DMAP in dichloromethane (Scheme 95 - A). The effect of substituents on both the *N*-arylsulfonyl and the aldehyde's aromatic ring moieties was also studied: higher conversions were obtained when an electron-donating group was attached to *N*-tosyl and an electron-withdrawing substituent was present in the imine. Unexpectedly, a change in solvent led, exclusively, to the formation of a tricyclic compounds via a cascade aza-Diels-Alder after the intramolecular aza-Michael addition (Scheme 95 - B). Finally, a mechanistic study detailing the stereochemical outcome of the reaction concluded that the attack of the *p*-quinol hydroxy group on the imine dictates the final stereochemistry of the oxazolidine ring.



Scheme 95. (A) Base-catalysed synthesis of 1,3-oxazolidines using DMAP; (B) Formation of a tricyclic compound via Aza Diels-Alder cascade catalysed by DABCO/LiClO₄.³⁰⁸

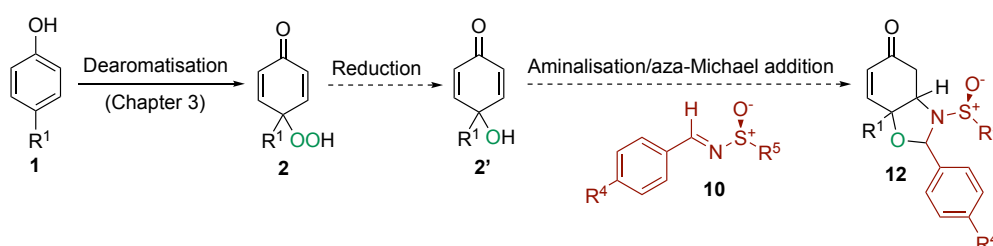
7.2. Aims and general strategy

The synthesis of novel compounds containing a 1,3-oxazolidine ring is highly desirable due to their potential medicinal properties and varied synthetic uses, as shown above. Although the asymmetric synthesis of 1,3-oxazolidines from *p*-quinols has been previously reported by Rubush,²⁴¹ the modest enantiomeric excess and low yield obtained motivates the development of new enantioselective routes. Therefore, the aims of this Chapter were:

- To explore whether the dearomatisation of *p*-substituted phenols can be applied to produce 1,3-oxazolidines.
- To extend this approach to the asymmetric synthesis of 1,3-oxazolidines.
- To develop a telescoped continuous flow process, using this new methodology, from *p*-substituted phenols.

To address these aims, the following strategy was adopted:

1. A synthetic route for the asymmetric telescoped synthesis of 1,3-oxazolidines **11** was proposed as a starting point, as shown in Scheme 96. It consists of three consecutive steps: dearomatisation of *p*-substituted phenols **1**, reduction of *p*-peroxyquinols **2**, and amination/Aza-Michael cascade. The reaction is to be performed in scCO₂ using singlet oxygen in a continuous flow regime with the intention to improve safety and scalability of the process.



Scheme 96. Proposed continuous flow telescoped synthesis of 1,3-oxazolidines **12** from *p*-substituted phenols **1**.

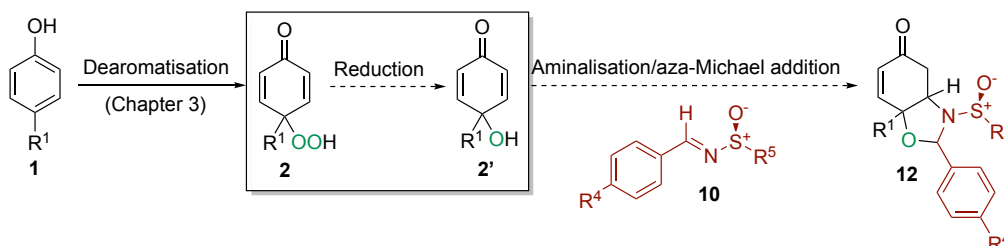
2. The first reaction to be investigated in batch was the formation of *p*-quinol **2'** from the reduction of *p*-peroxyquinol **2**.

3. Using *p*-quinol **2'** obtained previously, the cyclisation step was to be carried out with *N*-sulfinyl imine **10**.

7.3. Results and discussion

7.3.1. Synthesis of *p*-quinol 2a'

Given the dearomatisation of *p*-substituted phenols had already been studied in Chapter 3, the next step was to investigate the reduction of *p*-peroxyquinols **2** to form *p*-quinols **2'** (Scheme 97).

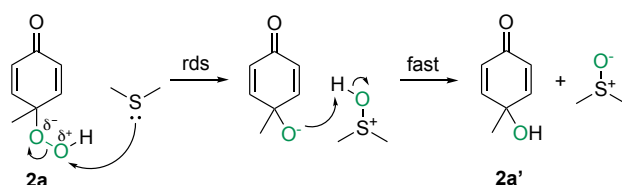


Scheme 97. Reduction of *p*-peroxyquinols **2** to *p*-quinols **2'** in the proposed asymmetric synthesis of 1,3-oxazolidines **12**.

p-Peroxyquinol **2** was reduced using dimethyl sulfide (DMS) as a reducing agent, following a protocol published by Adimurthy and co-workers.³⁸⁹ This methodology was particularly chosen as the only by-product formed is dimethyl sulfoxide (DMSO), which is a solvent that would not be expected to interfere in the future telescoped synthesis.

Reaction Mechanism

The generally accepted mechanism for this reduction involves a nucleophilic attack of the sulfur atom in DMS to the distal oxygen in *p*-peroxyquinol **2a**, followed by a S_N2 displacement to give *p*-quinol **2a'** (Scheme 98). A kinetics study has shown that the oxygen transfer to dimethyl sulfide is the rate-determining step (rds), followed by fast proton transfer from protonated dimethyl sulfoxide to form *p*-quinol **2a'**.³⁹⁰



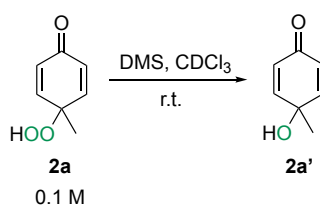
Scheme 98. Mechanism for the reduction of *p*-peroxyquinol **2a** to *p*-quinol **2a'** by dimethyl sulfide. 'Rds' indicates the rate-determining step.

Reduction of *p*-peroxyquinol **2a** with DMS in batch

The reaction was then carried out and optimised at room temperature, varying the amount of DMS, as shown in Table 34.

The reaction gave excellent yields in all experiments in a short amount of time. Considering yield, reaction time and equivalents of DMS for future telescoped synthesis, the best condition to be reproduced in continuous flow would be 4 eq. of DMS (Entry 2 – Table 34), which gives > 90% yield in only 30 min.

Table 34. Optimisation of the reduction of *p*-peroxyquinol **2a** reaction with DMS.

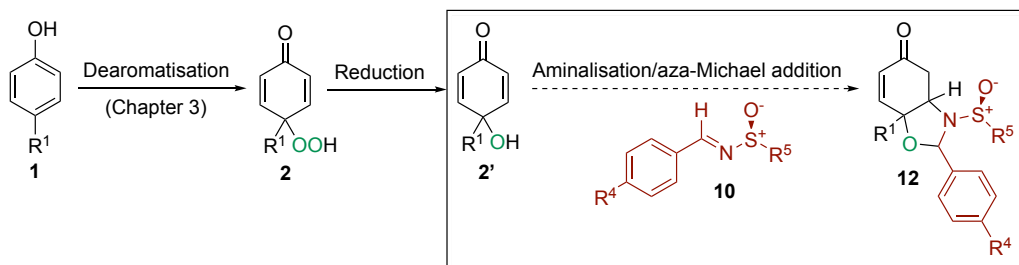


Entry	DMS (eq.)	Time (h)	NMR yield (%)
1	2	0.5	81
		1.0	97
2	4	0.5	93
		1.0	>99
3	6	0.5	>99
4	8	0.5	>99
5	10	0.5	>99

¹H NMR spectroscopy yields were obtained using biphenyl (0.05 eq.) as the internal standard.

7.3.2. Asymmetric synthesis of 1,3-oxazolidines

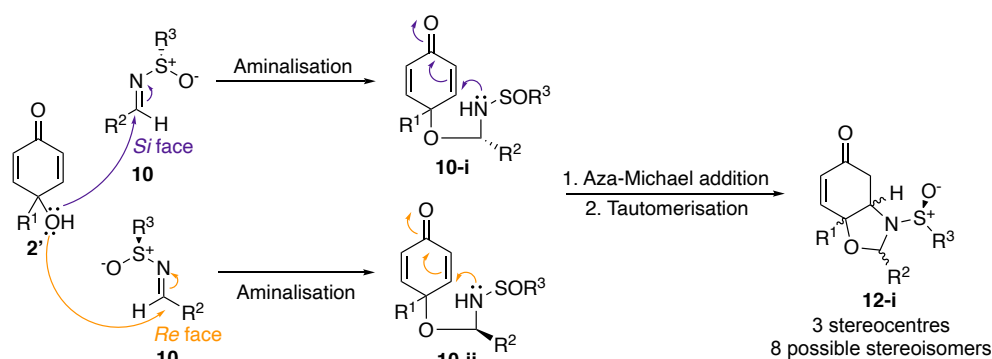
After finding the most efficient condition for the reduction of *p*-peroxyquinol **2a**, the aminalisation/Aza-Michael addition step of the synthesis of 1,3-oxazolidines **12** was explored.



Scheme 99. Aminalisation/Aza-Michael addition in the proposed asymmetric synthesis of 1,3-oxazolidines **12**.

Proposed Reaction Mechanism

The proposed mechanism of this reaction was based on work developed by Carreño *et al* (Scheme 100).³⁰⁸ The 1,2-addition of the hydroxide on *p*-quinol **2'** to the *N*-sulfinyl imine **10** can occur on both *Re* and *Si* faces. As mentioned previously, *N*-sulfinyl imine **10** as a chiral auxiliary is believed to favour one hemiaminal over the other (**10-i** and **10-ii**), as well as their respective 1,3-oxazolidines (**12-i** to **12-iv**). The stereochemical outcome of this reaction is difficult to be determined as the existent models to predict the diastereofacial selectivity of nucleophilic addition to *N*-sulfinyl imines vary depending on the reaction conditions.³⁴²

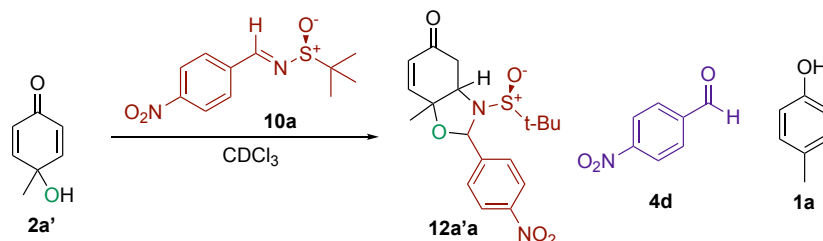


Scheme 100. Proposed mechanism for the synthesis of 1,3-oxazolidines **12** from *p*-quinols **2'** and *N*-sulfinyl imines **10**.

Attempted asymmetric synthesis of 1,3-oxazolidines in batch

Different parameters were screened for the synthesis of 1,3-oxazolidines **12** with *N*-sulfinyl imine **10a** (synthesised by Dr. J. Moore), including type of catalyst, catalyst loading, temperature, and addition of drying agents, as shown in Table 35.

Table 35. Summary of the conditions screened for the synthesis of 1,3-oxazolidines **12** in batch.



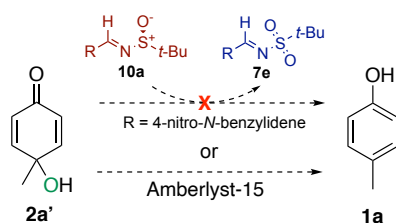
Entry	Catalyst	Catalyst loading	Temperature (°C)	Time (h)	NMR ratio 4d: 10a	NMR ratio 1a: 2a'
1	DMAP	0.15 eq.	r.t	24	No reaction	
2		1.0 eq.	r.t	24	No reaction	
3			40	24	No reaction	
4	Amberlyst-15	100% w/w	40	1	1: 9.5	1: 3.0
5*				1	1: 7.9	1: 0.8
				24	1: 2.9	1: 0.4

* Addition of 4 Å molecular sieves. The desired product 1,3-oxazolidine **12a'a** was not included in the table as it was unable to be synthesised in these conditions.

4-Dimethylaminopyridine (DMAP) has previously been reported to catalyse the synthesis of oxazolidines by facilitating the amination step.³⁰⁸ As DMAP ($\text{pK}_a = 9.7$)³⁹¹ is not a strong enough base to deprotonate the hydroxyl in *p*-quinol **2a'** ($\text{pK}_a = 13.1$),³⁹² it is more likely that the catalysis would occur via nucleophilic addition of DMAP to the imine, forming a more reactive electrophile. However, only starting materials were observed when a catalytic amount of DMAP was used in the reaction (Entry 1 – Table 35). Increasing the quantity of catalyst (Entry 2 – Table 35) or heating up to 40 °C (Entry 3 – Table 35), did not result in any reaction. One reasonable explanation could be that the lower electrophilicity in *N*-sulfinyl imines **9** compared to *N*-sulfonyl imines **7** hampers the nucleophilic attack of DMAP.

An acid catalysed version of this type of reaction using Amberlyst-15 has also been reported.²⁴¹ In 1 h of reaction (Entry 4 – Table 35), a ratio of aldehyde **4d**: *N*-sulfinyl imine

10a of 1: 9.5 was observed in the ^1H NMR spectroscopy, along with some impurities. A fraction of **2a'** was converted back to its corresponding phenol **1a**. It was thought initially that the re-aromatisation was aided by oxidation of *N*-sulfinyl imine **10a**, but *N*-sulfonyl imine **7e** signals were not found in the ^1H NMR spectroscopy spectrum of the reaction mixture. Another possibility is that Amberlyst-15 could activate **2a'** and facilitate the re-aromatisation of the ring to give *p*-cresol **1a** (Scheme 101).



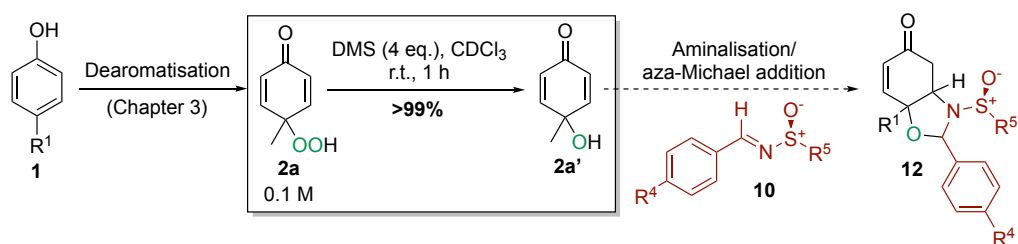
Scheme 101. Proposed routes for the re-aromatisation of *p*-quinol **2a'** to *p*-cresol **1a** via oxidation of *N*-sulfinyl imine **10a** to *N*-sulfonyl imine **7e**, or activation by Amberlyst-15. **X** represents a route that was disregarded due to lack of formation of *N*-sulfonyl imine **7e**.

To minimise hydrolysis of *N*-sulfinyl imine **10a**, 4Å molecular sieves were added to the reaction vessel in order to trap any water that could be formed during the reaction (Entry 5 – Table 35). However, hydrolysis of **10a** to **4d** and re-aromatisation of **2a** to **1a** continued to occur and even after 24 h of reaction, no 1,3-oxazolidine **12a'a** was formed.

7.4. Conclusions

Synthesis of *p*-quinol **2a'**

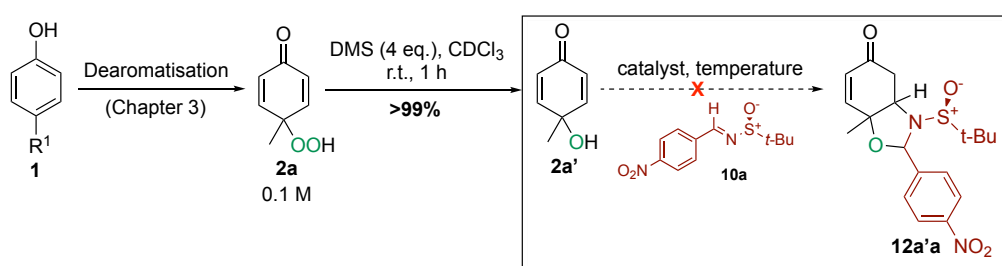
According to the strategy proposed for the asymmetric synthesis of 1,3-oxazolidines in this Chapter, the first step to be studied was the reduction of *p*-peroxyquinols **2**. The reaction was carried out using DMS as the reducing agent and further optimised, giving quantitative yield in only 1 h when 4 eq. of DMS was used at room temperature (Scheme 102).



Scheme 102. Optimised reduction of *p*-peroxyquinol **2a** to *p*-quinol **2a'** using DMS.

Asymmetric synthesis of *p*-quinol **2a'**

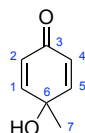
After optimising the reduction of *p*-peroxyquinol **2a**, the amination/Aza-Michael addition was investigated (Scheme 103). 1,3-Oxazolidine **12a'a** could not be formed in any of the experiments: DMAP-catalysed reactions resulted in no conversion of starting material, whilst Amberlyst-15 caused hydrolysis of the *N*-sulfinyl imine **10a** and re-aromatization to *p*-cresol **1a**.



Scheme 103. Attempted asymmetric synthesis of 1,3-oxazolidines **12a'a** from *p*-quinol **2a'** and *N*-sulfinyl imine **10a**. **X** represents that no product **12a'a** was formed in the reaction.

- **Reaction 5:** DMS (10.0 eq, 0.700 mmol, 50.0 μL). After 0.5 h of reaction, ^1H NMR spectroscopy = >99% yield of **2a'**.

4-Hydroxy-4-methylcyclohexa-2,5-dien-1-one **2a'**³⁹³

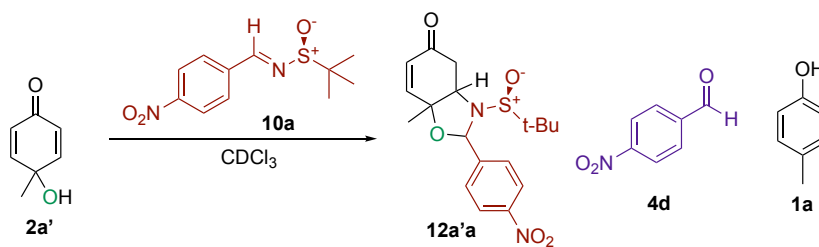


^1H NMR (400 MHz, Chloroform-*d*): δ 6.86 (d, $J = 10.1$ Hz, 2H, **1/5**), 6.05 (d, $J = 10.1$ Hz, 2H, **2/4**), 3.21 (s, 1H, **8**), 1.44 (s, 3H, **7**).

^{13}C NMR (101 MHz, Chloroform-*d*): δ 185.9 (**3**), 152.8 (**1/5**), 127.0 (**2/4**), 67.2 (**6**), 26.8 (**7**).

HRMS (ESI) m/z calcd $[\text{C}_7\text{H}_9\text{O}_2]^+$ ($[\text{M} + \text{H}]^+$): 147.0417, found 147.0408.

7.5.2. Synthesis of 1,3-oxazolidine 12a'a from *p*-quinol 2a' and (*E*)-2-methyl-*N*-(4-nitrobenzylidene)propane-2-sulfinamide 10a



Standard procedure: (*E*)-2-methyl-*N*-(4-nitrobenzylidene)propane-2-sulfinamide **10a** (1.0 eq, 0.299 mmol, 76.0 mg) and catalyst were added to a solution of *p*-quinol **2a'** (1.0 eq, 0.264 mmol, 37.0 mg) in CDCl₃. The solution was stirred, resulting in a yellow reaction mixture. ¹H NMR spectroscopy was recorded from a 0.6 mL sample, taken directly from the reaction mixture.

SET 1: base catalyst DMAP

- **Reaction 1:** 0.6 mL solution of **2a'** and DMAP (0.15 eq, 44.9 μmol, 6.00 mg) at room temperature. After 24 h of reaction, only starting materials were observed in the ¹H NMR spectroscopy.
- **Reaction 2:** similar conditions as Reaction 1, but DMAP (1.0 eq, 0.299 mmol, 37.0 mg). In 24 h of reaction, only starting materials were observed in the ¹H NMR spectroscopy.
- **Reaction 3:** similar conditions as Reaction 1, but at 40 °C. After 24 h of reaction, only starting materials were observed in the ¹H NMR spectroscopy.

SET 2: acid catalyst Amberlyst-15

- **Reaction 4:** 3 mL solution of **2a'** and Amberlyst-15 (100% w/w, 37.0 mg) at 40 °C. After 1 h of reaction, ¹H NMR spectroscopy ratio **4d**: **10a** was 1: 9.5 and **1a**: **2a'** was 1: 3.0.
- **Reaction 5, Test 1:** same conditions as Reaction 4, with addition of 4 Å molecular sieves to the reaction mixture. After 1 h of reaction, ¹H NMR spectroscopy ratio **4d**: **10a** was 1: 7.9, **1a**: **2a'** was 1: 0.8.
- **Test 2:** After 24 h of reaction, ¹H NMR spectroscopy ratio **4d**: **10a** was 1: 2.9 and **1a**: **2a'** was 1: 0.4.

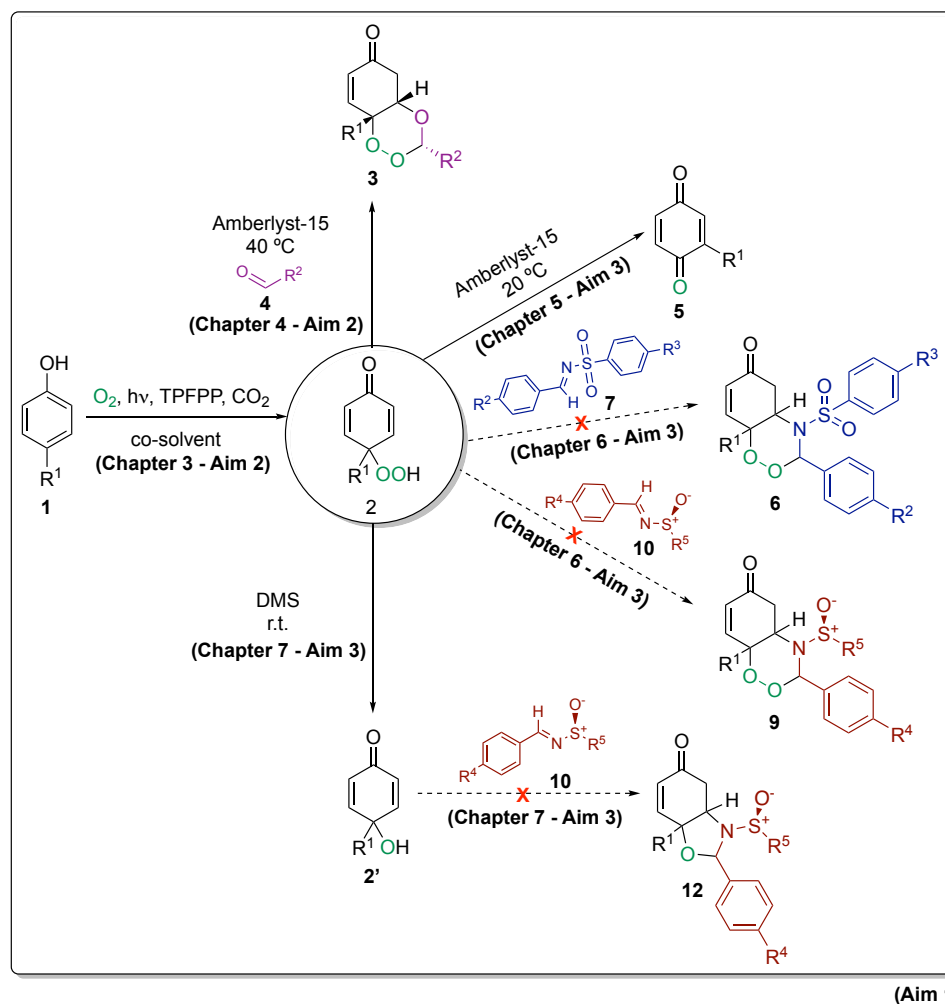
8. Final conclusions and future work

The conclusions and future work for this Thesis will be depicted for each chapter based on the aims outlined on Chapter 1 (Scheme 104), as repeated below:

Aim 1: To explore the applications of a custom-built high-pressure continuous flow photooxidation system.

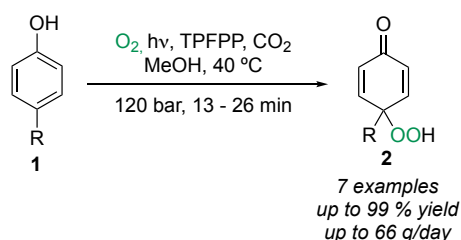
Aim 2: To conduct further studies on the photooxidation of *p*-substituted phenols **1** and telescoped synthesis of 1,2,4-trioxanes **3** previously developed in our group.

Aim 3: To investigate the applications of photooxidation of *p*-substituted phenols in telescoped syntheses of other molecular scaffolds with potential pharmaceutical interest (1,4-benzoquinones **5**, 1,2,4-dioxazinanes **6** and **9**, and 1,3-oxazolidines **12**).



*Scheme 104. Conclusion of the PhD Thesis highlighting the specific aims addressed in each chapter: Chapter 3 – photooxidation of *p*-substituted phenols **1** to *p*-peroxyquinols **2** (Aim 2); Chapter 4 – telescoped synthesis of 1,2,4-trioxanes **3** (Aim 2); Chapter 5 – telescoped synthesis of 1,4-benzoquinones **5** (Aim 3); Chapter 6 – telescoped synthesis of 1,2,4-dioxazinanes **6** and **9** (Aim 3); and Chapter 7 – telescoped synthesis of 1,3-oxazolidines **11** (Aim 3). Aim 1 is involved in all chapters. X means that the product could not be formed.*

Chapter 3: Continuous flow dearomatisation of *p*-substituted phenols using singlet oxygen in supercritical CO₂ (Aims 1 and 2)



Scheme 105. The continuous flow photooxidation of *p*-substituted phenols **1** using singlet oxygen in supercritical CO₂.

Aim 1: The high-pressure photooxidation flow system containing a sapphire photoreactor was employed in the continuous flow dearomatisation of *p*-substituted phenols **1** using singlet oxygen in supercritical CO₂. This setup enabled a safe and effective use of singlet oxygen by performing the photooxidation in a non-flammable solvent (CO₂) in a continuous flow regime, in which light penetration is enhanced and over-irradiation is avoided.

Aim 2: This methodology previously developed in our research group¹⁵² was further explored: the scope of reaction was expanded from four to eleven *p*-peroxyquinols **2**, with yields and productivities of up to 99% and 66 g/day, respectively (Scheme 105). This was a significant improvement when compared to projected productivities of 1.6 g/day and 12 g/day in previous works^{77, 169}

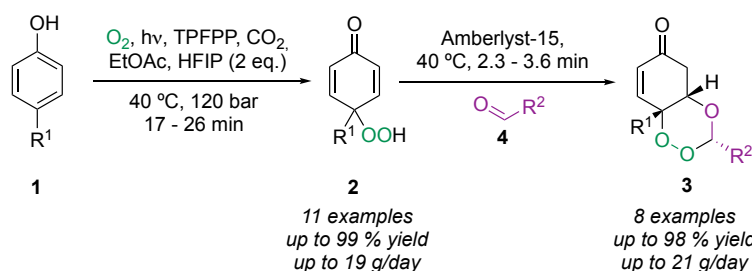
The substituent effect on the phenol **1** was also investigated. The degree of substitution did not have a significant impact on the yield, whereas the nature of the substituent, e.g. a *t*-Bu group, had a notable negative effect on the yield when compared to a methyl substituent. Steric hindrance and lone pair electron repulsion also had a negative influence on the yield when different types of substituents were examined. In addition, protecting groups such as *tert*-butoxycarbonyl (Boc) and methoxy (MeO) were not affected in the reaction conditions.

During this work, numerous challenges were addressed including the concentration of the starting solution, which was decreased depending on the solubility of the *p*-substituted phenol **1** or the forming *p*-peroxyquinol **2**. 4-(hydroxymethyl) phenol **1g** caused blockage in the system, so derivatisation was required to conduct the photooxidation. No

photooxidation product could be synthesised when an electron-withdrawing group was present at the *para* position in 4-hydroxybenzotrifluoride **1i**.

Future work: To further increase the scale of this reaction, a larger photo reactor or adding more photo reactors in series could be investigated. Although large quantities of *p*-peroxyquinols should not be isolated due to potential explosion hazards, this would be particularly interesting for multi-step synthesis as the *p*-peroxyquinols would be generated and used *in situ*. However, care should be taken regarding the overall concentration of oxygen and precipitation of solids during the process, as they can potentially cause explosions or blockages. In addition, in-line analysis could be incorporated in the continuous flow setup, such as high-pressure IR or NMR spectroscopy, to enable rapid analysis and optimisation. Future investigations could also explore the different reactivities of the *p*-peroxyquinol **2** building block, such as 1,2-addition to the carbonyl and cycloadditions.

Chapter 4: Continuous flow telescoped synthesis of 1,2,4-trioxanes (Aims 1 and 2)



Scheme 106. The continuous flow telescoped synthesis of 1,2,4-trioxanes **3** from photooxidation of *p*-substituted phenols **1**.

Aim 1: The continuous flow telescoped synthesis of 1,2,4-trioxanes **3** was performed in the high-pressure flow system, which was adapted to incorporate a thermo reactor (Scheme 106). The thermo reactor consists in a tubular reactor packed with an acid catalyst Amberlyst-15 and glass beads to aid mixing. The outlet of the photo reactor containing *p*-peroxyquinols **2** would then flow through the packed bed reactor together with a solution of aldehydes **4** to promote the acetalisation/oxa-Michael addition cascade.

Additional investigations were conducted using three different designs of thermo reactor in order to increase the yield for the acetalisation/oxa-Michael addition step. Although a small increase in yield (10%) was obtained for a model reaction, these are promising results for future reactor modifications.

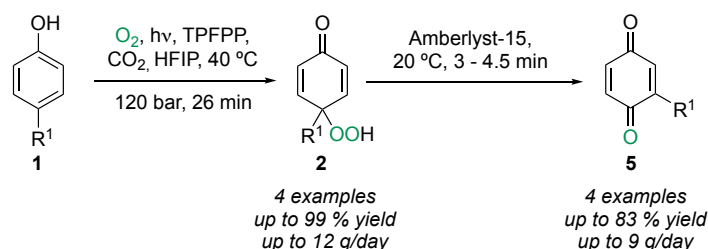
Aim 2: The first step of the process had to be re-optimised due to solvent incompatibility for the second step when MeOH was used as the co-solvent. Ethyl acetate with 2 equivalents of HFIP was found to be the optimal condition to perform both steps in sequence. Eleven *p*-peroxyquinols **2** were synthesised with yields of up to > 99%. Interestingly, 4-(4-hydroxyphenyl)-2-butanone **2m** bearing a ketone in *para* position spontaneously cyclised into spirocyclic peroxyhemiacetal **2m'**. Similar challenges associated with concentration of starting solution and blockages caused by free benzylic group were addressed in this chapter.

Using the methodology designed in our research group,¹⁵² eight 1,2,4-trioxanes **3** were synthesised. The scope was explored with various *p*-peroxyquinols **2** and aldehydes **4** counterparts, with yields and productivities of up to 98% and 21 g/day, respectively. Compared to previous methods in the literature,^{195, 233} productivities were significantly increased from < 300 mg/day to up to 21 g/day. Moreover, reaction times were efficiently

decreased from 12-48 h to 3.6 min. This protocol also enabled a safer synthesis of 1,2,4-trioxanes **3** by generating and reacting hazardous *p*-peroxyquinols **2** *in situ*. Toxic halogenated solvents such as dichloromethane previously used, were substituted by CO₂ with small quantities of co-solvent, minimising organic waste. Several challenges arose in this step of the process. For instance, purification of 1,2,4-trioxane **3hc** was attempted using flash column chromatography, 2D thin layer chromatography and crystallisation, but were unsuccessful. To facilitate isolation of the product, deprotection of the benzylic group in 1,2,4-trioxane **3hc** using TBAF was attempted, but only decomposition was observed. Four 1,2,4-trioxanes (**3cc**, **3dc**, **3hb**, and **3mc**) could not be synthesised either because of steric hindrance, deactivation of the 2,5-cyclohexenone ring, or unfavoured transition states.

Future work: The scope of the 1,2,4-trioxanes **3** could be explored using aldehydes **4** and *p*-peroxyquinols **2** bearing heterocyclic, electron-withdrawing, alkenyl, or alkynyl functional groups. Further scaling-up and *in vitro* tests for antimalarial and anticancer activities of these 1,2,4-trioxanes **3** should be considered, as this would be of high interest for pharmaceutical companies. Future studies could investigate additional functionalisation of these compounds. For instance, it has been reported that the double bond in the enone ring of the 1,2,4-trioxane **3** can react in Diels-Alder cycloaddition to form tricyclic structures.³⁰⁸ This reactive site can also be brominated, epoxidised, or reduced.¹⁹⁵ Finally, the continuous flow telescoped asymmetric synthesis of these 1,2,4-trioxanes **3** could be examined using, for example, chiral phosphoric acid catalysts.¹⁹⁵

Chapter 5: Continuous flow telescoped synthesis of 2-substituted 1,4-benzoquinones (Aims 1 and 3)



Scheme 107. The continuous flow telescoped synthesis of 2-substituted 1,4-benzoquinones **5** from photooxidation of *p*-substituted phenols **1**.

Aim 1: A methodology was developed in the continuous flow high-pressure system for the telescoped synthesis of 2-substituted-1,4-benzoquinones **5** from the photooxidation of *p*-substituted phenols **1** (Scheme 107). Similarly to the synthesis of 1,2,4-trioxanes **3** in Chapter 4, a tubular reactor packed with Amberlyst-15 was incorporated after the photo reactor to promote the 1,2-alkyl shift of the *para* substituent on *p*-peroxyquinol **2**.

Aim 3: Initial studies in batch to reproduce the conditions found in the literature²⁸² for the second step of the process were conducted using titanium chloride (TiCl₄) in dichloromethane. However, only decomposition of *p*-peroxyquinol **2a** bearing a methyl substituent at *para* position was observed. Thus, a series of parameters were screened in order to optimise the 1,2-alkyl shift of *p*-peroxyquinol **2a** in batch: concentration of substrate, temperature, acid catalysts and solvent systems. However, the best condition found using Amberlyst-15 at 40 °C in either toluene/HFIP or EtOAc/HFIP only gave traces of 1,4-benzoquinone **5a** (5%).

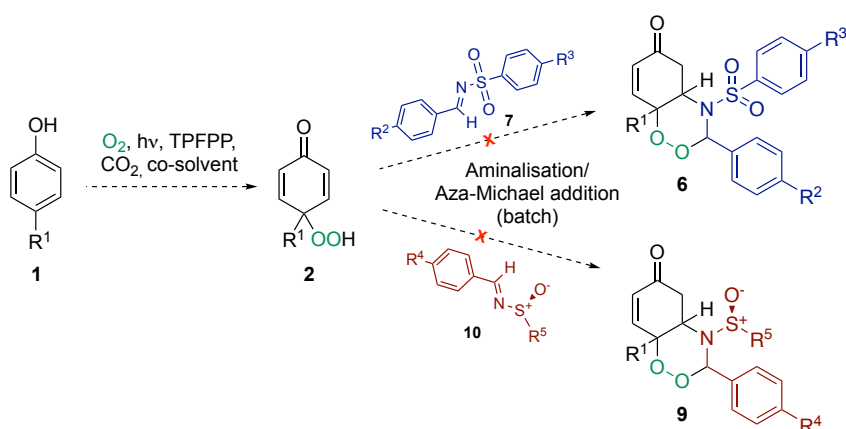
In order to confirm if the quantification methods were accurate, volatility tests were performed with 1,4-benzoquinone **5a**. The tests proved that **5a** co-evaporates with even mild solvent removal techniques, such as N₂ blown down. Different quantification methods were then compared, showing that HPLC and ¹H NMR spectroscopy using internal standard without solvent removal gave the same results.

When the substrate was changed to *p*-peroxyquinol **2n** with an isopropyl at the *para* position and optimisation of the reaction was carried out in batch, 1,4-benzoquinone **5n** was obtained in quantitative yields. Both the photooxidation of *p*-substituted phenol **1n** and the telescoped synthesis of **5n** were conducted in the continuous flow apparatus, resulting in an overall yield of 83% of **5n**.

In total, four 1,4-benzoquinones **5** were synthesised with overall yields and productivities of up to 83% and 9 g/day, respectively. Compared to the procedure found in the literature,²⁸² this protocol is atom efficient, substituting *t*-BuOOH for molecular oxygen. It is safer, as the *p*-peroxyquinols **2** are generated in small quantities at any one time and reacted *in situ* in a non-flammable solvent CO₂, instead of using large quantities of potentially explosive *t*-BuOOH. The scale and reaction time was improved from 1.8 g/day in batch to up to 9 g/day in a continuous flow regime with total residence time of 30 min. Moreover, the second step is performed at ambient temperature instead of -78 °C; the solvent was substituted for CO₂ with small amounts of HFIP as a co-solvent instead of dichloromethane; and the toxic TiCl₄ catalyst was replaced by Amberlyst-15, which is non-toxic and facilitates downstream purification.

Future work: The scope of the synthesis of 1,4-benzoquinones **5** could be further investigated with other *p*-substituted phenols **1**. Previous studies have found that a similar 1,2-alkyl shift of the *para* substituent occurs with high regioselectivity resulting in 2-substituted-1,4-benzoquinone **5**. To test this hypothesis, *p*-substituted phenols **1** bearing substituents at various positions should be tested. The migration of cyclic and spirocyclic substituents could be interesting to investigate. Allylic and benzylic *para* substituents have a strong ability to stabilise carbocations and are also potential candidates to be examined. The synthesis of 1,4-benzoquinone **5a** should be further optimised, since this strategy could be applied on the total synthesis of natural products such as Vitamin K₁ or coenzyme Q10.

Chapter 6: Continuous flow telescoped synthesis of 1,2,4-dioxazinanes (Aims 1 and 3)



Scheme 108. Attempted continuous flow telescoped synthesis of 1,2,4-dioxazinanes **6** and **9** from photooxidation of *p*-substituted phenols **1**.

Aim 1: The continuous flow telescoped synthesis of 1,2,4-dioxazinanes **6** and **9** was designed to be performed in the high-pressure flow setup in two consecutive steps: first, photooxidation of *p*-substituted phenols **1**, as shown in Chapter 3; and second, an aminalisation/aza-Michael addition cascade using either *N*-sulfonyl imines **7** or *N*-sulfinyl imines **10**, as shown in Scheme 108.

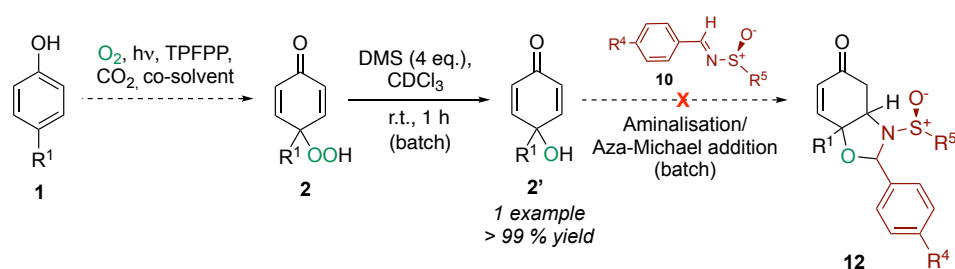
Aim 3: The second step of the racemic synthesis of *N*-sulfonyl-1,2,4-dioxazinanes **6** was tested in batch with *p*-peroxyquinol **2a** and two *N*-sulfonyl imines **7**, which were previously synthesised through condensation of sulfonamides **8** and aldehydes **4**. Similar conditions reported by Rubush were reproduced²⁴² using Amberlyst-15 as the acid catalyst, but no product was formed.

The asymmetric synthesis of *N*-sulfinyl-1,2,4-dioxazinanes **9** was then attempted with *p*-peroxyquinol **2a** and *N*-sulfinyl imine **10a**. After screening acid and base catalysts, temperatures and solvent, no product was obtained. In acidic conditions using Amberlyst-15, 1,2,4-trioxane **3nd** was formed instead. This is possibly due to a hydrolysis of *N*-sulfinyl imine **10a** into aldehyde **4d**, which then reacted with *p*-peroxyquinol **2a** through an acetalisation/oxa-Michael addition. Base catalysts only caused reduction of the *p*-peroxyquinol **2a** into *p*-quinol **2a'**.

Future work: Further studies could be conducted in order to enable the aminalisation/aza-Michael addition step. For example, *N*-sulfonyl imines **7** with different combinations of electron-donating/withdrawing groups at their benzene rings could be

tested, as only two were used in this chapter. Instead of *N*-sulfonyl imines **7**, imines with *N*-aliphatic substituents might enhance the nitrogen's nucleophilicity for the following Aza-Michael addition step and avoid steric hindrance issues. Additionally, *N*-sulfinyl imines **10** with a less strong electron-withdrawing group at the benzylidene ring could be interesting to investigate, as the NO₂ substituent makes the *N*-sulfinyl imines **10** highly reactive and more prone to hydrolysis. To avoid hydrolysis of both *N*-sulfonyl imines **7** and *N*-sulfinyl imines **10**, the experiments could be tested with thoroughly dried Amberlyst-15 to make sure that no moisture is present in the system.

Chapter 7: Continuous flow telescoped synthesis of 1,3-oxazolidines (Aims 1 and 3)



Scheme 109. Attempted continuous flow telescoped synthesis of 1,3-oxazolidines **12** from photooxidation of *p*-substituted phenols **1**.

Aim 1: The continuous flow telescoped synthesis of 1,3-oxazolidines **12** was designed to be performed in the high-pressure flow setup. The proposed synthetic route would start from the photooxidation of *p*-substituted phenols **1**, as shown in Chapter 3, followed by reduction to form *p*-quinol **2'**, which would then react with *N*-sulfinyl imine **10a** in an amination/aza-Michael addition cascade, as shown in Scheme 109.

Aim 3: The second step, the reduction of *p*-peroxyquinol **2a**, was the first to be investigated in batch, giving quantitative yields of *p*-quinol **2a'** after optimisation of reaction conditions reported in the literature using dimethyl sulfide as the reducing agent.³⁸⁹ The third step of the synthetic route was then examined in batch with *p*-quinol **2a'** and *N*-sulfinyl imine **10a** using either an acid (Amberlyst-15) or base catalyst (DMAP), reproducing similar protocols from the literature.^{241, 308} However, 1,3-oxazolidine **12a'a** could not be synthesised: No reaction was observed when using DMAP, and Amberlyst-15 caused hydrolysis of *N*-sulfinyl imine **10a**. In addition, *p*-substituted phenol **1a** was also identified in the reactions using Amberlyst-15 due to a possible re-aromatisation.

Future work: the telescoped synthesis of 1,3-oxazolidines **12** could focus on using other *N*-sulfinyl imines **10** bearing a neutral or electron-donating group in their benzylidene rings at *para* position. This is because the *N*-sulfinyl imine **10a** used possesses a nitro substituent which is strongly electron-withdrawing, making this compound highly reactive and prone to hydrolysis. A continuous flow telescoped synthesis of 1,3-oxazolidines **12** could be developed using *N*-sulfonyl imines **7** instead of *N*-sulfinyl imines **10**, as the reaction in batch has been previously reported.^{241, 308} For instance, the reduction of *p*-peroxyquinol **2a** performed in batch is promising to be transferred to the flow setup as it gave quantitative yields of *p*-quinol **2a'** and the only by-product DMSO would not interfere in subsequent steps.

8.1. Final words

Continuous flow photochemical processes have increasingly gained interest from both the scientific community and industries as a rapid and safe enabling tool for the synthesis of complex natural products and pharmaceutical compounds. However, the scalability of these processes is still limited, and the development of new reactor designs is needed to enable further breakthroughs.

In this PhD Thesis, the applications of high-pressure continuous flow photooxidations using singlet oxygen in supercritical CO₂ were further explored using a custom-built high-pressure flow system designed at the University of Nottingham. The photooxidation of *p*-substituted phenols provided a platform for multigram-scale telescoped syntheses of 1,2,4-trioxanes and 1,4-benzoquinones, both of which are scaffolds with potential medicinal properties such as antimalarial and anticancer. Although attempts to synthesise 1,2,4-dioxazinanes and 1,3-oxazolidines using this platform were unsuccessful, further studies could be conducted to find suitable conditions for these reactions using imines with different substituents whilst avoiding their hydrolysis.

As more studies are published showing the scalability, efficiency, and long-term cost benefits of continuous flow photochemical reactions, I anticipate wider uptake of these processes in chemical and pharmaceutical industries. In particular, I hope that industries keep developing more atom efficient and sustainable synthetic routes, for example using singlet oxygen as a traceless reagent and supercritical CO₂ as an alternative solvent.

Braira Abreu

9. References

1. Hartman, R. L., Flow chemistry remains an opportunity for chemists and chemical engineers. *Curr. Opin. Chem. Eng.* **2020**, *29*, 42-50.
2. Kappe, C. O., Continuous flow processing in the pharma industry – an unstoppable trend? *Eur. Pharm. Rev.* **2015**, *20*, 37-42.
3. Plutschack, M. B.; Pieber, B.; Gilmore, K.; Seeberger, P. H., The Hitchhiker's Guide to Flow Chemistry. *Chem. Rev.* **2017**, *117*, 11796-11893.
4. De Santis, P.; Meyer, L.-E.; Kara, S., The rise of continuous flow biocatalysis – fundamentals, very recent developments and future perspectives. *React. Chem. Eng.* **2020**, *5*, 2155-2184.
5. Guidi, M.; Seeberger, P. H.; Gilmore, K., How to approach flow chemistry. *Chem. Soc. Rev.* **2020**, *49*, 8910-8932.
6. Akwi, F. M.; Watts, P., Continuous flow chemistry: where are we now? Recent applications, challenges and limitations. *Chem. Commun.* **2018**, *54*, 13894-13928.
7. Baumann, M.; Moody, T. S.; Smyth, M.; Wharry, S., A perspective on continuous flow chemistry in the pharmaceutical industry. *Org. Process Res. Dev.* **2020**, *24*, 1802-1813.
8. Bogdan, A. R.; Dombrowski, A. W., Emerging trends in flow chemistry and applications to the pharmaceutical industry. *J. Med. Chem.* **2019**, *62*, 6422-6468.
9. Hughes, D. L., Applications of Flow Chemistry in the Pharmaceutical Industry—Highlights of the Recent Patent Literature. *Org. Process Res. Dev.* **2020**, *24*, 1850-1860.
10. Gérardy, R.; Emmanuel, N.; Toupay, T.; Kassin, V. E.; Tshibalonza, N. N.; Schmitz, M.; Monbaliu, J. C. M., Continuous flow organic chemistry: successes and pitfalls at the interface with current societal challenges. *Eur. J. Org. Chem.* **2018**, *2018*, 2301-2351.
11. Vapourtec R-series. <https://www.vapourtec.com> (13th June 2021),
12. Tube in Tube Membrane Reactor. <https://www.cambridgeactordesign.com/tube-in-tube-reactor/gastropod-membrane-reactor.html> (13th June 2021),
13. Ammonite. <https://www.cambridgeactordesign.com/ammonite> (13th June 2021),
14. Schwolow, S.; Neumüller, A.; Abahmane, L.; Kockmann, N.; Röder, T., Design and application of a millistructured heat exchanger reactor for an energy-efficient process. *Chem. Eng. Process. - Process Intensif.* **2016**, *108*, 109-116.
15. Reckamp, J. M.; Bindels, A.; Duffield, S.; Liu, Y. C.; Bradford, E.; Ricci, E.; Susanne, F.; Rutter, A., Mixing Performance Evaluation for Commercially Available Micromixers Using Villermaux–Dushman Reaction Scheme with the Interaction by Exchange with the Mean Model. *Org. Process Res. Dev.* **2017**, *21*, 816-820.

16. Jong, T.; Bradley, M., Flow-Mediated Synthesis of Boc, Fmoc, and Ddiv Monoprotected Diamines. *Org. Lett.* **2015**, *17*, 422-425
17. Straathof, N. J.; Cramer, S. E.; Hessel, V.; Noël, T., Practical photocatalytic trifluoromethylation and hydrotrifluoromethylation of styrenes in batch and flow. *Angew. Chem.* **2016**, *128*, 15778-15782.
18. Dallinger, D.; Gutmann, B.; Kappe, C. O., The Concept of Chemical Generators: On-Site On-Demand Production of Hazardous Reagents in Continuous Flow. *Acc. Chem. Res.* **2020**, *53*, 1330-1341.
19. Lehmann, H., A scalable and safe continuous flow procedure for in-line generation of diazomethane and its precursor MNU. *Green Chem.* **2017**, *19*, 1449-1453.
20. Mohamed, D. K. B.; Yu, X.; Li, J.; Wu, J., Reaction screening in continuous flow reactors. *Tetrahedron Lett.* **2016**, *57*, 3965-3977.
21. Ingham, R. J.; Battilocchio, C.; Hawkins, J. M.; Ley, S. V., Integration of enabling methods for the automated flow preparation of piperazine-2-carboxamide. *Beilstein J. Org. Chem.* **2014**, *10*, 641-652.
22. Weeranoppanant, N.; Adamo, A., In-Line Purification: A Key Component to Facilitate Drug Synthesis and Process Development in Medicinal Chemistry. *ACS Med. Chem. Lett.* **2020**, *11*, 9-15.
23. Dai, C.; Snead, D. R.; Zhang, P.; Jamison, T. F., Continuous-Flow Synthesis and Purification of Atropine with Sequential In-Line Separations of Structurally Similar Impurities. *J. Flow Chem.* **2015**, *5*, 133-138.
24. Deng, Q.; Lei, Q.; Shen, R.; Chen, C.; Zhang, L., The continuous kilogram-scale process for the synthesis of 2,4,5-trifluorobromobenzene via Gattermann reaction using microreactors. *Chem. Eng. J.* **2017**, *313*, 1577-1582.
25. Kolin, A., Demonstration of Parabolic Velocity Distribution in Laminar Flow. *Am. J. Phys.* **1953**, *21*, 619-620.
26. Godfrey, R. C.; Green, N. J.; Nichol, G. S.; Lawrence, A. L., Total synthesis of brevianamide A. *Nature Chem.* **2020**, *12*, 615-619.
27. Yang, Z., The Journey of Schinortriterpenoid Total Syntheses. *Acc. Chem. Res.* **2019**, *52*, 480-491.
28. Nicolaou, K. C.; Yang, Z.; Liu, J. J.; Ueno, H.; Nantermet, P. G.; Guy, R. K.; Claiborne, C. F.; Renaud, J.; Couladouros, E. A.; Paulvannan, K.; Sorensen, E. J., Total synthesis of taxol. *Nature* **1994**, *367*, 630-634.
29. Bloemendal, V. R. L. J.; Janssen, M. A. C. H.; van Hest, J. C. M.; Rutjes, F. P. J. T., Continuous one-flow multi-step synthesis of active pharmaceutical ingredients. *React. Chem. Eng.* **2020**, *5*, 1186-1197.
30. Jiao, J.; Nie, W.; Yu, T.; Yang, F.; Zhang, Q.; Aihemaiti, F.; Yang, T.; Liu, X.; Wang, J.; Li, P., Multi-Step Continuous-Flow Organic Synthesis: Opportunities and Challenges. *Chem. Eur. J.* **2021**, *27*, 4817-4838.

31. Porta, R.; Benaglia, M.; Puglisi, A., Flow Chemistry: Recent Developments in the Synthesis of Pharmaceutical Products. *Org. Process Res. Dev.* **2016**, *20*, 2-25.
32. Pastre, J. C.; Browne, D. L.; Ley, S. V., Flow chemistry syntheses of natural products. *Chem. Soc. Rev.* **2013**, *42*, 8849-8869.
33. Britton, J.; Raston, C. L., Multi-step continuous-flow synthesis. *Chem. Soc. Rev.* **2017**, *46*, 1250-1271.
34. Jaman, Z.; Sobreira, T. J.; Mufti, A.; Ferreira, C. R.; Cooks, R. G.; Thompson, D. H., Rapid On-Demand Synthesis of Lomustine under Continuous Flow Conditions. *Org. Process Res. Dev.* **2019**, *23*, 334-341.
35. Russell, M. G.; Jamison, T. F., Seven-Step Continuous Flow Synthesis of Linezolid Without Intermediate Purification. *Angew. Chem. Int. Ed.* **2019**, *58*, 7678-7681.
36. Corcoran, S., Unclogging the problems of flow chemistry. *Chemistry World* **2011**, *8*, 23-23.
37. Sedelmeier, J.; Ley, S. V.; Baxendale, I. R.; Baumann, M., KMnO₄-Mediated Oxidation as a Continuous Flow Process. *Org. Lett.* **2010**, *12*, 3618-3621.
38. White, T. D.; Alt, C. A.; Cole, K. P.; Groh, J. M.; Johnson, M. D.; Miller, R. D., How to Convert a Walk-in Hood into a Manufacturing Facility: Demonstration of a Continuous, High-Temperature Cyclization to Process Solids in Flow. *Org. Process Res. Dev.* **2014**, *18*, 1482-1491.
39. Nightingale, A. M.; Phillips, T. W.; Bannock, J. H.; De Mello, J. C., Controlled multistep synthesis in a three-phase droplet reactor. *Nat. Commun.* **2014**, *5*, 1-8.
40. Hook, B. D. A.; Dohle, W.; Hirst, P. R.; Pickworth, M.; Berry, M. B.; Booker-Milburn, K. I., A Practical Flow Reactor for Continuous Organic Photochemistry. *J. Org. Chem.* **2005**, *70*, 7558-7564.
41. Siopa, F.; António, J. P. M.; Afonso, C. A. M., Flow-Assisted Synthesis of Bicyclic Aziridines via Photochemical Transformation of Pyridinium Salts. *Org. Process Res. Dev.* **2018**, *22*, 551-556.
42. Amara, Z.; Poliakoff, M.; Duque, R.; Geier, D.; Franciò, G.; Gordon, C. M.; Meadows, R. E.; Woodward, R.; Leitner, W., Enabling the Scale-Up of a Key Asymmetric Hydrogenation Step in the Synthesis of an API Using Continuous Flow Solid-Supported Catalysis. *Org. Process Res. Dev.* **2016**, *20*, 1321-1327.
43. Noël, T.; Cao, Y.; Laudadio, G., The Fundamentals Behind the Use of Flow Reactors in Electrochemistry. *Acc. Chem. Res.* **2019**, *52*, 2858-2869.
44. Blanco-Ania, D.; Rutjes, F. P., Continuous-flow chemistry in chemical education. *J. Flow Chem.* **2017**, *7*, 157-158.
45. Coley, C. W.; Thomas, D. A.; Lummiss, J. A. M.; Jaworski, J. N.; Breen, C. P.; Schultz, V.; Hart, T.; Fishman, J. S.; Rogers, L.; Gao, H.; Hicklin, R. W.; Plehiers, P. P.; Byington, J.; Piotti, J. S.; Green, W. H.; Hart, A. J.; Jamison, T. F.; Jensen, K. F., A robotic platform for flow synthesis of organic compounds informed by AI planning. *Science* **2019**, *365*, eaax1566.

46. Trommsdorff, H., Ueber Santonin. *Ann. Pharm.* **1834**, *11*, 190-207.
47. Ciamician, G., The photochemistry of the future. *Science* **1912**, *36*, 385-394.
48. Glusac, K., What has light ever done for chemistry? *Nature Chem.* **2016**, *8*, 734-735.
49. Oelgemoller, M.; Jung, C.; Mattay, J., Green photochemistry: Production of fine chemicals with sunlight. *Pure Appl. Chem.* **2007**, *79*, 1939-1947.
50. Talukdar, J.; Wong, E. H. S.; Mathur, V. K., Caprolactam production by direct solar flux. *Sol. Energy* **1991**, *47*, 165-171.
51. Ravelli, D.; Protti, S.; Neri, P.; Fagnoni, M.; Albini, A., Photochemical technologies assessed: the case of rose oxide. *Green Chem.* **2011**, *13*, 1876-1884.
52. Turconi, J.; Griolet, F.; Guevel, R.; Oddon, G.; Villa, R.; Geatti, A.; Hvala, M.; Rossen, K.; Göller, R.; Burgard, A., Semisynthetic Artemisinin, the Chemical Path to Industrial Production. *Org. Process Res. Dev.* **2014**, *18*, 417-422.
53. Knowles, J. P.; Elliott, L. D.; Booker-Milburn, K. I., Flow photochemistry: Old light through new windows. *Beilstein J. Org. Chem.* **2012**, *8*, 2025-2052.
54. Rehm, T. H., Flow Photochemistry as a Tool in Organic Synthesis. *Chem. Eur. J.* **2020**, *26*, 16952-16974.
55. Sambiasco, C.; Noël, T., Flow photochemistry: Shine some light on those tubes! *Trends Chem.* **2020**, *2*, 92-106.
56. Williams, J. D.; Kappe, C. O., Recent Advances towards Sustainable Flow Photochemistry. *Curr. Opin. Green Sustainable Chem.* **2020**, 100351.
57. Cambie, D.; Bottecchia, C.; Straathof, N. J. W.; Hessel, V.; Noel, T., Applications of Continuous-Flow Photochemistry in Organic Synthesis, Material Science, and Water Treatment. *Chem. Rev.* **2016**, *116*, 10276-10341.
58. Raab, O., Über die wirkung Fluorescirender Stoffe auf Infusorien. *Z. Biol.* **1900**, *39*, 524-546.
59. Mulliken, R. S., Interpretation of the Atmospheric Oxygen Bands; Electronic Levels of the Oxygen Molecule. *Nature* **1928**, *122*, 505.
60. Mulliken, R. S., The Interpretation of Band Spectra Part III. Electron Quantum Numbers and States of Molecules and Their Atoms. *Rev. Mod. Phys.* **1932**, *4*, 1-86.
61. Kautsky, H.; de Bruijn, H., Die Aufklärung der Photolumineszenztilgung fluorescierender Systeme durch Sauerstoff: Die Bildung aktiver, diffusionsfähiger Sauerstoffmoleküle durch Sensibilisierung. *Naturwissenschaften* **1931**, *19*, 1043.
62. Gaffron, H., Über den Mechanismus der Sauerstoff-Aktivierung durch belichtete Farbstoffe, II. Mitteil.: Photoxydation im nahen Infrarot. *Ber. Dtsch. Chem. Ges.* **1935**, *68*, 1409-1411.
63. Kautsky, H., Reciprocal Action between Sensitizers and Oxygen in Light. *Biochem. Z.* **1937**, *291*, 271-284.
64. Khan, A. U.; Kasha, M., Red Chemiluminescence of Molecular Oxygen in Aqueous Solution. *J. Chem. Phys.* **1963**, *39*, 2105-2106.

65. Foote, C. S., Photosensitized oxygenations and the role of singlet oxygen. *Acc. Chem. Res.* **1968**, *1*, 104-110.
66. Krumova, K.; Cosa, G., Overview of Reactive Oxygen Species. In *Singlet Oxygen: Applications in Biosciences and Nanosciences*, 2016; Vol. 1, pp 1-21.
67. Imlay, J. A., Pathways of Oxidative Damage. *Annu. Rev. Microbiol.* **2003**, *57*, 395-418.
68. Scurlock, R. D.; Wang, B.; Ogilby, P. R., Chemical Reactivity of Singlet Sigma Oxygen ($b1\Sigma_g^+$) in Solution. *J. Am. Chem. Soc.* **1996**, *118*, 388-392.
69. Bodesheim, M.; Schmidt, R., Chemical Reactivity of Sigma Singlet Oxygen $O_2(1\Sigma_g^+)$. *J. Phys. Chem. A* **1997**, *101*, 5672-5677.
70. DeRosa, M. C.; Crutchley, R. J., Photosensitized singlet oxygen and its applications. *Coordin. Chem. Rev.* **2002**, *233*, 351-371.
71. Foote, C. S.; Clennan, E. L., Properties and Reactions of Singlet Dioxygen. In *Active oxygen in chemistry*, 1995; Vol. 2, pp 105-106.
72. Ogilby, P. R.; Foote, C. S., Chemistry of singlet oxygen. 42. Effect of solvent, solvent isotopic substitution, and temperature on the lifetime of singlet molecular oxygen. *J. Am. Chem. Soc.* **1983**, *105*, 3423-3430.
73. Hurst, J. R.; Schuster, G. B., Nonradiative relaxation of singlet oxygen in solution. *J. Am. Chem. Soc.* **1983**, *105*, 5756-5760.
74. Dupuis, P.; Roberge, R.; Sandorfy, C., The very low ionization potentials of porphyrins and the possible role of rydberg states in photosynthesis. *Chem. Phys. Lett.* **1980**, *75*, 434-437.
75. Adam, W.; Kazakov, D. V.; Kazakov, V. P., Singlet-Oxygen Chemiluminescence in Peroxide Reactions. *Chem. Rev.* **2005**, *105*, 3371-3387.
76. Fudickar, W.; Linker, T., Intermediates in the Formation and Thermolysis of Peroxides from Oxidations with Singlet Oxygen. *Aust. J. Chem.* **2014**, *67*, 320-327.
77. Carreño, M. C.; González-López, M.; Urbano, A., Oxidative de-aromatization of para-alkyl phenols into para-peroxyquinols and para-quinols mediated by oxone as a source of singlet oxygen. *Angew. Chem. Int. Ed.* **2006**, *45*, 2737-2741.
78. Ghogare, A. A.; Greer, A., Using Singlet Oxygen to Synthesize Natural Products and Drugs. *Chem. Rev.* **2016**, *116*, 9994-10034.
79. Wang, W.; Shi, R.; Zhang, W.; Sun, H.; Ge, X.; Li, C., Enhanced generation efficiency of singlet oxygen for methylene blue released from hydroxyapatite-MB@tannic acid-Fe(III) ions. *Pigm. Resin Technol.* **2019**, *48*, 185-196.
80. Chesneau, E.; Neckers, D. C., Electron transfer sensitized photobleaching of rose bengal induced by triplet benzophenones. *J. Photochem. Photobiol A* **1988**, *42*, 269.
81. Bonnett, R., Photosensitizers of the porphyrin and phthalocyanine series for photodynamic therapy. *Chem. Soc. Rev.* **1995**, *24*, 19-33.
82. Montalti, M., *Handbook of photochemistry*. CRC/Taylor & Francis 2006.

83. El'tsov, A. V., *Organic Photochromes*. Springer1990.
84. Monnerie, N.; Ortner, J., Economic Evaluation of the Industrial Photosynthesis of Rose Oxide via Lamp or Solar Operated Photooxidation of Citronellol. *J. Sol. Energy Eng.* **2001**, *123*, 171-174.
85. McConkey, B. J.; Hewitt, L. M.; Dixon, D. G.; Greenberg, B. M., Natural Sunlight Induced Photooxidation of Naphthalene in Aqueous Solution. *Water Air Soil Pollut.* **2002**, *136*, 347-359.
86. Oelgemoller, M., Solar Photochemical Synthesis: From the Beginnings of Organic Photochemistry to the Solar Manufacturing of Commodity Chemicals. *Chem. Rev.* **2016**, *116*, 9664-9682.
87. Shankar, R.; Shim, W. J.; An, J. G.; Yim, U. H., A practical review on photooxidation of crude oil: Laboratory lamp setup and factors affecting it. *Water Res.* **2015**, *68*, 304-315.
88. Lapkin, A. A.; Boddu, V. M.; Aliev, G. N.; Goller, B.; Polisski, S.; Kovalev, D., Photo-oxidation by singlet oxygen generated on nanoporous silicon in a LED-powered reactor. *Chem. Eng. J.* **2008**, *136*, 331-336.
89. Foote, C. S., Definition of Type I and Type II Photosensitized Oxidation. *Photochem. Photobiol.* **1991**, *54*, 659.
90. Quinn, J. C.; Kessell, A.; Weston, L. A., Secondary Plant Products Causing Photosensitization in Grazing Herbivores: Their Structure, Activity and Regulation. *Int. J. Mol. Sci.* **2014**, *15*, 1441-1465.
91. O'Mara, P.; Farrell, A.; Bones, J.; Twomey, K., Staying alive! Sensors used for monitoring cell health in bioreactors. *Talanta* **2018**, *176*, 130-139.
92. Greer, A., Christopher Foote's Discovery of the Role of Singlet Oxygen [1O₂ (1Δg)] in Photosensitized Oxidation Reactions. *Acc. Chem. Res.* **2006**, *39*, 797-804.
93. Hone, C. r. A.; Kappe, C. O., The Use of Molecular Oxygen for Liquid Phase Aerobic Oxidations in Continuous Flow. *Topics Curr. Chem.* **2020**, *377*, 67-110.
94. Gast, S.; Matthies, J. H.; Tuttlies, U. S.; Nieken, U., A Novel Experimental Setup for Kinetic Studies of Toluene Oxidation in the Homogeneous Liquid Phase. *Chem. Eng. Technol.* **2017**, *40*, 1445-1452.
95. Khan, F. I.; Ghoshal, A. K., Removal of Volatile Organic Compounds from polluted air. *J. Loss Prevent. Proc. Ind.* **2000**, *13*, 527-545.
96. DeSimone, J. M.; Guan, Z.; Elsbernd, C. S., Synthesis of Fluoropolymers in Supercritical Carbon Dioxide. *Science* **1992**, *257*, 945-947.
97. Clark, J. H.; Tavener, S. J., Alternative Solvents: Shades of Green. *Org. Process Res. Dev.* **2007**, *11*, 149-155.
98. Noyori, R., Supercritical Fluids: Introduction. *Chem. Rev.* **1999**, *99*, 353-354.
99. Heřmanská, M.; Stefánsson, A.; Scott, S., Supercritical fluids around magmatic intrusions: IDDP-1 at Krafla, Iceland. *Geothermics* **2019**, *78*, 101-110.

100. Trachenko, K.; Brazhkin, V. V.; Bolmatov, D., Dynamic transition of supercritical hydrogen: Defining the boundary between interior and atmosphere in gas giants. *Phys. Rev. E* **2014**, *89*, 032126.
101. Nahar, L.; Sarker, S. D., Supercritical fluid extraction in natural products analyses. In *Methods in molecular biology*, 2012; Vol. 864, p 43.
102. Beckman, E. J., Supercritical and near-critical CO₂ in green chemical synthesis and processing. *J. Supercrit. Fluids* **2004**, *28*, 121-191.
103. Savage, P. E., Organic Chemical Reactions in Supercritical Water. *Chem. Rev.* **1999**, *99*, 603-622.
104. Vadillo, V.; Sánchez-Oneto, J.; Portela, J. R.; Ossa, E. J. M., Problems in Supercritical Water Oxidation Process and Proposed Solutions. *Ind. Eng. Chem. Res.* **2013**, *52*, 7617-7629.
105. Beach, E. S.; Cui, Z.; Anastas, P. T., Green Chemistry: A design framework for sustainability. *Energy Environ. Sci.* **2009**, *2*, 1038-1049.
106. Mikami, K., *Green Reaction Media in Organic Synthesis*. 2005.
107. Andrzej, W.; Mirosław, M.; Sebastian, R., Analysis of pipeline transportation systems for carbon dioxide sequestration. *Arch. Thermodyn.* **2014**, *35*, 117-140.
108. Zosel, K., Separation with Supercritical Gases: Practical Applications. *Angew. Chem. Int. Ed.* **1978**, *17*, 702-709.
109. Kaplitz, A. S.; Mostafa, M. E.; Calvez, S. A.; Edwards, J. L.; Grinias, J. P., Two-dimensional separation techniques using supercritical fluid chromatography. *J. Sep. Sci.* **2021**, *44*, 426-437.
110. Cooper, A. I., Polymer synthesis and processing using supercritical carbon dioxide. *J. Mater. Chem.* **2000**, *10*, 207-234.
111. Montero, G. A.; Smith, C. B.; Hendrix, W. A.; Butcher, D. L., Supercritical Fluid Technology in Textile Processing: An Overview. *Ind. Eng. Chem. Res.* **2000**, *39*, 4806-4812.
112. Qi, H.; Gui, N.; Yang, X.; Tu, J.; Jiang, S., The application of supercritical CO₂ in nuclear engineering: A review. *J. Comp. Mult. Flows* **2018**, *10*, 149-158.
113. Padrela, L.; Rodrigues, M. A.; Duarte, A.; Dias, A. M. A.; Braga, M. E. M.; de Sousa, H. C., Supercritical carbon dioxide-based technologies for the production of drug nanoparticles/nanocrystals – A comprehensive review. *Adv. Drug Deliv. Rev.* **2018**, *131*, 22-78.
114. Bourne, R. A.; Han, X.; Poliakov, M.; George, M. W., Cleaner Continuous Photo-Oxidation Using Singlet Oxygen in Supercritical Carbon Dioxide. *Angew. Chem. Int. Ed.* **2009**, *48*, 5322-5325.
115. Worrall, D. R.; Abdel-Shafi, A. A.; Wilkinson, F., Factors Affecting the Rate of Decay of the First Excited Singlet State of Molecular Oxygen O₂(¹Δ_{g) in Supercritical Fluid Carbon Dioxide. *J. Phys. Chem. A* **2001**, *105*, 1270-1276.}
116. Jocelyn, P.; Julian, E., Supercritical carbon dioxide: a solvent like no other. *Beilstein J. Org. Chem.* **2014**, *10*, 1878-1895.

117. Casas, L.; Mantell, C.; Rodríguez, M.; Torres, A.; Macías, F. A.; Martínez de la Ossa, E., Effect of the addition of cosolvent on the supercritical fluid extraction of bioactive compounds from *Helianthus annuus* L. *J. Supercrit. Fluids* **2007**, *41*, 43-49.
118. Fritzsche, M., Note sur les carbures d'hydrogène solides, tirés du goudron de houille. *C. R. Chim.* **1867**, *64*, 1035-1037.
119. Windaus, A.; Brunken, J., Über die photochemische Oxydation des Ergosterins. *Liebigs Ann. Chem.* **1928**, *460*, 225-235.
120. Bergmann, W.; McLean, M. J., Transannular Peroxides. *Chem. Rev.* **1941**, *28*, 367-394.
121. Pibiri, I.; Buscemi, S.; Piccionello, A. P.; Pace, A., Photochemically produced singlet oxygen: applications and perspectives. *ChemPhotoChem* **2018**, *2*, 535-547.
122. Bourne, R. A.; Han, X.; Chapman, A. O.; Arrowsmith, N. J.; Kawanami, H.; Poliakoff, M.; George, M. W., Homogeneous photochemical oxidation via singlet O(2) in supercritical CO(2). *Chem. Commun.* **2008**, 4457-4459.
123. Han, X.; Bourne, R. A.; Poliakoff, M.; George, M. W., Strategies for cleaner oxidations using photochemically generated singlet oxygen in supercritical carbon dioxide. *Green Chem.* **2009**, *11*, 1787-1792.
124. Han, X.; Bourne, R. A.; Poliakoff, M.; George, M. W., Immobilised photosensitisers for continuous flow reactions of singlet oxygen in supercritical carbon dioxide. *Chem. Sci.* **2011**, *2*, 1059-1067.
125. Hall, J. F. B.; Han, X.; Poliakoff, M.; Bourne, R. A.; George, M. W., Maximising the efficiency of continuous photo-oxidation with singlet oxygen in supercritical CO2 by use of fluorous biphasic catalysis. *Chem. Commun.* **2012**, *48*, 3073-3075.
126. Hall, J. F. B.; Bourne, R. A.; Han, X.; Earley, J. H.; Poliakoff, M.; George, M. W., Synthesis of antimalarial trioxanes via continuous photo-oxidation with O-1(2) in supercritical CO2. *Green Chem.* **2013**, *15*, 177-180.
127. Amara, Z.; Bellamy, J. F. B.; Horvath, R.; Miller, S. J.; Beeby, A.; Burgard, A.; Rossen, K.; Poliakoff, M.; George, M. W., Applying green chemistry to the photochemical route to artemisinin. *Nature Chem.* **2015**, *7*, 489-495.
128. Kopetzki, D.; Lévesque, F.; Seeberger, P. H., A Continuous-Flow Process for the Synthesis of Artemisinin. *Chem. Eur. J.* **2013**, *19*, 5450-5456.
129. Wu, L. Q.; Abada, Z.; Lee, D. S.; Poliakoff, M.; George, M. W., Combining engineering and chemistry for the selective continuous production of four different oxygenated compounds by photo-oxidation of cyclopentadiene using liquid and supercritical CO2 as solvents. *Tetrahedron* **2018**, *74*, 3107-3112.
130. Wu, L. Q.; Lee, D. S.; Boufroua, H.; Poliakoff, M.; George, M. W., Photooxidation of Fulvenes in a Continuous Flow Photoreactor using Carbon Dioxide as a Solvent. *ChemPhotoChem* **2018**, *2*, 580-585.
131. Metzger, J.; Koll, P., High-pressure, high-temperature reactions in a flow reactor. Inter-molecular ene reactions in a high-pressure high-temperature flow apparatus. *Angew. Chem. Int. Ed.* **1979**, *18*, 70-71.

132. Metzger, J.; Hartmanns, J.; Koll, P., High-pressure, high-temperature reactions in a flow reactor. Thermic addition of alkanes to alkenes. *Tetrahedron Lett.* **1981**, *22*, 1891-1894.
133. Koll, P.; Metzger, J.; Bronstrup, B., High-pressure, high-temperature reactions in a flow reactor. Degradation of bio-polymers in a high-pressure high-temperature flow reactor. *Makromol. Chem. Rapid Comm.* **1982**, *3*, 365-369.
134. Subramaniam, B.; McHugh, M. A., Reactions in supercritical fluids-a review. *Ind. Eng. Chem. Process Des. Dev.* **1986**, *25*, 1-12.
135. Hawthorne, S. B., Analytical-scale supercritical fluid extraction. *Anal. Chem.* **1990**, *62*, 633A-642A.
136. Adschiri, T.; Hirose, S.; Malaluan, R.; Arai, K., Noncatalytic conversion of cellulose in supercritical and subcritical water. *J. Chem. Eng. Jpn.* **1993**, *26*, 676-680.
137. Lang, X. S.; Akgerman, A.; Bukur, D. B., Steady-state Fischer-Tropsch synthesis in supercritical propane. *Ind. Eng. Chem. Res.* **1995**, *34*, 72-77.
138. Palmer, M.; Ting, S., Applications for supercritical fluid technology in food processing. *Food Chem.* **1995**, *52*, 345-352.
139. Savage, P. E.; Gopalan, S.; Mizan, T. I.; Martino, C. J.; Brock, E. E., Reactions at supercritical conditions: applications and fundamentals. *AIChE J.* **1995**, *41*, 1723-1778.
140. York, P., Strategies for particle design using supercritical fluid technologies. *Pharm. Sci. Technol. Today* **1999**, *2*, 430-440.
141. Banister, J. A.; Lee, P. D.; Poliakoff, M., Flow reactors for preparative chemistry in supercritical-fluid solution - solvent-free synthesis and isolation of Cr(CO)₅(C₂H₄) and (η⁵-C₅H₅)Mn(CO)₂(η²-H₂). *Organometallics* **1995**, *14*, 3876.
142. Hitzler, M. G.; Smail, F. R.; Ross, S. K.; Poliakoff, M., Friedel-Crafts alkylation in supercritical fluids: continuous, selective and clean. *Chem. Commun.* **1998**, 359.
143. Hitzler, M. G.; Smail, F. R.; Ross, S. K.; Poliakoff, M., Selective catalytic hydrogenation of organic compounds in supercritical fluids as a continuous process. *Org. Process Res. Dev.* **1998**, *2*, 137-146.
144. Meehan, N. J.; Sandee, A. J.; Reek, J. N. H.; Kamer, P. C. J.; Leeuwen, P.; Poliakoff, M., Continuous, selective hydroformylation in supercritical carbon dioxide using an immobilised homogeneous catalyst. *Chem. Commun.* **2000**, 1497-1498.
145. Stephenson, P.; Licence, P.; Ross, S. K.; Poliakoff, M., Continuous catalytic asymmetric hydrogenation in supercritical CO₂. *Green Chem.* **2004**, *6*, 521-523.
146. Walsh, B.; Hyde, J. R.; Licence, P.; Poliakoff, M., The automation of continuous reactions in supercritical CO₂: the acid-catalysed etherification of short chain alcohols. *Green Chem.* **2005**, *7*, 456-463.
147. Stephenson, P.; Kondor, B.; Licence, P.; Scovell, K.; Ross, S. K.; Poliakoff, M., Continuous asymmetric hydrogenation in supercritical carbon dioxide using an immobilised homogeneous catalyst. *Adv. Synth. Catal.* **2006**, *348*, 1605-1610.

148. Bourne, R. A.; Stevens, J. G.; Ke, J.; Poliakoff, M., Maximising opportunities in supercritical chemistry: the continuous conversion of levulinic acid to gamma-valerolactone in CO₂. *Chem. Commun.* **2007**, 4632-4634.
149. Amandi, R.; Scovell, K.; Licence, P.; Lotz, T. J.; Poliakoff, M., The synthesis of o-cyclohexylphenol in supercritical carbon dioxide: towards a continuous two-step reaction. *Green Chem.* **2007**, *9*, 797-801.
150. Clark, P.; Poliakoff, M.; Wells, A., Continuous flow hydrogenation of a pharmaceutical intermediate, 4-(3,4-dichlorophenyl)-3,4-dihydro-2H-naphthalenydene -methylamine, in supercritical carbon dioxide. *Adv. Synth. Catal.* **2007**, *349*, 2655-2659.
151. Hall, J. Continuous photo-oxidation with 1O₂ in CO₂. PhD Thesis, University of Nottingham 2014.
152. Wu, L. Applications of photo-oxidation with 1O₂ in multistep reactions. PhD Thesis, University of Nottingham 2019.
153. Osterberg, P. M.; Niemeier, J. K.; Welch, C. J.; Hawkins, J. M.; Martinelli, J. R.; Johnson, T. E.; Root, T. W.; Stahl, S. S., Experimental Limiting Oxygen Concentrations for Nine Organic Solvents at Temperatures and Pressures Relevant to Aerobic Oxidations in the Pharmaceutical Industry. *Org. Process Res. Dev.* **2015**, *19*, 1537-1543.
154. Chapman, A. O. Reactions of molecular oxygen in supercritical carbon dioxide. PhD Thesis, University of Nottingham 2007.
155. Rebsdatt, S.; Mayer, D., Ethylene Glycol. In *Ullmann's Encyclopedia of Industrial Chemistry*, 2000.
156. Dolomanov, O. V.; Bourhis, L. J.; Gildea, R. J.; Howard, J. A. K.; Puschmann, H., OLEX2: a complete structure solution, refinement and analysis program. *J. Appl. Crystallogr.* **2009**, *42*, 339-341.
157. Sheldrick, G. M., SHELXT - Integrated space-group and crystal-structure determination. *Acta Crystallogr., Sect. A: Found. Crystallogr.* **2015**, *71*, 3-8.
158. Sheldrick, G. M., Crystal structure refinement with SHELXL. *Acta Crystallogr., Sect. C: Cryst. Struct. Commun.* **2015**, *71*, 3-8.
159. Roche, S. P.; Porco Jr., J. A., Dearomatization Strategies in the Synthesis of Complex Natural Products. *Angew. Chem. Int. Ed.* **2011**, *50*, 4068-4093.
160. Zheng, C.; You, S.-L., Advances in Catalytic Asymmetric Dearomatization. *ACS Cent. Sci.* **2021**, *7*, 432-444.
161. Quideau, S.; Pouységu, L.; Deffieux, D., Oxidative Dearomatization of Phenols: Why, How and What For? *Synlett* **2008**, 467-495.
162. Fan, R.; Ding, Q.; Ye, Y., Recent Advances in Phenol Dearomatization and Its Application in Complex Syntheses. *Synthesis* **2012**, *45*, 1-16.
163. Sun, W.; Li, G.; Hong, L.; Wang, R., Asymmetric dearomatization of phenols. *Org. Biomol. Chem.* **2016**, *14*, 2164-2176.

164. Baker Dockrey, S. A.; Lukowski, A. L.; Becker, M. R.; Narayan, A. R. H., Biocatalytic site- and enantioselective oxidative dearomatization of phenols. *Nature Chem.* **2018**, *10*, 119-125.
165. Casteel, A. D., Peroxy natural products. *Nat. Prod. Rep.* **1999**, *16*, 55-73.
166. Ding, L.; Maier, A.; Fiebig, H.-H.; Lin, W.-H.; Peschel, G.; Hertweck, C., Kandenols A–E, Eudesmenes from an Endophytic Streptomyces sp. of the Mangrove Tree *Kandelia candel.* *J. Nat. Prod.* **2012**, *75*, 2223-2227.
167. Niu, X.; Li, S.; Zhao, Q.; Lin, Z.; Sun, H.; Lu, Y.; Zhang, L.; Zheng, Q., A novel diterpene hydroperoxide, glutinosin C, from *Isodon glutinosa*. *Tetrahedron Lett.* **2002**, *43*, 5277-5280.
168. Kim, J. H.; Kim, D. H.; Baek, S. H.; Lee, H. J.; Kim, M. R.; Kwon, H. J.; Lee, C.-H., Rengyolone inhibits inducible nitric oxide synthase expression and nitric oxide production by down-regulation of NF- κ B and p38 MAP kinase activity in LPS-stimulated RAW 264.7 cells. *Biochem. Pharmacol.* **2006**, *71*, 1198-1205.
169. Endo, K.; Seya, K.; Hikino, H., Biogenesis-like transformation of solidoside to rengyol and its related cyclohexyletanoids of *forsythia suspensa*. *Tetrahedron* **1989**, *45*, 3673-3682.
170. Sidde, L. S. L.; Malathi, S.; Malathi, S. S., A brief review on *Clerodendrum indicum*. *Int. j. indig. herbs drugs.* **2018**, *3*, 1-4.
171. Barradas, S.; Carreño, M. C.; González-López, M.; Latorre, A.; Urbano, A., Direct Stereocontrolled Synthesis of Polyoxygenated Hydrobenzofurans and Hydrobenzopyrans from p-Peroxy Quinols. *Org. Lett.* **2007**, *9*, 5019-5022.
172. Tong, G.; Liu, Z.; Li, P., Stereocontrolled Construction of the Tricyclic Framework of Tiglianes and Daphnanes by an Oxidative Dearomatization Approach. *Org. Lett.* **2014**, *16*, 2288-2291.
173. Kalstabakken, K. A.; Harned, A. M., Asymmetric transformations of achiral 2,5-cyclohexadienones. *Tetrahedron* **2014**, *70*, 9571-9585.
174. Wipf, P.; Kim, Y., . π -Facial Selectivity in Nucleophilic Additions to 4,4-Disubstituted Dienones: Experimental Support for Electrostatic Control. *J. Am. Chem. Soc.* **1994**, *116*, 11678-11688.
175. Ward, J.; Johnson, A.; Clark, G.; Caprio, V., The Synthesis of Functionalised Bicyclo[3.3.1]nonanes Related to Huperzine A. *Synthesis* **2009**, *20*, 3411-3418.
176. Carreño, M. C.; Merino, E.; Ribagorda, M.; Somoza, Á.; Urbano, A., Enantioselective Synthesis of Natural Polyoxygenated Cyclohexanes and Cyclohexenes from [(p-Tolylsulfinyl)methyl]-p-quinols. *Chem. Eur. J.* **2007**, *13*, 1064-1077.
177. Hayashi, Y.; Gotoh, H.; Tamura, T.; Yamaguchi, H.; Masui, R.; Shoji, M., Cysteine-Derived Organocatalyst in a Highly Enantioselective Intramolecular Michael Reaction. *J. Am. Chem. Soc.* **2005**, *127*, 16028-16029.
178. Jones, K. M.; Hillringhaus, T.; Klussmann, M., A singlet oxygen approach to oxaspirocycles. *Tetrahedron Lett.* **2013**, *54*, 3294-3297.

179. Fischer, J.; Serier-Brault, H.; Nun, P.; Coeffard, V., Substrate-Selectivity in Catalytic Photooxygenation Processes Using a Quinine-BODIPY System. *Synlett* **2020**, *31*, 463-468.
180. Dubnikova, F.; Kosloff, R.; Almog, J.; Zeiri, Y.; Boese, R.; Itzhaky, H.; Alt, A.; Keinan, E., Decomposition of triacetone triperoxide is an entropic explosion. *J. Am. Chem. Soc.* **2005**, *127*, 1146-1159.
181. Dussault, P., Working with organic peroxides in the academic lab. In *Organic Peroxides: Safety Issues* University of Nebraska: Digital Commons, 2018.
182. Kraszewski, K.; Tomczyk, I.; Drabinska, A.; Bienkowski, K.; Solarska, R.; Kalek, M., Mechanism of Iodine(III)-Promoted Oxidative Dearomatizing Hydroxylation of Phenols: Evidence for a Radical-Chain Pathway. *Chem. Eur. J.* **2020**, *26*, 11584-11592.
183. Houk, K. N., Frontier molecular orbital theory of cycloaddition reactions. *Acc. Chem. Res.* **1975**, *8*, 361-369.
184. Leach, A. G.; Houk, K. N., Diels–Alder and ene reactions of singlet oxygen, nitroso compounds and triazolinediones: transition states and mechanisms from contemporary theory. *Chem. Commun.* **2002**, 1243-1255.
185. Aubry, J.; Pierlot, C.; Rigaudy, J.; Schmidt, R., Reversible Binding of Oxygen to Aromatic Compounds. *Acc. Chem. Res.* **2003**, *36*, 668-675.
186. Al-Nu'airat, J.; Dlugogorski, B. Z.; Gao, X.; Zeinali, N.; Skut, J.; Westmoreland, P. R.; Oluwoye, I.; Altarawneh, M., Reaction of phenol with singlet oxygen. *Phys. Chem. Chem. Phys.* **2019**, *21*, 171-183.
187. Gallegos, M.; Costales, A.; Pendas, A. M., Energetic descriptors of steric hindrance in real space: an improved IQA picture. *ChemPhysChem* **2021**, *22*, 775-787.
188. Yamazaki, Y.; Naganuma, J.; Gotoh, H., A theoretical, dynamical evaluation method of the steric hindrance in nitroxide radicals using transition states of model reactions. *Scientific reports* **2019**, *9*, 1-11.
189. Young, S. N., L-tyrosine to alleviate the effects of stress? *J. Psychiatry Neurosci.* **2007**, *32*, 224-224.
190. Page, P. C. B.; Buckley, B. R.; Farah, M. M.; Blacker, A. J., Binaphthalene-Derived Iminium Salt Catalysts for Highly Enantioselective Asymmetric Epoxidation. *Eur. J. Org. Chem.* **2009**, *2009*, 3413-3426.
191. Eske, A.; Ecker, S.; Fendinger, C.; Goldfuss, B.; Jonen, M.; Lefarth, J.; Neudörfl, J.-M.; Spilles, M.; Griesbeck, A. G., Spiro-fused and Annulated 1,2,4-Trioxepane-, 1,2,4-Trioxocane-, and 1,2,4-Trioxonane-Cyclohexadienones: Cyclic Peroxides with Unusual Ring Conformation Dynamics. *Angew. Chem. Int. Ed.* **2018**, *57*, 13770-13774.
192. Kumar, V.; Parmar, V. S.; Samuelson, L. A.; Kumar, J.; Cholli, A. L., Enzyme mediated oxidative polymerization of 4-hydroxybenzyl alcohol for optical applications. *J. Macromol. Sci. A* **2002**, *39*, 1183-1193.
193. Arcas, R.; Peris, E.; Mas-Marzá, E.; Fabregat-Santiago, F., Revealing the contribution of singlet oxygen in the photoelectrochemical oxidation of benzyl alcohol. *Sustainable Energy & Fuels* **2021**, *5*, 956-962.

194. Smith, J. M.; Vitali, F.; Archer, S. A.; Fasan, R., Modular Assembly of Macrocyclic Organo–Peptide Hybrids Using Synthetic and Genetically Encoded Precursors. *Angew. Chem. Int. Ed.* **2011**, *50*, 5075-5080.
195. Rubush, D. M.; Morges, M. A.; Rose, B. J.; Thamm, D. H.; Rovis, T., An Asymmetric synthesis of 1,2,4-trioxane anticancer agents via desymmetrization of peroxyquinols through a Brønsted acid catalysis cascade. *J. Am. Chem. Soc.* **2012**, *134*, 13554-13557.
196. Jung, S.; Inoue, A.; Nakamura, S.; Kishi, T.; Uwamizu, A.; Sayama, M.; Ikubo, M.; Otani, Y.; Kano, K.; Makide, K.; Aoki, J.; Ohwada, T., Conformational Constraint of the Glycerol Moiety of Lysophosphatidylserine Affords Compounds with Receptor Subtype Selectivity. *J. Med. Chem.* **2016**, *59*, 3750-3776.
197. Khan, Abu T.; Ghosh, S.; Choudhury, Lokman H., A Simple and Useful Synthetic Protocol for Selective Deprotection of tert-Butyldimethylsilyl (TBS) Ethers. *Eur. J. Org. Chem.* **2004**, *2004*, 2198-2204.
198. Pratesi, L., *Gazz. Chim. Ital.* **1885**, *14*.
199. Yin, L.-Y.; Hu, Y.-F.; Wang, H.-Y., The remarkable effect of organic salts on 1,3,5-trioxane synthesis. *Pet. Sci.* **2016**, *13*, 770-775.
200. Chatelard, C.; Dodin, M.; Martinez-Franco, R.; Tuel, A., Di- and trioxacyclohexane as structure directing molecules in the synthesis of zeolites omega and ECR-1. *Microporous Mesoporous Mater.* **2021**, *318*, 111015.
201. Suemitsu, C.; Kanazawa, A.; Aoshima, S., The “solid-state” ring-opening cationic polymerization of 1,3,5-trioxane: frozen polymerization for suppression of oligomer formation and synthesis of ultrahigh molecular weight polymers. *Polym. Chem.* **2021**, *12*, 822-830.
202. Teager, D. S.; Murray Jr, R. K., Oxidation of 2,4-didehydroadamantane. *J. Org. Chem.* **1993**, *58*, 5548-5550.
203. Tu, Y., The discovery of artemisinin (qinghaosu) and gifts from Chinese medicine. *Nat. Med.* **2011**, *17*, 1217-1220.
204. Organization, W. H. *World malaria report 2020: 20 years of global progress and challenges*: Geneva, Switzerland, 2020.
205. Jelínková, L.; Jhun, H.; Eaton, A.; Petrovsky, N.; Zavala, F.; Chackerian, B., An epitope-based malaria vaccine targeting the junctional region of circumsporozoite protein. *npj Vaccines* **2021**, *6*, 1-10.
206. Challenger, J. D.; Olivera Mesa, D.; Da, D. F.; Yerbanga, R. S.; Lefèvre, T.; Cohuet, A.; Churcher, T. S., Predicting the public health impact of a malaria transmission-blocking vaccine. *Nat. Commun.* **2021**, *12*, 1-12.
207. Where Malaria Occurs. <https://www.cdc.gov/malaria/about/distribution.html> (11 May 2021),
208. Anopheles Mosquito Facts & Identification. <https://www.orkin.com/other/mosquitoes/anopheles-mosquito> (11 May 2021),

209. Dai, Y.-F.; Zhou, W.-W.; Meng, J.; Du, X.-L.; Sui, Y.-P.; Dai, L.; Wang, P.-Q.; Huo, H.-R.; Sui, F., The pharmacological activities and mechanisms of artemisinin and its derivatives: a systematic review. *Med. Chem. Res.* **2017**, *26*, 867-880.
210. Do Artemisia annua L. compounds have SARS-CoV-2 antiviral potential? <https://www.news-medical.net/news/20210318/Do-Artemisia-annua-L-compounds-have-SARS-CoV-2-antiviral-potential.aspx> (11 May 2021),
211. Webster, H. K.; Lehnert, E. K., Chemistry of artemisinin: an overview. *Trans. R. Soc. Trop. Med. Hyg.* **1994**, *88*, 27-29.
212. Gao, F.; Sun, Z.; Kong, F.; Xiao, J., Artemisinin-derived hybrids and their anticancer activity. *Eur. J. Med. Chem.* **2020**, *188*, 1-14.
213. Efferth, T., Beyond malaria: The inhibition of viruses by artemisinin-type compounds. *Biotechnol. Adv.* **2018**, *36*, 1730-1737.
214. Lin, L.; Mao, X.; Sun, Y.; Cui, H., Antibacterial mechanism of artemisinin / beta-cyclodextrins against methicillin-resistant Staphylococcus aureus (MRSA). *Microb. Pathogen.* **2018**, *118*, 66-73.
215. Bai, X.; Pei, R.; Lei, W.; Zhao, M.; Zhang, J.; Tian, L.; Shang, J., Antidiabetic Effect of Artemether in Db/Db Mice Involves Regulation of AMPK and PI3K/Akt Pathways. *Front. Endocrinol.* **2020**, *11*, 1-9.
216. Li, G.; Yuan, M.; Li, H.; Deng, C.; Wang, Q.; Tang, Y.; Zhang, H.; Yu, W.; Xu, Q.; Zou, Y.; Yuan, Y.; Guo, J.; Jin, C.; Guan, X.; Xie, F.; Song, J., Safety and efficacy of artemisinin-piperaquine for treatment of COVID-19: an open-label, non-randomised and controlled trial. *Int. J. Antimicrob. Agents* **2021**, *57*, 1-7.
217. Cao, R.; Hu, H.; Li, Y.; Wang, X.; Xu, M.; Liu, J.; Zhang, H.; Yan, Y.; Zhao, L.; Li, W.; Zhang, T.; Xiao, D.; Guo, X.; Li, Y.; Yang, J.; Hu, Z.; Wang, M.; Zhong, W., Anti-SARS-CoV-2 Potential of Artemisinins In Vitro. *ACS Infect. Dis.* **2020**, *6*, 2524-2531.
218. Xia, M.; Liu, D.; Liu, Y.; Liu, H., The therapeutic effect of artemisinin and its derivatives in kidney disease. *Frontiers in pharmacology* **2020**, *11*, 380.
219. Ikram, N. K. B. K.; Simonsen, H. T., A Review of Biotechnological Artemisinin Production in Plants. *Front. Plant Sci.* **2017**, *8*, 1-10.
220. Uwimana, A.; Legrand, E.; Stokes, B. H.; Ndikumana, J.-L. M.; Warsame, M.; Umulisa, N.; Ngamije, D.; Munyaneza, T.; Mazarati, J.-B.; Munguti, K.; Campagne, P.; Criscuolo, A.; Ariey, F.; Murindahabi, M.; Ringwald, P.; Fidock, D. A.; Mbituyumuremyi, A.; Menard, D., Emergence and clonal expansion of in vitro artemisinin-resistant Plasmodium falciparum kelch13 R561H mutant parasites in Rwanda. *Nat. Med.* **2020**, *26*, 1602-1608.
221. Patel, O. P. S.; Beteck, R. M.; Legoabe, L. J., Exploration of artemisinin derivatives and synthetic peroxides in antimalarial drug discovery research. *Eur. J. Med. Chem.* **2021**, *213*, 1-45.
222. Choudhary, A.; Sinha, M.; Devi, A.; Jindal, S.; Goyal, K., A Review on Antimalarial 1, 2, 4-Trioxane Derivatives. *J. Drug Deliv. Ther.* **2020**, *10*, 240-253.
223. Chakroborty, S.; Bhanja, C.; Jena, S., Advances in the synthesis of biologically important 1, 2, 4-trioxanes. *Asian J. Biomed. Pharm. Sci.* **2012**, *2*, 1-8.

224. Payne, G. B.; Smith, C. W., Reactions of Hydrogen Peroxide. III. Tungstic Acid Catalyzed Hydroxylation of Cyclohexene in Nonaqueous Media. *J. Org. Chem.* **1957**, *22*, 1682-1685.
225. Singh, C., Preparation of β -hydroxyhydroperoxides by photooxygenation of allylic alcohols and their elaboration into 1, 2, 4-trioxanes. *Tetrahedron Lett.* **1990**, *31*, 6901-6902.
226. Jefford, C. W.; Jaggi, D.; Boukouvalas, J.; Kohmoto, S., Reaction of bicyclic endo peroxides with carbonyl compounds. A new approach to 1, 2, 4-trioxanes. *J. Am. Chem. Soc.* **1983**, *105*, 6497-6498.
227. Jefford, C. W.; Kohmoto, S.; Boukouvalas, J.; Burger, U., Reaction of singlet oxygen with enol ethers in the presence of acetaldehyde. Formation of 1, 2, 4-trioxanes. *J. Am. Chem. Soc.* **1983**, *105*, 6498-6499.
228. Jefford, C. W.; Jaggi, D.; Kohmoto, S.; Boukouvalas, J.; Bernardinelli, G., A New Approach to 1,2,4-Trioxanes from Cyclic Allylic Hydroperoxides. *Helv. Chim. Acta* **1984**, *67*, 2254-2260.
229. Singh, R.; Ishar, M. P. S., UV irradiation of arylidene- β -ionones in the presence of dioxygen: regioselective formation of stable endoperoxides. *Tetrahedron Lett.* **2003**, *44*, 1943-1945.
230. Gardner, E. J.; Squire, R. H.; Elder, R.; Wilson, R. M., Oxidative photoaddition of p-benzoquinone to cyclooctatetraene. Chemical application of the laser. *J. Am. Chem. Soc.* **1973**, *95*, 1693-1695.
231. Yamamoto, H.; Akutagawa, M.; Aoyama, H.; Omote, Y., Synthesis and reactions of 5-arylamino-1, 2, 4-trioxans. *J. Chem. Soc. Perkin Trans. 1* **1980**, 2300-2303.
232. Rudrapal, M.; Chetia, D.; Singh, V., Novel series of 1,2,4-trioxane derivatives as antimalarial agents. *J. Enzyme Inhib. Med. Chem.* **2017**, *32*, 1159-1173.
233. Rudrapal, M., Newer series of trioxane derivatives as potent antimalarial agents. *Med. Chem. Res.* **2018**, *27*, 653-658.
234. Hoar, T. P.; Jacob, W. R., Breakdown of Passivity of Stainless Steel by Halide Ions. *Nature* **1967**, *216*, 1299-1301.
235. Prat, D.; Hayler, J.; Wells, A., A survey of solvent selection guides. *Green Chem.* **2014**, *16*, 4546-4551.
236. Colomer, I.; Chamberlain, A. E. R.; Haughey, M. B.; Donohoe, T. J., Hexafluoroisopropanol as a highly versatile solvent. *Nat. Rev. Chem.* **2017**, *1*, 1-12.
237. Li, S.; Lv, X.; Ren, D.; Shao, C.; Liu, Q.; Xiao, J., Redox-triggered cascade dearomative cyclizations enabled by hexafluoroisopropanol. *Chem. Sci.* **2018**, *9*, 8253-8259.
238. Mareev, E.; Aleshkevich, V.; Potemkin, F.; Bagratashvili, V.; Minaev, N.; Gordienko, V., Anomalous behavior of nonlinear refractive indexes of CO₂ and Xe in supercritical states. *Optics express* **2018**, *26*, 13229-13238.

239. Broo, A.; Holm, P.; Judkins, R.; Li, L.; Lindstedt-Alstermark, E.-L.; Sandberg, P.; Swanson, M.; Weidolf, L.; Mrickmann, K. Non-anilinic derivatives of isothiazol-3(2H)-one 1,1-dioxides as liver X receptors modulators. 2006.
240. Barradas, S.; Hernández-Torres, G.; Urbano, A.; Carreño, M. C., Total Synthesis of Natural p-Quinol Cochinchinenone. *Org. Lett.* **2012**, *14*, 5952-5955.
241. Rubush, D. M.; Rovis, T., Stereoselective synthesis of dioxolanes and oxazolidines via a desymmetrization acetalization/Michael cascade. *Synlett* **2014**, *25*, 713-717.
242. Rubush, D. M. Progress toward the total synthesis of stemocurtisine and asymmetric synthesis of endoperoxide anticancer agents via Bronsted acid cascade catalysis. PhD Thesis, Colorado State University 2012.
243. Tsai, C.-Y.; Chen, L.-A.; Sung, K., TiCl₄-catalyzed synthesis of peroxyacetals from aldehydes. *Can. J. Chem.* **2012**, *90*, 321-325.
244. Yang, Z.; Xu, X.; Yang, C.-H.; Tian, Y.; Chen, X.; Lian, L.; Pan, W.; Su, X.; Zhang, W.; Chen, Y., Total Synthesis of Nannocystin A. *Org. Lett.* **2016**, *18*, 5768-5770.
245. Giedyk, M.; Turkowska, J.; Lepak, S.; Marculewicz, M.; ó Proinsias, K.; Gryko, D., Photoinduced Vitamin B12-Catalysis for Deprotection of (Allyloxy)arenes. *Org. Lett.* **2017**, *19*, 2670-2673.
246. Eyong, K. O.; Kuete, V.; Efferth, T., Quinones and Benzophenones from the Medicinal Plants of Africa. In *Medicinal Plant Research in Africa*, Elsevier: Oxford, 2013; pp 351-391.
247. Hayashi, N.; Ohnuma, T.; Saito, Y.; Higuchi, H.; Ninomiya, K., Structure and electronic properties of quinone dimers connected with acetylene and diacetylene linkages. *Tetrahedron* **2009**, *65*, 3639-3644.
248. Hayashi, N.; Yoshikawa, T.; Ohnuma, T.; Higuchi, H.; Sako, K.; Uekusa, H., Synthesis, Structure, and Properties of Benzoquinone Dimer and Trimers Bearing t-Bu Substituents. *Org. Lett.* **2007**, *9*, 5417-5420.
249. Abraham, I.; Joshi, R.; Pardasani, P.; Pardasani, R. T., Recent advances in 1,4-benzoquinone chemistry. *J. Braz. Chem. Soc.* **2011**, *22*, 385-421.
250. Dandawate, P. R.; Vyas, A. C.; Padhye, S. B.; Singh, M. W.; Baruah, J. B., Perspectives on Medicinal Properties of Benzoquinone Compounds. *Mini-Rev. Med. Chem.* **2010**, *10*, 436-454.
251. Kuete, V.; Efferth, T., Pharmacogenomics of Cameroonian traditional herbal medicine for cancer therapy. *J. Ethnopharmacol.* **2011**, *137*, 752-766.
252. Aussel, L.; Pierrel, F.; Loiseau, L.; Lombard, M.; Fontecave, M.; Barras, F., Biosynthesis and physiology of coenzyme Q in bacteria. *Biochim. Biophys. Acta, Bioenerg.* **2014**, *1837*, 1004-1011.
253. Fan, Y.; Liu, X.; Keyhani, N. O.; Tang, G.; Pei, Y.; Zhang, W.; Tong, S., Regulatory cascade and biological activity of *Beauveria bassiana* oosporein that limits bacterial growth after host death. *Proc. Natl. Acad. Sci. USA* **2017**, *114*, E1578-E1586.

254. Yıldırım, H., Synthesis, characterization, and biological evaluation of a set of new alkylthio substituted plastoquinones containing ester group. *J. Mol. Struct.* **2020**, *1203*, 1-7.
255. Saini, R., Coenzyme Q10: The essential nutrient. *J. Pharm. Bioallied Sci.* **2011**, *3*, 466-467.
256. Lee, C.-S., Excision Repair of 2,5-Diaziridinyl-1,4-Benzoquinone (DZQ)-DNA Adduct by Bacterial and Mammalian 3-Methyladenine-DNA Glycosylases. *Mol. Cells* **2000**, *10*, 723-727.
257. Tansuwan, S.; Pornpakakul, S.; Roengsumran, S.; Petsom, A.; Muangsin, N.; Sihanonta, P.; Chaichit, N., Antimalarial Benzoquinones from an Endophytic Fungus, *Xylaria* sp. *J. Nat. Prod.* **2007**, *70*, 1620-1623.
258. Belardi, J. K.; Micalizio, G. C., Studies on the Syntheses of Benzoquinone Ansamycin Antibiotics. Syntheses of the C(5)-C(15) Subunits of Macbecin I, Geldanamycin, and Herbimycin A. *Org. Lett.* **2006**, *8*, 2409-2412.
259. Sagnou, M.; Strongilos, A.; Hadjipavlou-Litina, D.; Couladouros, E., Synthesis of Novel Benzoquinones with Anti-Inflammatory Activity. *Lett. Drug Des. Discovery* **2009**, *6*, 172-177.
260. Wendlandt, A. E.; Stahl, S. S., Quinone-Catalyzed Selective Oxidation of Organic Molecules. *Angew. Chem. Int. Ed.* **2015**, *54*, 14638-14658.
261. Trost, B. M., Dehydrogenation Mechanisms. On the Mechanism of Dehydrogenation of Acenaphthene by Quinones. *J. Am. Chem. Soc.* **1967**, *89*, 1847-1851.
262. Inaba, K.; Takahashi, Y.-h.; Ito, K.; Hayashi, S., Critical role of a thiolate-quinone charge transfer complex and its adduct form in de novo disulfide bond generation by DsbB. *Proc. Natl. Acad. Sci. USA* **2006**, *103*, 287-292.
263. Wang, Z., Thiele-Winter Acetoxylation. In *Comprehensive Organic Name Reactions and Reagents*, 2010; pp 2762-2765.
264. Hosamani, B.; Ribeiro, M. F.; da Silva Júnior, E. N.; Namboothiri, I. N. N., Catalytic asymmetric reactions and synthesis of quinones. *Org. Biomol. Chem.* **2016**, *14*, 6913-6931.
265. Katritzky, A. R.; Fedoseyenko, D.; Mohapatra, P. P.; Steel, P. J., Reactions of p-Benzoquinone with Sulfur Nucleophiles. *Synthesis* **2008**, 777-787.
266. Alemán, J.; Cabrera, S.; Maerten, E.; Overgaard, J.; Jørgensen, K. A., Asymmetric Organocatalytic α -Arylation of Aldehydes. *Angew. Chem. Int. Ed.* **2007**, *46*, 5520-5523.
267. Alemán, J.; Richter, B.; Jørgensen, K. A., Organocatalytic Highly Enantioselective α -Arylation of β -Ketoesters. *Angew. Chem. Int. Ed.* **2007**, *46*, 5515-5519.
268. Nawrat, C. C.; Moody, C. J., Quinones as Dienophiles in the Diels-Alder Reaction: History and Applications in Total Synthesis. *Angew. Chem. Int. Ed.* **2014**, *53*, 2056-2077.

269. Hu, Q.-Y.; Zhou, G.; Corey, E. J., Application of Chiral Cationic Catalysts to Several Classical Syntheses of Racemic Natural Products Transforms Them into Highly Enantioselective Pathways. *J. Am. Chem. Soc.* **2004**, *126*, 13708-13713.
270. Zhou, G.; Corey, E. J., Short, Enantioselective Total Synthesis of Aflatoxin B2 Using an Asymmetric [3+2]-Cycloaddition Step. *J. Am. Chem. Soc.* **2005**, *127*, 11958-11959.
271. Sultan, S.; Bhat, M.-u.-S.; Rizvi, M. A.; Shah, B. A., Visible Light-Mediated [2 + 2] Cycloaddition Reactions of 1,4-Quinones and Terminal Alkynes. *J. Org. Chem.* **2019**, *84*, 8948-8958.
272. Wood, J. M.; da Silva Júnior, E. N.; Bower, J. F., Rh-Catalyzed [2 + 2 + 2] Cycloadditions with Benzoquinones: De Novo Access to Naphthoquinones for Lignan and Type II Polyketide Synthesis. *Org. Lett.* **2020**, *22*, 265-269.
273. Shukla, S.; Dubey, K. K., CoQ10 a super-vitamin: review on application and biosynthesis. *3 Biotech* **2018**, *8*, 1-11.
274. Coombes, C. L.; Moody, C. J., First Syntheses of 2,2-Dimethyl-7-(2'-methylbut-3'-en-2'-yl)-2H-chromen-6-ol and 2-(3'-Methylbut-2'-enyl)-5-(2'-methylbut-3'-en-2'-yl)-1,4-benzoquinone, Novel Prenylated Quinone Derivatives from the New Zealand Brown Alga *Perithalia capillaris*. *J. Org. Chem.* **2008**, *73*, 6758-6762.
275. Hewson, A. T.; Sharpe, D. A.; Wadsworth, A. H., Synthesis of P-Benzoquinones by Oxidation of N-Arylsulphonamides. *Synth. Commun.* **1989**, *19*, 2095-2099.
276. Chen, Y.; Ying, W.; Harmata, M., Oxidation of 4-methoxyanilines to 1,4-benzoquinones using ceric ammonium nitrate (CAN). *Tetrahedron Lett.* **2011**, *52*, 480-482.
277. Perri, S. T.; Foland, L. D.; Decker, O. H. W.; Moore, H. W., Synthesis of benzoquinones and annulated derivatives from conjugated ketenes. *J. Org. Chem.* **1986**, *51*, 3067-3068.
278. Maurya, H., Oxidizing Agent Applied for Quinone Synthesis: A Review. *Org. Chem. Ind. J.* **2016**, *12*, 1-41.
279. Teuber, H.-J.; Glosauer, O., Reaktionen mit Nitrosodisulfonat, XXVII: Über die Oxydation einiger weiterer Phenole. *Chem. Ber.* **1965**, *98*, 2643-2647.
280. van Dort, H. M.; Geursen, H. J., Salcomine-catalyzed oxidations of some phenols: A new method for the preparation of a number of para-benzoquinones. *Recl. Trav. Chim. Pays-Bas* **1967**, *86*, 520-526.
281. Murahashi, S. I.; Naota, T.; Miyaguchi, N.; Noda, S., Ruthenium-catalyzed oxidation of phenols with alkyl hydroperoxides. A novel, facile route to 2-substituted quinones. *J. Am. Chem. Soc.* **1996**, *118*, 2509-2510.
282. Murahashi, S. I.; Miyaguchi, N.; Noda, S.; Naota, T.; Fujii, A.; Inubushi, Y.; Komiya, N., Ruthenium-catalyzed oxidative dearomatization of phenols to 4-(tert-butylperoxy)cyclohexadienones: Synthesis of 2-substituted quinones from p-substituted phenols. *Eur. J. Org. Chem.* **2011**, *2011*, 5355-5365.

283. Murahashi, S.-I.; Fujii, A.; Inubushi, Y.; Komiya, N., Synthesis of 2-substituted quinones, vitamin K 3, and vitamin K 1 from p-cresol. BF₃·OEt₂-catalyzed methyl migration of 4- tert-butylidioxycyclohexadienones. *Tetrahedron Lett.* **2010**, *51*, 2339-2341.
284. Reinaud, O.; Capdevielle, P.; Maumy, M., Première synthèse totale d'une hydroxy-méthoxy-quinone: la dihydromaesanine. *Tetrahedron Lett.* **1985**, *26*, 3993-3996.
285. Martínez-Cifuentes, M.; Monroy-Cárdenas, M.; Millas-Vargas, J. P.; Weiss-López, B. E.; Araya-Maturana, R., Assessing Parameter Suitability for the Strength Evaluation of Intramolecular Resonance Assisted Hydrogen Bonding in o-Carbonyl Hydroquinones. *Molecules* **2019**, *24*, 1-13.
286. Kholdeeva, O. A.; Mel'gunov, M. S.; Shmakov, A. N.; Trukhan, N. N.; Kriventsov, V. V.; Zaikovskii, V. I.; Malyshev, M. E.; Romannikov, V. N., A new mesoporous titanium-silicate Ti-MMM-2: a highly active and hydrothermally stable catalyst for H₂O₂-based selective oxidations. *Catal. Today* **2004**, *91-92*, 205-209.
287. Brooke, G. M.; Forbes, E. J.; Richardson, R. D.; Stacey, M.; Tatlow, J. C., 372. Aromatic polyfluoro-compounds. Part XXI. Reactions of the pentafluorobenzenediazonium ion. *J. Chem. Soc.* **1965**, 2088-2094.
288. Mehta, G.; Pan, S. C., Total Synthesis of the Novel Antifungal Agent (±)-Jesterone. *Org. Lett.* **2004**, *6*, 811-813.
289. Boldron, C.; Aromí, G.; Challa, G.; Gamez, P.; Reedijk, J., Selective oxidative para C–C dimerization of 2,6-dimethylphenol. *Chem. Commun.* **2005**, 5808-5810.
290. Lin, Y.; Li, B.; Feng, Z.; Kim, Y. A.; Endo, M.; Su, D. S., Efficient Metal-Free Catalytic Reaction Pathway for Selective Oxidation of Substituted Phenols. *ACS Catal.* **2015**, *5*, 5921-5926.
291. Uliana, M.; Vieira, Y.; Maria, C.; Donatoni, A.; Corrêa, U.; Brocksom, T.; Brocksom, U., Oxidation of Mono-Phenols to para-Benzoquinones: a Comparative Study. *J. Braz. Chem. Soc.* **2008**, *19*, 1484-1489.
292. Wertjes, W. C.; Southgate, E. H.; Sarlah, D., Recent advances in chemical dearomatization of nonactivated arenes. *Chem. Soc. Rev.* **2018**, *47*, 7996-8017.
293. Okumura, M.; Sarlah, D., Visible-Light-Induced Dearomatizations. *Eur. J. Org. Chem.* **2020**, *2020*, 1259-1273.
294. Yuji, H.; Shunsuke, S.; Masatoshi, T.; Takeo, S., Selective Oxidation of P-alkylphenols With Tetraperoxymolybdate, [Mo(O₂)₄]=:a Preparative Method of a Dienone Hydroperoxide. *Chem. Lett.* **1973**, *2*, 651-654.
295. Saladino, R.; Neri, V.; Mincione, E.; Filippone, P., Selective oxidation of phenol and anisole derivatives to quinones with hydrogen peroxide and polymer-supported methylrhenium trioxide systems. *Tetrahedron* **2002**, *58*, 8493-8500.
296. Rockcliffe, D. A.; Martell, A. E., The stoichiometric and catalytic oxidation of various substrates with a novel macrocyclic binuclear copper(I) dioxygen complex as an intermediate. *J. Chem. Soc., Chem. Commun.* **1992**, 1758-1760.

297. Miecznikowski, J. R.; Caradonna, J. P.; Foley, K. M.; Kwiecien, D. J.; Lisi, G. P.; Martinez, A. M., Introduction to Homogenous Catalysis with Ruthenium-Catalyzed Oxidation of Alcohols: An Experiment for Undergraduate Advanced Inorganic Chemistry Students. *J. Chem. Educ.* **2011**, *88*, 657.
298. Wang, Y. W.; Duh, Y. S.; Shu, C. M., Thermal runaway hazards of tert-butyl hydroperoxide by calorimetric studies. *J. Therm. Anal. Calorim.* **2009**, *95*, 553-557.
299. Rodikova, Y. A.; Zhizhina, E. G.; Pai, Z. P., Alkyl-1,4-Benzoquinones – From Synthesis to Application. *ChemistrySelect* **2016**, *1*, 2113-2128.
300. González, R. R.; Gambarotti, C.; Liguori, L.; Bjørsvik, H. R., Efficient and green telescoped process to 2-methoxy-3-methyl-[1,4]benzoquinone. *J. Org. Chem.* **2006**, *71*, 1703-1706.
301. Reymond, H.; Vitas, S.; Vernuccio, S.; von Rohr, P. R., Reaction Process of Resin-Catalyzed Methyl Formate Hydrolysis in Biphasic Continuous Flow. *Ind. Eng. Chem. Res.* **2017**, *56*, 1439-1449.
302. Antonovskii, V. L.; Khursan, S. L., Thermolysis of organic peroxides in solution. *Russ. Chem. Rev.* **2003**, *72*, 939-963.
303. Pilkington, J. W.; Waring, A. J., Cyclohexadienones. Use of the dienone–phenol rearrangement in measuring migratory aptitudes of alkyl groups. *J. Chem. Soc., Perkin Trans. 2* **1976**, 1349-1359.
304. Trummal, A.; Lipping, L.; Kaljurand, I.; Koppel, I. A.; Leito, I., Acidity of Strong Acids in Water and Dimethyl Sulfoxide. *J. Phys. Chem. A* **2016**, *120*, 3663-3669.
305. Rumble, J. R.; Lide, D. R.; Bruno, T. J., *CRC handbook of chemistry and physics : a ready-reference book of chemical and physical data*. 100th ed.; Boca Raton, CRC Press 2019.
306. Wicks, Z. W., Jr., Jones, F.N., Pappas, S.P. and Wicks, D.A, Amino Resins. In *Organic Coatings*, 2007; pp 213-230.
307. Chang, Y.; Lee, C.; Bae, C., Polystyrene-based superacidic solid acid catalyst: synthesis and its application in biodiesel production. *RSC Adv.* **2014**, *4*, 47448-47454.
308. García-García, C.; Redondo, M. C.; Ribagorda, M.; Carreño, M. C., Reactions of p-quinols with aldehydes and imines: stereoselective access to polyheterobicyclic and tricyclic systems. *Eur. J. Org. Chem.* **2014**, *2014*, 7377-7388.
309. Kyasa, S. K. New Methods for Synthesis of Organic Peroxides and Application of Peroxide Electrophiles to Synthesis of Functionalized Ethers. University of Nebraska 2015.
310. Carniti, P.; Gervasini, A.; Biella, S.; Auroux, A., Intrinsic and Effective Acidity Study of Niobic Acid and Niobium Phosphate by a Multitechnique Approach. *Chem. Mater.* **2005**, *17*, 6128-6136.
311. Sabaa, M. W.; Madkour, T. M.; Yassin, A. A., Polymerization products of p-Benzoquinone as bound antioxidants for styrene-butadiene rubber: Part I—Preparation of quinone polymers. *Polym. Degrad. Stab.* **1988**, *22*, 195-203.

312. Daniels, I. N.; Wang, Z.; Laird, B. B., Dielectric Properties of Organic Solvents in an Electric Field. *J. Phys. Chem. C* **2017**, *121*, 1025-1031.
313. Smallwood, I. M., Ethyl acetate. In *Handbook of Organic Solvent Properties*, Smallwood, I. M., Ed. Butterworth-Heinemann: Oxford, 1996; pp 227-229.
314. Monticelli, S.; Castoldi, L.; Murgia, I.; Senatore, R.; Mazzeo, E.; Wackerlig, J.; Urban, E.; Langer, T.; Pace, V., Recent advancements on the use of 2-methyltetrahydrofuran in organometallic chemistry. *Monatsh. Chem.* **2017**, *148*, 37-48.
315. Smallwood, I. M., Acetonitrile. In *Handbook of Organic Solvent Properties*, Smallwood, I. M., Ed. Butterworth-Heinemann: Oxford, 1996; pp 289-291.
316. Smallwood, I. M., Methanol. In *Handbook of Organic Solvent Properties*, Smallwood, I. M., Ed. Butterworth-Heinemann: Oxford, 1996; pp 61-63.
317. Smallwood, I. M., Chloroform. In *Handbook of Organic Solvent Properties*, Smallwood, I. M., Ed. Butterworth-Heinemann: Oxford, 1996; pp 141-143.
318. Lide, D. R., *CRC Handbook of Chemistry and Physics*. 75th ed.; CRC Press Inc.: Boca Raton, 1994; Vol. 75.
319. Yakura, T.; Omoto, M.; Yamauchi, Y.; Tian, Y.; Ozono, A., Hypervalent iodine oxidation of phenol derivatives using a catalytic amount of 4-iodophenoxyacetic acid and Oxone[®] as a co-oxidant. *Tetrahedron* **2010**, *66*, 5833-5840.
320. Kim, S.; Matsubara, R.; Hayashi, M., Activated carbon-promoted dehydrogenation of hydroquinones to benzoquinones, naphthoquinones, and anthraquinones under molecular oxygen atmosphere. *J. Org. Chem.* **2019**, *84*, 2997-3003.
321. Love, B. E.; Duffy, B. C.; Simmons, A. L., Effects of reaction conditions on quinone/diquinone product ratios in the oxidation of 1,4-dimethoxybenzene derivatives with ceric ammonium nitrate. *Tetrahedron Lett.* **2014**, *55*, 1994-1997.
322. Ismail, B. B.; Pu, Y.; Guo, M.; Ma, X.; Liu, D., LC-MS/QTOF identification of phytochemicals and the effects of solvents on phenolic constituents and antioxidant activity of baobab (*Adansonia digitata*) fruit pulp. *Food Chem.* **2019**, *277*, 279-288.
323. Silva, D. C. M. N.; Bresciani, L. F. V.; Dalagnol, R. L.; Danielski, L.; Yunes, R. A.; Ferreira, S. R. S., Supercritical fluid extraction of carqueja (*Baccharis trimera*) oil: Process parameters and composition profiles. *Food Bioprod. Process.* **2009**, *87*, 317-326.
324. Baldauf, S.; Bode, J., Synthesis and Evaluation of Cyclic Acetals of Serine Hydroxylamine for Amide-Forming KAHA Ligations. *Synthesis* **2019**, *51*, 1273-1283.
325. Chemla, P., Stereoselective synthesis of (+)-hydantocidin. *Tetrahedron Lett.* **1993**, *34*, 7391-7394.
326. Ma, K.; Han, J.; Bao, L.; Wei, T.; Liu, H., Two Sarcoviolins with Antioxidative and α -Glucosidase Inhibitory Activity from the Edible Mushroom *Sarcodon leucopus* Collected in Tibet. *J. Nat. Prod.* **2014**, *77*, 942-947.

327. Riddell, F. G.; Berry, M. H.; Turner, E. S., The conformational analysis of tetrahydro-1,4,2-dioxazines. *Tetrahedron* **1978**, *34*, 1415-1423.
328. Pathipati, S. R.; Singh, V.; Eriksson, L.; Selander, N., Lewis Acid Catalyzed Annulation of Nitrones with Oxiranes, Aziridines, and Thiiranes. *Org. Lett.* **2015**, *17*, 4506-4509.
329. Liu, Y.; Ao, J.; Paladhi, S.; Song, C. E.; Yan, H., Organocatalytic Asymmetric Synthesis of Chiral Dioxazinanes and Dioxazepanes with in Situ Generated Nitrones via a Tandem Reaction Pathway Using a Cooperative Cation Binding Catalyst. *J. Am. Chem. Soc.* **2016**, *138*, 16486-16492.
330. Masubuti, H.; Endo, Y.; Araya, H.; Uekusa, H.; Fujimoto, Y., Establishment of Benzodioxazine Core Structure for Sarcodonin Class of Natural Products by X-ray Analysis. *Org. Lett.* **2013**, *15*, 2076-2079.
331. Yu, J.; Cai, C., FeCl₃-catalyzed [3+3]annulation between 3-oxirane-indolin-2-ones and nitrones to construct spiro[1,4,2-dioxazinan]oxindoles. *Mol. Diversity* **2017**, *21*, 761-768.
332. Wani, I. A.; Sayyad, M.; Ghorai, M. K., Domino ring-opening cyclization (DROC) of activated aziridines and epoxides with nitrones via dual-catalysis "on water". *Chem. Commun.* **2017**, *53*, 4386-4389.
333. Saba, S.; Domkowski, P. W.; Firooznia, F., Thermal Rearrangement of some Oxazolidine N-Oxides. 2-Alkyl-6-aryl-3,4-dihydro-2H-1,5,2-dioxazines. *Synthesis* **1990**, 921-923.
334. D. Jones, A.; W. Knight, D.; R. Thornton, S., On the Lewis acid-induced [1,3]-dipolar cycloaddition of allylic and homoallylic alcohols to N-methyl-C-phenyl nitrone. *J. Chem. Soc. Perkin Trans. 1* **1999**, 3337-3344.
335. Burchardt, A.; Geffken, D., Ringverengung von 1,5,2-Dioxazinan-3,6-dionen und 1,3,2,4-Dioxathiazinan-5-on-2-oxiden zu 1,2-Oxazetidin-3-onen. *Arch. Pharm. Pharm. Med. Chem.* **1990**, *323*, 967-970.
336. Piron, K.; Kenis, S.; Verniest, G.; Surmont, R.; Thuring, J. W.; ten Holte, P.; Deroose, F.; De Kimpe, N., Synthesis of gem-difluorinated 1,6-naphthyridine-5,7-diones. *Tetrahedron* **2012**, *68*, 6941-6947.
337. Meshcheryakov, V. I.; Moskalik, M. Y.; Kelling, A.; Schilde, U.; Ushakov, I. A.; Shainyan, B. A., Oxymethylation of trifluoromethanesulfonamide with paraformaldehyde in ethyl acetate. *Russ. J. Org. Chem.* **2008**, *44*, 311-316.
338. Tokala, V., Synthesis of 1, 2, 4-Dioxazinane, Bis-1,2,4-Dioxazinane, 1,2,4-Trioxanes and their Sugar Analogues as an Antimalarial drugs. *Int. J. Res. Appl. Sci. Eng. Technol.* **2018**, *6*, 2085-2093.
339. Das, A. K., Anticancer Effect of AntiMalarial Artemisinin Compounds. *Ann. Med. Health Sci. Res.* **2015**, *5*, 93-102.
340. Firsova, Y. N.; Lozinskaya, N. A.; Sosonyuk, S. E.; Proskurnina, M. V.; Zefirov, N. S., Stable synthetic equivalents of N-unsubstituted imines: Part 1. Synthesis. *Rev. J. Chem.* **2012**, *2*, 74-104.

341. Morales, S.; Guijarro, F. G.; García Ruano, J. L.; Cid, M. B., A General Aminocatalytic Method for the Synthesis of Aldimines. *J. Am. Chem. Soc.* **2014**, *136*, 1082-1089.
342. Ferreira, F.; Botuha, C.; Chemla, F.; Pérez-Luna, A., tert-Butanesulfinimines: structure, synthesis and synthetic applications. *Chem. Soc. Rev.* **2009**, *38*, 1162-1186.
343. Ellman, J. A.; Owens, T. D.; Tang, T. P., N-tert-butanesulfinyl imines: versatile intermediates for the asymmetric synthesis of amines. *Acc. Chem. Res.* **2002**, *35*, 984-995.
344. Mendes, J. A.; Costa, P. R.; Yus, M.; Foubelo, F.; Buarque, C. D., N-tert-Butanesulfinyl imines in the asymmetric synthesis of nitrogen-containing heterocycles. *Beilstein J. Org. Chem.* **2021**, *17*, 1096-1140.
345. Buchs, B.; Godin, G.; Trachsel, A.; de Saint Laumer, J.-Y.; Lehn, J.-M.; Herrmann, A., Reversible Aminal Formation: Controlling the Evaporation of Bioactive Volatiles by Dynamic Combinatorial/Covalent Chemistry. *Eur. J. Org. Chem.* **2011**, *2011*, 681-695.
346. Aggarwal, V. K.; Barbero, N.; McGarrigle, E. M.; Mickle, G.; Navas, R.; Suárez, J. R.; Unthank, M. G.; Yar, M., The fate of the tert-butylsulfinyl auxiliary after acid-promoted cleavage—a method for recycling t-BuSONH₂. *Tetrahedron Lett.* **2009**, *50*, 3482-3484.
347. Baidya, M.; Kobayashi, S.; Brotzel, F.; Schmidhammer, U.; Riedle, E.; Mayr, H., DABCO and DMAP—Why Are They Different in Organocatalysis? *Angew. Chem. Int. Ed.* **2007**, *46*, 6176-6179.
348. Raheem, I. T.; Jacobsen, E. N., Highly Enantioselective Aza-Baylis–Hillman Reactions Catalyzed by Chiral Thiourea Derivatives. *Adv. Synth. Catal.* **2005**, *347*, 1701-1708.
349. Stark, D. G.; O’Riordan, T. J. C.; Smith, A. D., Synthesis of Di-, Tri-, and Tetrasubstituted Pyridines from (Phenylthio)carboxylic Acids and 2-[Aryl(tosylimino)methyl]acrylates. *Org. Lett.* **2014**, *16*, 6496-6499.
350. Liu, X.; Xia, Q.; Zhang, Y.; Chen, C.; Chen, W., Cu-NHC-TEMPO Catalyzed Aerobic Oxidation of Primary Alcohols to Aldehydes. *J. Org. Chem.* **2013**, *78*, 8531-8536.
351. Siengalewicz, P.; Rinner, U.; Mulzer, J., Recent progress in the total synthesis of naphthyridinomycin and lemomycin tetrahydroisoquinoline antitumor antibiotics (TAAs). *Chem. Soc. Rev.* **2008**, *37*, 2676-2690.
352. Zmijewski, M. J.; Mikolajczak, M.; Viswanatha, V.; Hruby, V. J., Biosynthesis of the antitumor antibiotic naphthyridinomycin. *J. Am. Chem. Soc.* **1982**, *104*, 4969-4971.
353. Scott, J. D.; Williams, R. M., Total Synthesis of (–)-Tetrazomine. Determination of the Stereochemistry of Tetrazomine and the Synthesis and Biological Activity of Tetrazomine Analogues. *J. Am. Chem. Soc.* **2002**, *124*, 2951-2956.
354. Allan, K. M.; Stoltz, B. M., A Concise Total Synthesis of (–)-Quinocarcin via Aryne Annulation. *J. Am. Chem. Soc.* **2008**, *130*, 17270-17271.

355. Bernan, V.; Montenegro, D.; Korshalla, J.; Maiese, W.; Steinberg, D., Bioxalomycins, new antibiotics produced by the marine *Streptomyces* sp. LL-31F508: Taxonomy and fermentation. *J. Antibiot.* **1995**, *47*, 1417-1424.
356. Fukuyama, T.; Li, L.; Laird, A. A.; Frank, R. K., Stereocontrolled total synthesis of (+-)-cyanocycline A. *J. Am. Chem. Soc.* **1987**, *109*, 1587-1589.
357. Agami, C.; Couty, F., The Use of N-Boc-1,3-Oxazolidines as Chiral Auxiliaries in Asymmetric Synthesis. *Eur. J. Org. Chem.* **2004**, *2004*, 677-685.
358. Abadallah, H.; Gree, R.; Carrie, R., Syntheses asymetriques a l'aide d'oxazolidines chirales derivees de l'ephedrine. Preparation de formyl cyclopropanes chiraux. *Tetrahedron Lett.* **1982**, *23*, 503-506.
359. Colombo, L.; Di Giacomo, M.; Brusotti, G.; Milano, E., Camphor-derived 2-stannyl-N-Boc-1,3-oxazolidine: A new chiral formylanion equivalent for the asymmetric synthesis of 1,2-diols. *Tetrahedron Lett.* **1995**, *36*, 2863-2866.
360. Frieboes, K. C.; Harder, T.; Aulbert, D.; Strahringer, C.; Bolte, M.; Hoppe, D., Convenient Preparation of Stereochemically Homogeneous 2-Acyl-3-sulfonyl-1,3-oxazolidines and Diastereoselective Grignard Additions to Form Protected Enantiopure 2-Hydroxyalkanals. *Synlett* **1993**, 921.
361. Fioravanti, S.; Marchetti, F.; Pellacani, L.; Ranieri, L.; Tardella, P. A., Stereoselective aza-MIRC reactions on optically active (E)-nitro alkenes. *Tetrahedron: Asymmetry* **2008**, *19*, 231-236.
362. Adam, W.; Schambony, S. B., Diastereoselective Epoxidation of Oxazolidine-Substituted Alkenes by Dimethyldioxirane and m-Chloroperbenzoic Acid: π -Facial Control through Hydrogen Bonding by the Urea Functionality. *Org. Lett.* **2001**, *3*, 79-82.
363. Lacoste, J.-É.; Soucy, C.; Rochon, F. D.; Breau, L., 2-Vinyl-trans-octahydro-1,3-benzoxazine: Cyclization and 1,3-dipolar cycloaddition of nitrile oxides. *Tetrahedron Lett.* **1998**, *39*, 9121-9124.
364. Cardani, S.; Scolastico, C.; Villa, R., Synthesis of enantiomeric pure intermediate for the lactone portion of compactin and mevinolin. *Tetrahedron* **1990**, *46*, 7283-7288.
365. Adam, W.; Peters, K.; Peters, E.-M.; Schambony, S. B., Efficient Control of the Diastereoselectivity and Regioselectivity in the Singlet-Oxygen Ene Reaction of Chiral Oxazolidine-Substituted Alkenes by a Remote Urea NH Functionality: Comparison with Dimethyldioxirane and m-Chloroperbenzoic Acid Epoxidations. *J. Am. Chem. Soc.* **2001**, *123*, 7228-7232.
366. Wolf, C.; Xu, H., Asymmetric catalysis with chiral oxazolidine ligands. *Chem. Commun.* **2011**, *47*, 3339-3350.
367. Braga, A. L.; Appelt, H. R.; Schneider, P. H.; Rodrigues, O. E. D.; Silveira, C. C.; Wessjohann, L. A., New C₂-symmetric chiral disulfide ligands derived from (R)-cysteine. *Tetrahedron* **2001**, *57*, 3291-3295.

368. Jin, M.-J.; Jung, J.-A.; Kim, S.-H., New chiral phosphinooxazolidine ligands for palladium-catalyzed asymmetric allylic substitution. *Tetrahedron Lett.* **1999**, *40*, 5197-5198.
369. Raghavan, S.; Senapati, P., Oxazolidines as Intermediates in the Asymmetric Synthesis of 3-Substituted and 1,3-Disubstituted Tetrahydroisoquinolines. *J. Org. Chem.* **2016**, *81*, 6201-6210.
370. Bergmann, E. D., The Oxazolidines. *Chem. Rev.* **1953**, *53*, 309-352.
371. Singh, N.; Dar, A. A.; Kumar, A., A Simple and Efficient Approach for the Synthesis of 1,3-Oxazolidines from β -Amino Alcohols Using Grinding Technique. *ChemistrySelect* **2018**, *3*, 13675-13681.
372. Bulman Page, P. C.; Parkes, G. A.; Buckley, B. R.; Heaney, H.; Gholizadeh, M.; Steven Wailes, J., Microwave-assisted highly diastereoselective synthesis of oxazolidines derived from ketones and aminoalcohols. *Tetrahedron Lett.* **2008**, *49*, 6951-6954.
373. Sriramurthy, V.; Barcan, G. A.; Kwon, O., Bisphosphine-Catalyzed Mixed Double-Michael Reactions: Asymmetric Synthesis of Oxazolidines, Thiazolidines, and Pyrrolidines. *J. Am. Chem. Soc.* **2007**, *129*, 12928-12929.
374. Nimmagadda, S. K.; Zhang, Z.; Antilla, J. C., Asymmetric One-Pot Synthesis of 1,3-Oxazolidines and 1,3-Oxazinanes via Hemiaminal Intermediates. *Org. Lett.* **2014**, *16*, 4098-4101.
375. Tarannum, S.; Sk, S.; Das, S.; Wani, I. A.; Ghorai, M. K., Stereoselective Syntheses of Highly Functionalized Imidazolidines and Oxazolidines via Ring-Opening Cyclization of Activated Aziridines and Epoxides with Amines and Aldehydes. *J. Org. Chem.* **2020**, *85*, 367-379.
376. Elliott, L. D.; Wrigglesworth, J. W.; Cox, B.; Lloyd-Jones, G. C.; Booker-Milburn, K. I., 2,2-Difunctionalization of Alkenes via Pd(II)-Catalyzed Aza-Wacker Reactions. *Org. Lett.* **2011**, *13*, 728-731.
377. Fukata, Y.; Asano, K.; Matsubara, S., Asymmetric Synthesis of 1,3-Oxazolidines via Intramolecular Aza-Michael Addition by Bifunctional Organocatalysts. *Chem. Lett.* **2013**, *42*, 355-357.
378. Li, G.; Fronczek, F. R.; Antilla, J. C., Catalytic Asymmetric Addition of Alcohols to Imines: Enantioselective Preparation of Chiral N,O-Aminals. *J. Am. Chem. Soc.* **2008**, *130*, 12216-12217.
379. Cheng, D.-J.; Li, R.-Q.; Zhang, X.-S.; Zhao, L.; Wang, T.; Shao, Y.-D., Diastereoselective Synthesis of Functionalized Indoline N,O-Aminals: Unexpected Water-Involved Cascade Reaction of 3H-Indoles and Oxazol-5-(4H)ones. *Eur. J. Org. Chem.* **2020**, *2020*, 496-500.
380. Xie, L.; Dong, S.; Zhang, Q.; Feng, X.; Liu, X., Asymmetric construction of dihydrobenzofuran-2,5-dione derivatives via desymmetrization of p-quinols with azlactones. *Chem. Commun.* **2019**, *55*, 87-90.
381. Huang, B.; He, Y.; Levin, M. D.; Coelho, J. A. S.; Bergman, R. G.; Toste, F. D., Enantioselective Kinetic Resolution/Desymmetrization of Para-Quinols: A Case Study

in Boronic-Acid-Directed Phosphoric Acid Catalysis. *Adv. Synth. Catal.* **2020**, *362*, 295-301.

382. Guiso, M.; Marra, C.; Piccioni, F.; Nicoletti, M., Iridoid and phenylpropanoid glucosides from *Tecoma capensis*. *Phytochemistry* **1997**, *45*, 193-194.

383. Ata, A.; Kerr, R. G.; Moya, C. E.; Jacobs, R. S., Identification of anti-inflammatory diterpenes from the marine gorgonian *Pseudopterogorgia elisabethae*. *Tetrahedron* **2003**, *59*, 4215-4222.

384. McCarroll, A. J.; Bradshaw, T. D.; Westwell, A. D.; Matthews, C. S.; Stevens, M. F. G., Quinolins As Novel Therapeutic Agents. 7. Synthesis of Antitumor 4-[1-(Arylsulfonyl-1H-indol-2-yl)]-4-hydroxycyclohexa-2,5-dien-1-ones by Sonogashira Reactions. *J. Med. Chem.* **2007**, *50*, 1707-1710.

385. Evans, D. A.; Wong, R. Y., Synthesis of antibacterial p-quinols from marine sponges. Synthetic applications of "masked" quinones. *J. Org. Chem.* **1977**, *42*, 350-352.

386. Magdziak, D.; Meek, S. J.; Pettus, T. R. R., Cyclohexadienone Ketals and Quinolins: Four Building Blocks Potentially Useful for Enantioselective Synthesis. *Chem. Rev.* **2004**, *104*, 1383-1430.

387. Milić, D. R.; Gašić, M. J.; Muster, W.; Csanádi, J. J.; Šolaja, B. A., The synthesis and biological evaluation of A-ring substituted steroidal p-quinones. *Tetrahedron* **1997**, *53*, 14073-14084.

388. Carreño, M. C.; González, M. P.; Fischer, J., Synthesis and diels-alder reactions of (R)-4-hydroxy-4-p-tolylsulfanyl-methyl-2,5-cyclohexadienone. *Tetrahedron Lett.* **1995**, *36*, 4893-4896.

389. Samanta, S.; Ravi, C.; Joshi, A.; Pappula, V.; Adimurthy, S., Visible-light-induced aerobic dioxygenation of styrenes under metal- and additive-free ambient conditions. *Tetrahedron Lett.* **2017**, *58*, 721-725.

390. Amels, P.; Elias, H.; Wannowius, K.-J., Kinetics and mechanism of the oxidation of dimethyl sulfide by hydroperoxides in aqueous medium Study on the potential contribution of liquid-phase oxidation of dimethyl sulfide in the atmosphere. *J. Chem. Soc., Faraday Trans.* **1997**, *93*, 2537-2544.

391. Ko, K.; Nakano, K.; Watanabe, S.; Ichikawa, Y.; Kotsuki, H., Development of new DMAP-related organocatalysts for use in the Michael addition reaction of β -ketoesters in water. *Tetrahedron Lett.* **2009**, *50*, 4025-4029.

392. Novak, M.; Bonham, G. A.; Mulero, J. J.; Pelecanou, M.; Zemis, J. N.; Buccigross, J. M.; Wilson, T. C., Hydrolysis of N-acetyl-p-benzoquinone imines: pH dependence of the partitioning of a tetrahedral intermediate. *J. Am. Chem. Soc.* **1989**, *111*, 4447-4456.

393. Miyamoto, K.; Yokota, Y.; Suefuji, T.; Yamaguchi, K.; Ozawa, T.; Ochiai, M., Reactivity of Hydroxy-and Aquo (hydroxy)- λ^3 -iodane-Crown Ether Complexes. *Chemistry—A European Journal* **2014**, *20*, 5447-5453.